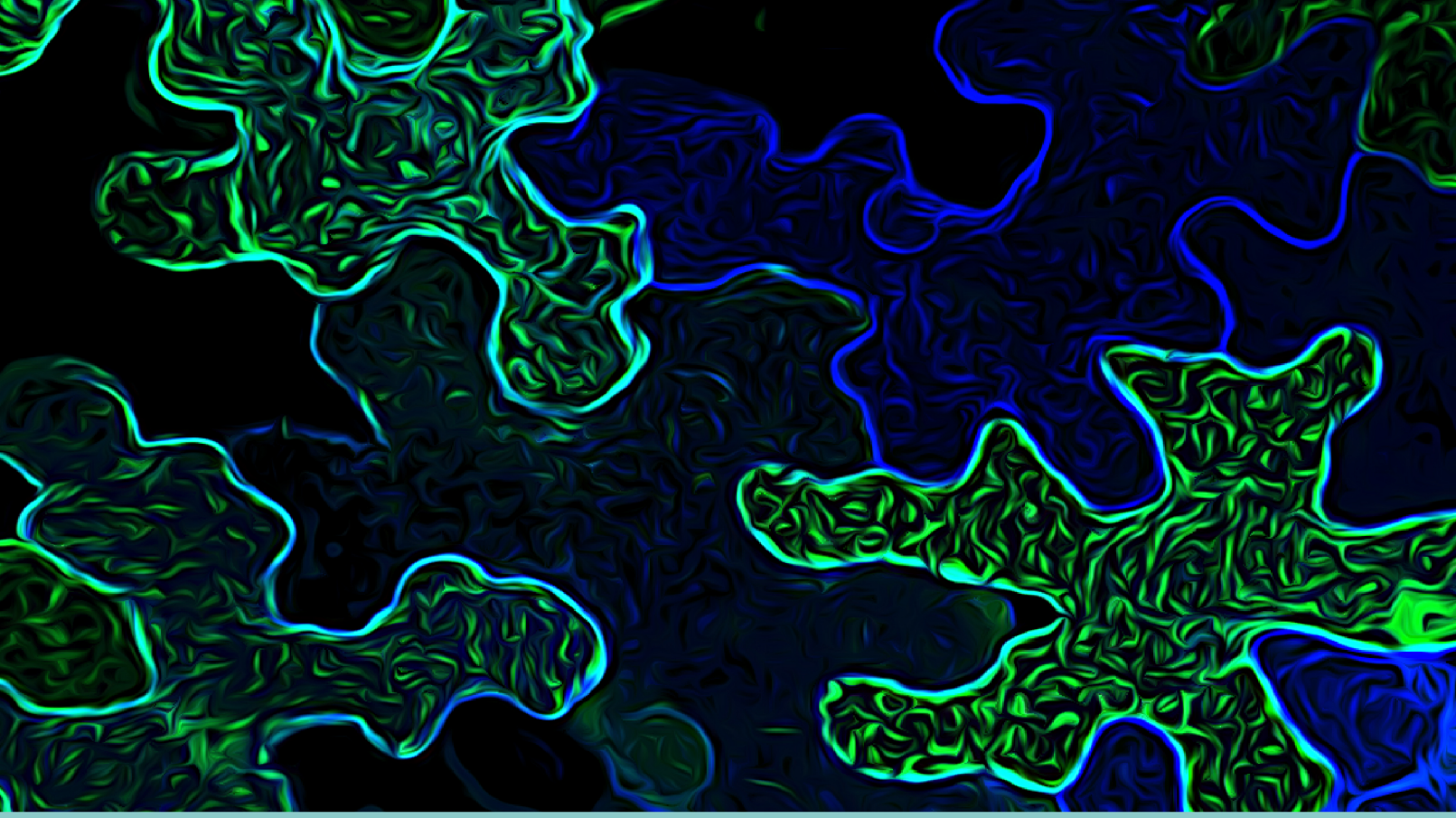

Doctoral thesis

Deciphering the intracellular dual targeting of the melon necrotic spot virus coat protein, its interaction with host factors and their roles in plant defense

María Saiz Bonilla

June 2023

Directors
Prof. Vicente Pallás
Dr. Jose A. Navarro

UNIVERSITAT POLITÈCNICA DE VALÈNCIA

Deciphering the intracellular dual targeting of the melon necrotic spot virus coat protein, its interaction with host factors and their roles in plant defense

María Saiz Bonilla

June 2023

Directors

Prof. Vicente Pallás

Dr. Jose A. Navarro

María Saiz Bonilla ha disfrutado de un contrato predoctoral de formación de personal investigador (FPI) (PRE-2018-84130) otorgado por el Ministerio de Ciencia e Innovación asociado al proyecto BIO2017-88321-R.

Este trabajo de tesis doctoral ha sido realizado con el apoyo económico de los proyectos de investigación del Ministerio de Ciencia e Innovación, BIO2017-88321-R y PID2020-115571RB-I00.

Don Vicente Pallás Benet, Doctor en Ciencias Biológicas, Profesor de Investigación del Consejo Superior de Investigaciones Científicas del Instituto de Biología Molecular y Celular de Plantas (Universidad Politécnica de Valencia-Consejo Superior de Investigaciones Científicas) de Valencia.

Don Jose Antonio Navarro Bohigues, Doctor en Ciencias Biológicas, Técnico Superior de Investigación del Consejo Superior de Investigaciones Científicas del Instituto de Biología Molecular y Celular de Plantas (Universidad Politécnica de Valencia-Consejo Superior de Investigaciones Científicas) de Valencia.

Don Frederic Aparicio Herrero, Doctor en Biología, Profesor Contratado Doctor (Universidad Politécnica de Valencia) de Valencia.

CERTIFICAN:

Que Doña María Saiz Bonilla, Graduada en Biología por la Universitat de Valencia, ha realizado bajo su dirección el trabajo que con título "Deciphering the intracellular dual targeting of the melon necrotic spot virus coat protein, its interaction with host factors and their roles in plant defense" presenta para optar al grado de Doctor en Biotecnología por la Universidad Politécnica de Valencia.

Y para que así conste a los efectos oportunos, firman el presente certificado en Valencia a ____ de_____ de 2023.

Vicente Pallás Benet **Jose Antonio Navarro Bohigues** **Frederic Aparicio Herrero**

Table of contents

SUMMARY

Plant viruses are the causal agents of many plant diseases and the subsequent economic losses, estimated to be US$60 billion worldwide each year. The melon necrotic spot virus (MNSV) is a small, single-stranded, positive-sense RNA virus that belongs to the genus *Gammacarmovirus* and encodes five proteins. The coat protein (CP) is composed of three distinct domains. The R domain is responsible for binding to different RNA molecules and can be divided into two subdomains: R_1 and R_2. This domain is connected to the S domain by the arm region, which is also part of the RNA binding domain. The main function of the S domain is genome protection and transmission when forming virions. It is followed by the P domain, which is the interaction site for the vector fungus zoospores. The discovery of a dual transit peptide in the amino-terminal part of the CP was the starting point of this thesis. Early in MNSV infection, the new synthesized CP is imported into chloroplasts and mitochondria, while the cytoplasmic pool increases as the infection progresses. Inhibiting this dual transport leads to an increase in the RNA silencing suppressor activity of the CP. However, far from resulting in an enhanced infection development, systemic spread was impaired. Therefore, the accumulation of cytoplasmic CP may cause an increase in viral replication and overexpression of p29, an auxiliary replicase that causes morphological alterations, ROS, and necrosis that may restrict viral movement. Thus, a new role for CP targeting would be to avoid excessive viral replication by modulating the suppressor activity to manage the balance between plant defense and viral counter-defense, leading to a compatible interaction.

Unfortunately, *Arabidopsis thaliana* is not a host for MNSV. Thus, to better understand the molecular mechanism behind the CP dual targeting, the receptors and pores of the *Nicotiana benthamiana* mitochondrial and chloroplast outer membrane translocons were genome identified, and some functional characterization was carried out. We assigned the following names NbToc75-III, NbToc34, NbToc90, NbToc120, NbToc159A, NbToc159B, NbTic22-III for chloroplast translocon components, and NbTom40, NbTom20-1, NbTom20-2, NbOm64 for mitochondrion translocon components. The functional characterization was mainly carried out by virus-induced gene silencing (VIGS) and RT-qPCR, revealing a functional redundancy higher than that reported for Arabidopsis homologs. Additionally, VIGS was also used to evaluate the relevance of each translocon component in MNSV infection, and together with

CP-receptor interaction studies performed by BiFC and Y2H, allowed us to identify NbToc159A for chloroplasts and NbOm64 for mitochondria as the main receptors involved in the CP organelle import. Moreover, silencing of NbToc34, NbToc75, or NbTom40 resulted in a generalized resistance not only to MNSV but also to turnip crinkle virus (TCV), and carnation mottle virus (CarMV), supporting the current idea that involves the chloroplast and mitochondrion physiological state in early defense response signaling.

Finally, a search for host factors interacting with the CP was performed by the innovative TurboID proximity labeling tool, which allows the detection of both direct/indirect and transient/stable interactions. Thus, a large number of candidate proteins were obtained that interacted either with the MNSV CP or with ΔNtCP, a cytoplasm-localized mutant. Eight interactors that showed a higher degree of confidence and were more relevant to viral defense were functionally analyzed by VIGS. Three of them, NbSIK1, NbSMU2, and NbMAP3K, showed a consistent and repetitive detrimental effect on MNSV RNA accumulation. After the validation of the interactions using another method and the analysis of the subcellular localization of the MNSV CP under each interactor silencing, two main hypotheses were proposed. Firstly, since the main function of NbSMU2 is related to messenger RNA regulation by splicing, this protein could be sequestered by the CP, causing the expression of proviral genes. On the other hand, NbSIK1 and NbMAP3K act as positive and negative regulators of the PTI response to infection, respectively. Moreover, both proteins interact with each other and are part of the MAP kinase cascade, so in our second hypothesis, CP would interact with this complex, promoting a negative regulation of PTI that would facilitate viral infection.

In summary, the work carried out in this thesis has allowed the identification and the mechanistic and functional analysis of the dual transport of the MNSV CP to chloroplasts and mitochondria. The results obtained provide both an extensive description of a new viral mechanism to attenuate plant defense and a promising study on host factors involved in the virus infection cycle.

RESUMEN

Los virus de plantas son los agentes causales de un gran número de enfermedades en plantas que ocasionan grandes pérdidas económicas. El virus de las manchas necróticas del melón (MNSV), es un pequeño virus de RNA monocatenario de polaridad positiva, perteneciente al género *Gammacarmovirus*, cuyo genoma codifica cinco proteínas. La proteína de cubierta (CP, del inglés "*coat protein*"), está formada por tres dominios distintos. El dominio R es el responsable de la unión a distintas moléculas de RNA y se puede dividir en dos subdominios: R_1 y R_2. Este dominio está conectado con el dominio S mediante la región "*arm*", que también forma parte del dominio de unión al RNA. La función principal del dominio S es la de protección y transmisión del genoma al formar viriones. Le sigue el dominio P, que es el sitio de interacción con las zoosporas del hongo vector. El descubrimiento de un péptido de transito dual en la región amino-terminal de la CP fue el punto de partida de esta tesis. Al inicio de una infección por MNSV, la CP nuevamente sintetizada es transportada al interior de cloroplastos y mitocondrias mientras que, una parte mucho menor se mantiene en el citoplasma aumentando a medida que avanza la infección. La inhibición de este transporte dual conlleva un aumento de la actividad supresora del silenciamiento del RNA de la CP. Sin embargo, lejos de provocar una mayor infección, la infección sistémica se ve particularmente afectada. Por tanto, la acumulación de la CP en el citoplasma puede provocar un aumento de la replicación viral pero a su vez una sobreexpresión de la p29, una replicasa auxiliar que ocasiona alteraciones morfológicas en las mitocondrias, puede provocar una explosión oxidativa y una necrosis que restringe el movimiento viral. De este modo, el transporte de la CP a los orgánulos podría evitar una replicación viral excesiva mediante la modulación de la actividad supresora para gestionar el equilibrio entre la defensa de la planta y la contradefensa viral favoreciendo una interacción compatible entre ambos.

Desafortunadamente, *Arabidopsis thaliana* no es huésped para el MNSV. Por tanto, para entender mejor el mecanismo molecular que rige el transporte de la CP a estos orgánulos, se identificaron los receptores y los poros de los translocones de las membranas externas de las mitocondrias y los cloroplastos en *Nicotiana benthamiana*, asignándose los siguientes nombres: NbToc75-III, NbToc34, NbToc90, NbToc120, NbToc159A, NbToc159B, NbTic22-III para componentes del translocón de los cloroplastos, y NbTom40, NbTom20-1, NbTom20-2,

NbOm64 para los de mitocondrias. Esta caracterización funcional se realizó principalmente mediante estudios de silenciamiento génico inducido por virus o VIGS y RT-qPCR, que mostró una redundancia funcional mayor que la observada entre los homólogos de Arabidopsis. Además, esta herramienta también se utilizó para evaluar la relevancia de cada componente bajo la infección por MNSV, y junto con los estudios de interacción CP-receptor realizados mediante BiFC y Y2H, nos permitió identificar NbToc159A para cloroplastos y NbOm64 para mitocondrias, como los principales receptores implicados en el transporte de la CP a estos orgánulos. A su vez, el silenciamiento de NbToc34, NbToc75 o NbTom40 resultó en una resistencia generalizada no solo a MNSV sino también al virus del arrugamiento del nabo (TCV) y al virus del moteado del clavel (CarMV), lo que respalda la idea actualmente aceptada y que involucra el estado fisiológico del cloroplasto y la mitocondria en la señalización temprana de la respuesta defensiva.

Finalmente, se realizó una búsqueda de factores del huésped que interaccionasen con la CP mediante la innovadora técnica de marcaje de proximidad con TurboID, una ligasa de biotina, que permite la detección de interacciones tanto directas e indirectas como transitorias y estables. Así, se obtuvo un gran número de proteínas candidatas utilizando la CP de MNSV y su mutante de localización citoplásmica, ΔNtCP. Ocho de las que presentaron un mayor grado de confianza y fueron más relevantes para defensa de las plantas frente a los virus fueron analizadas funcionalmente, de nuevo mediante VIGS. Tres de ellas, NbSIK1, NbSMU2 y NbMAP3K mostraron un efecto perjudicial constante y repetitivo sobre la acumulación del RNA viral. Después de la validación de las interacciones mediante otro método, y el análisis de la localización subcelular de la CP bajo el silenciamiento del interactor correspondiente, se establecieron dos hipótesis principales. En primer lugar, dado que la función principal de NbSMU2 está relacionada con el procesamiento y regulación del RNA mensajero, esta proteína podría ser secuestrada por la CP provocando la expresión de genes provirales. Por otro lado, NbSIK1 y NbMAP3K, actúan como reguladores positivo y negativo de la respuesta PTI a la infección, respectivamente. Además, ambas proteínas interaccionan entre sí y forman parte de la cascada de MAP quinasas, por lo que en nuestra segunda hipótesis, la CP interaccionaría con este complejo, promoviendo una regulación negativa de la PTI que facilitaría el desarrollo de la infección.

En resumen, el trabajo desarrollado en esta tesis ha permitido la identificación y el análisis mecanístico y funcional del transporte dual de la CP de MNSV a cloroplastos y mitocondrias. Los resultados obtenidos proporcionan, tanto una descripción extensa de un nuevo mecanismo viral para atenuar las defensas de las plantas, como un estudio prometedor de varios factores del huésped y su implicación en la defensa antiviral.

RESUM

Els virus de plantes són els principals causants de la major part de malalties en plantes i les conseqüents pèrdues econòmiques. El virus de les taques necròtiques del meló (MNSV) és un virus menut d'RNA monocatenari de polaritat positiva, pertanyent al gènere Gammacarmovirus, el genoma del qual codifica cinc proteïnes. La proteïna de coberta (CP, de l'anglès "*coat protein*"), està formada per tres dominis diferents. El domini R és el responsable de la unió a molècules diferents d'RNA i es pot dividir en dos subdominis: R1 i R2. Aquest domini està connectat amb el domini S mitjançant la regió "arm", que també forma part del domini d'unió a l'RNA. La funció principal del domini S és la de protecció i transmissió del genoma en formar virions. El segueix el domini P, que és el lloc d'interacció amb les zoospores del fong vector. El descobriment d'un pèptid de trànsit dual a la part aminoterminal de la CP va ser el punt de partida d'aquesta tesi. A l'inici d'una infecció per MNSV, la CP novament sintetitzada és transportada a l'interior dels cloroplasts i mitocondris mentre que, una part molt menor es manté al citoplasma augmentant a mesura que avança la infecció. La inhibició d'aquest transport dual comporta un augment de l'activitat supressora del silenciament de l'RNA de la CP. No obstant això, lluny de provocar una major infecció, la infecció sistèmica es va frenar. Per tant, l'acumulació de la CP al citoplasma pot provocar un augment de la replicació viral però alhora una sobreexpressió de la p29, una replicasa auxiliar que ocasiona alteracions morfològiques als mitocondris, una explosió oxidativa i necrosi que restringeix el moviment viral. D'aquesta manera, el transport de la CP als orgànuls podria evitar una replicació viral excessiva mitjançant la modulació de l'activitat supressora per gestionar l'equilibri entre defensa de la planta i contradefensa viral que condueixen a una interacció compatible entre tots dos. Per entendre millor el mecanisme molecular que regeix el transport de la CP a aquests orgànuls, es van identificar els receptors i els porus dels translocon de les membranes externes dels mitocondris i els cloroplasts a Nicotiana benthamiana, assignant-se els següents noms NbToc75-III, NbToc34, NbToc90, NbToc120, NbToc159A, NbToc159B, NbTic22-III per a components del translocó dels cloroplasts, i NbTom40, NbTom20-1, NbTom20-2, NbOm64 per als de mitocondris. Aquesta caracterització funcional es va realitzar principalment mitjançant estudis de silenciament gènic induït per virus (VIGS) i RT-qPCR, que va mostrar una redundància funcional més gran que l'observada entre els homòlegs d'Arabidopsis. A més, aquesta eina també es va utilitzar per avaluar la rellevància de cada

component sota la infecció per MNSV, i juntament amb els estudis d'interacció CP-receptor realitzats mitjançant BiFC i Y2H, ens va permetre identificar a NbToc159A per a cloroplasts i NbOm64 per a mitocondris, com els principals receptors implicats en el transport de la CP a aquests orgànuls. Alhora, el silenciament de NbToc34, NbToc75 o NbTom40 va resultar en una resistència generalitzada a MNSV, TCV i CarMV, la qual cosa recolza la idea que circula actualment i que involucra l'estat fisiològic del cloroplast i el mitocondri en la senyalització primerenca de la resposta defensiva. Finalment, es va fer una cerca de factors de l'hoste que interaccionessin amb la CP mitjançant la innovadora tècnica de marcatge de proximitat amb TurboID, una lligasa de biotina, que permet la detecció d'interaccions tant directes i indirectes com transitòries i estables. Així, es va obtenir un gran nombre de proteïnes candidates utilitzant la CP de MNSV i el seu mutant de localització citoplàsmica, ΔNtCP. Huit de les que van presentar un major grau de confiança i van ser més rellevants en defensa davant dels virus van ser analitzades funcionalment, novament mitjançant VIGS. Tres de elles, NbSIK1, NbSMU2 i NbMAP3K van mostrar un efecte perjudicial constant i repetitiu sobre l'acumulació de l'RNA viral. Després de la validació de les interaccions mitjançant un altre mètode, i l'examen de la localització subcel·lular de la CP sota el silenciament de cada interactor, es van establir dues hipòtesis principals. En primer lloc, atès que la funció principal de NbSMU2 està relacionada amb el processament i la regulació de l'RNA missatger, aquesta proteïna podria ser segrestada per la CP provocant l'expressió de gens provirals. D'altra banda, NbSIK1 i NbMAP3K actuen com a reguladors positiu i negatiu de la resposta PTI a la infecció, respectivament. A més, les dos proteïnes interaccionen entre si i formen part de la cascada de MAP quinases, per la qual cosa en la nostra segona hipòtesi, la CP interaccionaria amb aquest complex, promovent una regulació negativa de la PTI que facilitaria el desenvolupament de la infecció.

En resum, el treball desenvolupat en aquesta tesi ha permès la identificació i l'anàlisi mecanístic i funcional del transport dual de la CP de MNSV a cloroplasts i mitocondris. Els resultats obtinguts proporcionen, tant una extensa descripció d'una nova estratègia viral per atenuar les defenses de les plantes, com un estudi prometedor de diversos factors de l'hoste i la seva implicació en la defensa antiviral.

ABBREVIATIONS

PLANT VIRUSES		
AMV alfalfa Mosaic virus	**BaMV** bamboo Mosaic virus	**BCTV** beet curly top virus
CaMV culiflower mosaic virus	**CarmV** carnation mottle virus	**CMV** cucumber mosaic virus
CNV cucumber necrotic virus	**CymRSV** cymbidium ring spot virus	**MNSV** melon necrotic spot virus
PVX potato virus X	**PVY** potato virus Y	**PVYN^{NTN}** potato to potato virus Y^{NTN}
PepMV pepino Mosaic virus	**RCNMV** red clover necrotic mosaic virus	**TBSV** tomato bushy stunt virus
TCV turnip crinkle virus	**TEV** tobacco etch virus	**TMV** tobacco mosaic virus
ToCV tomato chlorosis virus	**TRV** tobacco rattle virus	**TSWV** tomato spotted wilt virus
TuMV turnip mosaic virus	**ToRSV** tomato ringspot virus	**TuMV** turnip mosaic virus
TYLCV tomato yellow leaf curl virus	**WSMV** wheat yellow mosaic virus	

aa Amino acids

ABA Abcisic acid

AGO Argonaute

AOX Alternative oxidase

APEX Ascorbate peroxidase

BiFC Bimolecular fluorescence complementation

BioID Bir A mutant

BRs Brassinosteroids

CHUP1 chloroplast unusual positioning1

CITEs Cap-independent translation enhancers

CKs Cytokinins

CLSM Confocal laser-scanning microscopy

coxP Cytochrome oxidase subunit IV

CP coat protein

cTP chloroplast targeting sequence

DCL Dicer-like RNases

DGB Double gene block

DNA Deoxyribonucleic acid

Dpi Days post-inoculation

DRB4 dsRNA-binding protein 4

dsRNA Double strand RNA

dTP Dual transit peptide

ER Endoplasmic reticulum

Et Etyhlene

ETI Effector-triggered immunity

Flg22 Flagellin2

FLS2 Receptor Flagellin-Sensitive 2

GFP Green fluorescent protein

GET Guied entry of tail-anchored proteins

glyrsP Glycyl-tRNA synthetase

gRNA Genomic RNA

GUN1 Genomes uncoupled 1

HA Hemagglutinin

HCPro Potyviral helper component proteinase

HEN1 HUA ENHANCER1

HR Hypersensitive response

IMS Intermembrane space

iRNA RNA silencing

ISR Induced systemic resistance

JA Jasmonic acid

LC-MS/MS liquid chromatography with tandem mass spectrometry analysis

MIM Mitochondrial import complex

MP Movement protein

MPP Mitochondrial processing peptidase

mRNA Messenger RNA

mTP Mitochondrial presequences

NES Nuclear export signal

NGE Nuclear gene expression

NRIP1 N receptor-interacting protein 1

nt nucleotide

OGE Organellar gene expression

ORF Open reading frame

PAMPs Pathogen-associated molecular patterns

PL Proximity labeling

POTRA polypeptide-transport-associated

PPI Protein-Protein interaction

PR pathogenesis-related genes

PRRs pattern recognition receptors

PTI pattern-triggered immunity

R Resistance

RDR/RdRP RNA-dependent RNA polymerases

RISC RNA-induced silencing complex

RNA Ribonucleic acid

RNAi RNA interference

ROS Reactive oxygen species

RSS RNA silencing suppression

SA Salicylic acid

SAM Sorting and assembly machinery

SAR Systemic acquired resistance

sgRNA Subgenomic RNA

siRNA Small interfering RNA

SPP Signal peptide peptidase

ssRNA Single-stranded RNA

Tic Translocon of the inner chloroplast membrane

Tim translocon of the inner mitochondrial membrane

Toc Translocon of the outer chloroplast membrane

Tom translocon of the outer mitochondrial membrane

TPR Tetratricopeptide repeats

UPL Ubiquitin proteasome system

UTR Untranslated region

VIGS Virus-induced gene silencing

VRC Viral replication complex

vRNA Viral RNA

VSR Viral suppressor of silencing

Y2H Yeast-two hybrid

General Introduction

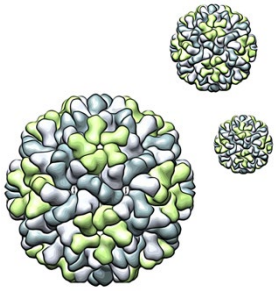

1. PLANT VIRUSES: HISTORY AND CHARACTERISTICS

A huge variety of parasites could infect plants, where viruses are the second group involved in plant pathogeny after fungi. Until 1833, when F. Unger published "Exanthemen der Pflanzen", plant diseases were thought to be caused by chemical alterations or adverse conditions. At the end of the 19th century, the development of a technique that filters microorganisms allowed to find out a connection between pathogenic bacteria and plant disease. In 1886 Adolf Mayer, studying the tobacco mosaic disease described by a student from Wageningen in 1857, discovered that "the juice from diseased plants obtained by grinding was a certain infectious substance for healthy plants". Mayer artificially transmitted for the first time a plant disease, the causal agent of which he demonstrated could not be seen or cultured and mistakenly reasoned that the disease was caused by a bacterium that lost activity upon filtration. In 1892, Dimitri Ivanovskij detected that the tobacco mosaic disease was caused by a filtered toxic substance. Then, Beijerinck characterized it as a contagious, living and soluble entity named as *contagium vivum fluidum* (van der Want and Dijkstra, 2006). In this line, the concept of virus was first referred to as a pathogen of minute dimensions unable to grow on artificial media. Almost at the same time the corpuscular nature of the virus was demonstrated studying the first animal virus (filterable) shown to be infectious causing the foot and mouth disease (FMDV). The fact that all organisms can harbor viruses was confirmed by the discovery of bacterial viruses, known as bacteriophage. These were first discovered by Frederick Twort (1877–1950) in England and by Felix d'Herelle (1873–1949), a Canadian working in France (see Pallás, 2007 for review).

The discovery of the tobacco mosaic virus (TMV) as the causal agent of the tobacco mosaic disease was the first example of a virus that infects plants and from which plant virology was born (Figure 1). TMV allowed to refine the concept of virus and better understand its components, turning it into a robust tool in plant biotechnology (Scholthof, 2004).

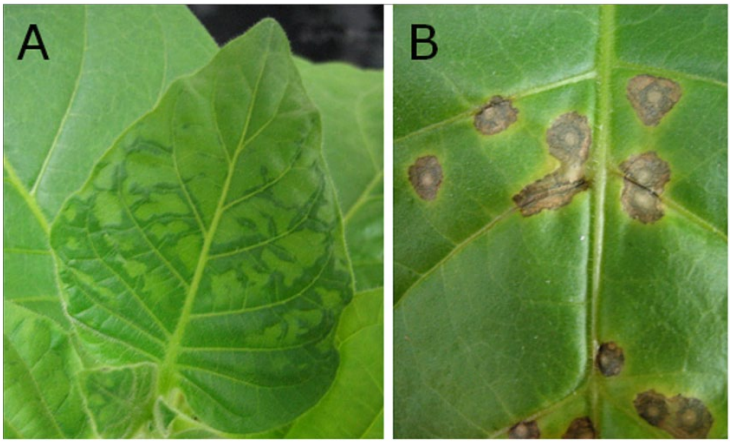

Figure 1. Systemic infection symptoms (A) and necrotic lesions (B) in tobacco mosaic disease caused by the tobacco mosaic virus (TMV). Images were taken and modified from Tobacco Mosaic Virus: The Beginning of Plant Virology, The American Phytopathological Society.

Viruses are the largest taxonomic group of emerging human, wildlife, and plant pathogens, responsible for nearly half of all reported emerging diseases (Elena *et al.*, 2014). Therefore, the study of plant viruses has become an important challenge because they are causal agents of a huge variety of plant diseases and, consequently, generate numerous economic losses. Moreover, its biological characterization is paramount for our knowledge about viral replication, genome expression, and plant defense (Ayllón *et al.*, 2016).

Most plant viruses are composed of a RNA genome enclosed within a nucleocapsid. Nevertheless, there is a wide variety of plant viruses with DNA or RNA genomes, singled or doubled stranded, monopartite or multipartite and with or without a lipid envelope surrounding the nucleocapsid. They are obligatory intracellular parasites with the ability to transmit their genomes. For that purpose, viruses have developed specific and restrictive characteristics such as small size, structural simplicity, and lack of metabolic activity (Marsh and Helenius, 2006). Indeed, plant viruses are cell-depending, and their main challenge will be overcoming plant physical and chemical barriers to achieve a viral infection (Navarro *et al.*, 2019). Then, pathogenesis, which is the process by which pathogen infection leads to disease, starts with developmental abnormalities, phenotypic manifestations, and physiological alterations (García and Pallás, 2015; Pallas and García, 2011).

1.1. A GENERAL VISION OF ALPHA-, BETA-, AND GAMMACARMOVIRUSES

Until 2015, carmoviruses were known as a unique genus that was later split into three different ones depending on the phylogenetic analysis of their RNA-dependent RNA polymerase (RdRP) (Navarro and Pallás, 2017; Pérez-Cañamás and Hernández, 2021). These genera were named *Alfacarmovirus, Betacarmovirus,* and *Gammacarmovirus,* with carnation mottle virus (CarMV), turnip crinkle virus (TCV), and melon necrotic spot virus (MNSV) as the respective type members. They all belong to the family *Tombusviridae* formed by small RNA viruses (around 30 nm in diameter) with rounded contour polyhedral particles. Other genera within this family are *Alphanecrovirus*, *Aureusvirus*, *Avenavirus*, *Betanecrovirus*, *Dianthovirus*, *Gallantivirus*, *Macanavirus*, *Machlomovirus*, *Panicovirus*, *Tombusvirus*, *Umbravirus,* and *Zeavirus*.

Members of the genera *Alphacarmovirus*, *Betacarmovirus,* and *Gammacarmovirus* are highly similar to those of the genus *Tombusvirus* in virion structure and morphology, genome organization, physicochemical properties, and epidemiological and ecological behavior, differing mainly in the genome size, which is smaller in all alpha-, beta-, and gammacarmoviruses, and ranges from 4 kb to 4.7 kb (Russo *et al.*, 1994).

1.1.1. Genomic organization, gene expression, and replication of alpha-, beta-, and gammacarmoviruses

Alpha-, beta-, and gammacarmoviruses are single-stranded RNA viruses of positive polarity with a compact genome that codes up to five overlapped open reading frames (ORF) (Russo et al., 1994; Pérez-Cañamás and Hernández, 2021). In both extremes of their genomic RNA (gRNA), there are two untranslated regions (UTR). At this point, it is important to notice the absence of CAP structures and poliA tails at the 5' at the 3' ends, respectively, which are unnecessary for infection development (Figure 2). Thus, these viruses must hijack the translational machinery of a host by employing non-canonical translation initiation mechanisms to produce viral proteins (Miras *et al.*, 2017; Truniger *et al.*, 2017).

Their first ORF (ORF1) has a weak stop codon and codifies for an auxiliary replicase ranging in size from 25-29 kb. Next, the weak stop codon read-through results in a second ORF that

codifies for the RNA-dependent RNA polymerase (ORF2), which contains the signature RdRp motifs and differs from genera *Alpha-*, *Beta-*, and *Gammacarmovirus*. The role of the auxiliary replicase in alpha-, betha-, and gammacarmovirus replication has not been studied, but in the related tombusviruses, this protein is central to the formation of the viral replicase complex (VRC) as it functions in RNA template selection and recruitment (Nagy, 2020). In addition, it promotes selfinteractions and interactions with the RdRp and numerous host proteins involved in the assembly, fidelity, and regulation of the replicase complex. The third and fourth ORF (ORF3 and ORF4) encode two small movement proteins (MP) that form the so-called double gene block of proteins (DGB) and are synthesized from the sgRNA 1 (Hull, 2002; Genovés *et al.*, 2006; Genovés *et al.*, 2009; Genovés *et al.*, 2010). Finally, the coat protein (CP) is encoded in the fifth ORF (ORF5) and expressed from the sgRNA 2. Beyond its structural role in viral genome binding and virion assembly, several functions have been assigned to the CP. Among them, the most shared refers to the ability of these proteins to act as suppressors of post-transcriptional gene silencing. In fact, TCV p38 is the first example of a viral structural protein with suppressor activity (Qu *et al.*, 2003).

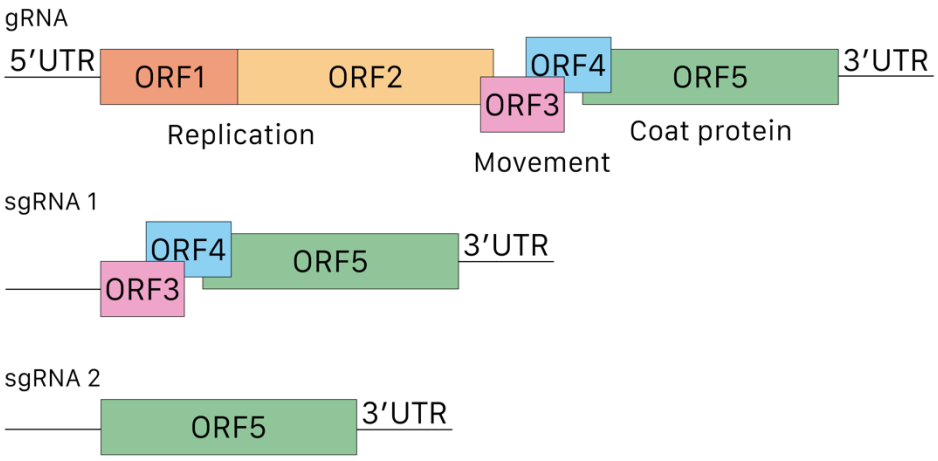

Figure 2. Genomic organization of alfa-, beta-, and gammacarmoviruses. The ORF are represented by boxes in the genomic RNA (gRNA) and subgenomic RNA (sgRNA 1 and sgRNA 2) whereas the UTR extremes are represented by solid lines. The functions of each genome region are also indicated.

Due to their positive polarity, these virus genomes could directly act as messenger RNA (mRNA) for their gene expression and replication. Strategically, the binding of the host cell ribosomes directly to the 5' end of the viral genome will rapidly translate the 5' proximal viral replicases, which are necessary to initiate the infection before mechanisms of plant defense are activated. Thus, to bring the ribosomes closer to the 5' end of the viral RNA and start viral

translation, these viruses rely on non-canonical initiation mechanisms. To this end, viral RNAs present elements with secondary and tertiary structure at their 3' UTR end called 3’ CITEs (3' cap-independent translation enhancers), which can extend up to the CP ORF. The 3' CITEs are binding sites for translation initiation factors of the eIF4E or eIF4G family that induce the binding of ribosomes or ribosomal subunits to the 5' end. For this, although with exceptions such as TCV, a long-distance interaction occurs with small secondary structures located in 5’-UTR (Simon and Miller, 2013; Simon, 2015; Blanco-Pérez *et al.*, 2016; Truniger *et al.*, 2017; Miras *et al.*, 2017). Next, the RdRp will produce complementary viral strands of the genomic RNA (gRNA), which will be used again as templates for the synthesis of positive strands of the viral gRNA. Instead, the gene expression of the MPs and CP, encoded centrally and 3’ proximally in viral gRNA, requires the production of the subgenomic RNA 1 and 2 (sgRNA 1 and 2), respectively, which act as mRNAs for being translated. This is a strategy for bringing their 5’ ends closer to the start codon of the downstream ORFs. They have the same 3’ UTR that gRNA, but both lack the 5’ proximal (sgRNA 1) and central (sgRNA 2) genes (Figure 2). The premature termination of the RdRp while copying the viral genome, due to the presence of either local secondary or long-distance higher-order structures, results in the synthesis of sgRNA complementary strands that are then used to transcribe the sgRNAs (Russo *et al.*, 1994). Otherwise, this strategy is thought to be mainly done to supplement with a high number of CP copies because of its multifunctionality, as stated below (Miller and Koev, 2000).

2. A BRIEF DESCRIPTION OF PROTEIN MULTIFUNCTIONALITY

In the last 80 years, the multifunctionality of proteins, a recurrent phenomenon in which proteins play two or more functional roles, has been broadly described. Indeed, it has been shown that between 20-26% of the characterized genes in yeast, flies, and humans code for multifunctional proteins, which are frequently related to virulence and diseases (Espinosa-Cantú *et al.*, 2020). Different non-mutually exclusive terms have been used in the literature to name multifunctional proteins. Although there is no consensus on their usage, they could be known as:

- Pleiotropic proteins. This qualifying is commonly used in genetic analysis when a null protein mutant affects different processes resulting in several quantifiable phenotypic effects.
- Multidomain proteins. This term applies to proteins with two or more globular domains, each performing one enzymatic but different function. Not all multidomain proteins are considered multifunctional if, for example, one part binds the cofactor, and the other couples with the substrate, but catalyzing a single reaction.
- Promiscuous proteins. This term is used for enzymes that bind multiple substrates, ligands, or other activity-unrelated macromolecules.
- Finally, moonlighting proteins have two or more different and independent functions that do not result from gene expression. Multitasking is an inherent property of most viral proteins, making them a promising target for animal therapeutic treatments and developing plant resistances, so that we will take particular notice of this phenomenon below.

The first moonlighting protein to be characterized was the delta-crystallin of the lens from birds and reptiles, which in other tissues played a catalytic role instead of a structural role as an argininosuccinate lyase enzyme (Piatigorsky *et al.*, 1988). Then, almost 700 moonlighting proteins were characterized, many of them related to human diseases such as cancer, immunity disorders, and the nervous system (Espinosa-Cantú *et al.*, 2020).

Moonlighting protein strategy is also used by small DNA and RNA viruses from animals and plants. For instance, the viral matrix protein VP40 from ebolaviruses performs three distinct activities during the infection cycle, each associated with a unique subunit organization. Inside the host cells, an octameric ring structure interacts with the viral RNA to control transcription, and a butterfly-shaped dimer moves toward the plasma membrane of the host cell. Once there, they undergo a rearrangement into linear hexamers creating a bigger filamentous matrix structure required for budding (Liu and Jeffery, 2020). Another example of moonlighting proteins is the major component of plant viruses, the coat protein (Weber and Bujarski, 2015). They are structural proteins that attend the viral genome in and out of host cells. Nevertheless, they not only exert protective and enveloping functions but also

participate in most stages of the viral cycle. For example, in addition to its structural role in viral particle assembly and genome encapsidation, the CP of MNSV can act as an RNA silencing suppressor due to its ability to bind sRNAs (Serra-Soriano *et al.,* 2017) and is responsible for the attachment to the zoospores of the fungus vector during horizontal transmission (Mochizuki *et al.*, 2008; Ohki *et al.*, 2010). Therefore, the CPs are considered a prototype of multifunctional proteins, whose main functions, besides their obvious structural role, are briefly reviewed below.

- Translation: in the non-polyadenylated alfalfa mosaic virus (AMV, genus *Alfamovirus*, family *Bromoviridae*) and ilarviruses, the CP may act as a poly(A)-binding protein through the interaction with the 3'-UTR of the viral genome and host factors such as eIF4G and eIFiso4G (Krab *et al.*, 2005). This binding is proposed to avoid the minus-strand promoter activity and enhances translation through a conformational switch between two RNA structures that converts the virus from a replicative to a translational mode (Bol, 1999; Pallas *et al.*, 2013).
- Replication: Principally in viruses with a single-stranded RNA (ssRNA) or double-stranded RNA (dsRNA) genome. For example, the association of the CP or N (nucleocapsid) protein of the tomato spotted wilt virus (TSWV) with its genome and RdRP is necessary for its replication and gene transcription (Kormelink, 2011). As mentioned above, the CP of AMV and ilarviruses also regulates the viral RNA (vRNA) synthesis and its localization during infection (Aparicio *et al.*, 2003; Reichert *et al.*, 2007).
- Movement: Cell-to-cell movement is CP-dependent in many viral genera, either because assembled viral particles or virions are required, or they form ternary complexes with MPs and the viral genome (Scholthof, 2005; Waigmann *et al.*, 2010). For instance, the binding of the potato virus X (PVX) CP to the 5' end of the vRNA and its MP is required for cell-to-cell movement (Lough *et al.*, 2007). Systemic movement is also dependent on CP in many genera, being carried out by virions or RNA-protein complexes (VNP) (Di Carli *et al.*, 2010; Waigmann *et al.*, 2010; Brizard *et al.*, 2006).
- Vector transmission: Viral transmission is generally by seeds, vegetative propagation, mechanical means, and vectors. For the latter, the formation of the virion and,

therefore, the CP is necessary. This is the case of MNSV, the tomato bushy stunt virus (TBSV), and cucumber necrosis virus (CNV). All of them are transmitted by the fungus *Olpidium bornovanus* through the interaction of the protruding domain of the CP and the glycoproteins of the zoospore membrane (Kakani *et al.*, 2001; Bol, 2008).

- Symptomatology: For the development of a viral infection, the interaction between the host and the pathogen is required (Pallas and García, 2011). Numerous studies show how mutations in viral CP can alter both the range of hosts and the appearance of symptoms. This is the case of TCV, tobamoviruses, luteoviruses and cucumoviruses (Lin and Heaton, 1999; Dawson, 1992; Zhang *et al.*, 1994; Sugiyama *et al.*, 2000). In addition, on many occasions, viral CP could act as an elicitor of the hypersensitive response (HR), as in cucumber mosaic virus (CMV), TCV, TMV, and PVX (Moffett, 2009).
- Plant defense: The main defense mechanisms in plants are mediated by resistance genes (R genes) and RNA silencing (iRNA), whose development could be influenced by the viral CP. For instance, CMV CP is related to the defense mediated by the resistance gene RCY (Soosaar *et al.*, 2005). On the other hand, the CPs of many viruses have been identified as silencing suppressors, such as TCV, PFBV and MNSV (Martínez-Turiño and Hernández, 2009; Serra-Soriano *et al.*, 2017; Thomas *et al.*, 2003).

2.1. THE COAT PROTEIN OF MELON NECROTIC SPOT VIRUS

The MNSV CP, as well as those of TCV and CarMV, is formed by three different domains (Figure 3). The amino-terminal domain, named as the R (random) domain, is an unstructured region responsible for binding to different RNA molecules, including the RNA genomes and small interfering RNAs (siRNA), which is essential for the CP role as viral suppressor of silencing (VSR) (Serra-Soriano *et al.*, 2017). The R domain is enriched in arginines, lysines, prolines, and glutamines and can be split into two subdomains (R_1 and R_2). It is connected to the S (shell) domain by an arm region that, together with the R_2 subdomain, is part of the RNA binding domain (BD). As we will see in chapter I, the R_1 subdomain is an essential region of the dual transit peptide that targets the CP to chloroplasts and mitochondria. The S domain is formed by eight antiparallel β-sheets with two helicoidal regions. The interaction among the S domain from different subunits forms a T=3 icosahedral shell. It is also connected with the P

(protruding) domain responsible for interacting with the zoospores of the fungus vector *Olpidium bornovanus* (Mochizuki *et al.*, 2008; Ohki *et al.*, 2010).

Nevertheless, regarding its primary sequence, length of R and P domains, and three-dimensional structure, the CP of MNSV is more similar to that of tombusviruses than to the gammacarmovirus CPs (Riviere *et al.*, 1989; Wada *et al.*, 2008). Indeed, it has been suggested that the CP gene could be acquired by recombination along a co-infection of MNSV and some tombusvirus since, compared to other viruses, whitin the family *Tombusviridae*, recombination appears to be a rather prevalent event between tombusviruses and carmoviruses (Boulila, 2011).

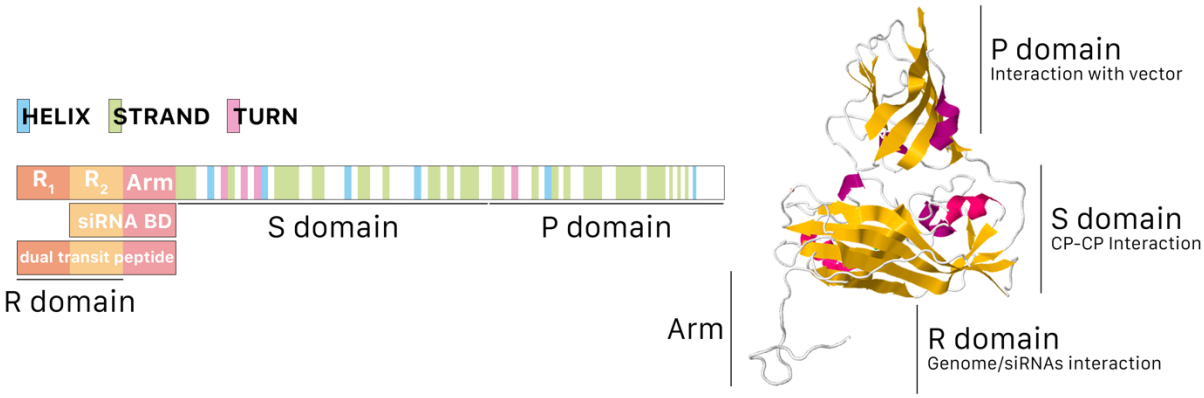

Figure 3. Schematic representation of structural domains (R, S, and P) that compose the melon necrotic spot virus (MNSV) coat protein (CP). The R_1 subdomain is shown as an orange box, the R_2 as a yellow box, and the arm region as a pink box. The CP linear representation shows the color-coded secondary structural elements for helix, strand, or turn. Also, a ribbon illustration of the MNSV CP subunit with β-sheets and α-helices is shown on the right. The R-domain (Met1–Asn60), which was disordered, is not shown in the drawing, but its position is indicated.

2.2. INTERACTION WITH HOST FACTORS

As obligated biotrophic pathogens, plant viruses must overcome plant defense barriers to multiplicate their genomes. All viruses share a small or multipartite compacted genome to lessen the effects of the lack of exonuclease proofreading activity of their RNA polymerases, and avoid high mutation rates and lethality. For a viral infection triggering, different phases such as viral particle disassembly, translation of viral genome, membrane modifications for the formation of viral replication complex (VRC), viral genome encapsidation, cell-to-cell movement, and long-distance transport must be completed by a minimal number of viral proteins (Wang, 2015).

Due to this simplicity and to achieve their multiplication and evolution, viruses need to hijack many cellular processes interacting with different host factors. They could be classified as proviral when host factors are required by viruses for infectious cycle development or, antiviral factors where viral proteins or nucleic acid are targeted by host factors to be eliminated by different mechanisms. Moreover, viruses use different mechanisms to overcome plant defense barriers, such as RNA silencing (Garcia-Ruiz, 2019).

Host factors implication in the virus cycle could occur through a direct interaction with a viral protein, being present in viral-host complexes, binding to non-protein components of viruses or being involved in signaling pathways and other cellular processes in relation to viral infection or plant immunity (Hsu and Spindler, 2012). Thus, the identification and characterization of host factors that interact with viruses is essential to understand not only how a viral infection is developed but also to establish targets for plant biotechnology. Table 1 represents a brief list of antiviral and proviral host factors in *Arabidopsis thaliana* (Garcia-Ruiz, 2019).

Table 1. Examples of host factors with antiviral and proviral activity. Adapted from Garcia-Ruiz, 2019; Hyodo and Okuno, 2016.

Activity	Host factor	Cell function	Viral mechanism and factor	Virus	Reference
Antiviral	APUM5	mRNA binding	Viral RNA translation, mRNA	CMV, turnip mosaic virus (TuMV)	Huh et al. (2013)
	RTM1, RTM2, RTM3	Protein binding	Virus movement, CP	Tobacco etch virus (TEV)	Chisholm et al., (2001); Decroocq et al., (2009)
	NBR1	Autophagy cargo receptor	Accumulation or activity of viral proteins, HC-Pro	TuMV	Hafrén et al., (2018)
	NBR1	Autophagy cargo receptor	Virions formation, CP	Cauliflower mosaic virus (CaMV)	Hafrén et al., (2017)
	RPP8	Protein binding	Cell death, CP	TCV	Cooley et al., (2000)

Proviral	eIF4E/eIFiso4E	5' CAP recognition	Viral protein translation, VPg	Potyviruses	Jiang and Laliberté, (2011)
	Arf1, Sar1	COPI/COPII vesicles biogenesis	VRC formation, replication protein	Red clover necrotic mosaic virus (RCNMV)	(Hyodo *et al.*, 2014)
	Sec39p	Vesicle transport	VRC formation, replication protein	TBSV	Sasvari et al., (2013)
	PLD	Phosphatidic acid production	RNA replication, auxiliary replicase	RCNMV	Hyodo et al., 2015)

2.2.1. Methods for studying protein-protein interaction (PPI)

Proteins operate in every developed process or complex inside cells as catalysts, transporters, inducers of the immune defense against pathogens, or activating signal transduction between cells. In most cases, the function of proteins takes place through their interactions (protein-protein interactions, PPI) rather than individually; therefore, the study of PPI and the identification of the proteins involved in these interactions is essential for understanding biological functions (Rao *et al.*, 2014; Lu *et al.*, 2020), mainly when the deregulation of the protein interaction network is responsible for diseases and disorders.

For that reason, a huge variety of methods for studying protein-protein interactions have been developed. They are classified as "*in vitro*" when the interaction study is made outside a living organism or in a controlled environment, *"in vivo"* when protein-protein interactions are analyzed inside an organism, or "*in silico*" when the techniques are performed by a computer or a simulation (Rao *et al.*, 2014). Table 2 summarizes the PPI methods developed for *in vivo, in vitro,* or *in silico* studies.

Table 2. Brief description of some protein-protein interaction (PPI) methods. Adapted from Rao et al., 2014.

Classification	Method	Description
In vitro	Tandem affinity purification mass spectroscopy (TAP-MS)	The foundation of TAP-MS is the double tagging of the target protein on its chromosomal locus, which is followed by a two-step purification procedure and mass spectroscopic analysis.

	Affinity chromatography	Important for detecting the weakest interactions in proteins.
	Coimmunoprecipitation	Coimmunoprecipitation establishes protein connections using a whole-cell extract that contains proteins in their native state among a diverse medley of cellular constituents.
	Protein microarrays	In a single experiment, it simultaneously analyzes thousands of parameters.
	Protein-fragment complementation	It could be used for any protein regardless of its expression level and molecular weight.
	Phage display	The protein of interest is incorporated into a single phage particle, followed by computational identification of potential interacting partners and a yeast two-hybrid validation step.
	X-ray crystallography	Allow the visualization of the protein structure changes when interacting with other molecules at the atomic level.
	NMR spectroscopy	Detect weak protein-protein interaction.
In vivo	Yeast 2 hybrid (Y2H)	Typically, Y2H starts with a protein screening against an interactor candidate's library.
	Proximity labelling	By engineered enzymes, an endogenous interaction is tagged in living cells (Qin *et al.*, 2021).
	Bimolecular fluorescence complementation	It is based on the interaction between two proteins fused to non-fluorescent portions of a fluorescent protein that results in the production of a fluorescent complex (Kerppola, 2008)
	Synthetic lethality	Useful for functional interactions. This approach results in mutations or deletions in two or more genes that are viable when isolated but fatal when combined under specific circumstances.
In silico	Ortholog-based sequence approach	Based on the pairwise local sequence methods and the homology of the query protein annotation in databases.
	Domain-pairs-based sequence approach	It predicts protein interactions based on connections between domains.
	Structure-based approaches	For proteins with similar structures (primary, secondary, or tertiary).

	Gene neighborhood	Based on functional linkage conservation among proteins.
	Gene fusion	Based on the idea that some proteins with single domains of one organism can produce multidomain proteins in other organisms.
	In silico 2 hybrid (I2H)	Based on the premise that the coevolution of interacting proteins is necessary to maintain its protein function.
	Phylogenetic tree	It predicts the protein-protein interaction based on the protein's evolutionary history.
	Phylogenetic profile	Determines if two proteins will interact when their evolutionary profiles are similar.
	Gene expression	Based on the hypothesis that proteins are more likely to interact if they belong to genes to the common expression-profiling clusters than proteins from genes belonging to separate clusters.

Due to its use in the work described in chapter IV, a special mention must be made to the recently developed proximity labeling (PL) technique. PL was created to overcome the traditional method limitations, such as the lack of detection of weak and transient interactions. It is based on the use of catalytic enzymes such as peroxidases or biotin ligases fused to the protein of interest. As a result, a short-lived reactive molecule will be encoded, and with the corresponding substrate complementation, all closest proteins in the living cell will be tagged. These interactor candidates will be identified by a liquid chromatography with tandem mass spectrometry analysis (LC-MS/MS) (Figure 4) (Qin *et al.*, 2021; Yang *et al.*, 2021).

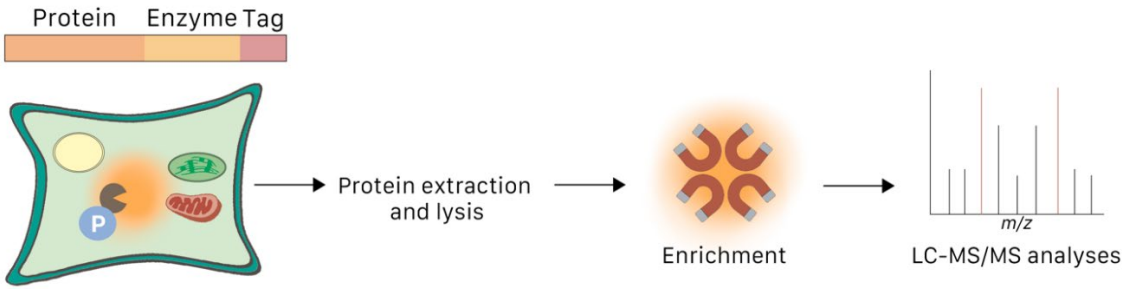

Figure 4. Overview of the proximity labeling (PL) approach. An enzyme with catalytic activity is fused to the protein of interest and a tag. After protein expression, protein extraction and lysis are carried out. This pull of proteins is enriched for positive interactors, which will be analyzed by an LC-MS/MS approach.

In this way, indirect, weak, transient, and hydrophobic PPI are also largely detected. Interestingly, it can also be used for protein-DNA or protein-RNA interactions. Additionally, PL has been employed for studying a wide range of biological processes, such as signal transduction networks, in a huge variety of cell types and different organisms like bacteria, yeast, or plants. Regarding PL limitations, catalytic enzyme, and tag fusion is a requirement that could alter the function, localization, or interactome of the protein of interest. Albeit, each PL enzyme used has different and specific characteristics to consider (Qin *et al.*, 2021).

Different catalytic enzymes are used in PL, the two most common are the Bifunctional ligase/repressor (BirA) mutant (known as BioID) and the ascorbate peroxidase (APEX). BioID comes from the biotin ligase mutant (R118G) of *Escherichia coli*, whose mutation promotes a promiscuous biotinylation (Roux *et al.,* 2012). Thus, BioID displays a major affinity for bioAMP and catalyzes the protein biotinylation with an optimal time of 18-24 hours. Upon the addition of biotin and ATP, BioID catalyzes biotin to form reactive biotinol-5'-AMP, which can promiscuously biotinylate the lysine residues of proteins that are in close proximity to the BioID enzyme (within a radius of 10 nm). With APEX, all neighboring proteins will be biotinylated in just 1 minute. However, it needs the use of H_2O_2, which is toxic to living cells. In order to overcome these limitations, a new PL enzyme was developed. TurboID combines combining the benefits of BioID and APEX. TurboID uses promiscuous biotin ligases (PBL) derived from the directed evolution of BirA in yeast, and has a shorter incubation time (3-6 hours) (Yang *et al.*, 2021).

2.3. PLANT RESPONSE TO PATHOGENS: A BRIEF DESCRIPTION OF PLANT IMMUNITY

As mentioned above, due to their simplicity, plant viruses rely entirely on host machinery and biological processes. Plant viruses enter the host cells by insect vectors or through opportunistic mechanical wounds, as opposed to animal viruses, which enter host cells via host surface receptors and endocytic activity (Navarro *et al.*, 2019). So, plants have improved their defense mechanisms to counteract viruses. These mechanisms are gene silencing, signaling by an immune receptor, defense mediated by hormones, degradation of proteins, and epigenetic regulation, being the first two mentioned the most studied (Calil and Fontes, 2017).

2.3.1. Effector-triggered immunity: resistance proteins (R) against viruses

The plant immune system has two levels of detection. The first one is pattern-triggered immunity (PTI) mediated by pattern recognition receptors (PRRs), which are localized in surfaces and identify the pathogen-associated molecular patterns (PAMPs) (Böhm *et al.*, 2014). The second level is the effector-triggered immunity (ETI), where virulence effectors secreted by pathogens inside the host are recognized, indirectly or directly, by immune receptors such as resistance proteins (R) (Jones and Dangl, 2006). The first R-gene identified, which confers resistance to the TMV, was the tobacco *N* gene (Whitham *et al.*, 1994). From this point, many R genes implicated in the defense against viral pathogens have been identified, many of them are part of (CC)-NB-LRR or Toll/interleukin-1 receptor (TIR)-NBS-LRR class (see Sett et al., 2022 for review).

Reactive oxygen species (ROS) production, calcium ion influx, MAPK activation, salicylic acid (SA) accumulation, and transcriptional reprogramming, including the induction of genes involved in defense responses, are typically associated with the immune responses downstream of R protein activation in plant-pathogen interactions. It also causes the production of a hypersensitive response (HR), which is frequently linked to programmed cell death of the infected and nearby cells, restricting the pathogen to the local site of infection (Calil and Fontes, 2017).

2.3.2. RNA silencing pathway and viral coevolution

RNA silencing or RNA interference (RNAi) is the major antiviral mechanism that plants use in plant-virus interactions. Basically, it is based on the action of RNA-dependent RNA polymerases (RDR) and the RNA-induced silencing complex (RISC), whose core consists of Argonauta (AGO) proteins, Dicer-like RNases (DCL), and double-stranded RNA binding proteins. When the viral cycle progresses, viral double-stranded RNA (dsRNA) or partially double-stranded hairpin RNA present in a host environment triggers RNAi. Thus, DCL4, in association with dsRNA-binding protein 4 (DRB4), cleaves the viral-dsRNA into small-interfering RNAs (siRNA) of 21 nucleotides, which will be loaded into AGO1, the major antiviral slicer, forming a RISC-loading complex. Before this, the siRNAs must be stabilized by 2u-O-

methylation by HUA ENHANCER1 (HEN1). This complex will be guided to RNA molecules with homologous sequences, which will be degraded in more molecules of siRNA (Pumplin and Voinnet, 2013). If DCL4 is repressed, DCL2 can substitute it, producing 22 nt vsiRNAs, while other members of the AGO family, like AGO7 may also be involved. The viral-derived siRNAs can also amplify the silencing through the RNA-dependent RNA polymerase 6 (RDR6) action. The viral RNA molecules cleaved by RISC and viral RNAs lacking 5'-or/and 3'- end might be recognized as aberrant RNAs, converted to dsRNA by RDR6, and processed again to siRNAs.

To counteract this mechanism, many viruses have coevolved by developing VSRs, which could act in different phases of RNAi, showing different modes of action. For instance, siRNA sequestration is typified by the tombusvirus p19 protein, the most studied viral silencing suppressor. Another well-known VSR is the potyviral helper component proteinase (HCPro), which also works at the viral-siRNA biogenesis level by ds siRNA binding and preventing the assembly of the RISC complex (Zhang *et al.*, 2015). Also, the p22 suppressor of tomato chlorosis virus (ToCV) prevents the cleavage of the dsRNAs by DCL (Landeo-Ríos *et al.*, 2016). In addition to binding small RNAs, the CMV 2b protein interacts with AGO1 and inhibits AGO1-mediated gene silencing, as has also been described for the CP of TCV (Csorba *et al.*, 2009).

Significant progress has been made recently in understanding the function of RNA silencing in plant antiviral responses. Indeed, the RNA-silencing pathway is commonly used through the virus-induced gene silencing (VIGS) approach for plant biotechnological research. Majorly, VIGS is preferably used to knock down a specific gene since it is easier and less time-consuming than genetic mutant production.

2.3.3. Defense mediated by plant hormones

Plant hormone production is essential for developmental processes and responses to environment, biotic, or abiotic stresses. Salicylic acid (SA), jasmonic acid (JA), and ethylene (ET) are mainly produced in response to biotic stress, albeit auxins (Auxs), brassinosteroids (BRs), cytokinins (CKs) and abscisic acid (ABA) have also been shown recently to participate in plant-pathogen interactions (Alazem and Lin, 2015). Some hormonal roles in plant defense against viruses are reviewed below:

- Salicylic acid (SA). It was first reported in relation to plant defense through viruses in the interaction between the gene *N* of tobacco and the TMV, albeit the SA response is also activated by tomato ringspot virus (ToRSV) and potato virus Y (PVY). SA action is essential for the initiation of systemic acquired resistance (SAR) through the recognition of *R* gene effectors and pathogenesis-related (PR) proteins PR-1 and PR-2 activation (Alazem and Lin, 2015). In this sense, many studies have shown that under SA signaling disruption or in defective SA accumulation mutants like Arabidopsis NahG plants, viruses widely expand, leading to infection and symptoms development (Baebler *et al.*, 2014).
- Jasmonic acid (JA). It is an oxylipin that, together with ET, controls another important type of systemic defense response: the induced systemic resistance (ISR) against necrotrophic pathogens (Thaler *et al.*, 2004). However, its signaling through virus defense is controversial mainly due to its antagonistic role with SA. For instance, the JA pathway is usually repressed under geminivirus infection, and it has been reported that the beet curly top geminivirus (BCTV) infection is disrupted under exogenous jasmonate treatment. Therefore, suppression of JA response is pivotal for completing the geminivirus infection cycle (Ascencio-Ibáñez *et al.*, 2008; Lozano-Durán *et al.*, 2011). Recently, Yang et al. report a regulatory network between jasmonate signaling and the RNA silencing pathway in rice antiviral immunity (Yang *et al.*, 2020). Rice stripe virus CP prompts jasmonate-AGO18 crosstalk, enhancing antiviral defenses. It should be pointed out that AGO18 is a member of the Argonaute protein clade specific only to monocotyledonous plants and functions to regulate the expression of a core component of the RNAi machinery. Thus, further studies are necessary to determine whether JA signaling also regulates the function of antiviral RNAi in dicotyledonous plants that do not encode a member in the AGO18 clade.
- Abscisic acid (ABA). It is a crucial element for developmental and abiotic stress in plants because it involves elemental processes such as seed germination or fruit ripening (Atkinson and Urwin, 2012; Rajjou *et al.*, 2012; Lee and Luan, 2012). However, the induction/repression of ABA synthesis by virus infection may fluctuate. An increase in ABA content after the viral infection has been reported, for example, in TMV-resistant tomato plants harboring the Tm-1 gene compared to susceptible plants. The bamboo

mosaic virus (BaMV) or cucumber mosaic virus (CMV) infection of *N. benthamiana* also increases the ABA content. Instead, TMV-infected tobacco showed a decrease in ABA levels at early infection stages. ABA was not induced during the early response to infection with potato to potato virus Y^{NTN} (PVY^{NTN}). In any case, the antiviral role of ABA has been demonstrated by increased virus resistance after ABA treatments. At the same time, inhibition of ABA biosynthesis or using ABA-deficient mutants accelerated systemic viral infections (Zhao and Li, 2021). ABA effect is antagonistic to SA and JA. It is essential in the early phases of the infection due to its role in stomatal closure and regulating the plasmodesmata conductivity by primed callose deposition (Alazem and Lin, 2015).

2.3.4. Epigenetic regulation in plant defense: m6A RNA methylation

The most prevalent internal change in cellular mRNA transcripts is the m6A modification. Approximately 25% of all cellular mRNA transcripts have undergone m6A modification, mostly in and around the 3' untranslated region (3'UTR) and the translation stop codon (Dominissini *et al.*, 2012; Meyer *et al.*, 2012). m6A RNA methylation was identified in the 1970s in a variety of viral systems, including the influenza virus, HSV1, and simian virus 40. Most intracellular stages of the viral life cycle have already shown to be affected by m6A modifications. Its effect was pro or antiviral, depending on the virus. To date, members of the families *Flaviviridae, Orthomyxoviridae, Paramyxoviridae, Retroviridae, Togaviridae, Picornaviridae, Polyomaviridae, Hepadnaviridae, Adenoviridae, Rhabdoviridae, Herpesviridae and Coronaviridae* have been reported to contain m6A modifications (Baquero-Perez *et al.*, 2021).

Studies on the m6A RNA modification in plants was also found in *A. thaliana,* and its conservation in plants and organelles points out m6A potential regulatory function in plant gene expression (Luo *et al.*, 2014; Wang *et al.*, 2017). Studies on the interaction of Alfalfa mosaic virus with host factors led to the identification of the first plant RNA demethylase, AtALKBH9B, which interacted with the coat protein (CP) modulating viral infection and the m6A levels in its genomic RNAs (Martínez-Pérez *et al.*, 2017; Alvarado-Marchena *et al.*, 2021) and playing a critical role for viral vascular movement in Arabidopsis (Martínez-Pérez *et al.*, 2021). Interestingly, under viral infection in plants, m6A levels have been found to change. In

particular, TMV infection caused *N. tabacum* m6A levels to drop (Li *et al.*, 2018) meanwhile, Zhang et al. found a significant variation in the m6A modification partterns between the resistant and susceptible varieties to wheat yellow mosaic virus (WSMV). More recently, it has been shown that m6A overexpression of a writer from *Solanum lycopersicum*, SlHAKAI, could negatively regulate pepino mosaic virus (PepMV) infection, inhibit viral RNA and protein accumulations by m6A affecting viral levels in tomato plants and vice versa (He *et al.*, 2023). All these results prove that plant would use m6A as a defense mechanism against plant viral infection (Yue et al., 2022).

3. THE ROLE OF PLANT ORGANELLES IN VIRAL INFECTION

Plant organelles are not only required for the functioning of the cell but also for the successful development of viral infections (Freed, 2004; Weiss, 2002). As pointed out in the section 2.2, plant viruses, as simple intracellular parasites, depend completely on host factors and cell routes. Although viruses use distinct mechanisms for their mobility and replication that vary across families, they need to target a variety of different subcellular compartments throughout their infectious cycle (Medina-Puche and Lozano-Duran, 2019). It is possible that the plant nucleus will be the most evident organelle that viruses alter. For instance, DNA viruses, such as geminiviruses and nanoviruses, modify the cell cycle to make the plant DNA replication machinery available for the replication of the viral genome (Hanley-Bowdoin *et al.*, 2013; Lozano-Durán, 2016). Moreover, DNA and RNA viruses primarily employ the nucleus to block RNA silencing by targeting VSRs (Csorba *et al.*, 2015).

In addition to employing endogenous organelle functions or reducing plant defensive outputs, viruses have the ability to reorganize cellular compartments to promote viral functions. Usually, positive polarity RNA viruses induce membrane remodeling to support the replication complex formation (Medina-Puche and Lozano-Duran, 2019). Some viral effects on plant organelles are summarized below (Glingston *et al.*, 2019) (Figure 5).

- Effect on endoplasmic reticulum (ER). Movement proteins (TGB2 and TGB3) of PVX cause ER reorganization and vesicular appearance (Ju *et al.*, 2005). Also, ER is modified by TMV for autophagosome production (Talbot and Kershaw, 2009).

- Effect on peroxisome. Cymbidium ring spot virus (CymRSV), TBSV, and CNV form small vesicles in peroxisomes of plant hosts (McCartney *et al.*, 2005; Panavas *et al.*, 2005; Russo *et al.*, 1983).
- Effect on Golgi apparatus. TuMV infection induces the amalgamation of ER, chloroplasts, and Golgi apparatus (Grangeon *et al.*, 2012).
- Vacuole alterations. The replicase-associated protein 1a and RdRP 2a of CMV form a replication complex in vacuole membranes (Huh *et al.*, 2011).
- Host ubiquitin proteasome system (UPL). PVX targets components of RNA silencing machinery such as AGO through proteasomal degradation (Chiu *et al.*, 2010).
- Effect on mitochondria. MNSV replication and its auxiliary replicase (p29) targeting to mitochondria membrane entail mitochondrial alterations (Gómez-Aix *et al.*, 2015).
- Effect on chloroplasts. Chloroplasts, but also mitochondria, play a central role in triggering the transcriptional activation of plant defense through the so-named retrograde signaling. In this sense, many viral proteins from unrelated viruses are targeted to chloroplasts. Therefore, the hijacking of these organelles might be a general strategy among plant viruses, not only for viral factory membrane recruitment and intracellular movement but also for targeting plant defense mechanisms. For instance, the C4 protein of tomato yellow leaf curl virus (TYLCV) is targeted at chloroplast for suppressing chloroplast-depended defense (Medina-Puche *et al.*, 2020). Alternatively, the CP of CNV is targeted to chloroplast stroma for interfering with plant defense response (Alam *et al.*, 2021). Remarkably, chloroplast distribution around the nucleus is a common response to pathogen sensing in *Nicotiana benthamiana* (Ding *et al.*, 2019).

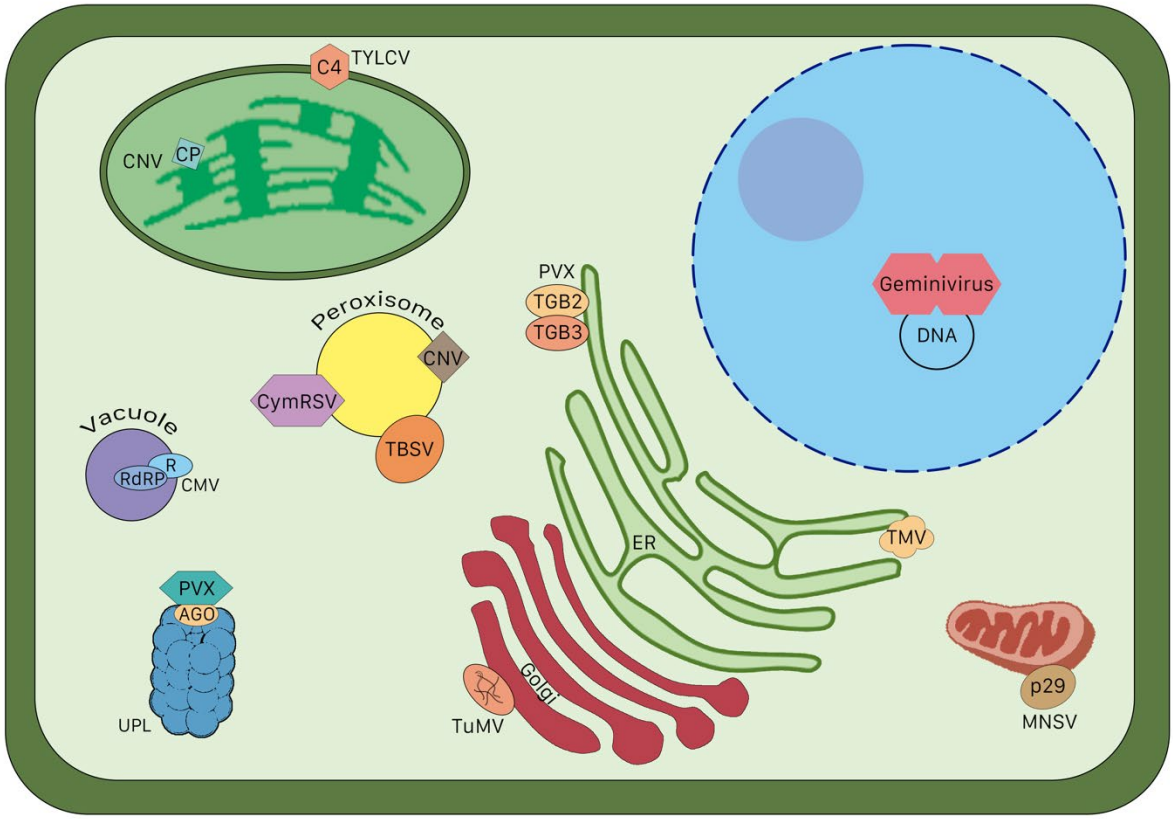

Figure 5. Examples of organelle function manipulation of plant viruses for viral process development, such as replication or immunity avoidance. Viruses represented are (from top to bottom): tomato yellow leaf virus (TYLCV), cucumber necrosis virus (CNV), potato virus X (PVX), cymbidium ringspot virus (CymRSV), tomato bushy stunt virus (TBSV), cucumber mosaic virus (CMV), tobacco mosaic virus (TMV), melon necrotic spot virus (MNSV) and turnip mosaic virus (TuMV). Adapted from Medina-Puche and Lozano-Duran, 2019.

3.1. THE RETROGRADE SIGNALLING IN PLANT CELLS

Plant genes are present in the nucleus or in the remnant genomes of the mitochondrion and chloroplast endosymbiotic organelles. In fact, energy-transducing system components are separately encoded by these compartment genomes, so their expression needs to be tightly regulated. Therefore, crosstalk between the nucleus and these organelles is essential for organelle biogenesis and plant growth, as well as for inducing stress responses, or adjusting to a dynamic environment (Mielecki *et al.*, 2020). In this context, retrograde signaling refers to the idea that changes in the developmental or metabolic state of mitochondria and chloroplasts serve as sources for signal molecules that communicate with the nucleus and alter the expression of nuclear genes (Kleine and Leister, 2016). In contrast, anterograde signaling concerns an organellar gene expression controlled by nuclear-encoded factors (Mielecki *et al.*, 2020).

The retrograde signals originating from plastids can be split into two categories, (i) related to the activity of chloroplasts in response to shifting environmental stimuli (operational control) and (ii) related to photosystem biogenesis, which occurs during plastid development and controls that subunits and cofactors are available in correct stoichiometry (biogenesis regulation) (Pogson et al., 2008). The generation of signal, transduction, and execution of retrograde signaling is poorly understood. There are still many knowledge gaps in the different routes described for chloroplast and mitochondrial retrograde signaling. In this way, retrograde signaling knowledge has been widely developed at three levels for chloroplasts and mitochondria (Wang *et al.*, 2020).

- 1. *The type of signals created in organelles.* Initially, the expression of genes involved in plastid biogenesis was formerly assumed to be regulated by a single plastid signal. Nowadays, multiple signals of different natures have been found (Kleine and Leister, 2013). They included: i) ROS as hydrogen peroxide (H_2O_2), singlet oxygen ($^1O_2$), and superoxide anion radical (O_2^-); ii) metabolites including β-cyclocitral, MEcPP (2-C-methyl-d-erythritol 2,4-cyclodiphosphate), PAP (3’-phosphoadenosine 5’-phosphate), and intermediates of the tetrapyrrole biosynthesis pathway, and iii) proteins such as the mitochondrial alternative oxidase (AOX), and the outer mitochondrial membrane protein 66 (OM66) (Huang et al., 2016; Exposito-Rodriguez et al., 2017).
- 2. *The transducers and effectors that relay signals from organelles to nucleus*, as the 3'-phosphoadenosine 5'-phosphate (PAP) phosphatase (SAL1), hypocotyl 5 (HY5), heat shock transcription factors, 5’–3’ exoribonucleases (XRNs), GENOMES UNCOUPLED1 (GUN1) or the plastid-encoded RNA polymerase (PEP) whose activation triggers a positive retrogade signal that synchronizes the expression of nuclear and chloroplast photosynthetic genes during plant development (Koussevitzky *et al.*, 2007; Díaz *et al.*, 2018).
- 3. *The executors*. They are nuclear gene expression factors that control transcription such as ABSCISIC ACID-INSENSITIVE4 (ABI4) or transcription factors of the ANAC, WHIRLY, and WRKY families (Giraud *et al.*, 2009; van Aken *et al.*, 2013).

From above, it is evident that mitochondria and chloroplasts can act as a hub for bioenergetic processes, but most notably in terms of viral infections, they are environmental signal integrators in plant cells and carriers of immunity-mediated response sending information through retrograde signaling pathways to the nucleus and other cell compartments (Pu et al., 2016; Yang et al., 2021). Regarding mitochondria, plant immunity response requires bioenergy production. Additionally, mitochondria actively alter intracellular metabolism, hormone-mediated signaling, signal transduction, produce reactive oxygen and nitrogen species, and activate programmed cell death to protect against pathogen attack (Wang *et al.*, 2022). Therefore, both organelles are obvious targets of plant pathogen effectors. For instance, the hypersensitive response (HR) can be suppressed by targeting a small fungus effector on both organelles (Tzelepis *et al.*, 2021). Besides, the *Meloidogyne javanica* nematode effector ROS suppressor (Mj-NEROSs) localizes in plastids where it interacts with Iron-Sulfur Proteins (ISP), interfering with the electron transport rate and ROS production (Stojilković *et al.*, 2022).

Chloroplasts are also a major site for the biosynthesis of phytohormones like SA and JA, signaling and its integration into immunity. Thus, it has been suggested that CNV CP is targeted to chloroplast stroma to interfere with some facets of the SA-mediated host defense response (Alam *et al.*, 2021). Furthermore, photosynthesis modification is a viral strategy to promote viral infection and set chloroplasts as an optimal niche (Zhao *et al.*, 2016).

4. PROTEIN IMPORT PATHWAY TO CHLOROPLASTS AND MITOCHONDRIA

Mitochondria and chloroplasts are endosymbiotic organelles with their own genomes, but only a few hundred proteins (about 10% of the total) are obtained by organellar gene expression (OGE). Obviously, this amount of proteins is far from sufficient to cover all the organelle tasks. The more functions fulfilled by chloroplasts and mitochondria, the more necessity for proteins that inevitably will be supplied by nuclear gene expression (NGE). In fact, about 20-25% of proteins encoded by a plant cell are localized in mitochondrial or chloroplast membranes, intermembrane spaces, mitochondrial matrix, or stroma of chloroplasts (Kaul *et al.*, 2000; Peeters and Small, 2001). Therefore, organelle protein codification in the nucleus genome implies the protein transport to the corresponding organelle after their synthesis in the cytoplasm (Bykov *et al.*, 2020; Rochaix, 2022). Two issues

make protein transport to mitochondria and chloroplasts remarkably different from that of the endomembrane system. As mentioned before, the presence of two genetic systems requires a coordinated signaling process between the nucleus and the endosymbiotic organelles for maintaining organelle function and biogenesis under these conditions (Woodson and Chory, 2008). Secondly, each semiautonomous organelle comprises more than one enveloping membrane and subcompartments, which multiplies the number of potential destinations.

Mitochondria and chloroplasts have evolved a complex protein transport mechanism that includes specific targeting signals in cargo proteins, a system of different sorting receptors, cytosolic chaperones, and transmembrane translocons. Previously to protein import into organelles, the presence of a targeting peptide signal in its N-terminal extreme is paramount, mainly for proteins destined to chloroplast stroma and mitochondrial matrix. Depending on their final organelle sublocalization, these targeting sequences vary in length, composition, and structure. For instance, mitochondrial presequences (mTP), which have an α-helix structure and a net positive charge, are targeting sequences that range in length from 15 to 55 amino acids. Instead, the presequence for chloroplast import, or chloroplast targeting sequence (cTP), is around 50 amino acids long, free of positively charged residues, unstructured, and enriched in serines (von Heijne and Nishikawa, 1991; Wiedemann and Pfanner, 2017).

On many occasions, it can also happen that one protein is transported to two different organelles, what is known as dual targeting. In this case, the protein localization signal is called a dual transit peptide (dTP). Two proteins can be produced from a single gene by having alternative transcription or translation starts, or alternative exon splicing. Finally, the N-terminus extreme of each of the two proteins represents a unique presequence (Figure 6A).

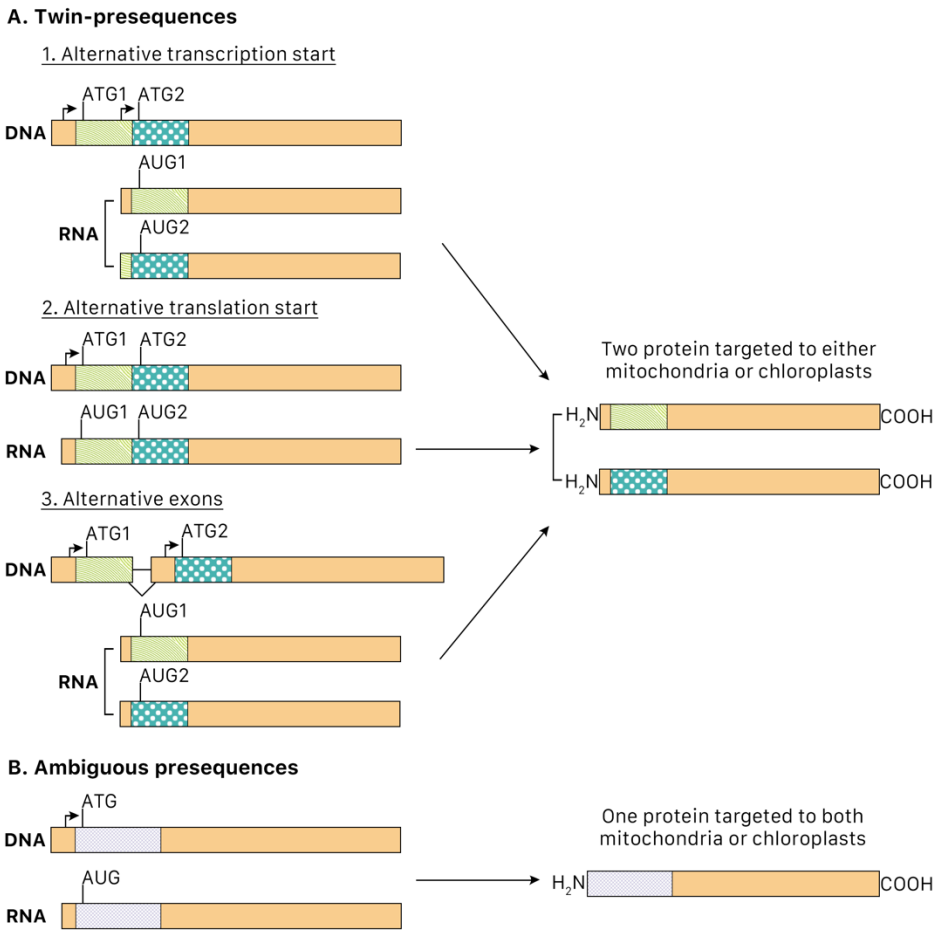

Figure 6. Dual targeting of proteins. (A) One gene can code for two proteins with distinct subcellular localization by alternative transcription start (1), alternative translation start (2), or alternative exon splicing (3). **(B)** Additionally, a single gene can produce a single polypeptide with a transit peptide consisting of cTP and mTP signals set in tandem or holding an ambiguous targeting signal, directing the protein to both mitochondria and chloroplasts. Adapted from (Peeters and Small, 2001).

Another possibility for dual targeting is the presence of twin presequences in a single translation product where mTP and cTP are placed in tandem at the N-terminal extreme (Figure 6B). However, the most extended dTP corresponds to an ambiguous peptide with common characteristics between mTP and cTP. The presence of ambiguous dTPs has already been well studied in the aminoacyl-tRNA synthetases (Berglund *et al.*, 2009) and, as we will see in the first chapter of this thesis, the CP of MNSV. However, it is not yet determined why ambiguous targeting peptides lack the high specificity of most organelle targeting sequences. A highly unlikely possibility is that dual transit peptides could be imported through non-general protein transport pathways that have not yet been discovered. Instead, the most plausible option is that dual transit peptides are imported through the same pathway as

proteins that are specifically targeted, so dTPs must be recognized by receptors of both mitochondrial and chloroplast import pathways (Peeters and Small, 2001).

Initial preprotein recognition and targeting toward both organelles is accomplished by the guidance complex, which is made up of Hsp70/90 family members and cytosolic factors that belongs to the 14-3-3 family. In particular, Hsp70 binds to hydrophobic and positive residues, and 14-3-3 mainly to phosphorylated serine (Zhang and Glaser, 2002). Next, the guide complex will carry preproteins toward the external membrane of the corresponding organelle based on their signal peptide.

Mitochondria and chloroplasts are double-membrane organelles with an intermembrane space and innermost compartment known as stroma in chloroplasts and matrix in mitochondria. Moreover, inside chloroplast stroma, there is a third membrane structure, thylakoids, where crucial proteins related to photosynthesis are found. For protein targeting, chloroplasts, and mitochondria have different complexes known as Toc (translocon of the outer chloroplast membrane) or Tom (translocon of the outer mitochondrial membrane) for their outer membrane and Tic (translocon of the inner chloroplast membrane) or Tim (translocon of the inner mitochondrial membrane) for their inner membrane (Zhang and Glaser, 2002). The transport complexes of both organelles are mechanically similar; however, they originated independently and are non-homologous (Carrie and Small, 2013).

4.1. THE TRANSLOCON COMPLEXES OF CHLOROPLASTS

4.1.1. Translocon of the outer chloroplast membrane: TOC

After cTP recognition by Hsp70, Hsp90, and 14-3-3 factors, preproteins are driven to the chloroplast membrane surface, where the translocon complex of the outer membrane is localized, mainly responsible for protein recognition. In plants, Toc is principally composed of two GTP-regulated receptors family, Toc34 and Toc159, and a proteinaceous channel, Toc75 (Jarvis, 2008) (Figure 7).

The Toc34 family comprises Toc33 and Toc34 isoforms meanwhile, the Toc159 family is formed by Toc90, Toc120, Toc132, and Toc159 in *Arabidopsis thaliana*. Regarding the

structure, both families share a GTPase domain (G), but the Toc34 family has a simple structure forming both monomers and dimers. The Toc159 family is more structure-complexed, and has a membrane anchoring domain (M) and a variable acidic domain (A) in its N-terminal extreme, except in Toc90. Toc75 is the major channel that interacts with the GTP-regulated receptors Toc34 and Toc159 for protein import into chloroplasts (Li and Chiu, 2010; Jarvis, 2008).

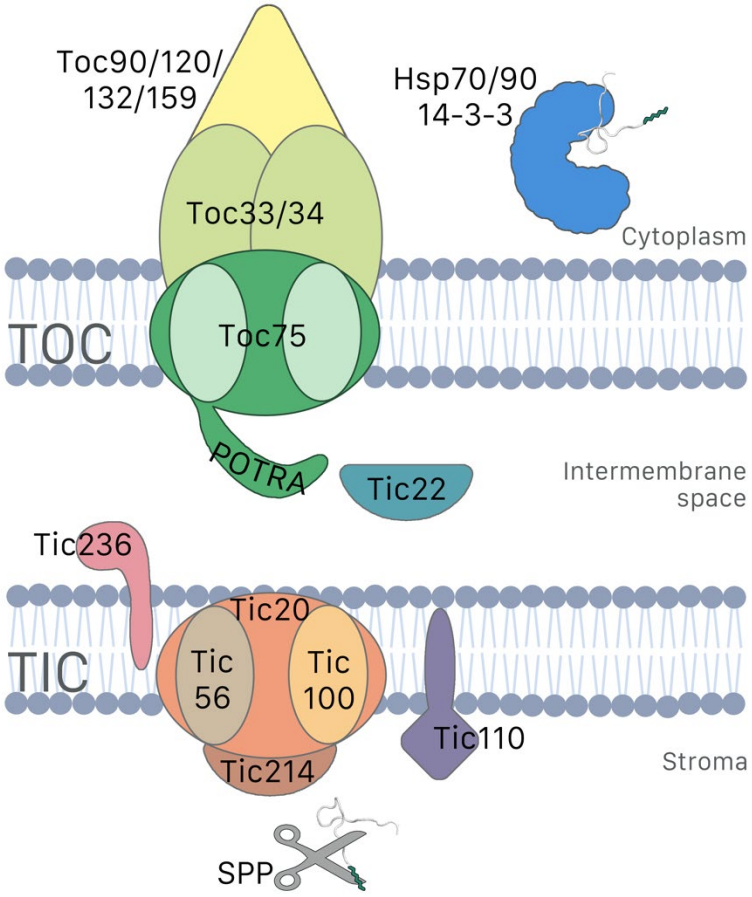

Figure 7. Model of protein translocation through chloroplast membranes. Preproteins are encoded in the nucleus and driven to the outer membrane of the chloroplasts by a guidance complex (Hsp70/90 and 14-3-3), which recognizes their transit peptide signals (cTP). After interacting with Toc159 and Toc34, the preproteins will reach the intermembrane space via the Toc75 channel. There, they will be recognized by Tic22 and Tic236, which direct them toward the main component of Tic. As soon as the preproteins reach the chloroplast stroma, the signal peptide peptidase (SPP) cleavages their cTP originating a mature protein.

The codification of different isoforms in the same family can lead to a differential function, expression, and some redundancy. In turn, the best way to determine these effects is the study of null mutants for each protein, mainly tested on *A. thaliana*. For instance, AtToc33 and AtToc159 are highly abundant in photosynthetic tissues, such as leaves, and AtToc34,

AtToc90, AtToc120, and AtToc132 are mostly expressed in non-photosynthetic tissues, such as roots (Jarvis, 2008; Gutensohn *et al.*, 2000; Andrès *et al.*, 2010). AtToc34 and AtToc33 exhibit some functional redundancy while having separate preferred precursor proteins, as it is shown in theirs simple mutants *toc34* and *toc33* (Figure 8A). Moreover, AtToc33 knockout could be complemented by AtToc34; meanwhile, a double mutant of AtToc34 family is embryo-lethal (Constan *et al.*, 2004; Hust and Gutensohn, 2006). For the AtToc159 family, *ppi2* mutant (AtToc159 knockout) presents a severe albino phenotype that cannot pass its cotyledon stage (Figure 8B), and could be partially complemented by AtToc90 and AtToc33 interaction (Infanger *et al.*, 2011). However, AtToc90 knockout (*ppi4*) did not present any phenotype. Likewise, the *toc132/toc120* double homozygote produced a *toc159*-like bleached phenotype, showing a highly redundant functioning between them (Figure 8B). On the contrary, its single mutants did not reveal any visible phenotype (Kubis *et al.*, 2004). The knockout of the main isoform of Toc75 in *A. thaliana*, *Toc75-III* was also embryo-lethal (Baldwin *et al.*, 2005).

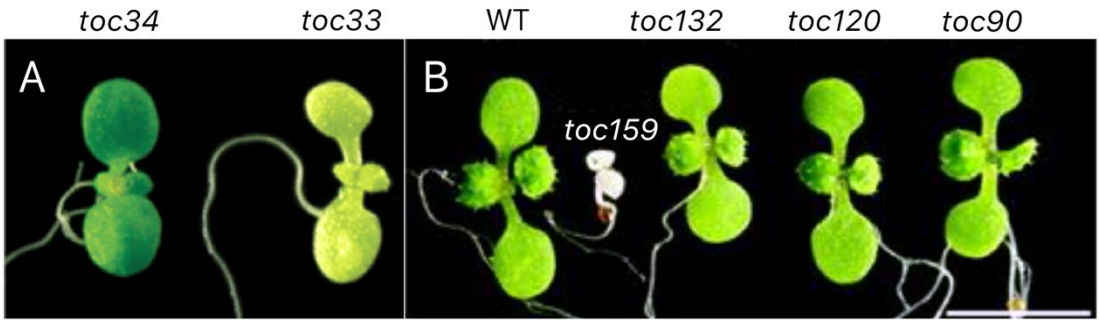

Figure 8. Visible phenotypes of TOC knockout mutants from *A. thaliana*. (A) Homozygous mutants for AtToc34 and AtToc33 family. **(B)** Homozygous mutants for AtToc159 members: AtToc90, AtToc120, AtToc132 and AtToc159. Both images were obtained from Constan *et al.*, 2004 and Kubis *et al*., 2004.

Two different models for preprotein recognition and import by Toc complex have been developed, and whether the initial recognition is done through Toc159 or Toc34 is still under discussion. Transit peptide is firsly recognized by Toc34 in the Toc34 receptor mode and the recognition is made by Toc159 in the Toc34 regulator mode (Wiesemann *et al.*, 2019). Furthermore, in most of the hypothesized models, the guidance complex is recognized by Toc34, and cTP binds to Toc159. Finally, preproteins pass to the intermembrane space through the Toc75 channel to eventually reach Tic (Li and Chiu, 2010; Gutensohn *et al.*, 2000).

4.1.2. Translocon of the inner chloroplast membrane: TIC

After preprotein import through the outer membrane of chloroplasts by Toc, it will reach stroma and thylakoids by Tic machinery (Figure 7). The first component is Tic22, which would act as a chaperone driving preprotein towards the inner membrane. Also, Tic22 functions coordinately with the soluble polypeptide-transport-associated (POTRA) domains of Toc75, proving close coordination between Toc and Tic at all stages of protein import (Richardson *et al.*, 2018). In *A. thaliana*, this chaperone gene encodes two functionally similar isoforms, AtTic22-III and AtTic22-IV. Despite the fact that AtTic22-IV has higher expression levels, only AtTic22-III knockout shows a phenotypic effect (Kasmati *et al.*, 2013).

Initially, a complex of around 1MDa responsible for translocation was discovered in the inner membrane of chloroplasts (Kikuchi *et al.*, 2009). It is composed of Tic20, Tic56, Tic100, and Tic214 being Tic20 the main component because it is responsible for the α-helical channel establishment (Kovács-Bogdán *et al.*, 2011; Campbell *et al.*, 2014). Moreover, the *tic20* mutant has reduced levels of protein accumulation in plastids, reduced photosynthesis potential, and consequently, growth deficiencies (Chen *et al.*, 2002; Hirabayashi *et al.*, 2011). The principal functions of the 1MDa complex components still need to be elucidated. However, Tic56 and Tic100 knockouts result in an albino seedling-lethal phenotype (Campbell *et al.*, 2014; Nakai, 2018).

Tic110 was the inner membrane translocation apparatus component first discovered. Unlike the other components, Tic110 did not belong to the 1MDa complex, so it is a universal or constitutive component. The Tic110 principal function is connected to the recruitment of chaperones to the stromal side of the Tic complex (Jarvis and Soll, 2002). Another protein integrated into the inner membrane but separated from Tic20 complex is Tic236. It has a domain oriented towards the intermembrane space, which interacts with Toc75. Its function is essential since the *tic236* mutant is embryo-lethal (Chen *et al.*, 2018).

Finally, when preprotein reaches the chloroplast stroma, the signal peptide peptidase (SPP) cleavages the transit peptide by recognizing a region of 10-15 amino acids. The SPP has a zinc-

binding domain, a pattern of the metallopeptidase family to which the mitochondrial processing peptidase also belongs (Jarvis, 2008).

4.2. TRANSLOCON COMPLEXES OF MITOCHONDRIA

4.2.1. Translocon of the outer mitochondrial membrane: TOM

Regarding mitochondria, after ribosomal translation of the preproteins, the guidance complex recognizes their mTPs and drives them toward the outer mitochondrial surface where the translocon complex of the outer membrane responsible for protein recognition is localized. Depending on the protein topology and targeting signal, five different protein import pathways have been characterized; however, in all of them, the Tom machinery takes part. First, hydrophilic proteins are imported into the matrix by the presequence translocase-associated motor. Intermembrane space (IMS) proteins are imported by the mitochondrial IMS import and and TOM compex. Precursors of β-barrel proteins, which are inserted into the outer membrane by the sorting and assembly machinery, are previously translocated through TOM to TIM like the precursors of metabolite carriers. Finally, the mitochondrial import complex (MIM) import α-helical proteins to outer membrane of mitochondria (Wiedemann and Pfanner, 2017).

In mammals and yeast, Tom complex is mainly formed by three receptors protein such as Tom20, Tom22, and Tom70, and a proteinaceous channel Tom40 (Figure 9). However, in plants, the Tom22 receptor is lacking, and there is not Tom20 and Tom70. Therefore, the channel Tom40 and a family of mammal and yeast non-homologous Tom20 receptors are part of the Tom complex in plants. The plant-specific mitochondrial outer membrane protein 64 (Om64) is also part of the preprotein plant import system; however, it does not belong to the Tom complex but is associated with it (Lister *et al.*, 2007).

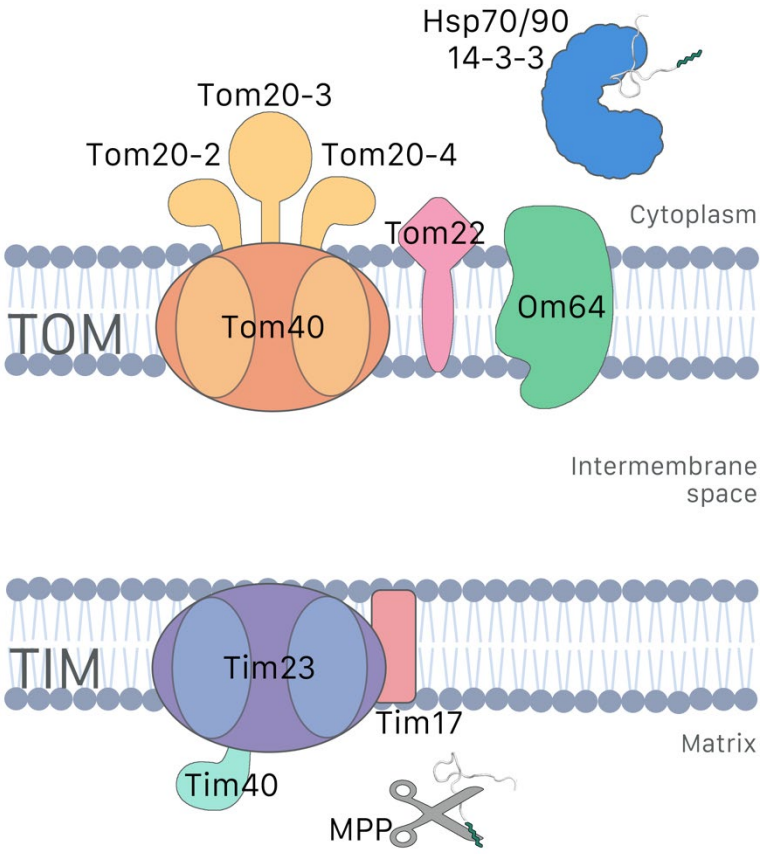

Figure 9. Model of protein translocation through the mitochondrial membranes. Preproteins are encoded in the nucleus and driven to the outer membrane of mitochondria by a guidance complex (Hsp70/90 and 14-3-3) which recognizes their presequences (mTP). After interacting with Om64 and Tom20, the preproteins will reach the intermembrane space via the Tom40 channel. Next, in the inner membrane of chloroplasts, preproteins will be recognized by Tim23 and Tim17. As soon as the preprotein reaches the mitochondrial matrix, MPP peptidase cleavages its mTP originating a mature protein.

Om64 has been identified as a paralogue of Toc64 from chloroplasts. Structurally, it has an N-terminal extreme anchored to the membrane and a tetratricopeptide repeat motif (TRP) domain at its C-terminal oriented to the cell cytoplasm. Om64 is mainly involved in interaction with mitochondrial precursor proteins and Tom complex at early stages. It also interacts with Hsp70/90 and 14-3-3 to prevent protein aggregation (Lister *et al.*, 2007; Nickel *et al.*, 2019).

In *A. thaliana*, the Tom20 family includes four different isoforms, Tom20-1, Tom20-2, Tom20-3, and Tom20-4. However, only Tom20-2, Tom20-3, and Tom20-4 are sufficiently expressed to be detected (Nickel *et al.*, 2019). Tom20 has an N-terminal extreme anchored to the outer membrane and acts as an initial receptor of the preprotein (Wiedemann and Pfanner, 2017; Lister *et al.*, 2007). Furthermore, overlapping roles have been observed in protein import to mitochondria. Indeed, *tom20-2/tom20-3/tom20-4* triple mutant, shows reduced protein

import rate and plant growth. Meanwhile, *tom20-2/tom20-3/tom20-4/om64* quadruple knockout is lethal at the embryo stage (Nickel *et al.*, 2019).

As an operative intermediary between Tom20 and Tom40, Tom22 acts as a multifunctional element, whose structural role is the most important (Kamenski *et al.*, 2007). Regarding Tom22 structure, in mammals and yeast, it has an acidic domain at its N-terminal extreme, which is absent in plants (Macasev *et al.*, 2000). Tom40 is a β-barrel protein with eight transmembrane domains that acts as the central subunit of the Tom complex being the principal entrance for mitochondrial preproteins (Kamenski *et al.*, 2007). Moreover, Tom40 knockdown of *A. thaliana* led to an early embryo-lethal phenotype that might have resulted from the lack of mitochondrial biogenesis during embryo development (Hu *et al.*, 2019).

As mentioned above, there are different import paths along Tom complex. Mainly in plants, mTP would be recognized by Om64 and transferred to Tom machinery. There, Tom20 acts as the principal receptor by mTP hydrophobic surface recognition, which Tom22 will join. Finally, preprotein will reach mitochondrial intermembrane space through the Tom40 channel (Nickel *et al.*, 2019; Young *et al.*, 2003; Wiedemann and Pfanner, 2017; Lister *et al.*, 2007).

4.2.2. Translocon of the inner mitochondrial membrane: TIM

Translocon receptor of the inner mitochondrial membrane or Tim complex is mainly formed by a translocon at the inner membrane and a translocation motor at the matrix (Kamenski *et al.*, 2007). The inner membrane translocon is different depending on preprotein substrate specificity, thus Tim differs from Tim23 or Tim22 complexes (Figure 9). While the Tim22 complex facilitates the import of a class of integral inner membrane proteins that do not carry a conventional matrix-targeting signal, the Tim23 complex mediates the import of preproteins with a positively charged matrix-targeting signal (Bauer *et al.*, 2000). Since Tim23 is the complex responsible for the import of mitochondrial matrix preproteins, we will focus on it.

The Tim23 complex is formed by Tim17, Tim23, and Tim44, where the C-terminal extreme of Tim23 is anchored to the inner membrane setting a proteinaceous channel; moreover, it is responsible for preprotein recognition. Tim17, which comprises four transmembrane segments, is associated with the Tim23 channel. Tim44 is also associated with the inner

membrane but faces the matrix space (Bauer *et al.*, 2000). Once preprotein reaches the mitochondrial matrix through the Tim23 complex, chaperone recruitment is done by Tim44, and the mitochondrial processing peptidase (MPP) in the matrix will remove the presequence of the protein (Wiedemann and Pfanner, 2017).

Justification and objectives

JUSTIFICATION AND OBJECTIVES

Plant viruses, as simple pathogens, have two main challenges to ensure their survival. They must develop mechanisms to overcome host defenses, such as the plant immune system triggering a hypersensitive response (HR), the RNA silencing mechanisms, or the new epigenetic regulation by N6-methyladenosine (m6A) modification. Also, viruses must guarantee their maintenance by evolving their components to play several roles during infection and acquiring counter-defense strategies to replicate in the cell or spread throughout the plant and between plants. To do this, plant viruses largely depend on host factors that will help in their replication and defense. In this sense, the melon necrotic spot virus (MNSV) coat protein (CP) is a multifunctional or moonlighting protein that could develop different tasks through the viral cycle. The research carried out in this doctoral thesis has been mainly focused on deciphering how the cellular distribution of the MNSV CP is achieved and how its multifunctionality is affected depending on its subcellular localization, with priority given to the interaction with host factors. Therefore, the following objectives were proposed:

- Objective 1. Study of the structural elements driving the MNSV CP targeting to chloroplasts, mitochondria, and altered-mitochondria or viral replication factories (VRC), and how these subcellular localizations affect the proper fulfilling of its different assigned tasks.
- Objective 2. Identification and characterization of the main components of the translocons of the outer membrane of chloroplasts (Toc) and mitochondria (Tom) in *Nicotiana benthamiana*, the experimental MNSV host used in this thesis.
- Objective 3. Identification and characterization of the Toc and Tom translocon receptors involved in the dual targeting of the MNSV CP to chloroplasts and mitochondria and their significance in viral infection.
- Objective 4. Knowledge acquisition and development of a new protein-protein interaction technique based on the biotin proximity labeling (PL) by specific ligases (TurboID) to find host interactors of the MNSV CP in the different subcellular compartments where it is located.

Chapter I

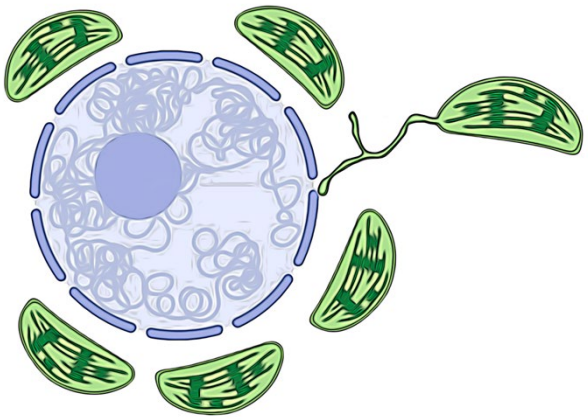

The mitochondrial and chloroplast dual targeting of a multifunctional plant viral protein modulates chloroplast-to-nucleus communication, RNA silencing suppressor activity, encapsidation, pathogenesis and tissue tropism.

Jose A. Navarro*, María Sáiz-Bonilla, Jesus A. Sanchez-Navarro and Vicente Pallas*

Department of Molecular and Evolutionary Plant Virology. Institute for Plant Molecular and Cell Biology. Consejo Superior de Investigaciones Científicas-Universitat Politècnica de València, Valencia, Spain.

*Corresponding authors: Vicente Pallas (vpallas@ibmcp.upv.es) and Jose Antonio Navarro (janavarr@ibmcp.upv.es)

Published as **Navarro, J. A., Saiz-Bonilla, M., Sanchez-Navarro, J. A., and Pallas, V.** (2021) The mitochondrial and chloroplast dual targeting of a multifunctional plant viral protein modulates chloroplast-to-nucleus communication, RNA silencing suppressor activity, encapsidation, pathogenesis and tissue tropism. *Plant J.*, **108**, 197–218.

Personal contribution. M.S-B performed and analyzed transitory expression and deletion experiments. J.A.S takes part in molecular cloning. J.A.N performed infection assays and analyzed the results. All authors discussed the results.

ABSTRACT

Plant defense against melon necrotic spot virus (MNSV) is triggered by the viral auxiliary replicase p29 that is targeted to mitochondrial membranes causing morphological alterations, oxidative burst, and necrosis. Here we show that MNSV coat protein (CP) was also targeted to mitochondria and mitochondrial-derived replication complexes (VRC), in close association with p29, in addition to chloroplasts. CP import resulted in the cleavage of the R/arm domain previously implicated in genome binding during encapsidation and RNA silencing suppression (RSS). We also show that CP organelle import inhibition enhanced RSS activity, CP accumulation, and VRC biogenesis but resulted in inhibition of systemic spreading, indicating that MNSV whole-plant infection requires CP organelle import. We hypothesize that to alleviate the p29 impact on host physiology, MNSV could moderate its replication and p29 accumulation by regulating CP RSS activity through organelle targeting and, consequently, eluding early-triggered antiviral response. Cellular and molecular events also suggested that S/P domains, which correspond to processed CP in chloroplast stroma or mitochondrion matrix, could mitigate host response inhibiting p29-induced necrosis. S/P deletion mainly resulted in a precarious balance between defense and counter-defense responses, generating either cytopathic alterations and MNSV cell-to-cell movement restriction or some degree of local movement. In addition, local necrosis and defense responses were dampened when RSS activity but not S/P organelle targeting was affected. Based on a robust biochemical and cellular analysis, we established that the mitochondrial and chloroplast dual targeting of MNSV CP profoundly impacts the viral infection cycle.

KEY WORDS

MNSV, chloroplasts, mitochondria, dual targeting, coat protein, silencing, hypersensitive response.

SIGNIFICANCE STATEMENT

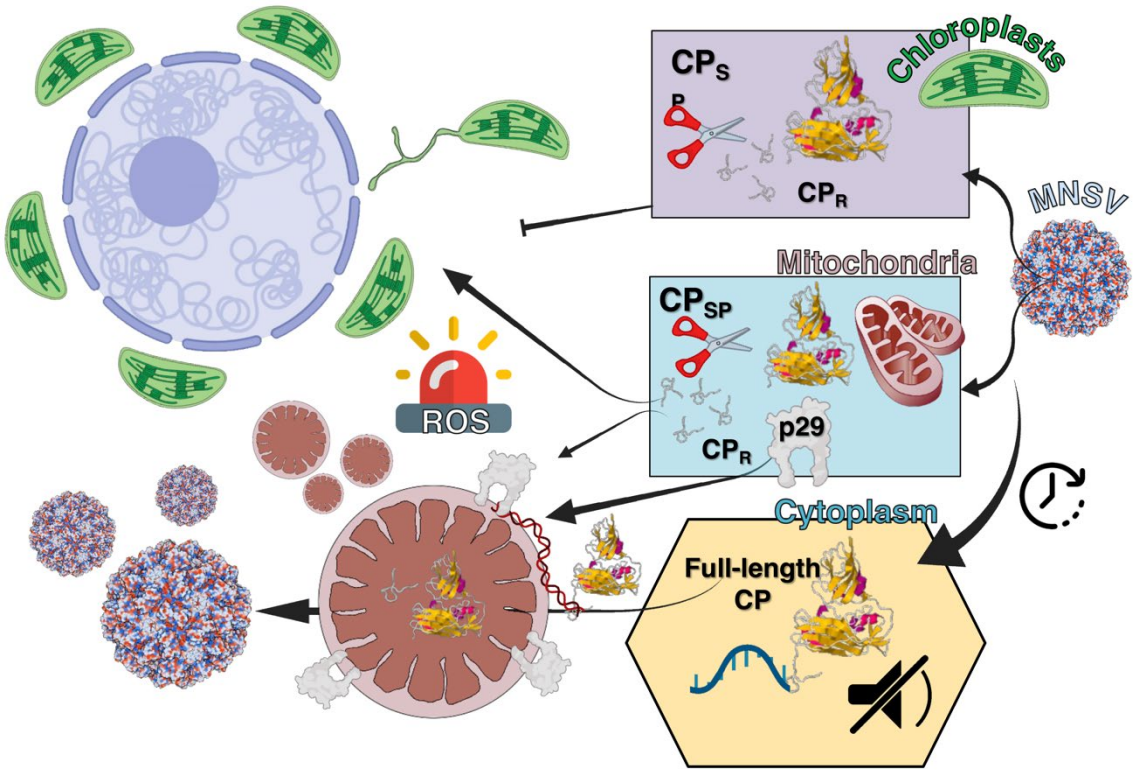

The importance of mitochondria and chloroplasts as stress recognition initial sites and signaling after cellular dysfunction is evident, although its involvement in plant–virus interactions remains unclear. Here, we show that a viral protein is organelle-targeted to modulate chloroplast-to-nucleus communication, RNA silencing suppression, encapsidation, pathogenesis and tissue tropism, making coat protein a remarkable multifunctional factor. Our results illuminate how plant viruses have evolved to evade plant defense and proliferate using a few proteins.

INTRODUCTION

Positive strand RNA plant viruses replicate in the cytoplasm of susceptible cells over or within specialized membranous compartments named viral replication factories or complexes (VRCs). VRCs are supposed to concentrate viral and host factors, generate a favorable environment for efficient replication and assembly, and protect RNA intermediates against host antiviral mechanisms such as RNA silencing (Laliberté and Sanfaçon, 2010). Besides, a growing body of evidence supports the VRC role in intra- and intercellular movement and long-distance transport through vascular tissues (Laliberté and Zheng, 2014; Wan *et al.,* 2015). It is still unclear how plant viruses orchestrate VRC scaffolding. Nevertheless, it is known that the alteration of membrane morphology is usually triggered by specific organelle targeting of viral proteins, most often those related to replication (Jin *et al.,* 2018). Once there, these proteins establish a network of interactions among other viral and host components, which are then incorporated into VRCs (Nagy, 2016).

Upon building these factories, viruses cause a profound remodeling and proliferation of host cell endomembranes and cytoskeleton, undermining the integrity and function of different organelles. Among them are chloroplasts, mitochondria, and peroxisomes, which contribute to maintaining the cellular homeostasis of signaling molecules such as reactive oxygen species (ROS) and phytohormones, and the endoplasmic reticulum (ER), which is a major protein folding compartment that bears the burden of new viral client proteins (Hernández *et al.,* 2016; Verchot, 2016; Su *et al.,* 2019; Loebenstein, 2009; Li *et al.,* 2016; Zhao *et al.,* 2016). Therefore, the impact of virus replication on organelle function together with viral protein accumulation could result in ROS or misfolded proteins exceeding normal levels. This late event eventually leads to ER stress, altered gene expression, and even hypersensitive response (HR)-related cell death (van Aken and van Breusegem, 2015; Pallas and García, 2011). Plant viruses as biotrophic parasites must reverse this adverse situation to preserve cell viability and generate compatible or tolerant interactions. Thus, they have coevolved a diversity of mechanisms to moderate their harmful effects on the host, not only including counter defense measures, such as suppression of RNA silencing, or inhibition of both oxidative burst and expression of plant innate immunity-associated genes but also self-attenuating their replication (Paudel and Sanfaçon, 2018).

VRC architecture and biogenesis have been mainly studied in members of the families Tombusviridae and Potyviridae (Jin et *al.,* 2018). Cytopathology studies by transmission electron microscopy showed that melon necrotic spot virus (MNSV) infection deeply modified the structure of mitochondria in melon, enlarging them and inducing big inner dilations as well as multi-vesiculation of the external and surrounding-dilation membranes (Gomez-Aix *et al.,* 2015). These altered mitochondria were frequently localized near plasmodesmata, indicating that they could play a role in the viral spread, always associated with the ER, lipid bodies, or droplets. Positive-sense viral RNAs, coat protein (CP), and replicative RNA intermediates (dsRNAs) were mainly detected in big inner dilations supporting the view that altered mitochondria constitute VRCs. In *N. benthamiana*, MNSV p29 auxiliary replicase was shown to associate with mitochondrial membranes upon an ectopic (Gomez-Aix *et al.,* 2015) or heterologous viral expression (Mochizuki *et al.,* 2009). Once there, p29 caused VRC-like modification of mitochondrial ultrastructure, loss of mitochondrial membrane potential (MPP), and necrosis, indicating a role for p29 in VRC formation and, probably, ROS activation of plant defense responses as described for cucumber necrosis virus (CNV) p33 (Rochon *et al.,* 2014).

Previous works by us and others showed that an oxidative burst accompanied melon response to MNSV infection. Briefly, hydrogen peroxide accumulation, which indicates mitochondrial damage, and cell wall fortification by callose deposition was found in local and systemic MNSV necrotic lesions (Fernández-Crespo *et al.,* 2017). Transcriptomic profiling of MNSV local infection unveiled deregulation of genes involved in defense response and oxidative stress (Gómez-Aix *et al.,* 2016). Comparative proteomic analysis of melon phloem exudates in response to MNSV infection revealed that differentially accumulated proteins were mainly involved in controlling redox balance and cell death, for example, an hsr203J HR marker-like carboxylesterase was up-accumulated, suggesting that HR could be activated (Serra-Soriano *et al.,* 2015). Jasmonic acid (JA) and salicylic acid (SA) are antagonistic phytohormones activated simultaneously in the same plants only in the case of effector-triggered immunity (ETI) (Betsuyaku *et al.,* 2018). Interestingly, SA, JA precursor 12-oxo-phytodienoic acid (OPDA), antioxidant ferulic acid, and detoxifying glutathione S-transferase mRNA levels increased

during the basal response of melon to MNSV, a plant response that was accentuated during hexanoic-primed systemic resistance (Fernández-Crespo *et al.,* 2017).

Systemic lethal necrosis, frequently observed in infection of MNSV family-related tombusviruses, was shown to be induced by auxiliary replicase with the indirect assistance of p19 suppressing plant defense mechanisms (Burgyán *et al.,* 2000). Similarly, the appearance of necrotic symptoms on melon cotyledons was enhanced by MNSV CP, which takes the role of p19 in RNA silencing suppression by increasing viral movement (Genoves *et al.,* 2006; Serra-Soriano *et al.,* 2017). MNSV CP consists of three major domains: a disordered N-terminal RNA-binding domain (R-domain), connected to the shell domain (S-domain) by a short and flexible arm, and the protruding domain (P-domain). Each domain plays different roles during infection, making MNSV CP an exceptional multifunctional protein. The R domain and the arm region are required for genome interaction and encapsidation, siRNA binding, and suppression of RNA silencing, the S domain has a structural function, whereas the P domain is involved in compatibility with fungus vector zoospores (Ohki *et al.,* 2010; Serra-Soriano *et al.,* 2017; Genoves *et al.,* 2006). MNSV CP also works as a host determinant since CP from melon isolates allows watermelon isolates to infect melon locally (Ohki *et al.,* 2008). Despite all this information, studies about CP subcellular localization, which are limited to the immunolocalizations mentioned above, and underlying molecular determinants are still lacking. Here we show that the R/arm region can act as an ambiguous transit peptide driving dual targeting of MNSV CP to mitochondria and chloroplasts in ectopic expression and during MNSV infection. CP was additionally found in altered mitochondria, resembling VRCs that moved along the cellular periphery of infected cells, supporting a link between intracellular movement and replication. We also evaluated the role of p29 in VRC biogenesis showing cellular events not previously described. Before necrosis appearance, ectopically expressed p29 was located around mitochondria displaying a swollen morphology and forming small ER-associated groups together with large juxtanuclear clusters. Based on cellular features, the effect of different CP mutations on MNSV infectivity, and expression levels of hypersensitive response, defense, and oxidative stress-related host genes, we propose new functions for MNSV CP, associated with its organelle targeting, in managing the balance between plant defense and virus counter-defense responses.

RESULTS

Transiently expressed MNSV CP has a dual localization to chloroplasts and mitochondria.

To study MNSV CP subcellular localization in plant cells, the green fluorescent protein (GFP) was fused to its C- or N-terminus (CP-GFP and GFP-CP, respectively) and transiently expressed in *N. benthamiana* leaves. The fluorescence, visualized under confocal laser scanning microscopy (CLSM) at 48 hpi, was mainly found in chloroplasts, as shown by the superposition of GFP and chlorophyll fluorescence, and in small and motile punctate bodies (Figure 1a and Movie S1) that overlapped with coxP-ChFP, a mitochondrial matrix marker (Figure 1b). Chloroplast-associated CP-GFP fluorescence was mainly observed in the stroma as revealed by its colocalization with NRIP1-ChFP, a stromal component (Caplan *et al.,* 2008) (Figure 1c), but not with CHUP1-ChFP, a chloroplast outer envelope protein (Oikawa *et al.,* 2008) (Figure 1d). Consistent with stromal localization, CP-GFP fluorescence was also detected in stromules (Figure 1e, up). Furthermore, CP-GFP fluorescence was frequently observed, forming discrete spots around chlorophyll fluorescence as described for CNV CP (Figure 1e, down). We found that these structures colocalized with the magnesium-protoporphyrin IX chelatase H subunit (CHLH/ABAR), a spanning chloroplast envelope receptor of ABA (Shang *et al.,* 2010) and tetrapyrrole sensor, which mediates plastid-to-nucleus retrograde signaling (Figure 1f) (Nott *et al.,* 2006). It has been reported that this pattern might result from the over-accumulation of chloroplast-targeted proteins that are prone to aggregate, such as viral CPs do (Chaudhary and Yadav, 2019; Perello *et al.,* 2016). In contrast, cells expressing GFP-CP showed nucleo-cytoplasmic fluorescence distribution (Figure 1g). It is known that the fusion of tags to the N terminus of the protein of interest interferes with plastid and mitochondrial localization signals, which are mainly located at this protein end. To solve this issue an internally GFP-tagged CP was constructed by inserting the fluorescent protein between the arm region and the S domain (R/arm-GFP-SP). This fusion protein has the advantage that the putative targeting signals present at the N and C terminus of the CP are not masked by the tag (Tanz *et al.,* 2013). After coexpression with coxP-ChFP, R/arm-GFP-SP showed a fluorescent pattern similar to that described above for CP-GFP, labelling mitochondria, chloroplasts, and chloroplast envelope-associated spots (Figure 1h). Therefore, CP-GFP and R/arm-GFP-SP reflect more accurately the actual subcellular localization of the CP than GFP-CP, revealing the presence of a dual-targeting signal at the N-terminus of the CP.

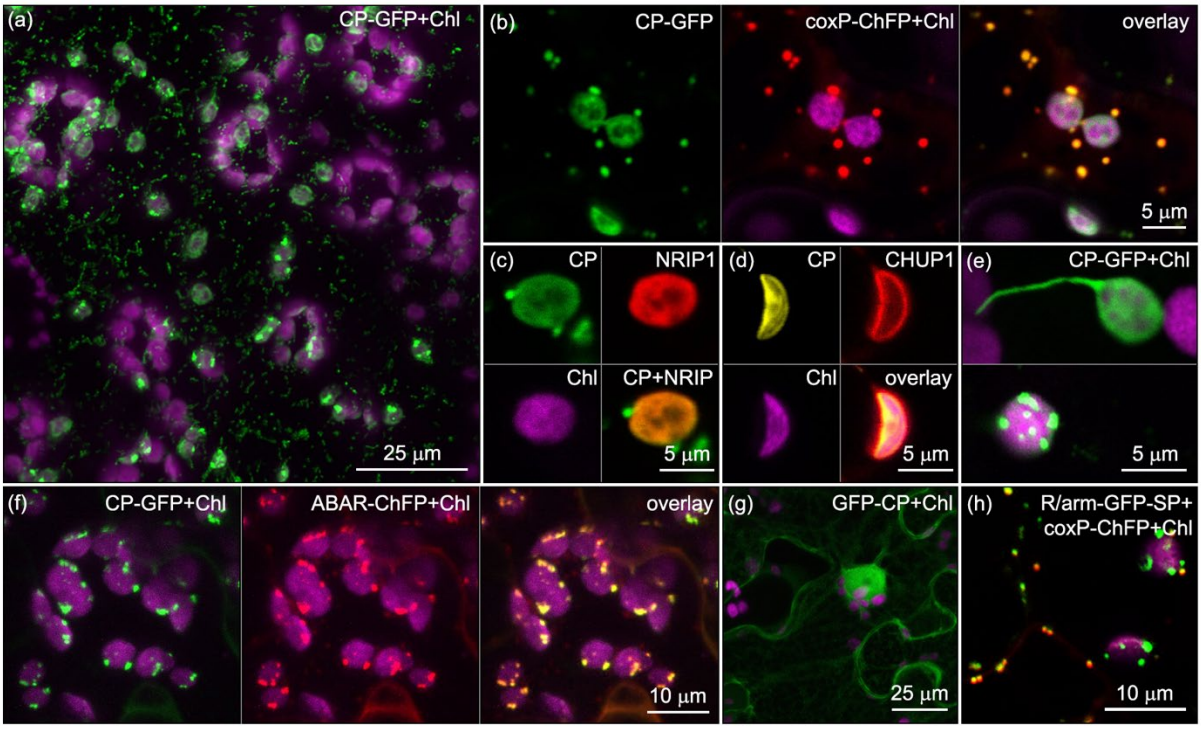

Figure 1. Subcellular localization of GFP-tagged CP upon transient expression in *N. benthamiana* leaves. (a) Z-stack projection showing CP-GFP distribution in epidermal and mesophyll cells **(b)** Coexpression of CP-GFP and the mitochondrial matrix marker, coxP-ChFP. **(c-d)** Image of a CP-GFP-labelled chloroplast expressing the stromal, NRIP1-ChFP (c), or outer-envelope, CHUP1-ChFP (d), proteins. **(e)** CP-GFP-labeled chloroplast showing a stromule (up) or envelope-associated spots (down). **(f)** Coexpression of CP-GFP and CHLH/ABAR-ChFP. **(g)** GFP-CP nucleo-cytoplasmic distribution in epidermal cells. **(h)** Coexpression of R/arm-GFP-SP and coxP-ChFP. Images correspond to single scans unless indicated. Chl, chlorophyll autofluorescence in magenta.

The N-terminal R/arm domain drives CP mitochondrial and chloroplast dual targeting and induces chloroplast-to-nucleus communication through stromule extension.

Although MNSV has been classified into the genus Gammacarmovirus, its CP shows a high degree of similarity to CPs in the genus Tombusvirus (Wada *et al.,* 2008; Riviere *et al.,* 1989). CPs from 16 out of 17 tombusviruses and MNSV CP were predicted to target chloroplasts and/or mitochondria by WoLF PSORT, LOCALIZER, and YLOC (Horton *et al.,* 2007; Sperschneider *et al.,* 2017; Briesemeister *et al.,* 2010) (Table S2). Accordingly, the N-terminal 39 amino acids of the CNV CP R domain were sufficient for mitochondrial import, whereas the arm region plus the first four aa (SVRI motif) of the S domain were required for chloroplast targeting (Hui *et al*., 2010; Xiang *et al.,* 2006). To reinforce this notion, we analyzed five tombusvirus CPs for their subcellular localization by using C-terminal GFP fusions. Except for tomato bushy stunt virus CP, the carnation Italian ringspot virus, cymbidium ringspot virus, Neckar river virus, and pelargonium necrotic spot virus CPs were localized in chloroplasts and mitochondria (Figure S1). In contrast to MNSV CP, some of these tombusvirus CPs also showed

a high degree of cytoplasmic localization. This result is consistent with previous work about CNV CP reporting that only 1–5% of this protein is targeted to chloroplast during infection (Xiang *et al.*, 2006). Alignment of the tombusvirus and MNSV N-terminal CP sequences showed that an asparagine/arginine-rich stretch at the protein start including an alanine residue at position 2, frequently found in dual and chloroplast (cTP) transit peptides (Pujol *et al.,* 2007), was the most conserved region in the R domain (Figure S2). Despite sequence variability, two adjacent alpha-helix (H1 and H2) were always predicted by JPred 4 (Drozdetskiy et al., 2015). Though cTPs usually are unstructured regions, they can form helices in membrane-mimetic environments. Some of these helices showed amphipathic properties, an mTP typical feature, as calculated by HeliQuest (Ge *et al.,* 2014; Gautier *et al.,* 2008). The arm region was more conserved than the R domain, but the SVRI motif embedded at the beginning of the S domain was only found in the Havel river virus and MNSV (SVKI). Instead, a GSVTV motif was mainly observed among the aligned sequences.

Considering the above-shared features, we examined the role of the MNSV CP N-terminal region in organelle import. We transiently expressed R/arm-GFP, which includes R and arm domains of the MNSV CP, and R/arm/S19-GFP, which also covers the first 19 aa of the S domain, including the SVKI motif and a 14-3-3 chaperone binding like-domain (RXnpSXP) (Xiang *et al.,* 2006) (Figure S2 and S3). Fluorescence distribution revealed that S domain sequences were not required for transport as both proteins were efficiently targeted to both organelles and additionally to nucleoli (Figure 2a-c). Chloroplast peripherally-located spots were not observed, but a high number of chloroplasts extended stromules and, frequently, they were found in perinuclear clusters tightly embracing nuclei through stromules that extend and coil around (Figure 2d-f). To determine the extent of stromule induction, we coexpressed NRIP-ChFP with CP-GFP, R/arm-GFP, and glyrsP-GFP, a dual mitochondrial and chloroplast marker used for steady-state control (Duchêne *et al.,* 2001), and quantified the percentage of chloroplasts with NRIP-ChFP-labelled stromules. As expected, the percentage increased with the presence of R/arm-GFP (28.8%, t=6.0, and p=0.0002) compared to control (10.3%). Stromule induction also occurs, but to a lesser extent, with CP-GFP (19.0%, t=4.4 and p=0.00006) (Figure 2g).

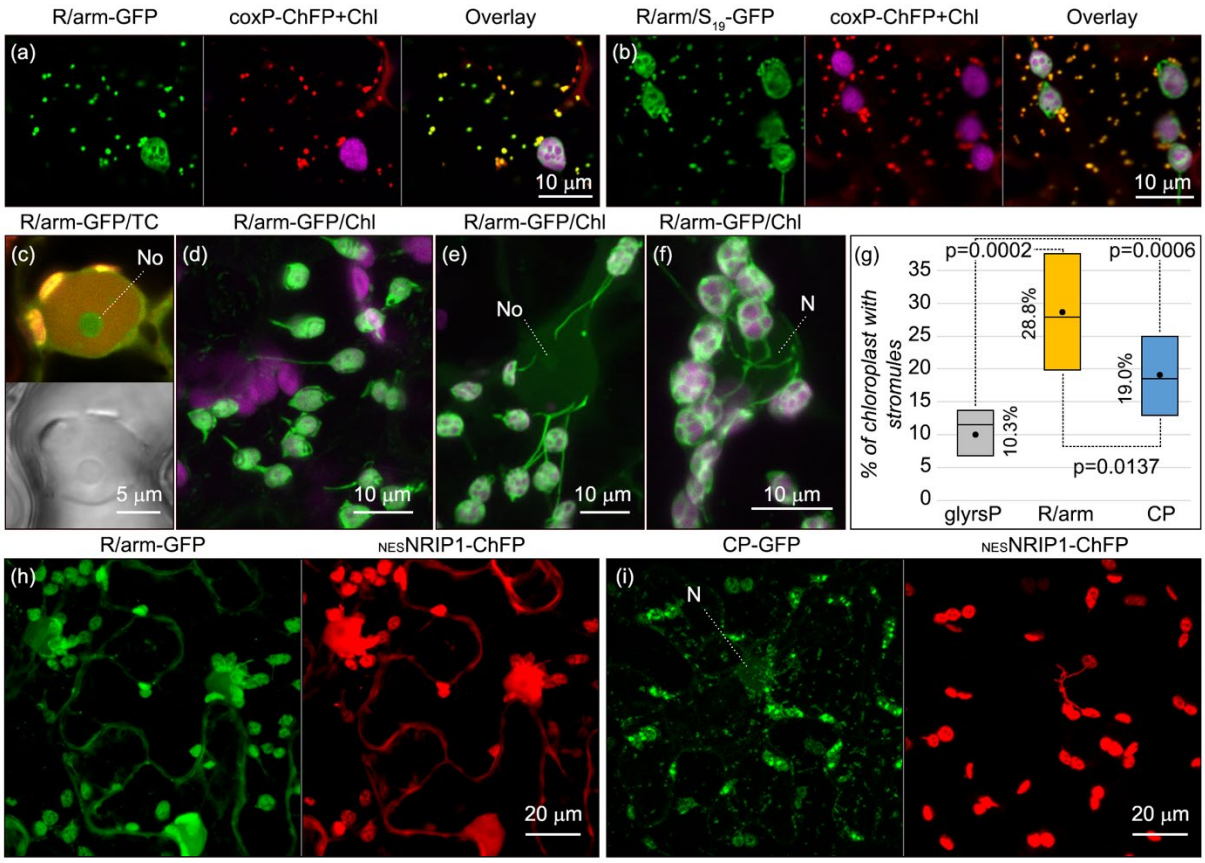

Figure 2. R/arm domain induces chloroplast stromule extension towards nucleus leading to chloroplast-to-nucleus communication. (a-b) Single scan images showing R/arm-GFP (a) and R/arm/S19-GFP (b) in chloroplasts (Chl, magenta) and mitochondria (coxP-ChFP). **(c)** Single scan image showing R/arm-GFP in the nucleolus (up) and the corresponding transmitted channel, TC (down). **(d-f)** CLSM images showing R/arm-GFP in chloroplast and stromules over the cytoplasm (d), near (e) and around (f) the nucleus, N. **(g)** Boxplot showing the percentage of NRIP-labelled chloroplasts with stromules in the presence of glyrsP-GFP, R/arm-GFP, and CP-GFP from three biological replicates. The lower and upper limits of the boxes are plotting the min and max values, respectively, whereas the lines dividing them represent the median values. Points inside boxes represent the mean from the three replicates, $p<0.05$ indicates statistical significance. **(h-i)** Coexpression of $_{NES}$NRIP1-ChFP with R/arm-GFP (H) or CP-GFP (i). Accumulation of $_{NES}$NRIP1-ChFP in the nucleus was higher upon R/arm-GFP than CP-GFP expression. Chl, chlorophyll autofluorescence in magenta. No, nucleolus. N, nucleus. Images correspond to Z-stack projections unless indicated.

Chloroplast perinuclear clustering and stromule induction appear to be a general response upon plant pathogen perception in *N. benthamiana* and could be elicited by ROS (Ding *et al.,* 2019; Krenz *et al.,* 2012). Besides, stromules have been shown to facilitate chloroplastic NRIP1 and reactive oxygen species transport to the nucleus during effector-triggered immunity (ETI) induced by the helicase domain (p50) of the tobacco mosaic virus (TMV) replicase, activating defense responses (Hanson and Hines, 2018). To examine whether stromule induction by R/arm-GFP is also accompanied by retrograde chloroplast-to-nucleus communication, we used a well-established approach based on the fusion of a nuclear export signal (NES) to NRIP1-ChFP N-terminus ($_{NES}$NRIP-ChFP). Therefore, $_{NES}$NRIP-ChFP nuclear localization is only

possible when it travels through stromules from the chloroplast where both N-terminal transit peptide and NES are cleaved (Caplan *et al.,* 2015). CLSM analysis at 48 hpi revealed that, in addition to chloroplasts, $_{NES}$NRIP1-ChFP fluorescence was observed in the nucleus and cytoplasm when expressing with R/arm-GFP (Figure 2h) but not CP-GFP (Figure 2i) nor other controls such as GFP, CPΔ(R/arm)-GFP and glyrsP-GFP (Figure S4).

Dissecting R/arm domains reveals that the R1 subdomain is required but not sufficient for dual targeting.

To further define the sequences involved in CP targeting, we performed fine mapping of the R/arm domains by deletion analysis (Figure S3). Either removal of both the R and arm domains in CPΔ(R/arm)-GFP or only the R domain in CPΔR-GFP, completely abolished organelle targeting of both proteins that, instead, showed a nucleo-cytoplasmic localization (Figure 3a-b). Though some cytoplasmic background was observed, arm deletion in CPΔarm-GFP did not affect dual import (Figure 3c). Within the R domain, the amino acid composition of the first 30 positions is enriched in basic, hydrophobic, and proline residues. In contrast, acidic or helix breaker glycine residues are lacking (Figure S5), which matches with that described for dTPs (Ge *et al.,* 2014). Interestingly, asparagine instead of serine is also overrepresented. The next 30 positions in the R domain or those in the arm region show a more diverse composition. Therefore, we defined two R subdomains (R1 and R2) of 30 aa, including H1 and H2, respectively (Figure S2). Other mutants were generated by deleting each R subdomain either alone, CPΔR1-GFP and CPΔR2-GFP, or in combination with the arm region, CPΔ(R1/arm)-GFP and CPΔ(R2/arm)-GFP (Figure S3). CLSM analysis revealed that CPΔR1-GFP, CPΔ(R1/arm)-GFP, and CPΔ(R2/arm)-GFP showed a nucleo-cytoplasmic localization (Figure 3d, f, and g, respectively). Small bodies, which did not colocalize with coxP-ChFP, were occasionally observed in some cells expressing CPΔR1-GFP (Figure 3d, arrows). Proper import to mitochondria and chloroplasts was neither affected in CPΔR2-GFP, except for some cytoplasmic background (Figure 3e). The same result was observed in CP(R81A)-GFP harboring R81A mutation, which reduces CP RNA silencing suppression capacity (Serra-Soriano *et al.,* 2017) (Figure 3h). As expected, fluorescence nucleo-cytoplasmic distribution was observed in N-terminal GFP fusions (Figure S6). These results indicated that the R1 subdomain was essential but not sufficient for an efficient dual organelle import since either the R2 subdomain or arm region was also required.

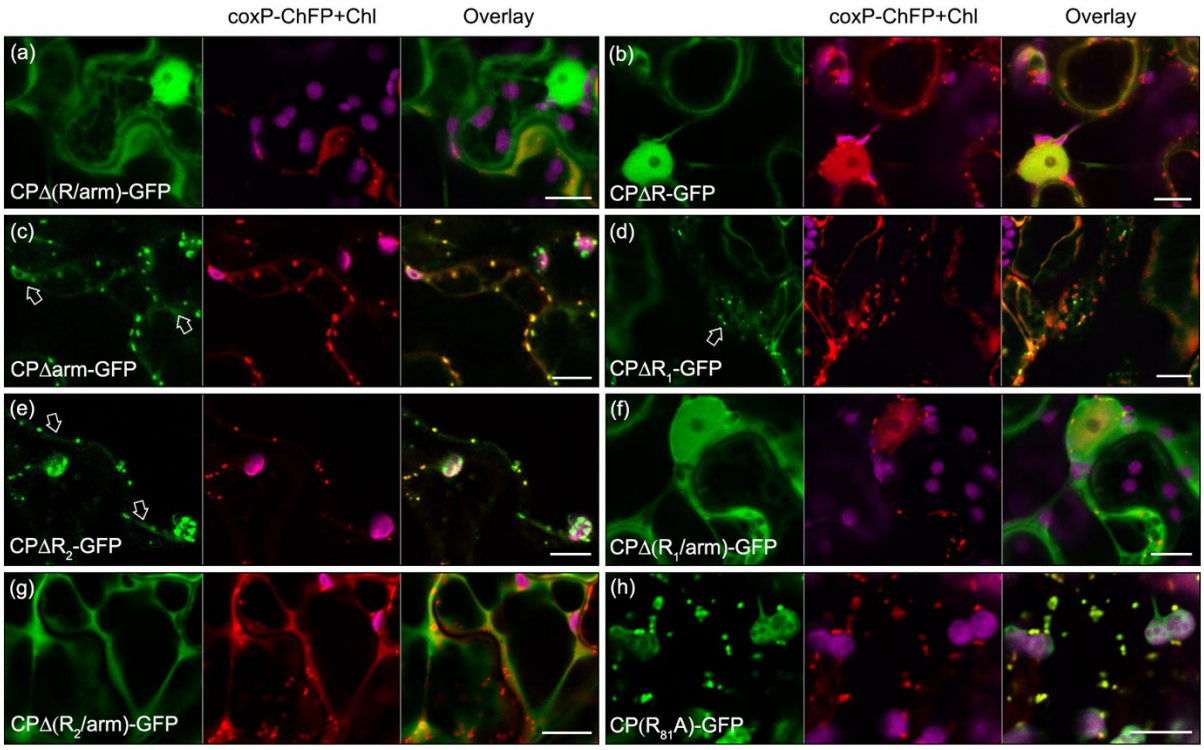

Figure 3. Subcellular localization of C-terminal GFP fusions of MNSV CP mutants in leaves of *N. benthamiana*. Each panel to the left corresponds to the indicated CP mutant. Panels in the middle are merged images showing coxP-ChFP and chlorophyll (Chl, magenta). Each panel to the right shows the overlay of the above two panels. Arrows in (c) and (e) pointed at cytoplasmic fluorescence, whereas the arrow in (d) pointed to CPΔR1-GFP spots not colocalizing with mitochondria. Scale bars: 10 µm. Images correspond to single scans.

Immunoblot analyses showed that the size of nucleocytoplasmic GFP-tagged CPs was as theoretically estimated (Figure S7a). In contrast, the size of CP-GFP, CPΔarm-GFP, and CPΔR2-GFP, which were dually targeted, was smaller than predicted but similar to CPΔ(R/arm)-GFP. Full-length CPΔarm-GFP and CPΔR2-GFP were slightly detected, most likely associated with the cytoplasmic fluorescence observed in these proteins (Figure S7b). Besides, R/arm-GFP or R/arm/S19-GFP size was similar to GFP (Figure S7c). Together, these results indicate that fusion proteins properly imported to both organelles undergo proteolytic R/arm region cleavage as estimated by size comparison.

MNSV CP has an R_1 subdomain-dependent localization to mitochondria, chloroplasts, and mitochondrial-derived VRCs during infection.

To rule out the possibility that MNSV CP dual localization could be due to high protein abundance during transient expression from 35Sx2 promoter or different posttranslational mechanisms occurring in healthy vs infected cells, we evaluated CP-GFP localization when expressed under the control of its promoter during infection. To do that, GFP was inserted

into the MNSV construct behind CP, generating pMNSV(CP-GFP). In vitro transcripts were inoculated in *N. benthamiana* leaves, and CLSM analysis at five dpi revealed small fluorescent infection foci (Figure 4a and Movie S2). Some differences were found between mesophyll and epidermal cells most likely representing early or late stages of infection, respectively. In the formers, CP-GFP fluorescence was mainly localized to chloroplast stroma and occasionally in stromules (Figure 4a, inset). The spotted distribution around chloroplast, described above, was rarely observed except in mesophyll cells at the leading edge of the focus, which corresponds to a very early stage of the infection (Figure 4b).

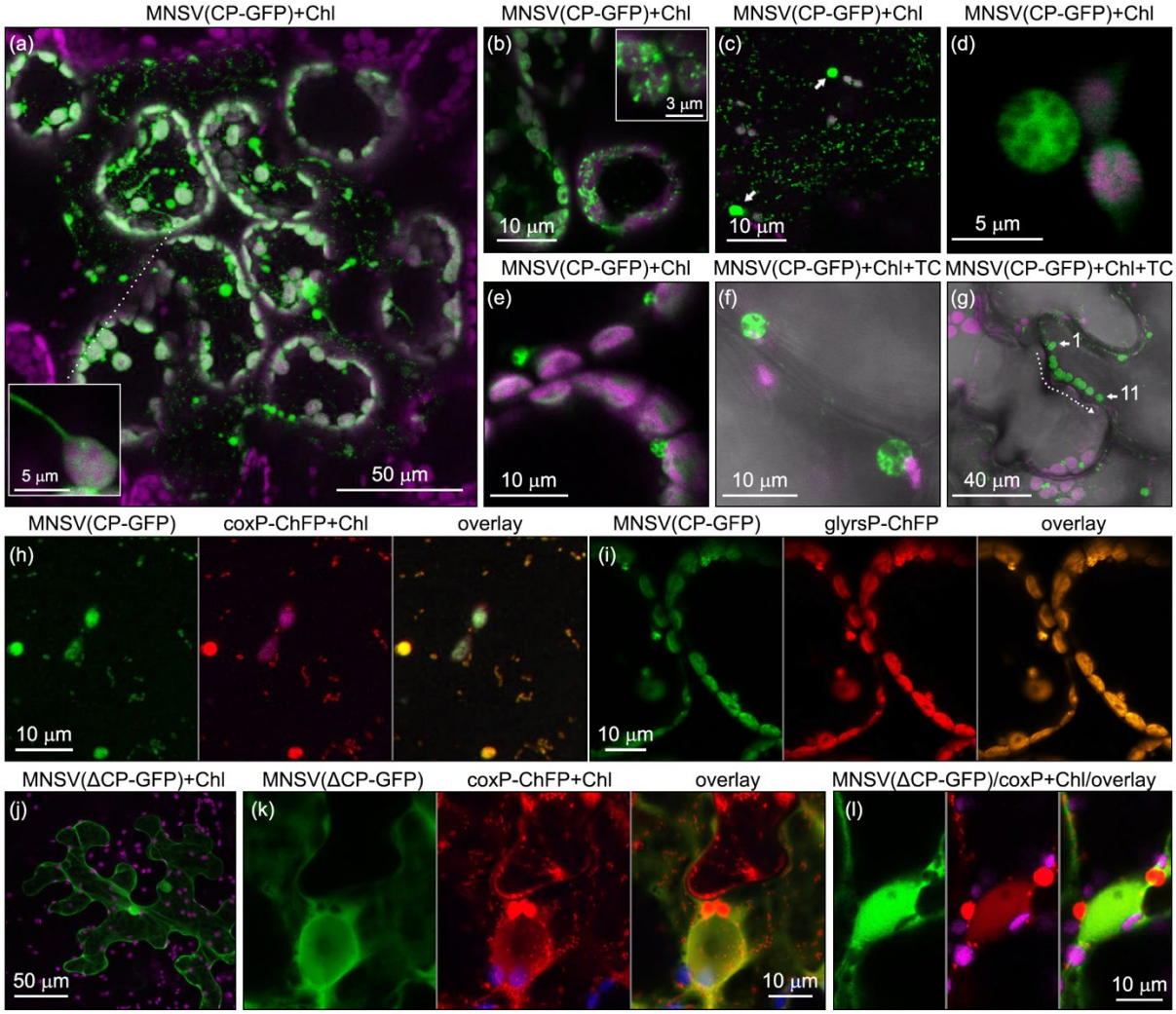

Figure 4. CP-GFP subcellular localization during MNSV infection in leaves of *N. benthamiana* at five dpi. (a) CLSM image showing an MNSV(CP-GFP) infection focus. Inset, Single scan showing a chloroplast with CP-GFP in the stroma and extended stromule. **(b)** CLSM showing mesophyll cells at the MNSV(CP-GFP) infection focus edge. Inset, chloroplasts with CP-GFP envelope-associated spots. **(c)** CLSM image showing CP-GFP fluorescence in chloroplasts, small bodies resembling mitochondria, and round structures (arrows) in epidermal MNSV(CP-GFP) infected cells. **(d)** Single scan of a mitochondrial-derived round structure showing uneven fluorescence distribution inside. **(e-f)** Single scans of the adjacent region between two mesophyll (e) or epidermal

(f) MNSV(CP-GFP) infected cells showing the peripheral localization of mitochondrial-derived round structures. (g) Stack projection of 11-time series scans (frame time 0.78 s) showing the displacement of a mitochondrial-derived round structure from positions 1 to 11. **(h-i)** Colocalization of CP-GFP with the mitochondrial marker coxP-ChFP (h) and dual marker glyrsP-ChFP (i) in MNSV(CP-GFP) infected cells. **(j-l)** CLSM images showing MNSV(ΔCP-GFP) infected epidermal cells, either alone (in j) or together with the mitochondrial matrix marker coxP-ChFP (in k-l). Chl, chlorophyll in magenta. TC, transmitted channel. CLSM images correspond to Z-stack projections unless indicated.

In epidermal cells, CP-GFP fluorescence was also found in chloroplasts, but mainly in small bodies resembling mitochondria and bigger round structures (13.00±3.43 per cell), which were about 3.34±1.20 µm in diameter (Figure 4c). These structures, which were less frequently observed in mesophyll cells (only 2.6±1.3 per cell in 30% of analyzed cells), showed an uneven internal distribution of fluorescence, which confers them the appearance of swollen mitochondria with inner vesicles (Figure 4d). The majority were peripherally located in mesophyll and epidermal cells, with some having a certain degree of mobility (Figure 4e-g and Movie S3). Colocalization of small bodies and round structures with coxP-ChFP and glyrsP-ChFP confirmed our assumption about their mitochondrial origin (Figure 4h-i). These swollen mitochondria were similar in form, size, internal organization, intracellular distribution, mitochondrial origin, and CP presence to MNSV VRCs previously described in melon (Gomez-Aix et al., 2015), suggesting that they could also constitute viral replication sites. In contrast, inoculation of MNSV(ΔCP-GFP), in which the CP was replaced by the GFP, resulted in local movement impairment since only single epidermal cells showing nucleo-cytoplasmic fluorescence were observed (Figure 4j). Therefore, CP-GFP must retain some degree of functionality allowing cell-to-cell movement of MNSV(CP-GFP). Altered mitochondria were still observed in MNSV(ΔCP-GFP) infected cells after transient expression of coxP-ChFP (Figure 4k-l).

To determine whether proteolytic processing also occurs during infection, MNSV CP was tagged at the C-terminus with influenza hemagglutinin (HA) epitope into an MNSV infectious construct, generating pMNSV(CP-HA). In addition, HA-tag was also inserted between the arm region and the S domain in pMNSV(CHAP). In vitro transcripts of wild type and both HA-tagged MNSV constructs were inoculated in *N. benthamiana* leaves. The amounts of viral RNAs and HA-tagged CPs were analyzed at different days post-inoculation (dpi). Regardless of whether the CP was HA-tagged or not, MNSV genomic and subgenomic RNAs were early detected at 2-3 dpi and highly accumulated at 6 dpi (Figure 5a). At 7-8 dpi, similar necrotic lesions were

observed in all inoculated leaves (Figure 5b). At 3-4 dpi, CP-HA and CHAP immunodetection resulted in two bands of approximately 35.04±0.24 and 32,07±0,33 kDa (Figure 5c and d, respectively), identical to those observed when CP-HA was produced by agroinfiltration (Figure 5c), and resembling the pattern of the cleaved products reported after immunodetection of CNV CP (Ghoshal et al., 2015). This observation indicates that MNSV CP could be transported to mitochondria and chloroplasts also during infection undergoing N-terminal processing. At 8 dpi, a band of 44,09±0.33 kDa corresponding either to the whole CP-HA or CHAP (theoretical size: 43.03 kDa) was detected. However, the intensities of bands corresponding to the cleaved CP were always higher than that of the complete ones. These results contrast with what was found in CNV infection, where only 1-5% of the CP was reported to target chloroplasts and mitochondria (Xiang et al., 2006).

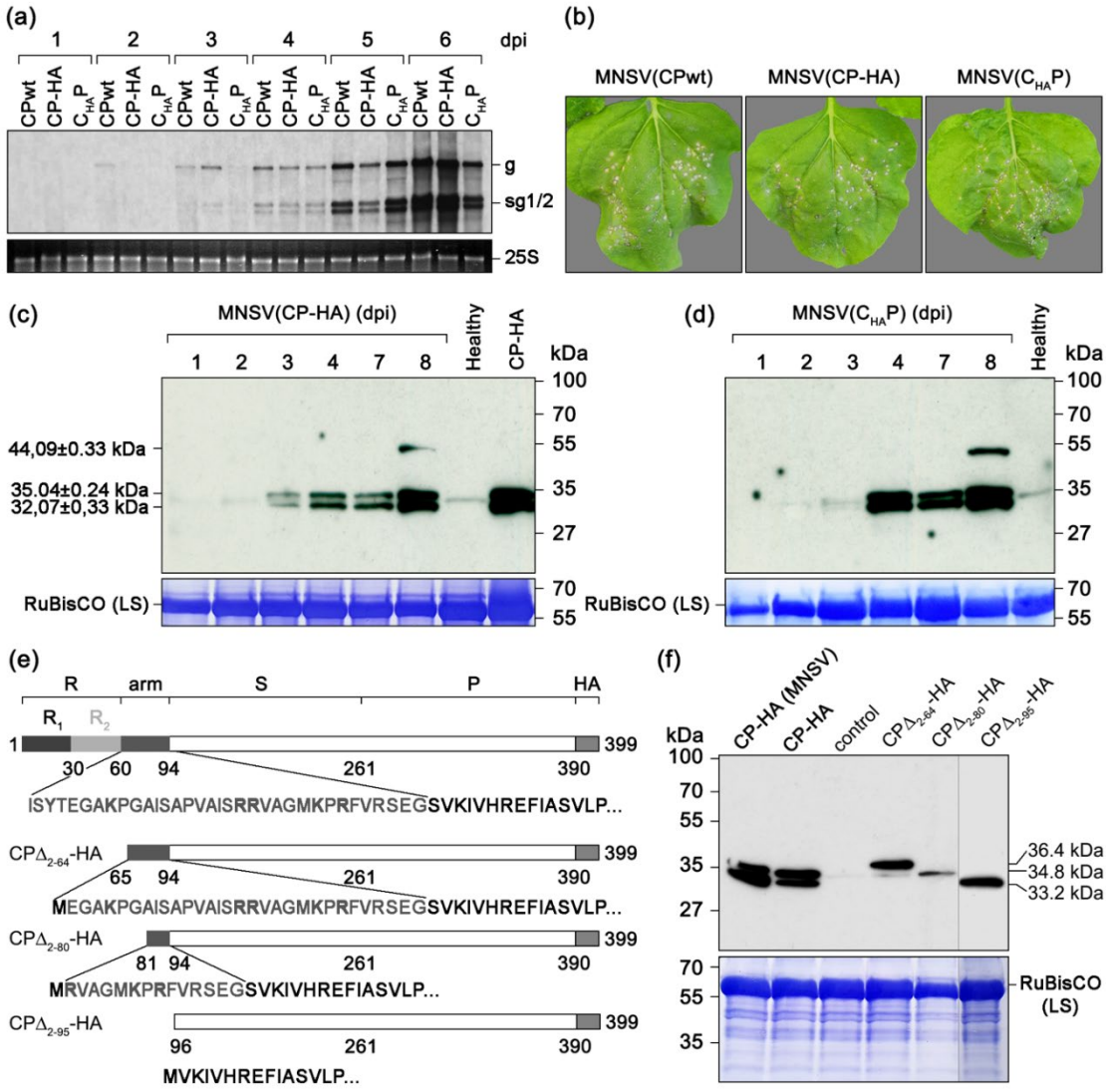

Figure 5. CP-HA undergoes cleavage at two different points during both infection and agroinfiltration. **(a)** Northern blot analysis of MNSV RNAs at the indicated days post-inoculation. The position of genomic and

both subgenomic RNAs is indicated. Ethidium staining of ribosomal RNA 25S is shown as loading control. **(b)** Images of *N. benthamiana* leaves inoculated with the indicated viral RNAs taken at 8 dpi. **(c-d)** Immunodetection of CP-HA and $C_{HA}P$ expressed from MNSV genome during local infection of *N. benthamiana* at the indicated dpi (MNSV(CP-HA)). The last track in (c) corresponds to CP-HA obtained 48 h after agroinfiltration of a binary plasmid in *N. benthamiana.* Leaves from three plants were analyzed at each time point and mixed in one sample. The molecular weight of the resulting bands was estimated by linear regression and indicated. **(e)** Schematic representation of the MNSV CP domains (R, arm, S, and P plus the HA tag) and the three CP-HA deletion proteins starting at position 65 ($CP\Delta_{2\text{-}64}$-HA), 81 ($CP\Delta_{2\text{-}80}$-HA), and 96 ($CP\Delta_{2\text{-}95}$-HA). (f) Size comparison of the two CP-HA cleavage products obtained either from MNSV infection or agroinfiltration with $CP\Delta_{2\text{-}64}$-HA, $CP\Delta_{2\text{-}80}$-HA, and $CP\Delta_{2\text{-}95}$-HA by Western blot. The size of $CP\Delta_{2\text{-}64}$-HA, $CP\Delta_{2\text{-}80}$-HA, and $CP\Delta_{2\text{-}95}$-HA is indicated on the right. Coomassie blue stainings are shown as loading controls. The positions of the protein molecular weight markers with sizes in kDa are indicated.

Considering the estimated size of the bands and the results previously published about CNV CP, three MNSV CP-HA deletion proteins starting at position 65 ($CP\Delta_{2\text{-}64}$-HA), 81 ($CP\Delta_{2\text{-}80}$-HA), and 96 ($CP\Delta_{2\text{-}95}$-HA) were designed (Figure 5e). After agroinfiltration, the three proteins were analyzed by western blot, and their migration was compared with CP-HA (Figure 5f). The upper and lower cleavage products obtained from both MNSV(CP-HA) infection or CP-HA agroinfiltration co-migrated with $CP\Delta_{2\text{-}80}$-HA and $CP\Delta_{2\text{-}95}$-HA, indicating that CP processing in mitochondria and chloroplasts may occur at two different but close points, one of them within the arm region but near the arm/S domain junction where most likely the second one occurs, as previously described for CNV CP (Ghoshal et al., 2015).

To further evaluate whether R/arm-GFP expression during infection also acts as a cytopathogenic elicitor, we generated pMNSV(R/arm-GFP) by deleting both S and P domains in pMNSV(CP-GFP). Although very small multicellular foci were occasionally observed (Figure 6a), the infection was mainly restricted to single cells at five dpi (Figure 6b). R/arm-GFP localization in multicellular foci was similar to that described above for CP-GFP in MNSV(CP-GFP) except that VRCs were more frequently detected. Approximately 70% of mesophyll cells displayed numerous VRCs ubiquitously distributed throughout the cell (Figure 6a, inset). VRC number per mesophyll cell was also significantly higher than that observed in MNSV(CP-GFP) foci (12.36±7.87, t=4 and p=0.0021), although no difference was observed between epidermal cells (12.83±4.07, t=0.086 and p=0.9). In contrast, no fluorescence-labeled VRCs were detected in unicellular foci. Instead, most chloroplasts extended stromules to and contacted the nucleus forming perinuclear clusters as occurred upon transient R/arm-GFP expression (Figure 6b-d). Moreover, colocalization with coxP-ChFP revealed that mitochondria in these unicellular foci mainly showed an abnormal ring-shaped morphology similar to spheroids and

annular mitochondria observed in animal cells and Arabidopsis protoplasts, respectively, before stress-induced cell death (Scott and Logan, 2008; Miyazono et al., 2018) (Figure 6e-f).

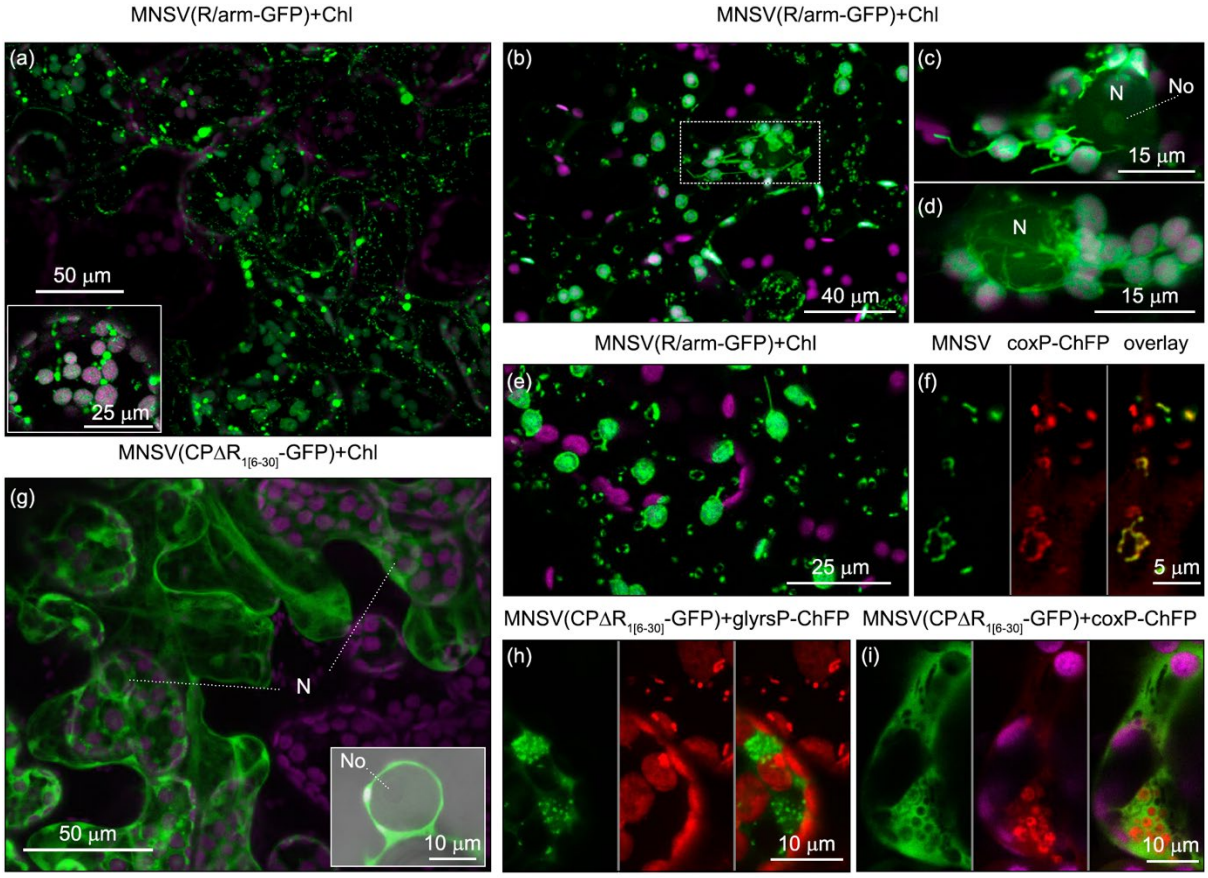

Figure 6. Subcellular localization of R/arm-GFP and CPΔR$_{1[6-30]}$-GFP during MNSV infection in leaves of *N. benthamiana* at 5 dpi. (a) CLSM image of a local MNSV(R/arm-GFP) infection foci. R/arm-GFP fluorescence was found in chloroplasts, normal and swollen mitochondria (VSM). Inset shows an infected mesophyll cell. **(b)** CLSM image of an isolated single cell infected by MNSV(R/arm-GFP). Single scan magnification of the dotted rectangle is shown in **(c)**. A detailed view of a juxtanuclear cluster of chloroplasts and cytoplasm with ring-shaped mitochondria are shown in **(d)** and **(e)**, respectively. **(f)** Single scan images showing colocalization of ring-shaped mitochondria with coxP-ChFP. **(g)** CLSM image of a local MNSV(CPΔR$_{1[6-30]}$-GFP) infection foci. Inset shows CPΔR$_{1[6-30]}$-GFP fluorescence in the cytoplasm around the nucleus merged with the transmitted channel. **(h)** CLSM images of two adjacent mesophyll cells showing the different distribution of mitochondria (coxP-ChFP) between the MNSV(CPΔR$_{1[6-30]}$-GFP) infected cell on the left, and the healthy one, on the right. **(i)** Single scan of an MNSV(CPΔR$_{1[6-30]}$-GFP) infected mesophyll cell showing a large and single cluster of mitochondrial-derived round structures labeled with coxP-ChFP. Chl, chlorophyll in magenta. TC, transmitted channel. CLSM images correspond to Z-stack projections unless indicated.

To study the relevance of the R1 subdomain in CP import during infection, an additional construct, pMNSV(CPΔR$_{1[6-30]}$-GFP), containing a deletion of the aa positions 6-30, was made. Due to overlapping between contiguous p7B and CP ORFs, the first five aa positions (MAMVR) of the R$_1$ subdomain remained. After 4-5 days post-inoculation, only small multicellular foci were detected showing CPΔR$_{1[6-30]}$-GFP fluorescence in the cytoplasm but not in the nucleus

of both mesophyll and epidermal cells (Figure 6g and Movie S4). Some cells also showed small bodies that did not colocalize with dual marker glyrsP-ChFP (Figure 6h). Expression of coxP-ChFP also confirmed the presence of VRCs in infected mesophyll cells, but they were found in groups or even forming a single large cluster consisting of more than 15 units (Figure 6i). This situation contrasts with that observed in mesophyll cells infected with MNSV(CP-GFP) or MNSV(R/arm-GFP), suggesting that although CP is not necessary for VRC formation, it could modulate their biogenesis and dynamic behavior.

MNSV p29 auxiliary replicase was localized at the boundaries of swollen mitochondria that form ER-associated small clusters and large juxtanuclear aggregates.

To further evaluate the contribution of p29 in mitochondrial modification, VRC formation, and its relationship with CP, we ectopically expressed a fluorescent-tagged p29 either alone or in combination with a mitochondrial matrix marker or CP. When p29 was expressed alone, the most striking observation, not described previously, was the appearance of a large round-shaped structure (11.95±2.22 µm in long axis) near the nucleus, together with free and vesicle-associated punctate bodies over the cytoplasm in epidermal cells (Figure 7a-b) or peripherally located in mesophyll cells (Figure 7c). Single scan analysis along Z-axis revealed that juxtanuclear structures consisted of a large cluster of size-heterogeneous vesicles showing uneven p29-GFP accumulation around them (Figure 7a, inset and Movie S5). Interestingly, large clusters and cytoplasmic bodies/vesicles were found in association with the ER (Figure 7d). To assess the nature of these structures, the mitochondrial matrix marker coxP-ChFP and p29-GFP were coexpressed. In a general view, both proteins appeared to overlap partially (Figure 7e-f) but, magnification images revealed that coxP-ChFP was actually in close association with the p29-labelled cytoplasmic bodies or inside vesicles (Figure 7g-h). Accordingly, coxP-ChFP and p29-GFP aggregated together in juxtanuclear structures as before (12.14±1.67 µm in long axis, $t=0.33$, and $p=0.73$), but their distribution profiles were opposite to each other, suggesting different localization. p29 could be associated with membranes of altered mitochondria, as reported previously, and coxP-ChFP in the matrix (Figure 7i-k). On the other hand, upon coexpression with p29-ChFP, CP-GFP fluorescence was observed inside p29-GFP-labelled vesicles in smaller juxtanuclear structures (9.87±2.34 µm in long axis, $t=3.4$, and $p=0.0015$) (Figure 7l-m), indicating that CP-GFP behaved as a mitochondrial matrix protein.

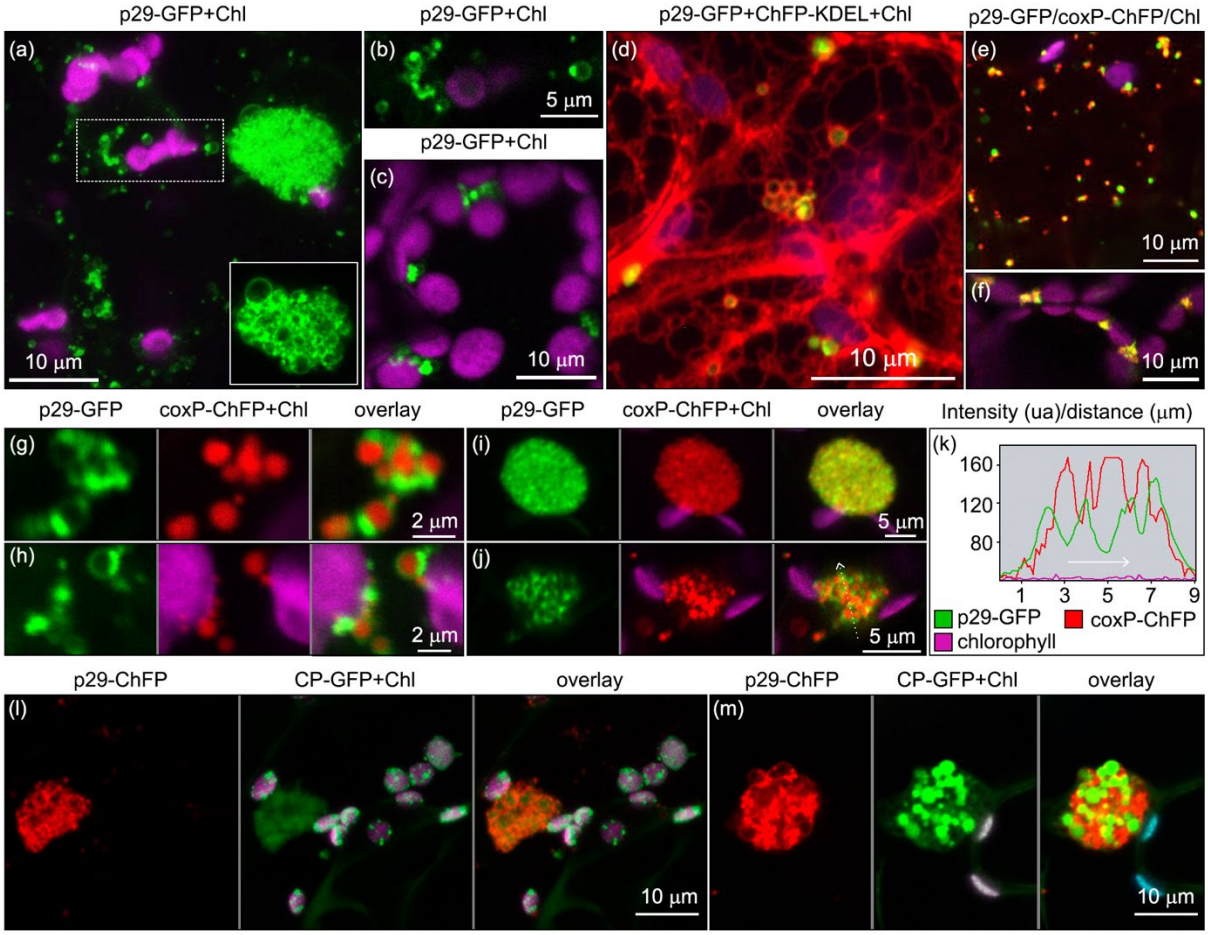

Figure 7. Transient expression of p29 auxiliary replicase can induce mitochondrial swelling and aggregation in leaves of *N. benthamiana*. **(a)** p29 subcellular localization in epidermal cells. A juxtanuclear structure single scan is shown on the bottom inset. **(b)** Single scan magnification of the dotted rectangle in (a). **(c)** Single scan showing p29-GFP bodies and vesicles peripherally located in mesophyll cells. **(d)** p29-GFP localization in the nuclear envelope, ER and ER-associated bodies. **(e-f)** Coexpression of p29-GFP and coxP-ChFP in epidermal (e) and mesophyll (f) cells. **(g-h)** Single scans showing p29-labeled cytoplasmic vesicles containing coxP-ChFP. **(i)** coxP-ChFP localization in a large oval-shape aggregate upon coexpression with p29-GFP. **(j)** Single scan showing the differential distribution of coxP-ChFP and p29-GFP in large aggregates. **(k)** Fluorescence intensity profile of indicated fluorophores plotted versus distance along the arrow in (j). **(l)** CLSM image showing CP-GFP localization in a large aggregate near the nucleus upon coexpression with p29-ChFP. **(m)** Single scan showing an aggregate of p29-ChFP labeled vesicles showing CP-GFP fluorescence inside.

MNSV CP import into mitochondria and chloroplasts could prevent p29-induced necrosis but compromises RNA silencing suppressor and encapsidation capacities.

Mochizuki *et al*. showed that p29 expressed from a CMV-based vector modifies mitochondrial membrane structures generating mitochondrial damage and necrosis in *N. benthamiana* (Mochizuki *et al.,* 2009). Accordingly, we have shown that p29 transient expression induced mitochondrial swelling and juxtanuclear aggregation but also triggered necrosis in localized areas at 5-6 dpi in single expression or together with GFP, CP□(R/arm)-GFP, and R/arm-GFP (Figure 8a). Necrosis was most prominent and affected the whole leaf when p29 was

coexpressed either with the silencing suppressor HCPro of tobacco etch virus or CPΔR_1-GFP. Instead, p29-HA coexpression with CP-GFP either abolished (left side of the panel) or considerably reduced (right side of the panel) necrosis appearance. Western blot analysis performed at 1, 2, 3, and 4 dpi, before necrosis appearance, showed that the levels of p29-HA in the presence of GFP, CPΔ(R/arm)-GFP, R/arm-GFP, or CP-GFP were not significantly different from each other (F=3.82, p=0.058), but all of them were significantly lower than those found in HCPro and CPΔR_1-GFP coexpressions (F=75, p<0.0001, calculated at two dpi, and adjusted p values for multiple comparisons with CP are shown in Figure 8b). Northern blot analysis at two dpi was consistent with Western blot results since p29-HA mRNA accumulated more in the presence of HCPro, which showed the highest levels, or CPΔR_1-GFP, than CP and the rest of the proteins (Figure 8c). Therefore, the higher p29 levels, the greater is necrosis, but, at equal amounts, only the complete CP attenuated necrosis. In previous work, using 16c GFP-transgenic plant system, we showed that siRNA binding through the R2/arm region confers to CP and CPΔR_1, RNA silencing suppressor activity at systemic, but not local, level (Serra-Soriano *et al.,* 2017). The results presented here suggest that CPΔR_1 acts as a strong local suppressor favoring p29 expression but, in contrast to HCPro, this effect was only noticeable earlier after CPΔR_1 expression. This could be the reason for negative results in the 16c system since samples were analyzed at five dpi. To clarify this issue, we used a new approach based on an alfalfa mosaic virus (AMV) RNA 3 expression vector and transgenic *N. tabacum* plants that express the P1 and P2 subunits of the AMV replicase (P12 plants) (Martínez-Pérez *et al.,* 2019). This method is a fast and reliable technique based on the correlation between symptomatology on inoculated leaves and suppressor activity. According to reported data, inoculation of P12 leaves with AMV RNA 3 expressing CP or GFP did not produce local symptoms. In contrast, AMV RNA 3 expressing CPΔR_1 generated extended necrotic lesions (Figure 8d). These data together indicate that CPΔR_1 is more efficient than CP as a suppressor at local level. Nevertheless, to further investigate this notion, we introduced CPΔ$R_{1[6\text{-}30]}$-HA into the construct pMNSV(CPΔ$R_{1[6\text{-}30]}$-HA), and the corresponding transcripts were inoculated in *N. benthamiana*. Viral RNA and CPΔ$R_{1[6\text{-}30]\text{-}HA}$ accumulation in infected leaves were compared with those obtained with the wild-type variant at eight dpi (Figure 8e). Depending on the sample, MNSV(CPΔ$R_{1[6\text{-}30]}$-HA) RNA levels were lower than or similar to wild type, but the levels of the single uncleaved CPΔ$R_{1[6\text{-}30]}$-HA band, which was detected, were

consistently higher than those of the two cleaved CP-HA products obtained in wild type infection. Therefore, the potential of CP to suppress RNA silencing is compromised by its organelle targeting that implies its cytoplasmic depletion and its R/arm domain processing, a region essential for its role as RNA silencing suppressor (Serra-Soriano *et al.,* 2017).

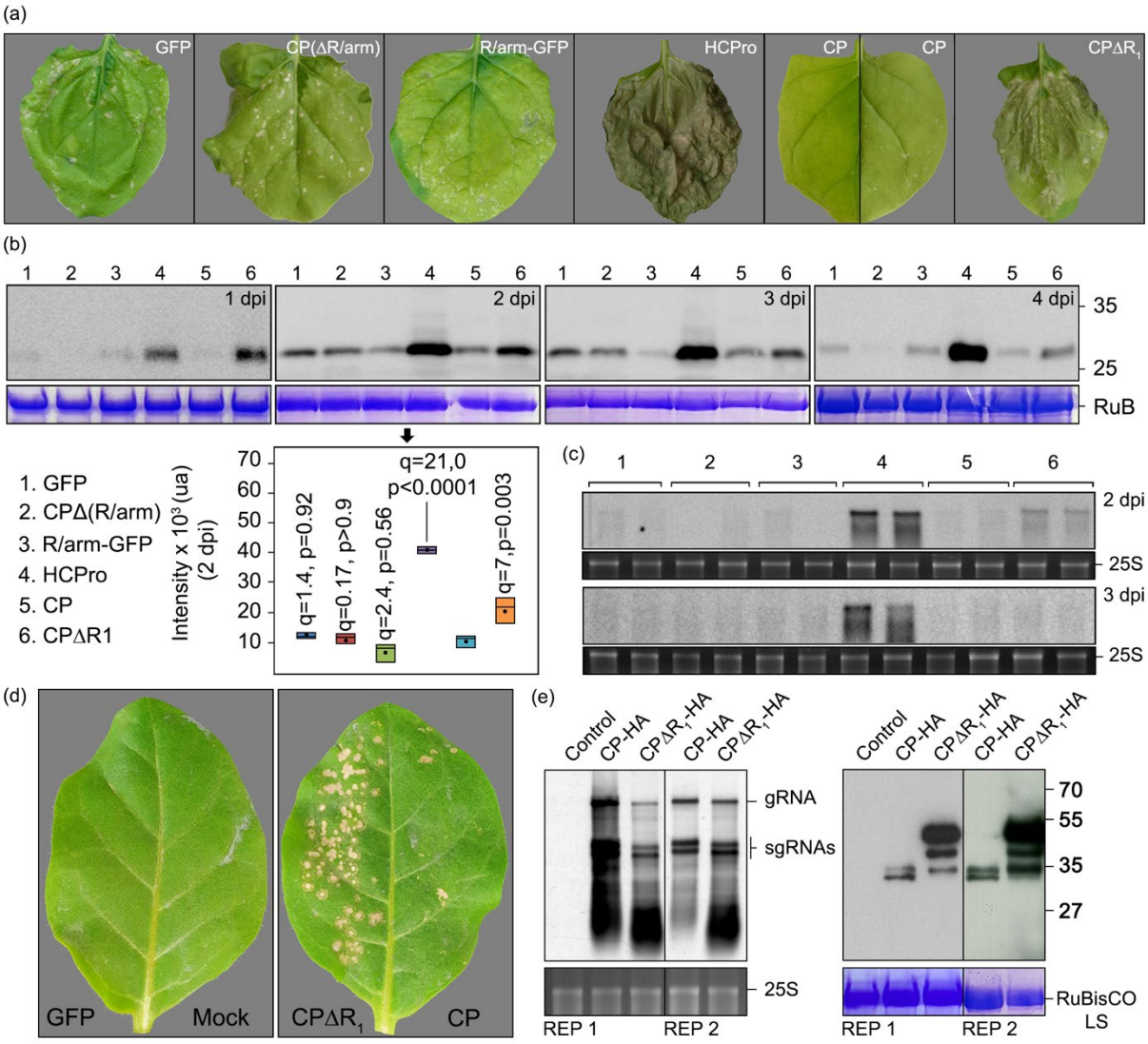

Figure 8. CP-GFP inhibition of p29-HA induced necrosis in transient expression assays and analysis of RNA silencing suppressor capacity of MNSV CPΔR1. (a) Effect of GFP, CPΔ(R/arm)-GFP, R/arm-GFP, CPΔR1, CP or TEV HCPro on p29-HA induced necrosis upon coexpression in leaves of *N. benthamiana*. Images were taken at six dpi. **(b)** Representative Western blot analysis to detect p29-HA in protein extracts from *N. benthamiana* leaves coexpressing the indicated proteins at 1,2, 3 and 4 dpi. Boxplot represents the chemiluminescence intensity of p29-HA band from three independent replicates at two dpi. The lower and upper limits of the boxes are plotting the min and max values, respectively, whereas the lines dividing them represent the median values. Points inside boxes represent the mean from the three replicates. $p<0.05$ indicates statistical significance. Coomassie blue staining of RuBisCO is shown as loading control. **(c)** Northern blot analysis from two independent replicates to detect p29-HA mRNA. RNAs were extracted from leaves coexpressing the indicated proteins at 2 and 3 dpi. Ethidium bromide staining of 25S ribosomal RNA is shown as loading control. **(d)** Comparison of the silencing suppressor activity of CP and CPΔR1, using AMV RNA 3 expression vector and transgenic P12 plants of *N. tabacum*. AMV RNA 3 transcripts expressing GFP, CP or CPΔR1 were inoculated on different leaf halves as

indicated. (e) Analysis of the accumulation of viral RNAs and CP in MNSV(CPΔR$_{1[6-30]}$-HA) and MNSV(CP-HA) by Northern blot (left) and Western blot (right), respectively. Three replicates were performed consisting of a tissue mix from three plants. Two of them are shown.

Considering that the R2/arm domain is also required for MNSV genome encapsidation (Serra-Soriano *et al.,* 2017), virus assembly could also be affected by CP processing upon organelle import. To examine this view, virions were isolated from photosynthetic (leaves and stems/petioles) and non-photosynthetic (roots) infected tissues. The process was repeated three times (two replicates are shown in Figure 9a) and consistently showed that virions accumulated in inverse proportion to the photosynthetic capacity of the tissue, higher in roots (10-20 times) and stems/petioles (5-10 times) than in leaves, where they were barely detected. To analyze whether the differential accumulation of virions could be related to different processing levels of the CP, we express CP-HA in *N. benthamiana* plants using a tobacco rattle virus (TRV)-based binary vector, TRV2$_{promPEBV}$[CP-HA] (MacFarlane and Popovich, 2000). This heterologous expression system ensures that transit peptide is not precluded by virion assembly and only uncoated CP is detected. A TRV vector expressing ChFP was generated, TRV2$_{promPEBV}$[ChFP], to visualize the virus spreading through the plant. One week after inoculation of *N. benthamiana*, TRV2$_{promPEBV}$[ChFP] fluorescence was observed in upper leaves, stems, and roots (Figure 9b). At this time, proteins from three TRV2$_{promPEBV}$[CP-HA] infected plants were extracted and analyzed by Western blot. According to that observed above during MNSV infection (Figure 4b), two CP-HA cleavage products of approximately the same size as before were detected (protein sizes calculated by regression analysis of electrophoretic mobility are shown in Figure 9c). Consistent with the tissue-specific accumulation of virions, full-length CP-HA (theoretical size 43.03 kDa) was detected in all root samples and, at least, in stem replicate two.

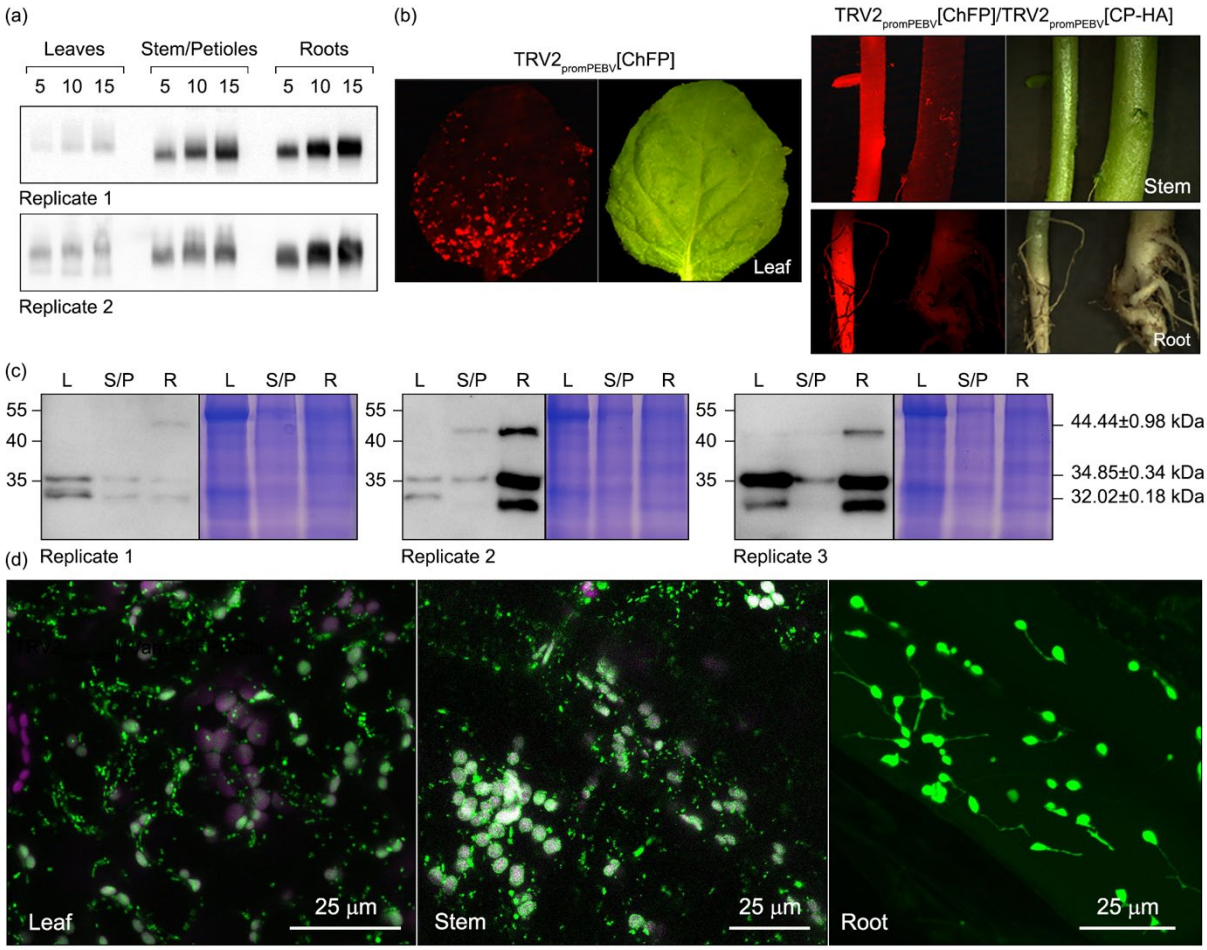

Figure 9. MNSV virion accumulation, CP-HA processing, and R/arm-GFP subcellular localization in leaves, stems, and roots. (a) Northern blot analysis of MNSV virions isolated from roots, stems, and petioles and leaves of MNSV infected *N. benthamiana* plants in two independent replicates. Equal extract volumes (5, 10, and 15) from the same fresh weight of each tissue were loaded. **(b)** Images of leaves, stems, and roots of *N. benthamiana* plants infected with $TRV_{promPEBV}$[ChFP] or $TRV_{promPEBV}$[CP-HA] taken under white or ultraviolet/rhodamine filter light one week after inoculation. **(c)** Western blot analysis to detect CP-HA expressed from a tobravirus-based vector in roots (R), stems and petioles (S/P), and leaves (L) of *N. benthamiana*. Results from three different plants are shown. Coomassie blue staining is shown as loading control. Protein sizes calculated by regression analysis of electrophoretic mobility are shown on the right. The positions of the protein molecular weight markers with sizes in kDa are indicated on the left. **(d)** Confocal images of cells from leaves, stems, and roots of *N. benthamiana* plants infected with TRV1 plus $TRV2_{promPEBV}$[R/arm-GFP] one week after inoculation.

In contrast, no full-length CP was observed in leaves. In any case, a high proportion of processed CP was still observed in all tissues. To explain this, we analyzed CP subcellular localization in stems and roots with an additional TRV vector expressing R/arm-GFP, $TRV2_{promPEBV}$[R/arm-GFP]. One week after inoculation, $TRV2_{promPEBV}$[R/arm-GFP] fluorescence was observed in mitochondria and chloroplasts of upper leaves and stems (Figure 9d). In roots, R/arm-GFP labeled non-photosynthetic plastids, since chlorophyll fluorescence was not detected, mainly clustered around the nucleus and showing long stromules. This targeting of

the R/arm-GFP to non-photosynthetic plastids could explain the high degree of CP-HA processing still observed in this tissue. Moreover, fluorescent mitochondria were also detected in roots but compared with green tissues, considerably fewer of them were observed.

Effect of R/arm CP mutations on MNSV infectivity and HR-related gene expression.

To explore how CP mutations affected MNSV infection in *N. benthamiana*, two-week-old seedlings were inoculated with in vitro transcripts of MNSV and all N-terminal deletion mutants used in this study as well as $R_{81}A$ point mutant. Five days later, leaves inoculated with MNSV-CPΔR_1 or MNSV-CP($R_{81}A$) showed necrotic or chlorotic symptoms, respectively, whereas the rest of the mutants caused no local symptoms. MNSV-CPΔ(R/arm) was taken as representative of symptomless variants for further analysis (Figure S8). Necrotic lesions generated by MNSV-CPΔR_1 were significantly smaller than those observed in wild-type MNSV infections (0.78±0.47 vs 2.17±1.07 mm2, t=5.8, p<0.0001). At 15 days post-inoculation, necrosis nearly or fully covered MNSV inoculated leaves whereas, in MNSV-CPΔR_1, local symptoms still consisted of well-defined necrotic lesions (3.73±1.35 mm2) (Figure S8). Only 2 out of 30 (6.7%) plants inoculated with MNSV-CPΔR_1, versus 27 out of 30 (90%) of those inoculated with MNSV, showed systemic symptoms (Figure S8). Those consisted of necrosis associated with local lesions, chlorotic in the beginning, stems and interveinal tissue of upper leaves, leaf malformation, dwarfing, and occasionally plant death (Figure S8). All plants inoculated with MNSV-CP($R_{81}A$), and the rest of the mutants remained symptomless at systemic level. MNSV systemic infection was confirmed by dot-blot hybridization analysis (Figure S8).

Samples from inoculated leaves were collected at five dpi and total RNA extracted. Although CPΔR_1 could enhance early viral replication compared to CP($R_{81}A$), the northern-blot analysis revealed that MNSV-CPΔR_1 and MNSV-CP($R_{81}A$) RNAs accumulated similar to each other (q=1.9, p=0.58) although significantly lower than wild-type viral RNAs (q=7.6, p=0.003; q=9.5, p=0.0007, respectively). In contrast, RNAs from MNSV-CPΔ(R/arm), which was selected as representative of symptomless mutants, were barely detected compared to wild-type viral RNAs (q=17.5, p<0.0001) (Figure 10a). All events described here, including mitochondrial swelling and aggregation, stromules induction, as well as necrosis and systemic resistance, are

consistent with a hypersensitive response (HR) (Scott and Logan, 2008; Mur *et al.,* 2007). To impede pathogen spreading, HR causes the rapid death of cells at the initial point of infection concurrent with the production of ROS and defense gene upregulation (Heath, 2000). Therefore, we examined the RNA expression of ZAT10, a regulatory transcription factor for oxidative stress signaling (Fujita *et al.,* 2009), APX2, an antioxidant cytosolic ascorbate peroxidase (Caverzan *et al.,* 2012), HR markers HIN1 (Gopalan *et al.,* 1996) and HSR203J (Pontier *et al.,* 1998) and pathogenesis-related PR1 (van Loon, 1997) genes by quantitative real-time reverse transcription PCR (qRT-PCR) shown in Figure 10b. PCR results indicated that, except for APX2, all markers were induced in MNSV and MNSV-CP□R1 infections in the same order of magnitude (Figure 10b). HIN1 and PR1 were strongly upregulated to levels similar to those seen in homologous HIN1 (Li *et al.,* 2012) and other members of the PR family (Fister *et al.,* 2016) under biotic stress. In comparison to HIN1, a lower induction was observed for the second HR marker HSR203J (4-5 fold). Nevertheless, it has been described that HSR203J and HIN1 are induced approximately at the same order of magnitude early upon pathogen attack, but when necrosis appeared, HIN1 upregulation further increased while HSR203J induction fell to one-tenth of HIN1 (Li *et al.,* 2012). Considering that MNSV infected samples were taken at five dpi when necrosis was macroscopically visible, HSR203J mRNA levels might be within the expected values. Concerning ZAT10, it was 14 and 11-fold induced in MNSV and MNSV-CPΔR_1 infections, respectively. These values are similar to those reported for abiotic (Rossel *et al.,* 2007) and biotic stresses such as the induced by the necrotrophic fungus Botrytis cinerea in Arabidopsis (AbuQamar *et al.,* 2006). Compared with previous data, PR1 was barely induced (6-fold) in non-necrotic MNSV-CP(R_{81}A) and MNSV-CPΔ(R/arm) infection, whereas the rest of the markers were not significantly induced. APX2 was not significantly upregulated in any case ($F=2.17$, $p=0.15$).

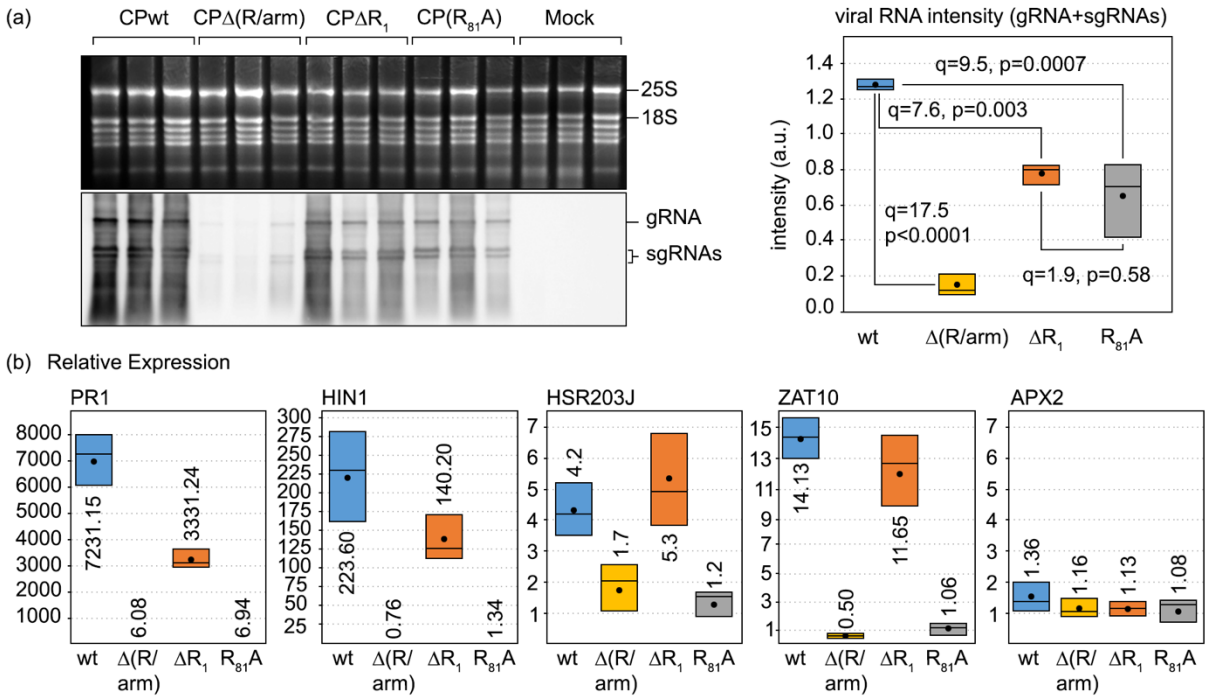

Figure 10. Analysis of ZAT10, HIN1, HSR203J, and PR1 gene expression by qRT-PCR in *N. benthamiana*. **(a)** Northern blot to detect MNSV RNAs in MNSV, MNSV-CPR_1, MNSV-CP$_{R81A}$, and MNSV-CPΔ(R/arm) inoculated leaves. Ethidium bromide staining of ribosomal RNAs is shown as loading control. RNAs from leaf pools of three independent assays are shown. Boxplot represents the genomic plus subgenomic MNSV RNA band chemiluminescence intensities from three replicates. Points inside boxes represent the mean from three replicates. $p<0.05$ indicates statistical significance. **(b)** Relative expression of PR1, HIN1, HSR203J, and ZAT10 genes analyzed by qRT-PCR in RNA samples from leaves inoculated with MNSV and the indicated mutants at five dpi. Mock corresponds to RNAs from leaves rubbed with inoculation buffer. Boxplots represent the relative expression in three biological replicates. The lower and upper limits of the boxes are plotting the min and max values, respectively, whereas the lines dividing them represent the median values. Points inside boxes represent the mean from the three replicates. $p<0.05$ indicates statistical significance.

DISCUSSION

Dual targeting is emerging as an evolutionary solution for some plant pathogens, constrained by small genomes, to expand and diversify protein function. However, only a few examples of dual targeting to mitochondria and chloroplasts, mainly including some fungus effectors and CNV CP, have been described (Liu *et al.,* 2018; Petre *et al.,* 2015; Hui *et al.,* 2010). Here we show that MNSV CP is also dually targeted to these organelles during ectopic expression, as well as to mitochondrial-derived VRCs in infected cells, and unravel the implications that this ambiguous targeting has on the viral infection cycle. Prediction analysis revealed that mitochondrial and/or chloroplast targeting could be extended among tombusvirus CPs, indicating that MNSV CP similarity is beyond structural features. Sequences in the R/arm domain were required in MNSV and CNV CP import, but we found some differences in dTP

structural organization. Mitochondrial and chloroplast targeting information rely on distinct regions in CNV dTP (Hui *et al.,* 2010), whereas MNSV dTP seems to contain a unique ambiguous signal. It is known that sorting information is mainly localized within the 19 N-terminal amino acids of transit peptides. Accordingly, the R_1 subdomain showed similar mTP and cTP traits except for the presence of polar asparagine instead of serine (Berglund *et al.,* 2009; Ge *et al.,* 2014). This bias towards nitrogenous asparagine was observed in the apicoplast transit peptide of the malaria parasite Plasmodium falciparum, which was hypothesized to be caused by differences in codon usage and nitrogen disposal (Ralph *et al.,* 2004). R_1 subdomain was shown to be essential but not sufficient for CP organelle import since, regardless of their primary structure, either R_2 subdomain or arm regions were also required. As previously described for some Arabidopsis proteins, a 60 aa minimum length could be necessary since it was proposed that longer than 20 aa spacer between cTP and mature protein relieves steric hindrance, enabling the binding of essential translocators (Shen *et al.,* 2017; Berglund *et al.,* 2009). Therefore, R_2/arm regions, which are relevant RNA binding domains (Serra-Soriano *et al.,* 2017), are acting here as a mere spacer between R_1 and the folded S domain.

Developmental and physiological states of mitochondria and chloroplasts play a role in sensing environmental conditions and eliciting adaptive plant responses. In this process, coordinated organelle-to-nucleus retrograde signaling, which results in nuclear expression changes and, occasionally, cell death, is essential (Reape *et al.,* 2015; Wang *et al.,* 2020). Also, mitochondria and chloroplasts have been revealed as critical organelles in regulating plant-virus interactions (Li *et al.,* 2016; Zhao *et al.,* 2016). Mitochondria and chloroplasts can coordinate plant defense response and cell death through shared retrograde signaling pathway components, some of them targeting both organelles (Wang *et al.,* 2020; Yang *et al.,* 2021). Moreover, several key antioxidative enzymes in the ascorbate-glutathione cycle and mitochondrial anti-apoptotic proteins from animals are also dually targeted to mitochondria and chloroplasts in plants. ACD2, which protects against cell death caused by *P. syringae*, was localized in both organelles in Arabidopsis young seedlings but only in chloroplasts in mature leaves. Interestingly, MNSV CP was rarely immunolocalized in chloroplasts of melon cotyledons suggesting that dual localization could be host- or tissue-dependent (Miras *et al.,* 2020; Gomez-Aix *et al.,* 2015). In

any case, the same authors reported that the expression of many chloroplast and photosynthesis-related genes was inhibited during MNSV infection of melon cotyledons (Gómez-Aix *et al.,* 2016). Mitochondria and chloroplasts are thus valuable targets for plant pathogenic effectors to efficiently interfere with retrograde signaling and control immune response (Petre *et al.,* 2015; Liu *et al.,* 2018).

Two MNSV components produced HR-compatible cytopathic effects on mitochondria and/or chloroplasts, uncovering their role in plant perception of the pathogen. On the one hand, the R/arm domain induced chloroplast clustering around the nucleus and communication among them through stromule extension (see a summary of the functions of the different domains of MNSV CP in Table S1). Degradation of signal peptides generated in mitochondria and chloroplasts is essential for proper plant development (Kmiec *et al.,* 2014). Therefore, after viral CP processing inside the organelles, peptide accumulation derived from the R/arm domain could exceed the capacities of the organellar oligopeptidases to degrade them. This situation could be perceived by chloroplasts and mitochondria as a stress signal triggering their movement to and communication with the nucleus. It has been reported that this is a general response to pathogen challenge during pattern-triggered immunity (PTI) and ETI, allowing pro-defense signals, such as ROS and NRIP1, to travel into the nucleus triggering cell death. This was evidenced by enhanced HR-like cell death response to *Pseudomonas syringae* in Arabidopsis knockouts constitutively expressing stromules (Caplan *et al.,* 2015; Ding *et al.,* 2019).

On the other hand, the interaction of p29 with the mitochondrial membrane induced mitochondrial swelling, aggregation, and subsequent signaling events leading to necrosis. Similar findings have previously revealed that chemical induction of ROS production in Arabidopsis protoplasts caused a rapid and consistent change in mitochondrial morphology that preceded cell death (Scott and Logan, 2008). Moreover, we showed that *N. benthamiana* necrotic response to MNSV was associated with upregulation of salicylic acid-, HR- and oxidative stress-related genes. Although we cannot rule out the possibility that other APX isoforms are induced, downregulation of APX activity through transcriptional and translation repression and posttranslational modifications has been described to promote oxidative burst needed for programmed cell death (de Pinto *et al.,* 2012). All these cellular and molecular

events together suggest that MNSV-host compatible interaction may result from an inefficient HR that usually does not stop disease progression but reinitiates in newly infected cells. This assumption fits closely with the observed trailing necrosis associated with vascular tissues, including stems, petioles, and interveinal regions, occasionally killing the plant (Balint-Kurti, 2019).

Previous studies have suggested that CP mitochondrial and chloroplast targeting may assist, early in infection, CNV uncoating process since both organelles are often found closely associated with peroxisomes, where CNV replicates (Hui *et al.,* 2010). Even if that was true for MNSV, we found experimental evidence suggesting that CP organelle targeting affects later infection stages. MNSV infection initiated by uncoated RNAs was negatively affected when organelle targeting, but not the rest of known CP functions, was impaired in MNSV-CPΔR_1. Moreover, MNSV RNA encapsidation was prominent and associated with unprocessed CP presence in non-photosynthetic tissues like roots or stems, where chloroplasts are lacking or fewer than in leaves (Maksymowych et al., 1993; Kobayashi and Masuda, 2013), indicating that virion assembly rate could also be regulated by this mean. To increase genome encapsidation specificity, virion assembly should take place near replication sites. MNSV CP targeting mitochondrial-derived VRCs could provide the most efficient way to bring together the main virion components, CP, and viral RNAs. However, we showed that CP behaves like a mitochondrial matrix protein, most likely undergoing R/arm processing and becoming useless for genome binding. One possibility is that the processing rate of mitochondrial cargo could be modulated at some infection stages allowing or not encapsidation from CP mitochondrial pool. In this sense, mitochondrial processing peptidase expression was reported to be down or upregulated in susceptible and resistant melon, respectively, especially five days after infection with the resistance-breaking MNSV-Mα5/3'264, an MNSV(Al/264)-like chimeric virus (Gómez-Aix et al., 2016).

Apart from that mentioned above, we propose an additional role for MNSV CP, associated with its organelle targeting, in managing the balance between plant defense and virus counter-defense responses leading to a compatible interaction (Table S1). Some plant viruses mitigate symptoms to persist in the host, decreasing the accumulation and/or activity of key viral effectors by genome translation repression, degradation through host pathways, and

posttranslational modification (Paudel and Sanfaçon, 2018). Our results indicated that organelle targeting and processing compromise viral counter-defense since MNSV CP was shown to fulfill its RNA silencing suppression task in the cytoplasm by siRNA sequestration through the R_2/arm region and preventing the spread of systemic silencing (Serra-Soriano *et al.,* 2017). Similarly, TBSV p19 cytoplasmic depletion upon translocation into the nucleus by ALY proteins negatively affects its silencing suppressor activity (Canto *et al.,* 2006). We showed that necrosis induction was p29 dose-dependent, and thus it could be closely linked to high infection levels mediated by antiviral RNA silencing suppression. In this sense, the accumulation of MNSV-CPΔR_1 holding CPΔR_1, which still allows genome binding and encapsidation (Serra-Soriano *et al.,* 2017), has enhanced RNA silencing suppression capacity but fails to localize in both organelles and was negatively affected or impaired at local or systemic level. Although MNSV-CPΔR_1 accumulation was significantly lower than MNSV, the induction of pathogen and HR-related gene markers was in the same order of magnitude. The high levels of CPΔR_1 in the cytoplasm likely enhance viral RSS activity favoring early p29 overaccumulation. Far from improving MNSV replication, this magnifies mitochondrial alteration reinforcing antiviral defense or accelerating its activation as occurs when coexpressing p29 and CPΔR_1. Thus, CP organelle targeting and processing might be considered as a mechanism to avoid excessive RSS activity in green parts where uncoated replicating genomes can spread protected inside motile VRCs but, in turn, could facilitate horizontal transmission through the interaction of vector fungus zoospores with virions accumulated in roots. Remarkably, MNSV accumulation was previously observed to be significantly higher in infected melon roots than in cotyledons or leaves (Gosalvez-Bernal *et al.,* 2008). Melon roots have also been reported as a tissue where RNA silencing occurs (Herranz *et al.,* 2015). This remarkable tissue tropism can now be explained by the lack of CP processing and concomitant RSS activity and virion accumulation in roots observed here.

Our results also indicate that S/P domains, which correspond to organelle mature CP, could mitigate the appearance of necrosis and cytopathic alterations, possibly interfering with plant response. CP, but not R/arm-GFP, expression inhibited p29-induced necrosis when coexpressed at equivalent levels. Induction of stromules was attenuated, and chloroplast-to-nucleus movement and communication were not observed when the whole CP was used.

MNSV-CP($R_{81}A$), holding CP($R_{81}A$), which had reduced suppressor activity but still targets both organelles, accumulated at similar MNSV-CPΔR_1 levels but did not induce necrotic lesions nor modify gene marker expression. In contrast, when S/P domains were replaced by GFP in MNSV(R/arm-GFP), the infection was mainly restricted to initially infected cells showing exacerbated cytopathic effects that affected mitochondria and chloroplasts. Some MNSV(R/arm-GFP) foci were observed, suggesting the existence of a rather unstable balance between defense and counter-defense mechanisms that occasionally inclines in favor of progression. Moreover, the number of VRCs significantly increases in MNSV(R/arm-GFP) foci, as happened in MNSV(CPΔR_1-GFP). This situation raises the question of whether mitochondrial morphology changes leading to VRC building are due to a direct effect of p29 on membrane curvature upon recruiting host membrane-deforming proteins, as described for tombusvirus p33 on peroxisome membranes (Nagy, 2016) or, indirectly result from membrane potential disruption that makes mitochondria grow into larger structures. These last options could be emphasized in MNSV(R/arm-GFP) by S/P absence and in MNSV(CPΔR_1-GFP) by cytoplasmic location and enhanced RSS activity. Yet still, the possibility that host and MNSV work in concert to build VRCs cannot be ruled out.

At the time of writing this manuscript, Alam *et al.* published an article about CNV CP targeting addressing part of the objectives described in this work. Similar to MNSV CP, these authors reported that CNV CP targeting the chloroplast stroma inhibits necrosis induced by CNV p33 and TBSV p19 and interferes with host defense response modulating SA signaling pathway (Alam *et al.,* 2021). However, previous work by the same group suggested that only 1–5% of the CNV CP is targeted to chloroplast during infection (Xiang *et al.,* 2006). This result contrasts with our observation where both CP and virions were barely detected in leaves during MNSV infection, suggesting a much higher percentage of organelle targeting for MNSV CP than for CNV CP. Therefore, mechanisms controlling the equilibrium to generate a compatible interaction in both pathosystems could not be exactly similar and most likely rely on the presence in CNV of a TBSV p19-like silencing suppressor, p20, that is absent in gammacarmoviruses (Hao *et al.,* 2011). Whether MNSV CP organelle targeting function is beyond a self-attenuation mechanism to not prematurely harm plant host or has a more direct

implication interfering with antiviral plant signaling starting in mitochondria and chloroplasts needs further investigation

In summary, cytoplasmic and organellar CP could be similar to echoproteins, a term that refers to identical, or nearly identical proteins, having different functions in different subcellular compartments (Yogev *et al.,* 2011). On the one hand, proteolytic processing of CP after targeting mitochondria and chloroplasts could result in two CP-derived peptides, both of them unsuitable for RNA silencing suppression and genome encapsidation. The overaccumulation of the split R/arm region could be perceived as a signal molecule for danger acting then as an elicitor whereas the rest of the CP (S/P domains) could be considered as an effector interfering with plant defence signaling starting in these organelles. On the other hand, after reaching a certain threshold of viral replication, the organellar targeting of the CP could be prevented, for example, by masking dTP through interactions with other CP molecules or different viral and host proteins, giving rise to a subpopulation of non-processed cytoplasmic CP suitable to function in RNA silencing suppression and genome encapsidation.

EXPERIMENTAL PROCEDURES

Molecular cloning.

For subcellular localization studies using an agro-mediated transient expression, MNSV CP, CP mutant (Figure S2), and p29 ORFs were PCR-amplified from available clones (Serra-Soriano *et al.,* 2017), digested and fused in-frame to the 5’ or 3’ ends of GFP by cloning them into a modified pBluescript including the CaMV 35Sx2 promoter and PoPit terminator. p29 ORF was also fused in-frame to the 5’ or 3’ ends of ChFP. Next, CP, all CP mutant and p29 expression cassettes were liberated by *SacI* or *HindIII* digestion, respectively, to be cloned into pMOG800 (Knoester *et al.,* 1998). For subcellular localization studies during MNSV infection, pMNSV(Al) (Genoves *et al.,* 2006) was modified by replacing its 3’-UTR from that of MNSV-264 isolate (Díaz *et al.,* 2004) generating pMNSV(Al/264). pMNSV(CP-GFP) and pMNSV(CP-HA) were obtained by linearizing pMNSV(Al/264) by inverse PCR and cloning either GFP or HA after CP using type IIs *BveI* restriction enzyme. pMNSV(CPΔR_1[6-30]-GFP), pMNSV(CPΔR_1[6-30]-HA), and pMNSV(R/arm-GFP) were generated by deletion of positions 6-30 of R_1 subdomain or S/P domains in pMNSV(CP-GFP) or pMNSV(CP-HA), as appropriate, by inverse PCR and self-

ligation through cohesive *BveI* ends. For MNSV infection studies in *N. benthamiana*, pMNSV(Al/264) was the basis to introduce R/arm, R, arm, R_1, R_2, and R_2/arm deletions by inverse PCR and self-ligation through cohesive *BveI* ends. To obtain the R_1/arm deletion mutant, the arm region was deleted from pMNSV(CPΔR_1) following the same procedure as before. R_{81}A point-mutation was introduced in pMNSV(Al/264) by inverse PCR using complementary primers. A tobacco rattle virus (TRV) expression system was used for CP-HA/ChFP expression in leaves, stems, and roots (MacFarlane and Popovich, 2000). For this purpose, C-terminal HA-tagged CP and ChFP ORFs were combined with pea early-browning virus (PEBV) CP subgenomic promoter by overlapping PCR and cloned into pTRV2 using Gateway technology (Liu *et al.,* 2002). Vectors were named TRV2$_{promPEBV}$[CP-HA] and TRV2$_{promPEBV}$[ChFP], respectively. Additionally, the alfalfa mosaic virus (AMV) RNA 3 expression system (Martínez-Pérez *et al.,* 2019) was used to compare the silencing suppressor capacity between CP and CPΔR_1. Both proteins were cloned under the control of a duplicated RNA4 subgenomic promoter into a modified RNA3 vector using appropriate restriction enzymes (Sanchez-Navarro *et al.,* 2001). The oligonucleotides used are listed in Table S3.

Subcellular fluorescent markers.

Transit peptides of yeast cytochrome oxidase subunit IV (coxP, matrix) (Köhler *et al.,* 1997) and Arabidopsis glycyl-tRNA synthetase (glyrsP, stroma, and matrix) (Duchêne *et al.,* 2001), as well as the chloroplastic *N. benthamiana* proteins, magnesium-protoporphyrin IX chelatase H subunit (CHLH/ABAR, outer envelope) (Shang *et al.,* 2010), N receptor-interacting protein 1 (NRIP1, stroma) (Caplan *et al.,* 2008) and chloroplast unusual positioning1 (CHUP1, outer envelope) (Oikawa *et al.,* 2008), were RT-PCR amplified from corresponding total RNAs and fused to fluorescent protein N-terminus following the same procedure described above. Markers obtained were designed as coxP-ChFP, glyrsP-ChFP/GFP, ABAR-ChFP, NRIP1-ChFP, and CHUP1-ChFP, respectively. Besides, the HIV-1 Rev nuclear export signal (NES) was fused to NRIP1ChFP N-terminus ($_{NES}$NRIP1-ChFP), including the corresponding sequence in the forward primer. The oligonucleotides used are listed in Table S3.

Protein expression and Western blot analysis.

Transient expression of proteins from binary vectors was performed using the *Agrobacterium tumefaciens* (C58C1) infiltration method in *N. benthamiana*. Overnight transformed bacteria

cultures were collected and adjusted to an OD600 of 0.2 with 10 mM MgCl2, 10 mM MES pH 5.6, and 150 µM acetosyringone. These suspensions were introduced in four-week-old leaves by infiltration into the abaxial side. For experiments requiring coexpression of two proteins, bacterial cultures were mixed before infiltration. Fluorescence was visualized at 48 hours post infiltration using confocal microscopy. For TRV-mediated expression, pTRV1 in combination with $TRV2_{promPEBV}$[CP-HA] or $TRV2_{promPEBV}$[ChFP] bacterial cultures were adjusted to an OD600 of 1 and mixed before infiltration. Plants were kept in growth chambers at 16 h light, 25 °C, and 8 h dark, 22 °C. Two weeks after infiltration, ChFP fluorescence was visualized under UV light using a rhodamine filter in a Leica MZ16 fluorescence stereomicroscope. For Western blot analysis, proteins were extracted from 100 mg of fresh tissue using 500 µl of Laemmli buffer and crude extracts clarified by centrifugation. After heat denaturing, 10 µl of each extract were analyzed by polyacrylamide gel electrophoresis and wet-transferred to PVDF membranes. Immunodetection was performed using a monoclonal antibody against GFP C-terminus or HA epitope. Blots were developed by chemiluminescence and examine using a Fujifilm LAS-3000 Imager. Densitometry was performed using Fujifilm Image Gauge V4.0.

Confocal laser scanning microscopy, image processing, and statistical analysis.

Subcellular localization analysis was conducted with an inverted Zeiss LSM 780 confocal microscope. eGFP and ChFP fluorescence were imagined by 488 and 561 nm laser excitation, respectively. The corresponding emission detection windows were 492–532 and 590–630, respectively. The chlorophyll excitation wavelength was 488 nm, and fluorescence was detected above 700 nm. Image processing and analysis, including overlays, Z-stack projections, movies, and estimation of p29 cluster sizes and areas, was performed using FIJI (Schindelin *et al.,* 2012) or ZEN 2011. Quantification of the stromule induction was done in epidermal cells marked with NRIP1-ChFP. Maximum intensity 2D projections of 30 z-stack slices were taken by confocal microscopy, each one including 5-6 cells (n=10, three replicates). Stromules and chloroplasts were counted using the MiToBo Cell Counter plugin of FIJI. Stromule induction was calculated as the number of chloroplast with stromules per total chloroplast number. Statistical significances at the 95% confidence level ($\alpha = 0.05$) were determined using Graphpad Prism ($p < 0.05$) through unpaired parametric t-test with Welch's correction as well as one-way ANOVA and Tukey's post-hoc test for multiple comparisons.

Virus inoculation.

GFP-recombinant, wild type, and mutated MNSV transcripts were synthesized in vitro using *PstI*-linearized vectors. Transcripts were quantified and used to infect two-week-old *N. benthamiana* plants by rubbing them on leaves (4-5 µg/leaf) with phosphate buffer (30 mM, pH 7.0) and carborundum. For subcellular studies, each RNA variant was inoculated in three leaves from three different plants. For infectivity studies, ten plants per RNA variant were inoculated. Three independent replicates were made, leaving some time between them. Plants were grown under long-day photoperiods as described above.

Total RNA extraction and Northern blot analysis.

For Northern blot, total RNA was isolated with RiboZol RNA Extraction Reagent Samples, electrophoresed on a denaturing gel (1X MOPS, 5% formaldehyde, 1.3% agarose) and capillary-transferred to nylon membranes in 10X SSC (1,5 M NaCl, 0,15 M sodium citrate). For dot blot, nucleic acids were isolated using the Dellaporta method (Dellaporta *et al.,* 1983) and spotted (300 ng) onto nylon membranes. Hybridization was performed using a digoxigenin-labelled riboprobe against MNSV CP or p29. Viral RNA detection was conducted using CSPD chemiluminescent substrate and Fujifilm LAS-3000 Imager. Densitometry was performed using Fujifilm Image Gauge V4.0.

Virion purification.

Two weeks after MNSV(Al/264) RNA inoculation, 10 g of stems/petioles, systemic leaves or roots were collected and homogenized in liquid nitrogen. The frozen powder was dissolved in 0.2 M sodium acetate, pH 5.0, and centrifuged at 7,700×g. After supernatant filtering, virions were pelleted by centrifugation at 146,000×g for 2 h through a 20% sucrose cushion and resuspended in 50 µl of 10 mM Tris-HCl, pH 7.3. For virions analysis, samples were electrophoresed (40 mM Tris-acetate, 1 mM EDTA, pH 8.0, agarose 1%), transferred to nylon membranes, and analyzed as described before. Three independent replicates were performed.

Real-time quantitative reverse transcription PCR.

DNase I treatment was performed to remove genomic DNA from RNA samples. First-strand cDNA was synthesized from 0.5 µg of total RNA using RevertAid H Minus Reverse Transcriptase and specific oligonucleotides (Table S3). qRT-PCR was carried out with the ABI 7500 Fast Real-

Time PCR detection system using PyroTaq EvaGreen qPCR Supermix, specific oligonucleotides, and recommended qPCR cycles. Specific oligonucleotides were designed using Primer3Web 4.1.0. Oligonucleotide efficiencies were tested by qRT-PCR using tenfold serial dilutions of the corresponding cDNA. MNSV-inoculated leaf samples from ten plants per each analyzed construct were pooled per assay generating three biological replicates. Each biological replicate was run in triplicate. Three reference genes encoding the elongation factor 1-α (EF1α, TC19582), F-BOX family protein (F-BOX, Niben.v0.3.Ctg24993647), and Protein phosphatase 2A (PP2A, TC21939) were used to normalize the expression levels (Liu *et al.,* 2012). The samples from Mock inoculated plants were used as control.

SUPPLEMENTARY MATERIAL

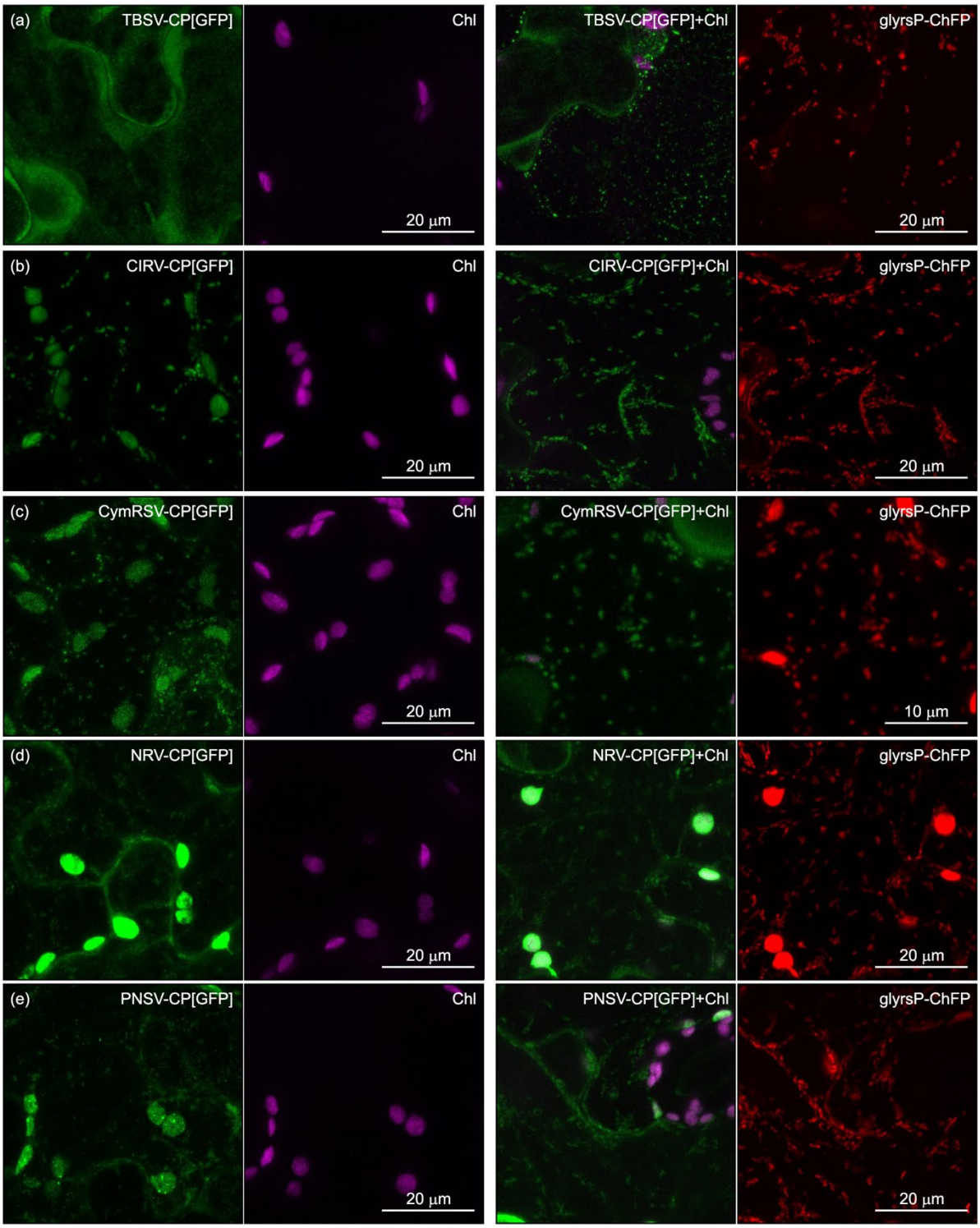

Figure S1. Subcellular localization of five coat proteins from members of the genus Tombusvirus.

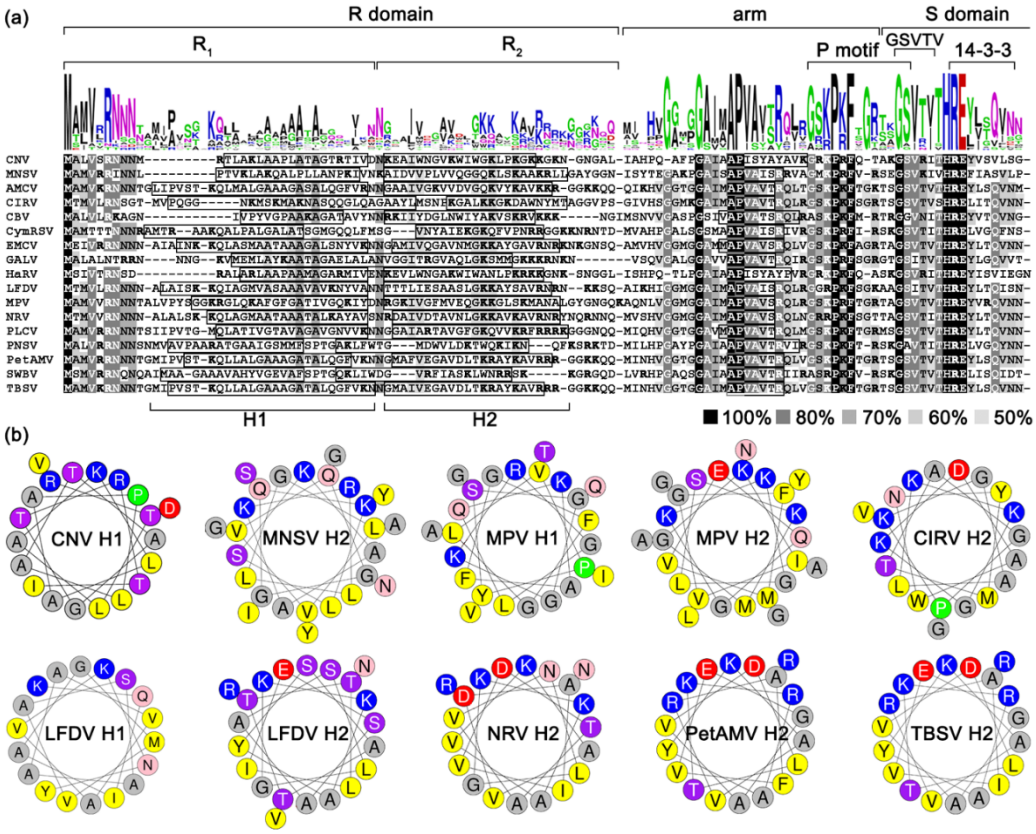

Figure S2. Multiple amino acid sequence alignment of the coat protein N-terminal regions of MNSV and 16 members of genus *Tombusvirus* and helical wheel presentation of some amphipathic α-helices in the N-terminal regions of MNSV and tombusvirus CPs.

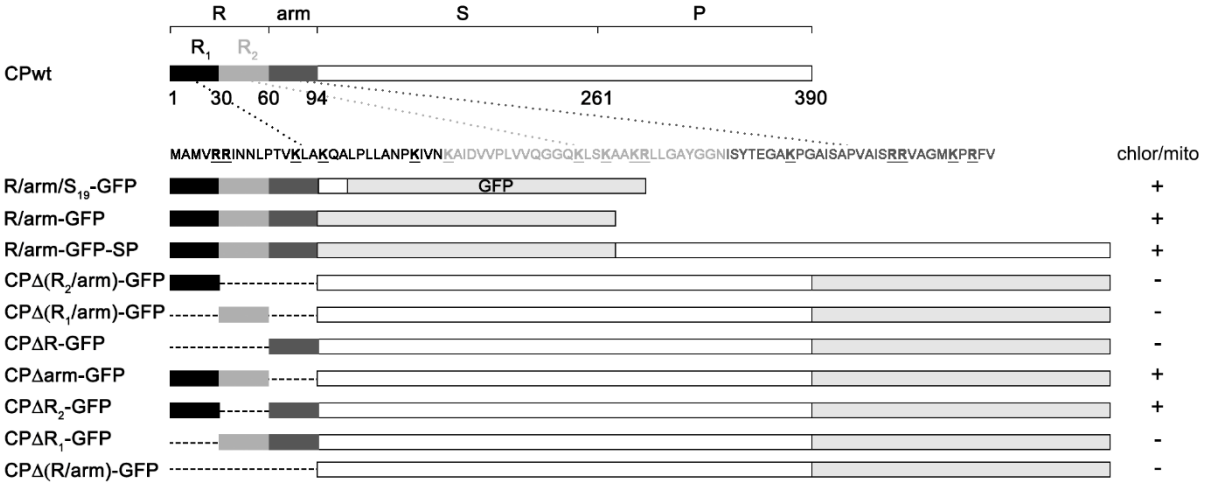

Figure S3. Schematic representation of the MNSV CP domains (R, arm, S, and P) and mutants used in this study.

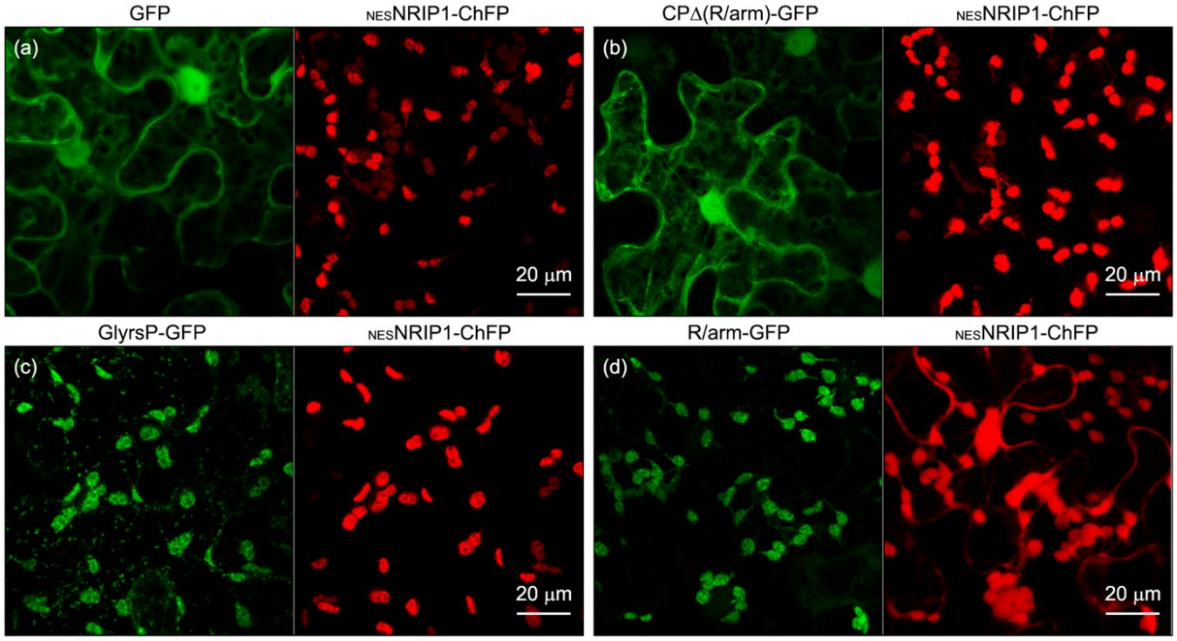

Figure S4. Coexpression of NESNRIP1-ChFP with GFP, CPΔ(R/arm)-GFP, glyrsP-GFP, and R/arm-GFP.

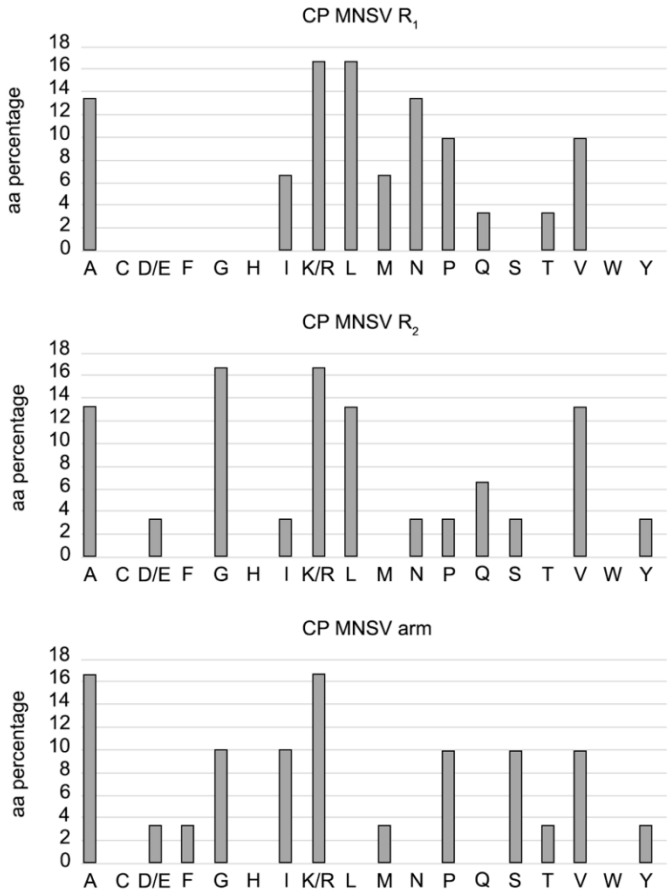

aa	R_1	R_2	arm
A	13,3	13,3	16,7
C	0,0	0,0	0,0
D+E	0,0	3,3	3,3
F	0,0	0,0	3,3
G	0,0	16,7	10,0
H	0,0	0,0	0,0
I	6,7	3,3	10,0
K+R	16,7	16,7	16,7
L	16,7	13,3	0,0
M	6,7	0,0	3,3
N	13,3	3,3	0,0
P	10,0	3,3	10,0
Q	3,3	6,7	0,0
S	0,0	3,3	10,0
T	3,3	0,0	3,3
V	10,0	13,3	10,0
W	0,0	0,0	0,0
Y	0,0	3,3	3,3

Figure S5. Amino acid composition of the MNSV CP R_1, R_2, and arm regions.

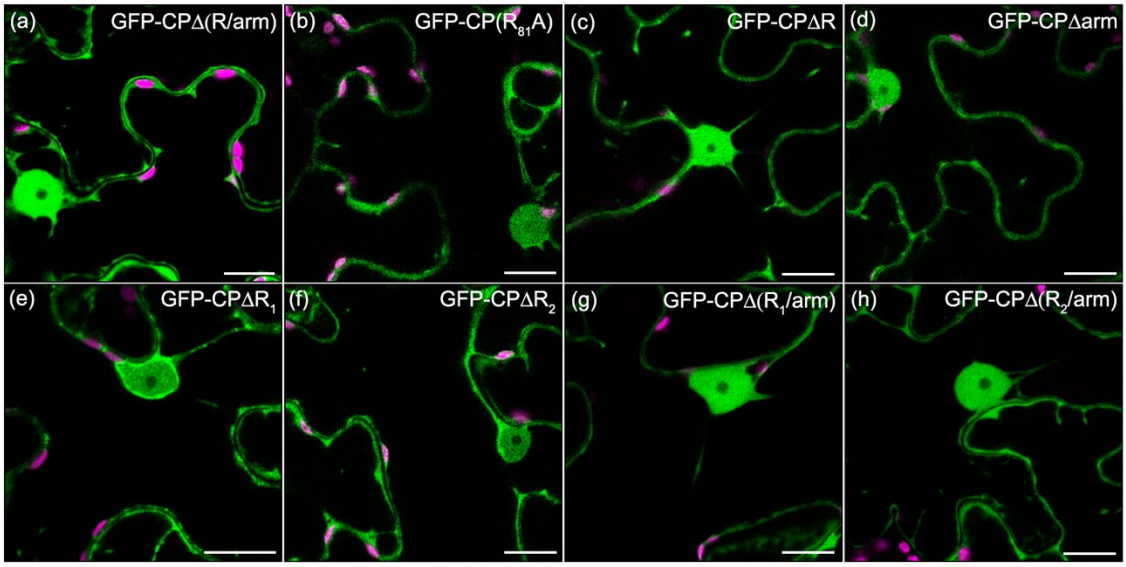

Figure S6. Subcellular localization of the MNSV CP deletion mutants fused to the GFP C terminus in leaves of *N. benthamiana* at 48 hpi.

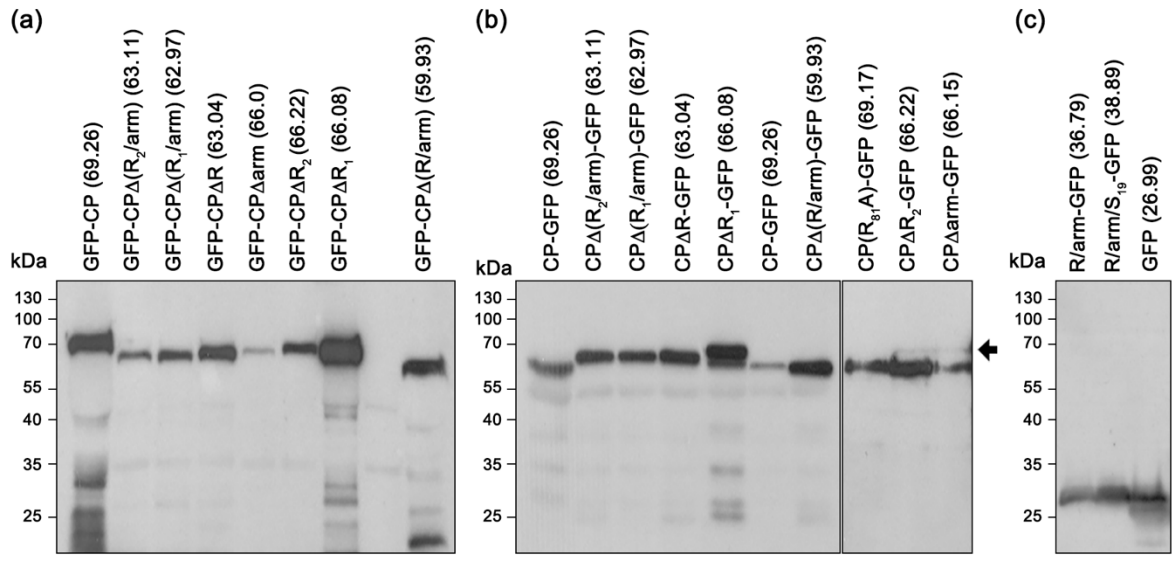

Figure S7. Western blot analysis of the GFP-tagged MNSV CP and deletion mutants transiently expressed in leaves of *N. benthamiana*.

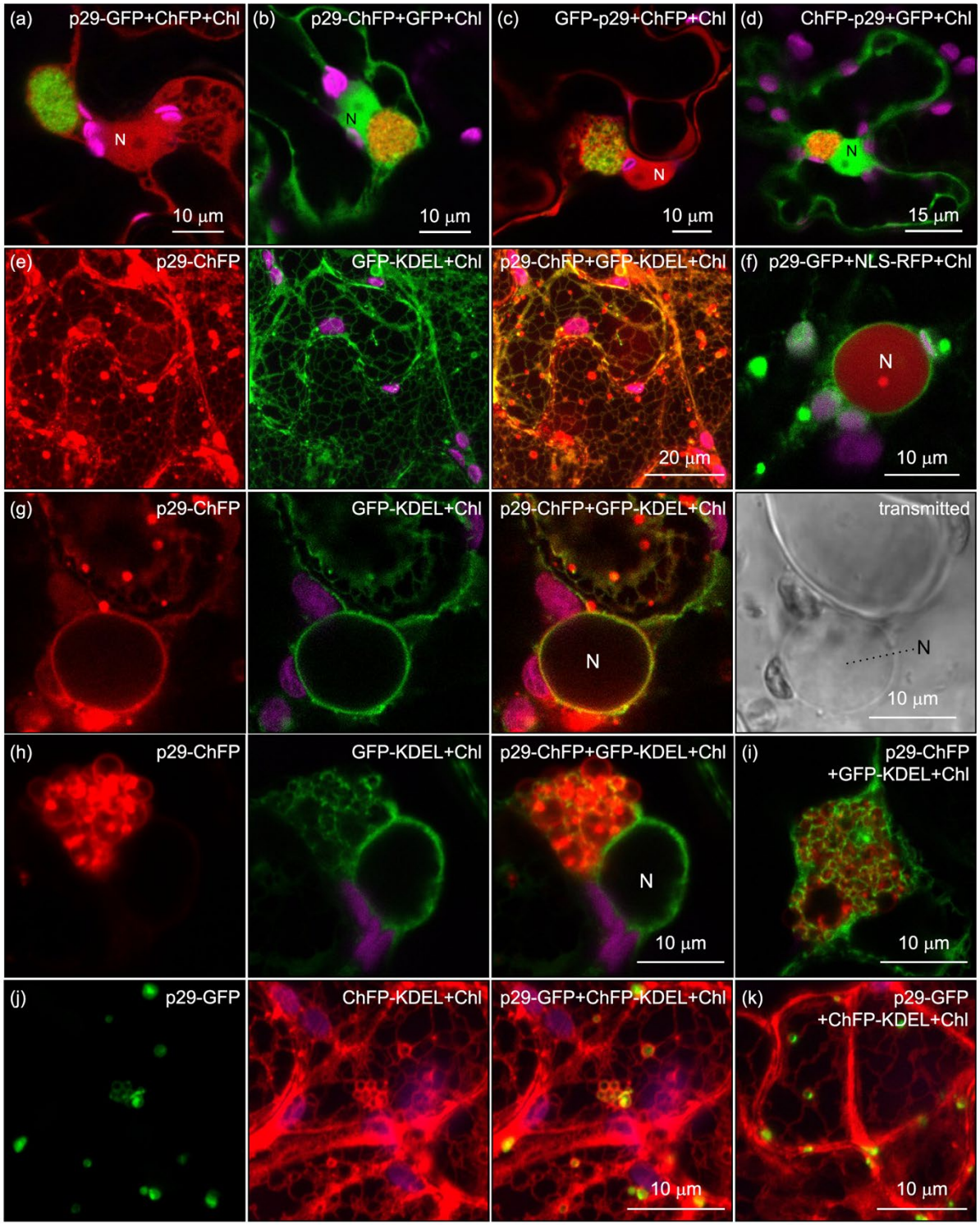

Figure S8. Effect of CP mutations on MNSV infectivity in *N. benthamiana*.

Table S1. Functions of the different domains of melon necrotic spot virus coat protein.

Domain	Subdomain	Function	Reference
R (RNA binding)	R_1	- Essential part of dual transit peptide in chloroplast and mitochondria targeting - Putative elicitor of plant defence in chloroplasts and mitochondria	This work
	R_2	- siRNA binding/RNA silencing suppression - Viral genome binding/encapsidation - Required as transit peptide spacer in chloroplasts and mitochondria targeting - Putative elicitor of plant defence in chloroplasts and mitochondria	Genoves *et al*., 2006 Serra-Soriano *et al*., 2017 This work
Arm region		- siRNA binding/RNA silencing suppression - Viral genome binding/encapsidation - Required as spacer in chloroplast and mitochondria targeting - Putative elicitor of plant defence in chloroplasts and mitochondria	Genoves *et al*., 2006 Serra-soriano *et al*., 2017 This work
S (Shell)		- Virion assembly - Putative effector of plant defence in mitochondria and chloroplasts	Riviere *et al*., 1989 Wada *et al*., 2008
P (Protruding)		- Compatibility with and transmission by the fungal vector *Olpidium bornovanus* - Putative effector of plant defence in mitochondria and chloroplasts	Ohki *et al*., 2010

Table S2. Prediction of CP subcellular localization of MNSV and 18 tombusviruses.

Virus	WoLF PSORT	LOCALIZER	YLOC
Melon necrotic spot virus	chlo*: 9.5**, chlo_mito: 7.5	chlo: 0.978***, mito: 0.966	mito: 82.15%***, vacu: 11.2%
Artichoke mottled crinkle vi	chlo: 13, E.R._vacu: 1	chlo: 0.998, mito: 0.835	mito: 75.4%, chlo: 14.7%
Carnation Italian ringspot vi	chlo: 11, vacu: 3	chlo: 0.996	chlo: 95%, pero:2.5%
Cucumber bulgarian virus	chlo: 10.5, chlo_mito: 6	chlo: 1.0, mito: 0.968	mito: 83.1%, chlo: 6%
Cucumber necrosis virus	chlo: 8, mito: 5	chlo: 0.952, -	mito: 95%, chlo: 3.8%
Cymbidium ringspot virus	chlo: 11, mito: 3	chlo: 1.0, mito: 0.995	mito: 88.3%, pero: 5.8%
Eggplant mottled crinkle vir	chlo: 14	chlo: 0.995, mito: 0.889	mito: 47.9%, cyto: 25.9%
Grapevine Algerian latent vi	chlo: 5, cyto: 2.5	chlo: 0.977, mito: 0.967	pero: 46.1%, mito: 44.2%

Havel River virus	chlo: 7.5, chlo_mito: 6.5	chlo: 0.995, -	cyto: 37.7%, mito: 27.7%
Limonium flower distortion	chlo: 13, vacu: 1	chlo: 0.993, mito: 0.961	mito: 65.1%, vacu: 12.7%
Moroccan pepper virus	chlo: 9, mito: 2	chlo: 0.992, mito: 0.9	mito: 81.9%, chlo: 11.3%
Neckar River virus	chlo: 12, mito: 2	chlo: 0.994, mito: 0.957	mito: 94.1%, chlo: 2.6%
Pelargonium leaf curl virus	chlo: 13, mito: 1	chlo: 0.997, mito: 0.981	mito: 75.1%, pero: 14%
Pelargonium necrotic spot v	chlo: 8, mito: 3	chlo: 0.99, mito: 0.946	mito: 84.2%, chlo: 12.7%
Petunia asteroid mosaic viru	chlo: 11, mito: 2	chlo: 0.998, mito: 0.974	mito: 95.7%, pero: 1.9%
Sitke waterborne virus	chlo: 10, vacu: 3	chlo: 0.998, mito: 0.994	mito: 85.1%, chlo: 11%
Tomato bushy stunt virus	chlo: 9, cyto: 2	chlo: 0.998, mito: 0.974	mito: 81.9%, pero: 6.9%
Maize necrotic streak virus	cyto: 10, nucl: 2	- -	nucl: 68.5%, cyto: 24.5%%

*The localization sites are abbreviated to four-letter codes with dual localization denoted by joining the four-letter codes v underscore character.

**The numbers roughly indicate the number of nearest neighbours (proteins in the WoLF PSORT training data that have tl similar localization

features) to the query which localizes to each site.

*** location probability. For YLOC, the two most probable locations are shown.

Table S3. List of oligonucleotides used in this study.

Cloning of CP MNSV(Al) isolate (DQ339157) in binary and infectious vectors

Position	sense	sequence	wt/mutation	PCR template
2816-2832	Forward	atcg**CCATGG**CGATGGTTAGACG (NcoI)	wt	pG-CPwt
3988-3972	Reverse	atcg**TCTAGA**TTAGGCGAGGTAGGCTG (XbaI) (stop)	$CP\Delta R_2$	$pG\text{-}CP\Delta R_2$
3986-3968	Reverse	atcg**TCTAGA**GGCGAGGTAGGCTGTTTC (XbaI) (non stop)	CPΔarm	pG-CPΔarm
			$CP\Delta(R_2/arm)$	$pG\text{-}CP\Delta(R_2/arm)$
			CP_{R81A}	$pG\text{-}CP_{R81A}$
2906-2925	Forward	atcg**CCATGA**AAGCTATAGATGTGGTTCC (PagI)	$CP\Delta R_1$	$pG\text{-}CP\Delta R_1$
3988-3972	Reverse	atcg**TCTAGA**TTAGGCGAGGTAGGCTG (XbaI) (stop)	$CP\Delta(R_1/arm)$	$pG\text{-}CP\Delta(R_1/arm)$
3986-3968	Reverse	atcg**TCTAGA**GGCGAGGTAGGCTGTTTC (XbaI) (non stop)		
89-110	Forward	atcg**CCATGA**ATGGATACTGGTTTGAAATTTC (PagI)	wt	pMNSV(Al)

895-874	Reverse	atcg**GCTAGC**CTAGTTGACCAACTTGAAAGCC (NheI) (stop)		
892-871	Reverse	atcg**GCTAGC**GTTGACCAACTTGAAAGCCTTC (NheI) (non stop)		
2906-2929	Forward	atcg**ACCTGC**ACGTTAGAAAAGCTATAGATGTGGTTCC (BveI)	CPΔR$_1$	MNSV(Al/264)
2834-2816	Reverse	atcg**ACCTGC**TGCGTCTAACCATCGCCAT (BveI)		
2996-3016	Forward	atcg**ACCTGC**ACGTAAATATTTCGTACACTGAGGGTGCC (BveI)	CPΔR$_2$	MNSV(Al/264)
2909-2885	Reverse	atcg**ACCTGC**CTTTATTTACAATTTTAGGGTTCG (BveI)		
3086-3106	Forward	atcg**ACCTGC**ACGTCAACCGATCGGAAGGATCTGTGAAG (BveI)	CPΔarm	MNSV(Al/264)
2995-2969	Reverse	atcg**ACCTGC**ACGTGTTGCCTCCATAAGCGCCAAGCAATC (BveI)		
3085-3106	Forward	atcg**ACCTGC**ACGTAAATCGATCGGAAGGATCTGTGAAG (BveI)	CPΔ(R$_2$/arm)	MNSV(Al/264)
2909-2886	Reverse	atcg**ACCTGC**CTTTATTTACAATTTTAGGGTTCGC (BveI)		
3086-3106	Forward	atcg**ACCTGC**ACGTCAACCGATCGGAAGGATCTGTGAAG(BveI)	CPΔ(R$_1$/arm)	MNSV(CPΔR$_1$)
2995-2969	Reverse	atcg**ACCTG**CACGTGTTGCCTCCATAAGCGCCAAGCAATC(BveI)		
2995-3016	Forward	atcg**ACCTGC**ACGTTAGCATTTCGTACACTGAGGGTGCC (BveI)	CPΔR	MNSV(Al/264)
2829-2810	Reverse	atcg**ACCTGC**ACGTGCTAACCATCGCCATTTGTAG (BveI)		
3086-3106	Forward	atcg**ACCTGC**ACGTTAGCCGATCGGAAGGATCTGTGAAG (BveI)	CPΔ(R/arm)	MNSV(Al/264)
2829-2810	Reverse	atcg**ACCTGC**ACGTGCTAACCATCGCCATTTGTAG (BveI)		
3041-3073	Forward	GTCGCTATTAGTCGG*gc*AGTGGCTGGTATGAAG	CP(R$_{81}$A)	MNSV(Al/264)
3073-3041	Reverse	CTTCATACCAGCCACT*gc*CCGACTAATAGCGAC		
CP and ChFP cloning in TRV expression system				
Acces number	**sense**	**sequence**		
X15883	Forward	**GGGGACAAGTTTGTACAAAAAAGCAGGCT**TCTGTGAGGCATTGCTCTTTTG (attB1)	PEBV CP subgenomic promoter	
	Reverse	CACTTACCCGAGTTAACGAGATGGCGATGGTTAGACGC		
DQ339157	Forward	**GGGGACAAGTTTGTACAAAAAAGCAGGCT**TCTGTGAGGCATTGCTCTTTTG (attB1)	PEBV CP promoter/MNSV CP-HA	
	Reverse	**GGGGACCACTTTGTACAAGAAAGCTGGGT**GCTAAGCGTAATCTGGAACATCG (attB2)		
MK160997	Forward	CACTTACCCGAGTTAACGAGATGGTGAGCAAGGGCGAG	Cherry fluorescent protein, ChFP	
	Reverse	**GGGGACCACTTTGTACAAGAAAGCTGGGT**GTTACTTGTACAGCTCGTCCATG (attB2)		
	Forward	**GGGGACAAGTTTGTACAAAAAAGCAGGCT**TCTGTGAGGCATTGCTCTTTTG (attB1)	PEBV CP promoter/ChFP	
	Reverse	**GGGGACCACTTTGTACAAGAAAGCTGGGT**GTTACTTGTACAGCTCGTCCATG (attB2)		
Fluorescent subcellular marker cloning in binary vectors				
Access number	**sense**	**sequence**	**Protein/transit peptide**	
At3g25690	Forward	atcg**ACATGT**TTGTCCGGATAGGGTTTG (PciI)	*A. thaliana* chloroplast unusual positioning 1, CHUP1	
	Reverse	atcg**GCTAGC**GTTTACAGATTCTTCTTCATTGC (NheI)		
At3g48110	Forward	atcg**CCATGG**CCATCCTCCATTTCTC (NcoI)	*A. thaliana* glycine-tRNA ligase transit peptide	
	Reverse	atcg**GCTAGC**CTGGAGGCGTTGAATCGC (NheI)		
EU332891	Forward	atcg**TCATGA**GAATTCTTTCCCTTCCC (PagI)	*N. benthamiana* chloroplast N receptor-interacting protein 1 (NRIP1)	
	Reverse	atcg**GCTAGC**AGAGTCAGTCGGAAGACC (NheI)		
EU332891	Forward	atcg**CCATGG**ATGCTTCAGCTACCACCGCTTGAGAGACTTACTCTTAGAATTCTTTCCCTTCCCTC (NcoI)	HIV-1 Rev nuclear export signal (NES)-NRIP1	
	Reverse	atcg**GCTAGC**AGAGTCAGTCGGAAGACC (NheI)		

At5g13630	Forward	atcg**ACATGT**CTTCGCTTGTGTATTC (PscI)	Mg-chelatase H Subunit (CHLH)/ABA receptor, CHLH/ABAR
	Reverse	atcg**ACATGT**TCGATCGATCCCTTCGATCTTG (PscI)	
NM_001181052	Forward	atcg**CCATGG**ATGCTTTCACTACGTCAATC (NcoI)	S. cerevisiae Cytochrome c oxidase subunit IV transit peptide
	Reverse	atcg**GCTAGC**GGATCCGGGTTTTTGCTGAAG (Nhe)	

List of oligonucleotides used in this study for quantitative RT-PCR

Acces number	sense	sequence	
Niben101Scf04717g02003.1	Forward	GCTGCCTTTGCAATTGTTTT	Harpin induced-like protein 1,HIN1
	Reverse	TGTCAACGTAGCATCGGTCA	
Niben101Scf05283g00016.1	Forward	AGAACAAGAGCAAACGCCGT	HSR203J-like protein
	Reverse	TTTAAGCTCCTCCACCGCCG	
Niben101Scf00107g03008.1	Forward	CATGGTCAATACGGCGAAAA	Pathogenesis-related protein 1, PR1
	Reverse	CCACACACCTGTCCTTGAGC	
Niben101Scf17237g00001.1	Forward	TTTGCCACAAGGCTTTTCCT	Zinc finger protein 10-like protein, ZAT10
	Reverse	GCGCCTCCGTCTGAAGTAGT	
Niben101Scf07050g00006.1	Forward	AGGATTTGAGGGAGCATGGA	Ascorbate peroxidase 2, APX2
	Reverse	AGGGCGGAAAACTGGATCTT	

Sequences in bold refer to the indicated restriction enzyme cleavage or attb recombination sites
Underlined sequences correspond to cohesive ends resulting from BveI restriction
Lowercase italic sequences correspond to amino acid point-mutation.

The following supplementary information can be accessed in section *Supporting information* of the following web page: https://onlinelibrary.wiley.com/doi/full/10.1111/tpj.15435

Movie S3. Time-lapse series showing the movement of CP-GFP-labelled round structures at 48 hpi in epidermal cells of *N. benthamiana.*

Movie S4. Z-stack movie showing that juxtanuclear structures consisted of a large cluster of size-heterogeneous p29-GFP labeled vesicles.

Movie S5. 360° 3D reconstruction of Figure 6g showing an MNSV(CPΔR_1-GFP) infection focus at 5 dpi in *N. benthamiana*.

Chapter II

Molecular characterization, targeting and expression analysis of chloroplast and mitochondrion protein import components in *Nicotiana benthamiana*.

María Sáiz-Bonilla[1], Andrea Martín Merchán[2], Vicente Pallás[1]*, Jose A. Navarro [1]*

[1]Laboratory of Plant Molecular Virology, Institute for Plant Molecular and Cell Biology, Department of Molecular and Evolutionary Plant Virology, Consejo Superior de Investigaciones Científicas-Universitat Politècnica de València, Valencia, Spain.

[2]Current address: Centre for Research in Agricultural Genomics (CRAG), CSIC-IRTA-UAB-UB, Bellaterra, Barcelona, Spain

*Corresponding authors: Vicente Pallas (vpallas@ibmcp.upv.es) and Jose Antonio Navarro (janavarr@ibmcp.upv.es)

Published as **Sáiz-Bonilla, M., Martín-Merchan, A., Pallás, V. and Navarro, J.A.** (2022) Molecular characterization, targeting and expression analysis of chloroplast and mitochondrion protein import components in *Nicotiana benthamiana*. *Front Plant Sci*, **13**, 1040688.

Personal contribution. M.S-B and A-M-M performed molecular cloning and BiFC. Bioinformatic analysis was carried out by J.A.N. BiFC, Y2H, VIGs, and analysis of the results was performed by M.S-B. and J.A.N. All authors discussed the results.

ABSTRACT

Improved bioinformatics tools for annotating gene function are becoming increasingly available, but such information must be considered theoretical until further experimental evidence proves it. In the work reported here, the genes for the main components of the translocons of the outer membrane of chloroplasts (Toc) and mitochondria (Tom), including preprotein receptors and protein-conducting channels of *N. benthamiana*, were identified. Sequence identity searches and phylogenetic relationships with functionally annotated sequences such as those of *A. thaliana* revealed that *N. benthamiana* orthologs mainly exist as recently duplicated loci. Only a Toc34 ortholog was found (NbToc34), while Toc159 receptor family was composed of four orthologs but somewhat different from those of *A. thaliana*. Except for NbToc90, the rest (NbToc120, NbToc159A and NbToc159B) had a molecular weight of about 150 kDa and an acidic domain similar in length. Only two orthologs of the Tom20 receptors, NbTom20-1 and NbTom20-2, were found. The number of the Toc and Tom receptor isoforms in *N. benthamiana* was comparable to that previously reported in tomato and what we found in BLAST searches in other species in the genera *Nicotiana* and *Solanum*. After cloning, the subcellular localization of *N. benthamiana* orthologs was studied, resulting to be identical to that of *A. thaliana* receptors. Phenotype analysis after silencing together with relative expression analysis in roots, stems and leaves revealed that, except for the Toc and Tom channel-forming components (NbToc75 and NbTom40) and NbToc34, functional redundancy could be observed either among Toc159 or mitochondrial receptors. Finally, heterodimer formation between NbToc34 and the NbToc159 family receptors was confirmed by two alternative techniques indicating that different Toc complexes could be assembled. Additional work needs to be addressed to know if this results in a functional specialization of each Toc complex.

KEY WORDS

Nicotiana benthamiana, chloroplasts, mitochondria, translocon receptor, TOC, TOM, protein transport.

INTRODUCTION

Over time, the vast majority of the genes (93–99%) from the prokaryotic ancestors of the mitochondria and plastids in plants were lost or/and transferred to the nucleus. Currently, mitochondria and chloroplasts contain close to a thousand or several thousand proteins, respectively, but at best, their remnant endosymbiont genomes encode only about a hundred of them. These numbers imply that encoding organelle-destined proteins must be transported back into the respective organelle after their synthesis in the cytosolic ribosomes (Bykov *et al.,* 2020; Rochaix, 2022). In addition, the majority of the oligomeric protein complexes found in mitochondria and plastids, such as ribosomes, electron transport chains, or even the most abundant enzyme in the world, the ribulose-1,5-bisphosphate carboxylase/oxygenase, consist of subunits of dual genetic origin (Priesnitz and Becker, 2018; Ramundo *et al.,* 2020). A tightly nuclear-organelle coordinated mechanism must exist to maintain organelle function and biogenesis in these circumstances. This system must ensure the availability of the different subunits encoded on separated and compartmentalized genomes in the correct stoichiometry for complex assembly and their appropriate transport at the time and place required. The latter process was highly dependent on the successful acquirement of an organellar protein import apparatus that, despite mitochondria appeared much earlier than plastids during eukaryotic cell evolution, arose *de novo* in both organelles. Although mitochondrion and chloroplast transport systems do not share any homology, they are mechanistically similar (Peeters and Small, 2001; Kunze and Berger, 2015).

Reciprocal crosstalk between the nucleus and both mitochondria and chloroplasts is necessary to coordinate their respective gene expression and ensure the appropriate synthesis of protein working in common complexes during biogenesis and plant growth (Woodson and Chory, 2008). Nevertheless, mitochondria and chloroplasts are not only organelles primarily devoted to energy conversion. Their involvement in sensing environmentally stressful conditions, cell death and redox signaling is currently more than evident and known to be related to their physiological state (Kleine and Leister, 2016; Wang *et al.,* 2020). In response to changes in current functions, mitochondria and chloroplasts can coordinately initiate a signaling cascade, known as the retrograde response pathway, to modulate the expression of nuclear genes (Wang *et al.,* 2020). Therefore, these organelles have become logical targets for

pathogen effectors. Small fungus effectors target mitochondria and chloroplasts to suppress the hypersensitive response (Tzelepis *et al.,* 2021), and the localization of the coat protein of cucumber necrosis virus into the chloroplast stroma attenuates host defense response (Alam *et al.,* 2021). More recently, we have also shown that the mitochondrial and chloroplast dual targeting of melon necrotic spot virus coat protein modulates chloroplast-to-nucleus communication, mitigating tissue necrosis and favoring the local and systemic spread of the infection (Navarro *et al.,* 2021).

Mitochondria and chloroplasts are surrounded by a double-membrane that defines an intermembrane space and an innermost subcompartment termed stroma in chloroplasts or matrix in mitochondria. In addition, chloroplast stroma holds a third membrane system called thylakoids. It consists of a set of interconnected and highly specialized stacked membrane sacs where many essential photosynthesis-related proteins are located. Sorting newly synthesized proteins and their import into the correct organelle and/or intraorganellar compartment requires the presence of specific targeting signals mostly located at the N-terminus in the case of the mitochondrial matrix and stromal proteins, the well-known transit peptide (TP) and presequence, respectively. Although internal or C-terminal targeting signals exist, they are mainly found in proteins destined for organelle membranes or intermembrane spaces (Shi and Theg, 2013; Murcha *et al.,* 2014; Kunze and Berger, 2015). The targeting of precursor proteins from the cytosol to mitochondria or chloroplasts also requires the help of some chaperones, especially members of the Hsp70/90 families, and, specifically for chloroplast import, several cytosolic factors belonging to the 14-3-3 family of phosphoserine binding proteins. Both are thought to maintain precursor proteins in an unfolded, transport-competent state (May and Soll, 2000; Voos and Röttgers, 2002; Flores-Pérez and Jarvis, 2013). Once inside the organelle, targeting signals of these preproteins can undergo or not a specific cleavage giving rise to mature proteins (Teixeira and Glaser, 2013). The main chloroplast or mitochondrion gateway is a proteinaceous channel that, together with several membrane-associated receptors, forms a complex translocon protein machinery called Toc (translocase of the outer chloroplast membrane) or Tom (translocase of the outer mitochondrial membrane). Soluble proteins further destined for chloroplast stroma and mitochondrial matrix pass across the inner membranes through a second translocon known as Tic (translocon of the inner chloroplast

membrane) and Tim17:23 (translocon of the inner mitochondrial membrane 17:23), respectively (Murcha *et al.,* 2014; Richardson *et al.,* 2014).

The central core of the Toc complex is composed of two GTP-regulated receptors, Toc34 and Toc159, that bind to the TPs of preproteins and initiate the protein import through Toc75, a β-barrel membrane channel (Eckart *et al.,* 2002; Hinnah *et al.,* 2002). In vascular plants, Toc34 and Toc159 exist in multiple isoforms, allowing them to form structurally different Toc complexes. Thus, the import of a specific subset of proteins could be driven by each Toc complex in response to environmental factors and/or the developmental and physiological state (Ivanova *et al.,* 2004; Kubis *et al.,* 2004; Dutta *et al.,* 2014; Wiesemann *et al.,* 2019). The membrane topology of Toc75 and, especially, the orientation of its soluble N-terminal polypeptide transport-associated (POTRA) domains have been a matter of debate during the last decade since they were reported by different researchers either facing the cytoplasm or chloroplast intermembrane space. The final model of protein translocation may differ depending on POTRA orientation: in the intermembrane space, POTRA domains and Tic22 are suggested to act as chaperones that facilitate preprotein transfer to the Tic complex (Kasmati *et al.,* 2013; Gross *et al.,* 2020); alternatively, a cytoplasmic exposure of the POTRA domains, which provides a Toc33 binding site, could regulate the GTPase activity of the TOC receptors (Sommer *et al.,* 2011).

More than five protein import pathways operate in plant mitochondria depending on protein topology, but all of them employ the Tom complex to a greater or lesser extent (Bausewein *et al.,* 2020). The core subunit of the Tom complex is the transmembrane β-barrel protein Tom40 (Rapaport and Neupert, 1999; Hu et al., 2019), while precursor protein recognition with presequences generally occurs via the family of the Tom20 receptors. In addition, plant-specific receptor Om64 (outer membrane 64) is a paralogue of Toc64 that could play a role analogous to Tom71 and Tom70 in yeast and animals, respectively, in cytosolic chaperone binding and insertion of hydrophobic and

multispanning α-helical proteins of the outer membrane (Lister *et al.,* 2007; Murcha *et al.,* 2014).

Concerning resident proteins of chloroplasts and mitochondria in green plants and except for a few examples, such as *Pisum sativum* and *Solanum lycopersicum*, the most intensively studied components of the organellar import systems are by far those of *Arabidopsis thaliana* (Stengel *et al.,* 2009; Paul *et al.,* 2013; Yan *et al.,* 2014). *A. thaliana* is still the most appreciated model species for plant genomic research, most likely due to the availability of both the whole sequence of its small genome and unique genetic resources. Nevertheless, the difference between *A. thaliana* and other plant species is that forward and reverse functional genetics is highly implemented in *A. thaliana* due to the easy availability of an extensive collection of genetically modified loss- and gain-of-function lines. (Bouché and Bouchez, 2001). Because of this, *A. thaliana* has, by far, the best-annotated genome, which integrates annotations based on literature evidence together with curations from the scientific community (Berardini *et al.,* 2015).

Nicotiana benthamiana is also emerging as an alternative tool for research in innate immunity and defense signaling during host-pathogen interaction. The main reason for this is its high susceptibility to many pathogens, such as viruses, bacteria, fungi, and many more. This particular feature makes it highly responsive to virus-based vectors and agrobacterium infiltration methods, which have been developed to express and purify foreign proteins, identificate protein-protein interactions and determine the subcellular localization of fluorescent protein-tagged proteins (Goodin *et al.,* 2008; Bally *et al.,* 2018). Concerning plant genomic research, sequences from two independent drafts assembly of the *N. benthamiana* genome, Sol Genomics Network and Nicotiana benthamiana Genome and Transcriptome Sequencing Consortium (benthgenome), began to be publicly available a decade ago but now are practically completed providing a considerable amount of information (Bally *et al.,* 2018). Improved bioinformatics tools for the annotation of gene function are becoming increasingly available, but such information must be considered theoretical until further experimental evidence proves it. The arrival of the virus-induced gene silencing (VIGS) technique has dramatically accelerated the process, especially in the virus hypersusceptible *N. benthamiana*, by which plant molecular biologists can unravel the gene functions in other plants rather than *A. thaliana.* In addition, the ease with which *N. benthamiana* can be handled to generate stable transgenic lines and transiently express proteins has also facilitated rapid forward

genetic screens. Despite all the above, the number of experimental validations of *N. benthamiana* gene functions found in the research literature is still minimal.

Here, we take advantage of the advances made in publicly available draft genomes and genome-based proteomes of *N. benthamiana* to identify the core components of the translocases of the outer membrane of chloroplasts and mitochondria. We also provide experimental evidence about their function based on their similarities with *A. thaliana* orthologs, phylogenetic analysis with its close relatives, identification of signatures in protein structures, subcellular localization, phenotypes of silenced plant, expression profiles at different tissues and stages, and characterization of physical interactions. Our findings will help to guide future studies about interactions between host preproteins and import machinery receptors to understand better the distinct organelle protein import pathways but, at the same time, to know how plant pathogens hijack host machinery for their own profit while taking advantage of the benefits of *N. benthamiana* as a research tool.

RESULTS

Identification of the receptors and the main channel component of Toc and Tom from *N. benthamiana.*

To identify the putative receptors and the main channel component of Toc and Tom complexes in *N. benthamiana*, a BLASTp search was conducted using *A. thaliana* amino acid (aa) sequences (Supplementary Table S2) and the *N. benthamiana* genome v1.0.1 (available at Sol Genomics Network, https://solgenomics.net). The aa sequences of *N. benthamiana* showing the highest identity were tentatively designated as NbToc34, NbToc90, NbToc120, NbToc159A, NbToc159B, NbTic22-III, NbTic22-IV, NbToc75-III, NbTom20-1, NbTom20-2, NbOm64 and NbTom40 (Figure 1 and Table 1). At least two *N. benthamiana* aa sequences, denoted by a number (e.g., NbToc34.1 and NbToc34.2), were identified for each *A. thaliana* query protein. The corresponding gene structures were visualized using the Genome Browser Tool (https://solgenomics.net) and the Niben v1.0.1 genome. The size and number of exons of each pair of genes were similar or identical. Still, they differed in intron/exon arrangement as well as in their chromosome location (NbLab330 database) and, occasionally, in their transcriptional orientation (Supplementary Figure 1 and Supplementary Table S3). All of them were supported by mRNA-seq evidence in the Niben v1.0.1 gene model and they also matched

with NibSet-1 and NbDE protein datasets with a minimum sequence identity of 94.3% (Supplementary Table S3) (Kourelis et al., 2019; Schiavinato et al., 2019). These findings indicated that each pair of sequences are not caused by polymorphisms between different sequenced samples and assembly errors but corresponded to different gene copies.

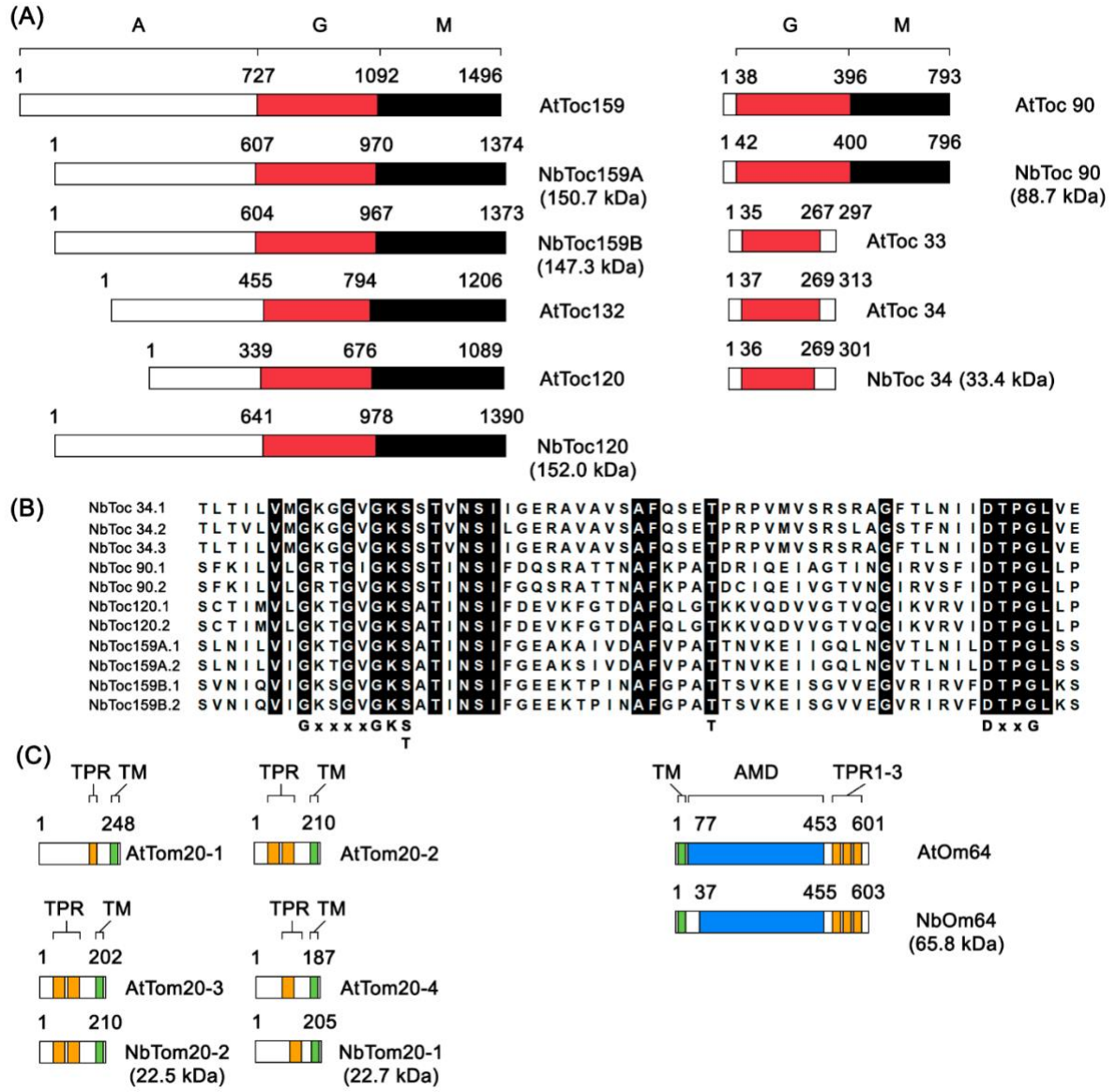

Figure 1. Structural comparison of the core components of the Toc and Tom complexes in *N. benthamiana* and *A. thaliana*. (A) Schematic alignment of the domain organization of Toc34 and Toc159 family receptors in *N. benthamiana* and *A. thaliana*. The positions of the acidic domains (A, white boxes), the GTPase domains (G, red boxes) and the membrane anchor domain (M, black boxes) are shown. The sizes of the *N. benthamiana* orthologs in kDa are indicated to the right of each representation. The numbers above each drawing correspond to the amino acid positions at the domain boundaries. **(B)** Amino acid alignment of the region of the G domains of the *N. benthamiana* Toc receptors holding the P-loop (G1) motif (GxxxxGKS/T), the threonine in switch-I (G2) and the residues DxxG of switch-II (G3). **(C)** Schematic alignment of the domain organization of isoforms of Tom20 and Om64 receptors in *N. benthamiana* and *A. thaliana*. The positions of the transmembrane domains (TM, green boxes), the tetratricopeptide repeats (TPR, orange boxes) and the amidase domain (AMD, blue boxes) are shown. The sizes of the *N. benthamiana* orthologs in kDa are indicated to the right

of each representation. The numbers above each drawing correspond to the amino acid positions at the domain boundaries.

Table 1. Amino acid sequence identity among Tom and Toc receptors of *Nicotiana benthamiana* and *Arabidopsis thaliana*.

	AtTom20-1	AtTom20-2	AtTom20-3	AtTom20-4	AtOm64	
NbTom20-1	42.92%	57.07%	58.91%	59.35%		
NbTom20-2.1	41.08%	56.93%	60.39%	58.28%		
NbTom20-2.2	42.57%	56.93%	58.41%	57.75%		
NbOm64					64.45%	
NbOm64-like					49.39%	
	AtToc90	**AtToc120**	**AtToc132**	**AtToc159**	**AtToc34**	**AtToc33**
NbToc90.1	51.95%	38.31%	38.06%	34.54%	27.15%	25.92%
NbToc90.2	51.96%	40.02%	39.89%	37.13%	28.43%	26.93%
NbToc120.1	38.83%	60.51%	56.68%	32.08%	28.75%	26.93%
NbToc120.2	38.83%	60.33%	56.59%	32.23%	28.11%	26.93%
NbToc159A.1	33.03%	31.31%	30.53%	41.55%	29.07%	27.94%
NbToc159A.2	32.03%	31.22%	30.29%	39.62%	28.75%	27.60%
NbToc159B.1	34.42%	36.17%	34.10%	52.65%	26.19%	26.59%
NbToc159B.2	34.17%	35.72%	34.27%	49.63%	26.19%	26.59%
NbToc34.1	26.57%	29.90%	30.56%	30.23%	67.44%	61.95%
NbToc34.2	25.41%	29.37%	30.03%	29.04%	64.35%	60.26%
	AtTic22-III	**AtTic22-IV**		**AtTom40**	**AtToc75-III**	
NbTic22-III.1	61.85%	29.62%	**NbTom40.1**	73.07%		
NbTic22-III.2	58.87%	28.62%	**NbTom40.2**	72.75%		
			NbTom40.3	68.80%		
			NbTom40.4	69.11%		
NbTic22-IV.1	27.79%	59.57%	**NbToc75-III.1**		78.28%	
NbTic22-IV.2	26.55%	53.28%	**NbToc75-III.2**		77.01%	
	A domain		**G domain**		**M domain**	
NbToc90 vs AtToc90			54.31%		49.49%	

NbToc120 vs AtToc120	11.2%	86.35%	71,35%
NbToc120 vs AtToc132	11.64%	87.24%	71.84%
Toc159A vs AtToc159	16.47%	55.09%	65.59%
Toc159B Vs AtToc159	21.02%	69.14%	73.64%

Besides, *N. benthamiana* contains a complex allotetraploid genome formed by interspecific hybridization of two diploid progenitors. The maternal ancestor was probably a species in section *Noctiflorae*, which introgressed some DNA from a species in section *Petunioides* (*N. attenuate*), while the paternal parent belonged to section *Sylvestres* (Schiavinato *et al.,* 2020). This means that at least two homeologs per gene could be found (Bally *et al.,* 2018). Schiavinato et al. used phylogenetic distances to assign a parental origin to the *N. benthamiana* genes (NibSet-1 gene models, http://bioinformatics.boku.ac.at/NicBenth/Download/) (Schiavinato *et al.,* 2019) and scaffolds (Sol Genomics Network). Based on their data, we analyzed the parental origin of all the identified proteins in this work. Except for NbTic22-IV aa sequences, which had a paternal origin, a maternal source was assigned to the rest, indicating that each pair of sequences are not homeologs (Supplementary Table S3). This is possible because new hybridizations during the pseudodiploidization process led to losses in some genomic regions and even whole chromosomes (Bally *et al.,* 2018). Nevertheless, phylogenetic relationships to other Toc and Tom receptors from related and distant species suggested a close relationship between most of the analyzed *N. benthamiana* sequences and their parental species (Supplementary Figures 2 to 5).

In *A. thaliana*, the Toc receptors either belong to Toc34 or Toc159 families consisting of two or four different genes coding for AtToc33/34 and AtToc90/120/132/159, respectively (Figure 1A). Four aa sequences of a putative *N. benthamiana* ortholog of AtToc34 were found (NbToc34.1-4). NbToc34.1 and NbToc34.3, as well as NbToc34.2 and NbToc34.4, were near-

identical aa sequences (Supplementary Table S3). However, structural similarities such as the size and number of exons as well as transcriptional orientation were higher between the corresponding genes of NbToc34.1 and NbToc34.2 and between NbToc34.3 and NbToc34.4, but some indels were observed only in the last pair. It is noteworthy that *NbTOC34.1-3* had a maternal origin while *NbTOC34.4* was declared "orphan"; thus, they most likely arose from recent gene duplication events. NbToc34.1 and NbToc34.2 shared 67.44% and 64.35% overall aa sequence identity, respectively, with AtToc34 but 61.95% and 60.26% with AtToc33 (Table 1). Thus, we considered both as NbToc34 orthologs. The phylogenetic tree generated in this study, which includes some *Nicotiana sp*. and *Solanum sp*. (family *Solanaceae*), *A. thaliana*/*lyrata* (family *Brassicaceae*) and *Cucumis sativus* (family *Cucurbitaceae*) sequences retrieved from NCBI database, showed that Toc34 aa sequences of members of the family *Solanaceae* grouped into two clades (80% bootstrap support), and NbToc34.1 and NbToc34.2 fell into each one of them (Supplementary Figure 2).

Four pairs of aa sequences were found concerning putative orthologs belonging to the Toc159 family (Supplementary Table S3). One of them showed an estimated molecular weight of about 88.7 kDa (Figure 1A) and shared the highest overall aa sequence identity with AtToc90 (NbToc90.1, 51.95% and NbToc90.2, 51.96%, Table 1). Both sequences fell into a clade (100% bootstrap support) exclusively composed of Toc90 samples from species of the genus *Nicotiana* (Supplementary Figure S2). The members of the *A. thaliana* Toc159 family were numbered according to their molecular weight; thus, based on their predicted molecular masses of about 150 kDa (Figure 1A), the remaining three pairs of *N. benthamiana* aa sequences could correspond to AtToc159 orthologs. However, one of them shared the highest identity in the whole sequence with AtToc120 (60.51% and 60.33%) and AtToc132 (56.68% and 56.59%). The aa sequence identity was even higher for the G (86,35% and 87.24%) and D (71.35% and 71,84%) domains (Table 1). We also show that they fell into a clade (100% bootstrap support) exclusively composed of aa sequences from the genus *Nicotiana* that were annotated as Toc120 in the NCBI database (Supplementary Figure S2) and related with AtToc120/132. Following the trend of what has been done in other orthologs of similar and higher sizes from *Nicotiana* and *Solanum* species, we named them NbToc120.1 and NbToc120.2 (Supplementary Table S3). The other two pairs of deduced aa sequences shared

an identity ranging from 39.62% to 52.65%, approximately, with AtToc159 (Table 1). As they are also clustered in two divergent clades, they are both likely to be different Toc159 isoforms to which we arbitrarily assigned the names NbToc159A and NbToc159B. A third sequence, NbToc159A.3, sharing a high identity with NbToc159A.1 and NbToc159A.2 was also identified but lacking near 300 aa in its amino end. We also constructed a phylogenetic tree with orthologs of AtTicIII or AtTicIV from some species belonging to the genera *Solanum* and *Nicotiana* found in the NCBI search. Sequences were equally distributed into two groups (99% bootstrap support), each including either AtTicIII or AtTicIV (Supplementary Figure S3).

Despite the difference in their molecular sizes, all Toc receptors share a central conserved GTPase domain (G-domain) and members of the Toc159 family also share a conserved C-terminal membrane anchor domain (M-domain) and a variable N-terminal acidic domain (A-domain), which in *A. thaliana* is also variable in length (AtToc120: 339 aa; AtToc132: 455 aa, AtToc159: 727 aa). In contrast, the A domain of NbToc120 (641 aa), NbToc159A (607 aa), and NbToc159B (604 aa) showed a similar length but still a low degree of sequence identity (8.23%-14.07%) (Figure 1A). Analysis of *N. benthamiana* aa sequences of Toc receptors using the NCBI Conserved Domain Database (http://www.ncbi.nlm.nih.gov/Structure/cdd/wrpsb.cgi) confirmed the presence of the G domain (cl38936: P-loop_NTPase) with the five canonical guanine nucleotide-binding motifs (G1-5). The P-loop (G1) motif (GxxxxGKS/T), the threonine in switch-I (G2) and the residues DxxG of switch-II (G3) were conserved (Figure 1B). In addition to the G domain, the M domain (pfam11886, TOC159_MAD) was also identified in NbToc90, NbToc120 and NbToc159A/B, confirming that all of them have the same characteristic tripartite domain organization.

Regarding mitochondria, Tom20 is the principal receptor of the Tom complex, and in *A. thaliana*, there are up to four isoforms of Tom20 (AtTom20-1 to AtTom20-4). AtTom20 belongs to the tetratricopeptide repeat (TPR) superfamily and, contrary to what happens in animals and fungi, it is anchored to the mitochondrial outer membrane through a C-terminal transmembrane domain (Ghifari et al., 2018) (Figure 1C). Only two ortholog proteins, which we have designed as NbTom20-1 (22.7 kDa) and NbTom20-2 (22.5 kDa), were identified by searching in both Sol Genomics Network and the Nicotiana benthamiana Genome and Transcriptome Sequencing Consortium (https://benthgenome.qut.edu.au). *TOM20-1.1* and

TOM20-2.1/2 have six exons of nearly identical sizes, but the first two were absent in *NbTOM20-1.2.* Interestingly, *TOM20-2.1* and *TOM20-2.2* showed different transcriptional orientations. Our phylogenetic analyses also revealed that almost all *Nicotiana sp*. sequences were separated into two clusters (83% bootstrap support), each of which included one of the *N. benthamiana* variants (Supplementary Figure S4). Amino acid sequence comparison of NbTom20-1 and NbTom20-2 with *A. thaliana* isoforms revealed that the highest identity was with AtTom20-4 (59.35%) and AtTom20-3 (60.39%-58.41%), respectively (Table 1). According to motif prediction by TPRpred, two TPR motifs were predicted in both AtTom20-3 and NbTom20-2 in a similar position (41-74 and 86-119 vs 41-74 and 79-112, respectively), but only one in both AtTom20-4 (81-116) and NbTom20-1 (79-114). A hydrophobic region was also predicted at the Ct of both NbTom20-1 (positions 178-192) and NbTom20-2 (positions 174-187) using the Dense Alignment Surface method (Figure 1B).

The 64-kDa outer envelope protein, Om64, is not present in yeast or mammals, but it seems to play a role as an import receptor in some vascular plants (Carrie *et al.,* 2010). Here, we found three putative *N. benthamiana* orthologs of 58.98, 62.43 and 65.80 kDa that were annotated just as Glutamyl-tRNA(Gln) amidotransferase subunit A and showed 64.45%, 47.10% and 49.91% amino acid identity with AtOm64. The smallest two differed in the insertion of 45 aa but were highly similar in shared sequence (95.87%). However, they differed quite from the largest ones (49.82% and 50.53%). In *A. thaliana*, the aa sequence of AtOm64 is about 51% identical to the chloroplast localized AtToc64-III. Thus, the smallest two may correspond to orthologs of AtToc64-III, with which they share a higher amino acid sequence identity (63.10% and 66.50%) (Table 1 and Supplementary Table S3). In this sense, both aa sequences clustered with AtToc64-III while the third sequence, which was then named NbOm64, grouped with AtOm64 and other Om64 aa sequences from the genera *Solanum* and *Nicotiana* (97% bootstrap support) (Supplementary Figure S4). In *A. thaliana*, AtOm64 has an N-terminal transmembrane anchor region followed by a globular cytosolic region that shows sequence similarity to an amidase and contains three TPR at the C-terminus (Carrie *et al.,* 2010) (Figure 1B). Analysis of NbOm64 using the NCBI Conserved Domain Database confirmed the presence of the amidase superfamily domain (pfam01425) and the three TPR (positions

486-518, 521-552 and 554-580). A putative transmembrane domain was also predicted at its Nt (positions 15-29) using the Dense Alignment Surface method (Figure 1C).

Finally, Toc75 and Tom40 are the central channels for protein translocation across the chloroplast and mitochondria outer membranes, respectively. Both are transmembrane β-barrel proteins. In addition, Toc75 also contains three POTRA domains, followed by the C-terminal membrane-spanning β-barrel (Rapaport and Neupert, 1999; Panigrahi et al., 2015). In *A. thaliana*, four Toc75-related genes have been identified, AtToc75-I, AtToc75-III, AtToc75-IV and AtToc75-V -(renamed AtOEP80), but only AtToc-III is proposed to form the protein conducting channel in Toc complexes (Baldwin et al., 2005). Two sequences corresponding, as mentioned above, to a unique putative ortholog of AtToc75-III in *N. benthamiana* (Supplementary Figure S1) were found to share 92.2% identity between them and 78.28% and 77.01% aa sequence identity with AtToc75-III. As expected, both clustered into the group of Nicotiana sequences (99% bootstrap support) (Supplementary Figure S5). As putative *N. benthamiana* orthologs of AtTom40, we found four similar aa sequences near-identical two by two in sequence and exon structure of its corresponding genes, NbTom40.1/2 and NbTom40.3/4 (Figure S1 and Supplementary Table S3). Although a maternal origin was assigned for all of them, phylogenetic analysis showed that NbTom40.1/2 and NbTom40.3/4 were grouped with *N. noctiflora* and N. sylvestris, respectively (Supplementary Figure S5).

Nicotiana benthamiana and *A. thaliana* orthologs show identical subcellular localization after transient expression.

Subcellular localization largely influences protein function by controlling interactor accessibility. Thus, to complete our bioinformatics analysis, we evaluated the subcellular localization of the *N. benthamiana* Toc and Tom receptors and channels identified above, making a comparison with *A. thaliana* ortholog proteins in plant cells. To do that, cDNA of the *N. benthamiana* proteins denoted by number one in Supplementary Table S3, in addition to their *A. thaliana* orthologs, were RT-PCR amplified and cloned into the appropriate vectors. Except for Toc75-III and Tom40, the green fluorescent protein (GFP) was fused to their C- or N-terminus, and next, they were transiently expressed in *N. benthamiana* leaves. The fluorescence was visualized under laser scanning confocal microscopy (LSCM) at 48 hpi, but C-terminally GFP-tagged Toc159 family members produced a very weak or no fluorescent signal.

It has been reported that adding a bulky tag may mask the sorting information, which is localized at the Ct of the Toc receptors from both Toc34 and Toc159 families, resulting in the proteasome-mediated degradation of the mistargeted fusion proteins (Lung and Chuong, 2012). Nevertheless, fluorescence was visualized properly in the corresponding fusions harboring an N-terminal GFP (Figures 2 to 4).

Regarding Toc75-III and Tom40, Toc75-III has a bipartite Nt targeting signal that is cleaved by the stromal and the intermembrane space localized type I signal peptidase (Tranel and Keegstra, 1996), and, although the Tom40 targeting signal has not been still resolved, it was shown that the fusion of GFP at the N terminus of human Tom40 abolished its mitochondrial targeting (Humphries et al., 2005). Therefore, we only analyzed the C-terminally fused versions (Figure 2A-D). AtToc75-III and NbToc75-III gave a circular, rim-like fluorescence pattern surrounding the chlorophyll fluorescence (pseudocolored in magenta), probably located on the chloroplast surface, that is consistent with the localization of AtToc75-III in the chloroplast outer membrane (Figure 2A-B). AtTom40-GFP and NbTom40-GFP were observed in small punctate structures within *N. benthamiana* epidermal cells. Visualization of mitochondria in these cells with the mitochondrial matrix marker coxP-ChFP (in red) revealed that many punctate structures were associated with these organelles (Figure 2C-D).

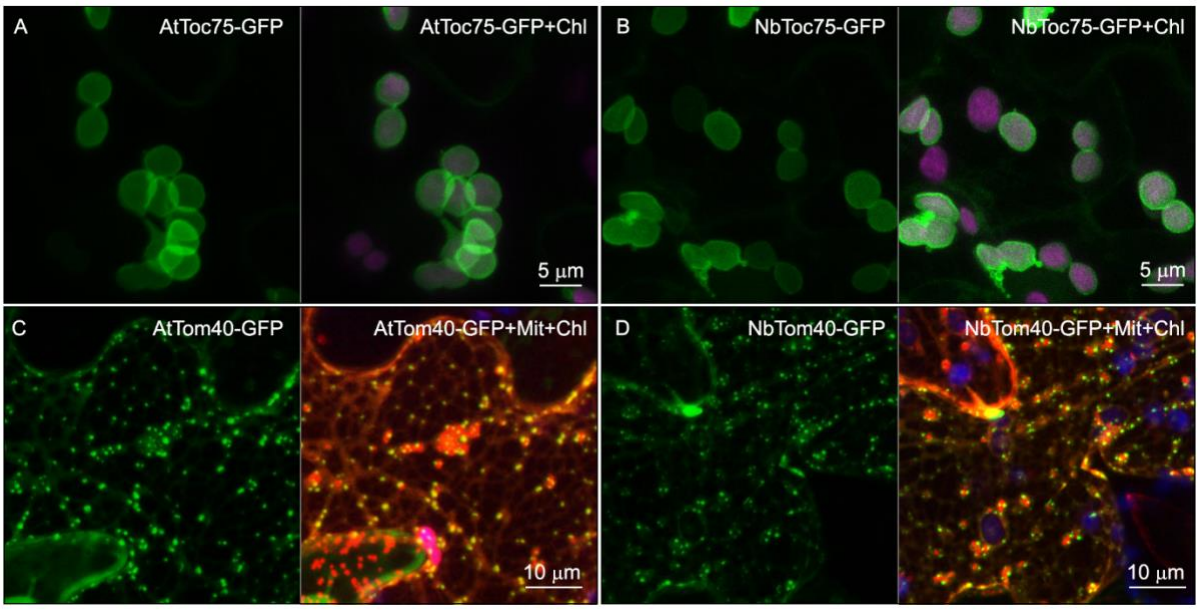

Figure 2. Subcellular localization of Toc (Toc75-III) and Tom (Tom40) channels in *N. benthamiana* and *A. thaliana*. GFP fusion proteins (green channel), indicated in the upper part of each panel, were expressed in

epidermal cells of *N. benthamiana* by transient expression mediated by agrobacterium. All images correspond to Z-stack projections taken two days after infiltration. Chlorophyll fluorescence is shown in magenta (Chl). To better visualize the rim of fluorescence surrounding the chloroplast in A and B, the green channel alone (left panel) and merged with the magenta channel (right panel) are shown. The red channel in C and D corresponds to the mitochondrial matrix marker, coxP-ChFP (Mit).

In addition to chloroplast outer envelope localization, the *A. thaliana* and *N. benthamiana* Toc receptors of both Toc34 and Toc159 families fused to the GFP C-terminus were also abundant in the cytoplasm, indicating that they partition between soluble and membrane fractions (Figure 3A-K). A similar pattern was observed with Nt and Ct GFP fusions of AtTic22-III and NbTic22-III, but more diffuse fluorescence throughout chloroplast was observed instead of forming the rim-like pattern (Figure 3L-M and Supplementary Figure S6). AtToc33-GFP, AtToc34-GFP and NbToc34-GFP mainly produced diffuse fluorescent signals in the cytoplasm and, only occasionally, showed the rim-like distribution around chloroplasts (Supplementary Figure S6).

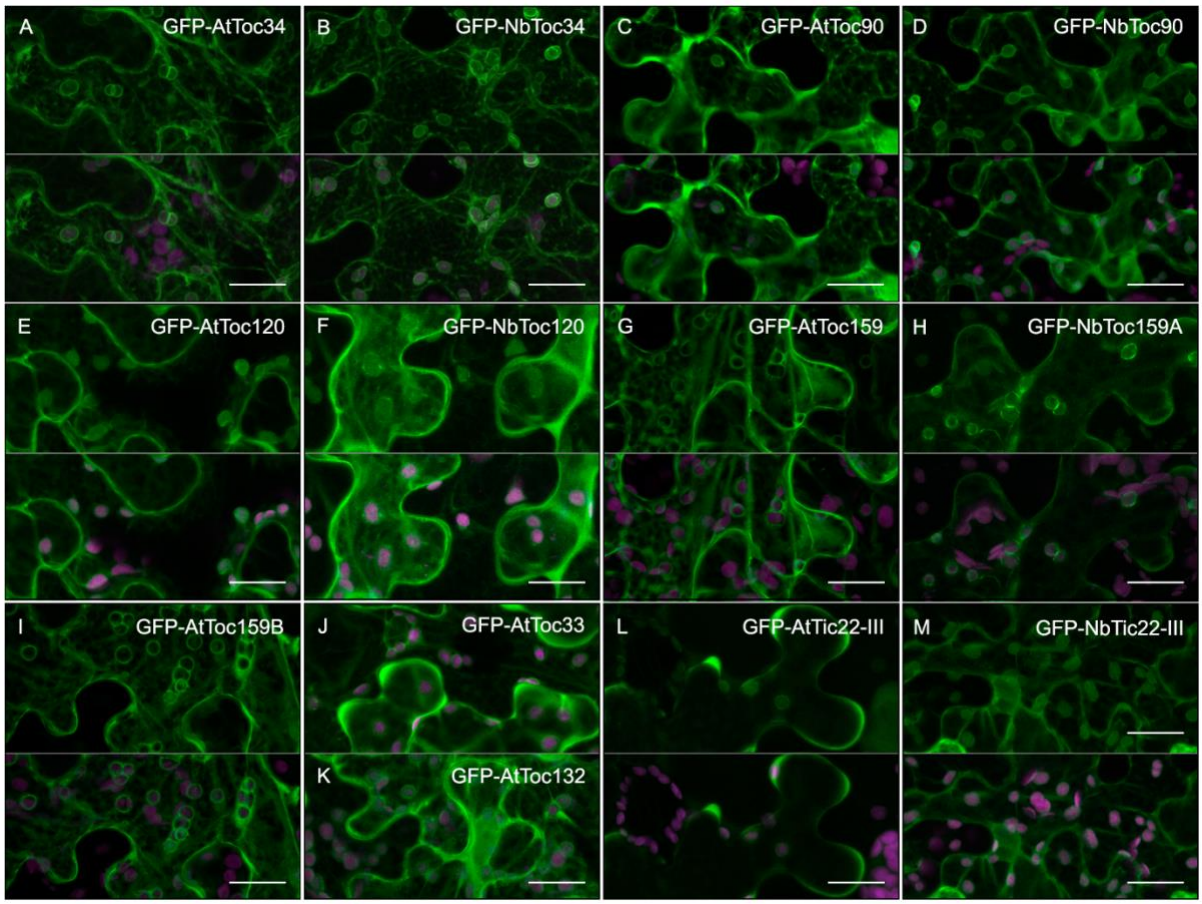

Figure 3. Subcellular localization of Toc receptors in *N. benthamiana* and *A. thaliana*. GFP fusion proteins (green channel), indicated in the upper part of each panel, were expressed in epidermal cells of *N. benthamiana* by transient expression mediated by agrobacterium. All images correspond to Z-stack projections taken two days

after infiltration. Chlorophyll fluorescence is shown in magenta. To better visualize the rim of fluorescence surrounding the chloroplast, the green channel alone (upper part of each panel) and merged with the magenta channel (bottom part of each panel) are shown. Scale bars correspond to 20 µm.

Expression of *A. thaliana* and *N. benthamiana* isoforms of Tom20 harboring a C-terminal GFP tag resulted in endoplasmic reticulum (ER) mistargeting (Figure 4A-B, E-F and Supplementary Figure S6). GFP N-terminally tagged versions were also located in the ER. Still, they mainly produced rims surrounding the chloroplasts (chlorophyll fluorescence pseudocolored in magenta) and mitochondria (chloroplast and mitochondrion dual marker, glyRS-ChFP in red) (Figure 4C-D, G-J and Supplementary Figure S6). Overexpression of both AtOm64-GFP and NbOm64-GFP produced fluorescent vesicles of different sizes evenly distributed over the cytoplasm and occasionally aggregated (Figure 4K-L). Upon coexpression with coxP-ChFP, red fluorescence was observed inside the vesicles indicating that they correspond to mitochondria that have suffered some swallowing alteration, most likely due to membrane protein overexpression (Figure 4M). In contrast to AtOm64-GFP and NbOm64-GFP, which seem to be targeted appropriately to the outer mitochondrial membrane, GFP-AtOm64 and GFP-NbOm64 produced a cytoplasmic fluorescent pattern (Supplementary Figure S6). GFP tagging to the AtOm64 and NbOm64 N-termini probably disrupted their mitochondrial anchoring that is mediated by their Nt transmembrane domains.

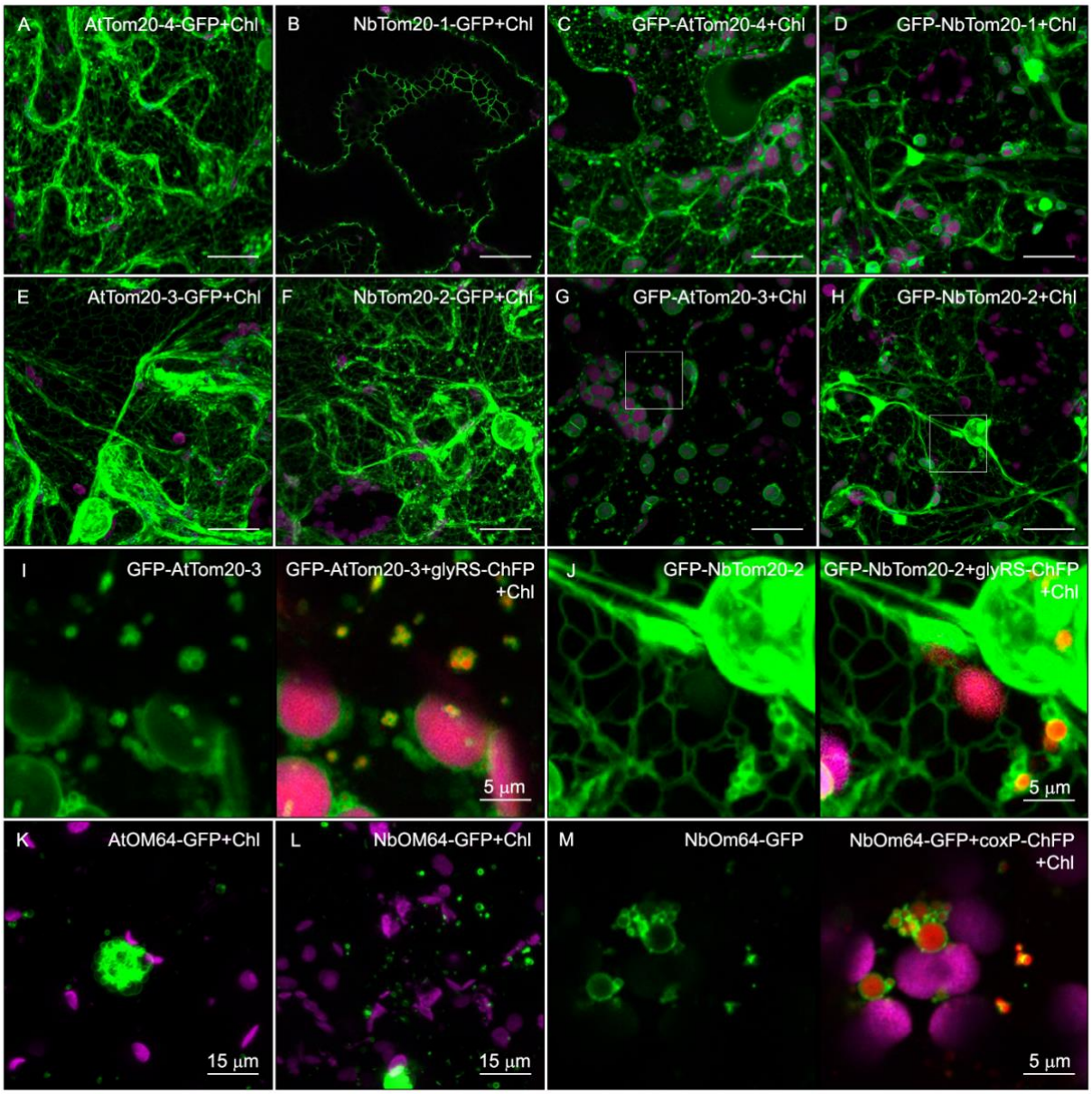

Figure 4. **Subcellular localization of Tom receptors in *N. benthamiana* and *A. thaliana***. GFP fusion proteins (green channel), indicated in the upper part of each panel, were expressed in epidermal cells of *N. benthamiana* by transient expression mediated by agrobacterium. All images correspond to Z-stack projections taken two days after infiltration. The red channel either corresponds to the mitochondrion and chloroplast dual marker glyRS-ChFP or the matrix marker, coxP-ChFP, as indicated. Chlorophyll fluorescence is indicated (Chl) and shown in magenta. I and J panels correspond to a magnification of the area delimited by the box in panels G and H, respectively. Scale bars correspond to 20 µm unless indicated.

Developmental phenotypes of *N. benthamiana* plants silenced for genes encoding Tom/Toc receptors and channels.

To go deeper into the function of the individual Toc/Tom receptors and channels in *N. benthamiana*, we decided to silence them using a viral-induced gene silencing (VIGS) approach (Liu et al., 2002). We were able to generate VIGS constructs with a tobacco rattle virus binary

system (pTRV1 plus pTRV2 vectors) that have the potential to target all gene copies. pTRV2 carrying the complete mGFP5 gene, pTRV2[GFP], was used as control. VIGS was performed with 2 weeks old *N. benthamiana* plants. Three weeks later, silenced plants were compared with control plants. *NbTOC90-*, *NbTOC120-*, *NbTOC159A*, *NbTIC22-III*, *NbTOM20.1-*, *NbTOM20-2-* and *NbOM64*-silenced plants showed no visible phenotype except for the typical TRV symptoms, such as mildly curved leaves and a very slight but unevenly distributed chlorosis, mainly in young leaves (Figure 5A). In contrast, *NbTOM40-*, *NbTOC75-III-*, *NbTOC34-* and *NbTOC159B*-silenced plants showed different developmental phenotypes depending on the silenced gene. *NbTOM40*-silenced plants showed leaf and petiole necrosis that produced some constriction sites, finally causing the leaf to wither and die. Plant growth was also arrested, most likely due to this phenotype (Figure 5B). The VIGS lines for *NbTOC75-III* (Figure 5C) and *NbTOC34* (Figure 5D) showed similar strong albino phenotypes with occasional necrosis around the veins, dwarfism of newly emerging leaves and severe arrested growth. In contrast, the *NbTOC159B*-silenced plants only had a slightly pale phenotype. Silencing of both *NbTOC159A* and *NbTOC159B* did not accentuate the phenotype of *NbTOC159B*-silenced plants (Figure 5G). Still, the silencing of both *NbTOC159A* and *NbTOC159B* plus *NbTOC120* led to a variegated phenotype with green and albino leaf regions and occasional distortion (Figure 5H).

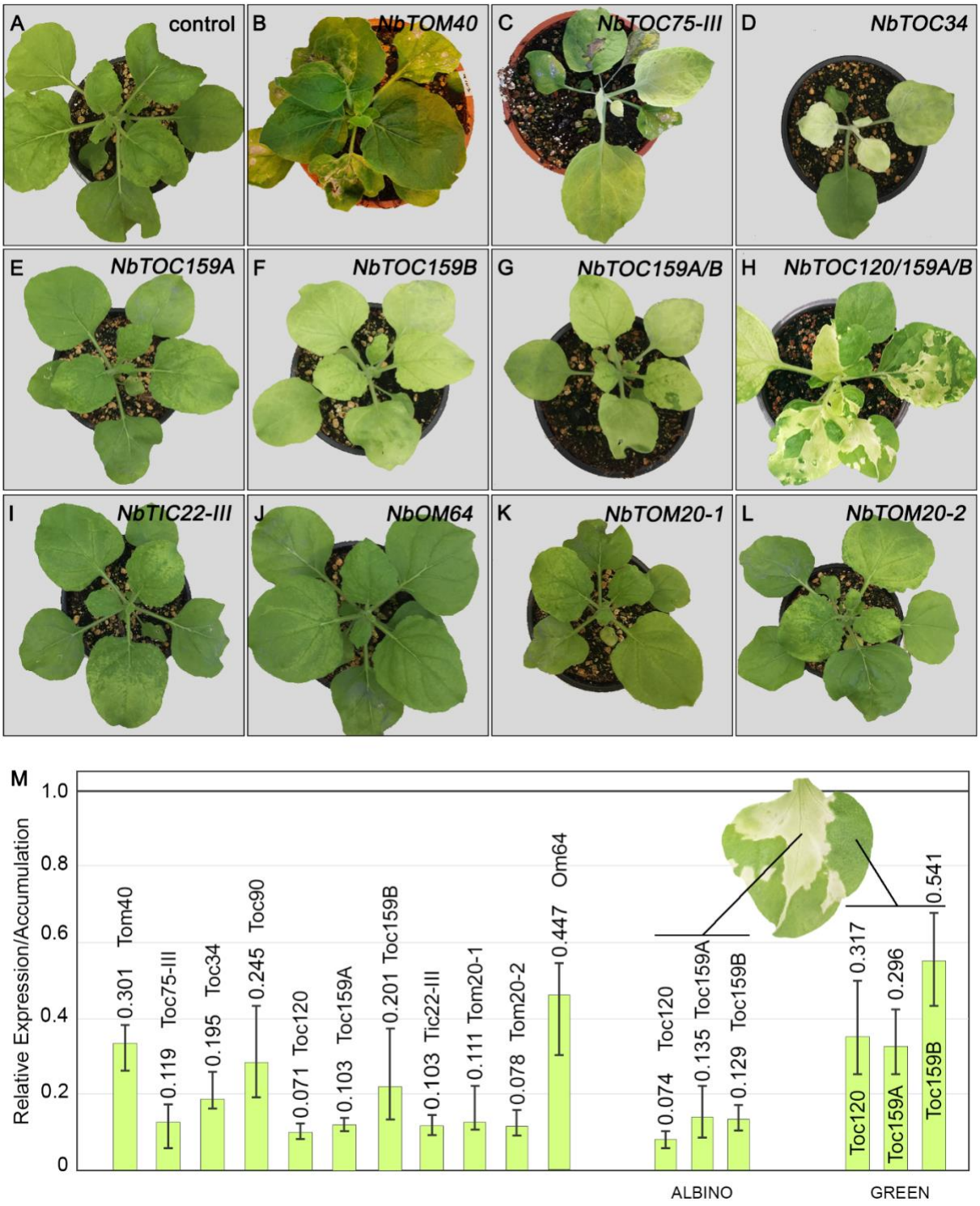

Figure 5. Analysis of the phenotype of the *N. benthamiana* plants silenced for each core component of the Toc and Tom complexes using viral-induced gene silencing mediated by TRV. **(A-L)** Phenotype of the *N. benthamiana* plants silenced for each indicated gen. Images were taken three weeks after infiltration with pTRV1 and each variant of the pTRV2 construct. Control corresponds to a plant infiltrated with pTRV1 and pTRV2[GFP]. The phenotype of both *NbTOC90-*, and *NbTOC120*-silenced plants were as control. **(M)** Relative gene expression of *NbTOM40*, *NbTOC75-III*, *NbTOC34*, *NbTOC90*, *NbTOC120*, *NbTOC159A*, *NbTOC159B*, *NbTIC22-III*, *NbTOM20-1*, *NbTOM20-2* and *NbOM64* in the corresponding *N. benthamiana* silenced plants. The relative gene expression of NbTOC120, NbTOC159A and NbTOC159B in green and albino regions from variegated leaves is shown on the

right. An RNA mix from three different plants was used in each case. Expression levels in the control plant were used as reference sample. The error bars indicate the RQ minimum and maximum.

To check the expression levels of the targeted genes, quantitative RT-PCR was performed using gene-specific primers. Infiltrated pTRV2[GFP] plus pTRV1 plants were used as a positive control. The mRNA expression levels of all genes were reduced in silenced plants compared to the levels in control plants three weeks after TRV infection. Although the silencing levels varied, the silencing efficiency ranged from 70% (NbTom40) to 93% (NbToc120), except for Om64, for which we reached up to 55% at best. Albino and green leaf regions in *NbTOC120/159A/159B* silenced plants were associated with high and moderate levels of gene silencing, respectively (Figure 5M).

Expression profiles of the Toc and Tom receptors from *N. benthamiana.*

The knowledge of gene expression profiles can provide useful information about their regulation and function. Therefore, to gain an insight into the potential functional differences of the members of the *N. benthamiana* families of Toc and Tom receptors, we analyzed their relative expression by RT-qPCR in photosynthetic (leaves and stems) and non-photosynthetic (roots) tissues at different weeks after germination (2, 4 and 6). Total RNAs extracted from a mix of leaves, stems and roots was used as reference sample. Expression levels of the *NbTOC34* gene showed practically uniform levels of relative expression in all tested tissues and stages (2W: p=0.053 and F=3.95; 4W: p=0.381 and F=1.136; 6W:p=0.208 and F=1.90) (Figure 6A). In contrast, the highest expression of the four Toc159 family members was generally observed in leaves, while stem and roots displayed less but similar relative levels of transcripts (Figure 6B-E). The largest difference between the levels of transcripts in leaves and stem/root tissues was observed with *NbTOC90*, two weeks after germination, since transcripts were nearly undetectable in stems and roots ($p<0.0001$ and F=139.5). This difference became increasingly smaller at four ($p<0.0001$ and F=41.46) and six (p=0.143 and F=6.675) weeks after germination not only in this gene but also in *NbTOC120* (2W: p=0.013 and F=6.97; 4W: p=0.051 and F=4.031; 6W:p=0.136 and F=2.475) (Figure 6C) and *NbTOC159B* (2W: p=0.048 and F=4.14; 4W: p=0.046 and F=9.87; 6W:p=0.056 and F=3.86) (Figure 6B) but, contrastingly, it became larger in *NbTOC159A* (2W: p=0.011 and F=15.28; 4W: p=0.0002 and F=24.75; 6W:p=0.003 and F=21.64) (Figure 6D).

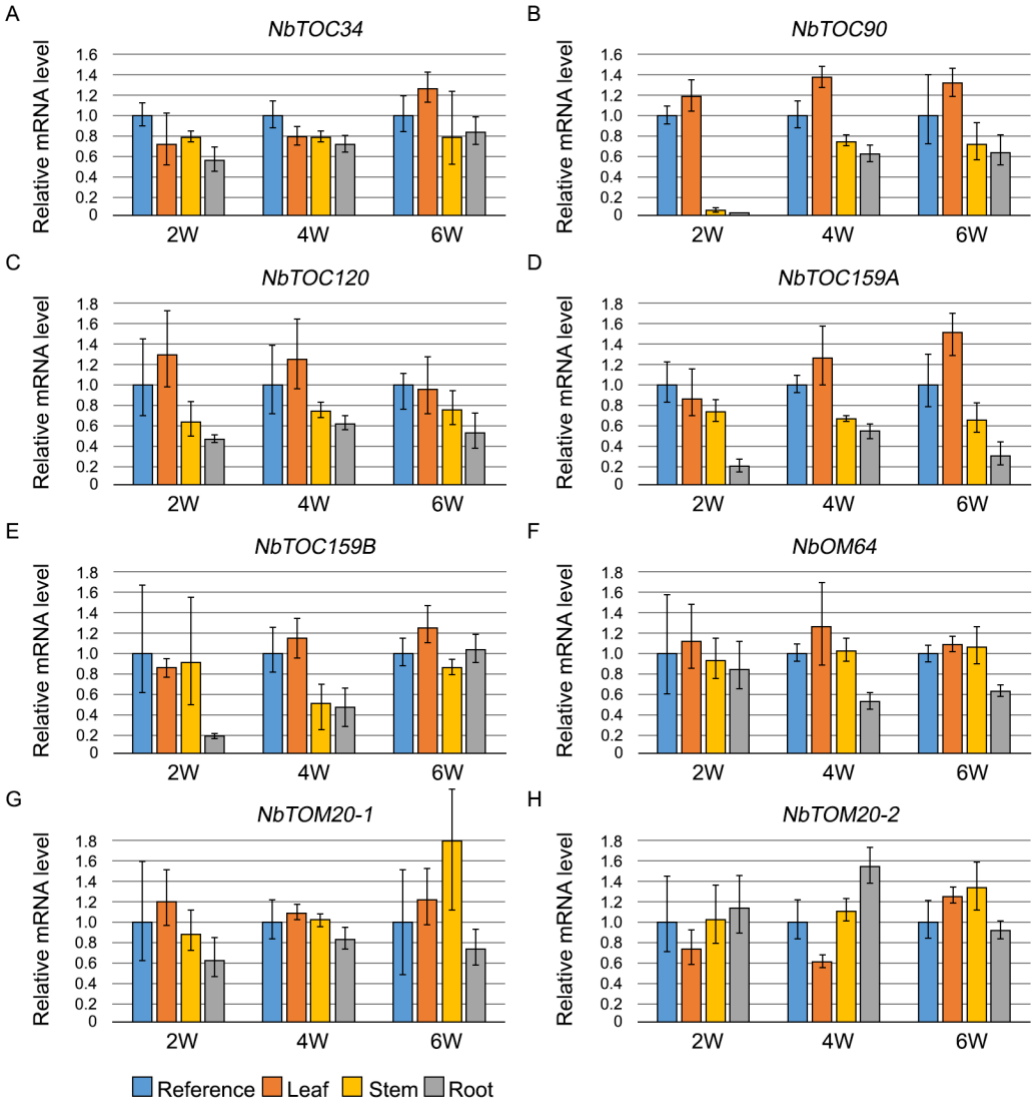

Figure 6. Relative gene expression of *NbTOC34* **(A)**, *NbTOC90* **(B)**, *NbTOC120* **(C)**, *NbTOC159A* **(D)**, *NbTOC159B* **(E)**, *NbTIC22-III* **(F)**, *NbOM64* **(G)**, *NbTOM20-1* **(H)** and *NbTOM20-2* **(I)** genes in leaves (orange), stems (yellow) and roots (cool grey) analyzed by RT-qPCR at two (2W), four (4W) and six (6W) weeks after germination. The mean value from three different plants is shown. Total RNAs extracted from a mix of leaves, stems and roots was used as reference sample (blue). Error bars correspond to ±SD.

Concerning mitochondrial receptors, the relative expression of *NbOM64* gene 2 weeks after germination was similar in all tissues (p=0.713; F=0.47) but its expression in roots relative to leaves and stems significantly decreased at four (p=0.0167, F=6.309; $p_{leaf\ vs\ root}$= 0.0169) and six (p=0.0028, F=11.54; $p_{control\ vs\ root}$= 0.00108; $p_{leaf\ vs\ root}$= 0.0035; $p_{stem\ vs\ root}$= 0.0068) weeks after germination (Figure 6F). Although there was not a significant difference in the relative expression of *NbTOM20.1* in different tissues and stages (2W: p=0.202 and F=1.94; 4W: p=0.141 and F=2.41; 6W:p=0.177 and F=2.11), it seems that there is a tendency towards

higher relative expression in photosynthetic tissues than in roots (Figure 6G). This trend seems to be inverted at least two and four weeks after germination in *NbTOM20.2* (2W: p=0.383 and F=1.16; 4W: p=0.0005 and F=18.97; 6W:p=0.027 and F=5.27) (Figure 6H).

Interaction of NbToc34 with the members of the Toc159 family in *N. benthamiana.*

Biochemical studies performed in *A. thaliana* have shown that a complex network of interactions can occur between the members of the Toc34 family and those of the Toc159 family through its GTPase domains. Particularly, AtToc159 preferentially associates with atToc33, while AtToc120 and AtToc132 especially interact with AtToc34, which in the absence of client proteins, also form homodimers. In addition, genetic and molecular studies have revealed that the acidic domain of the Toc receptors interacts with transit peptides of different client proteins. Therefore, structurally diverse Toc complexes can be assembled depending on the identity and relative abundance of the translocon receptors showing different abilities for preprotein recognition and translocation (Dutta et al., 2014; Schnell, 2019). To explore this possibility in *N. benthamiana*, we carried out bimolecular fluorescence complementation (BiFC) and yeast two-hybrid (Y2H) assays. Briefly, we fused each of the GFP fragments (see Materials and Methods section) to the amino and carboxyl terminus of the bait (NbToc34) and prey proteins (NbToc90, NbToc120, NbToc159A and NbToc159B) to generate Nt [YFP]-Bait/Prey, Ct [YFP]-Bait/Prey, Bait/Prey-Nt[YFP] and Bait/Prey-Ct[YFP] recombinant proteins. We screened all eight combinations for fluorescence complementation by LSCM: Bait-Ct[YFP]+Nt[YFP]-Prey, Ct[YFP]-Bait+Nt[YFP]-Prey, Bait-Nt[YFP]+Ct[YFP]-Prey, Nt[YFP]-Bait+Ct[YFP]-Prey, Bait-Ct[YFP]+Prey-Nt[YFP], Ct[YFP]-Bait+Prey-Nt[YFP], Bait-Nt[YFP]+Prey-Ct[YFP] and Nt[YFP]-Bait+ Prey-Ct[YFP] (Supplementary Table S4). Two days after infiltration, the fluorescent signal was detected in the combinations shown in Figure 7 but not with the other options and negative controls (Supplementary Table S4 and Supplementary Figure S7). The GFP fluorescence resulting from NbToc34 homodimerization was consistently observed in the cytoplasm and chloroplast surfaces in three out of four combinations (Figure 7A-C) and, occasionally, in $_{Ct[GFP]}$Toc34+$_{Nt[GFP]}$Toc34 (Figure 7D). Interestingly, the number of positive combinations including NbToc34 and NbToc90/120/159A/159B were dependent on each receptor, with NbToc159A showing the highest number of them (5/8, Figure 7E-I), followed by NbToc159B (4/8, Figure 7J-M), NbToc120 (3/8, Figure 7N-O) and NbToc90 (1/8, Figure 7P).

In contrast to that observed with NbToc34 homodimerization, only two positive combinations were show in cytoplasm and chloroplast envelope (Figure 7G and 7N) while fluorescence in the rest of positive interactions was mainly located at the cytoplasm with occasional punctate structures but not in the nucleus. At least for AtToc159, it was shown that a cytoplasmic pool is active for interaction with AtToc33 lacking the membrane anchoring domain (Hiltbrunner et al., 2001) and exhibits specific transit peptide binding (Smith et al. 2004). Therefore, the visualization of receptor interactions in the cytoplasm is possible.

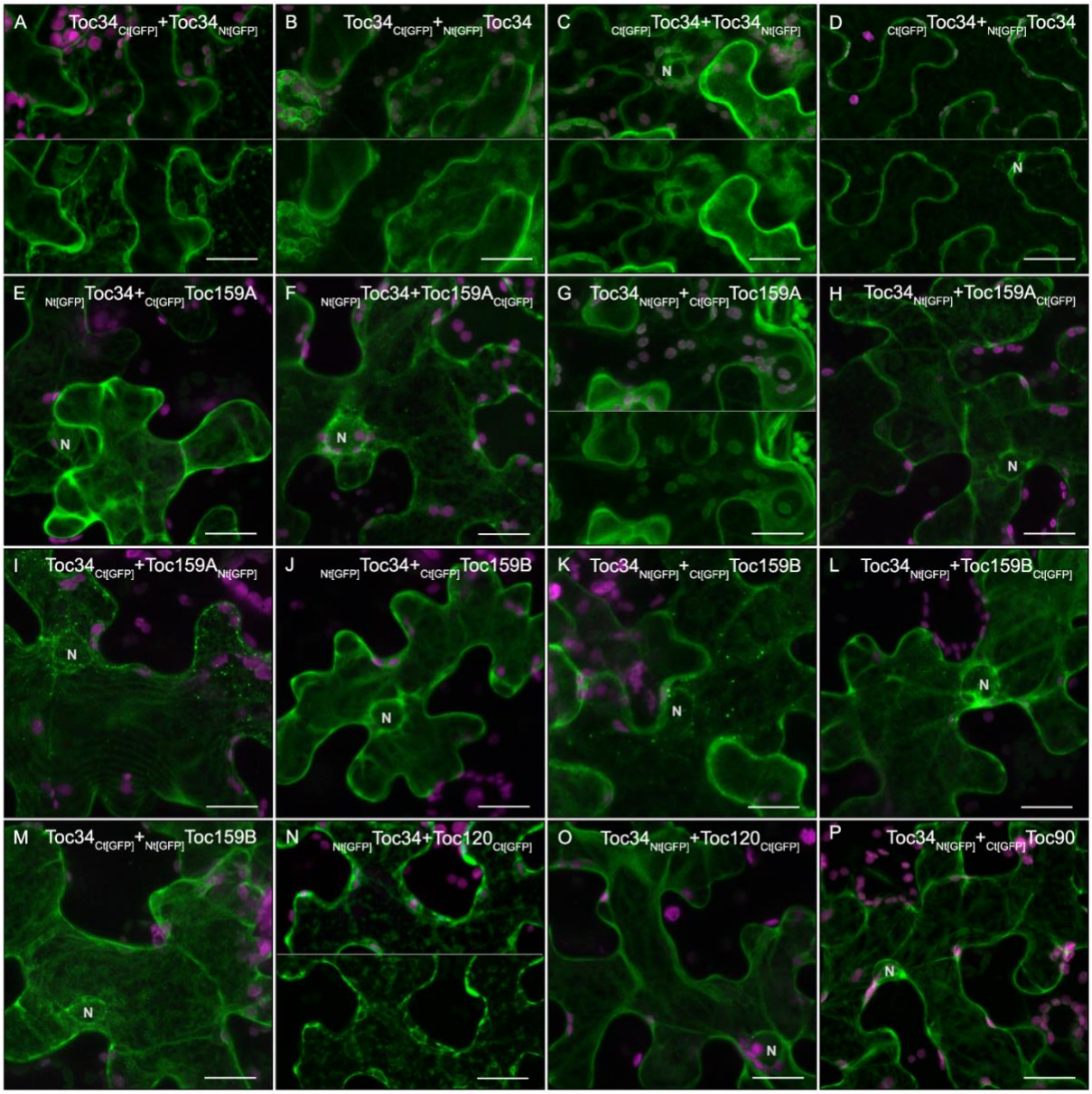

Figure 7. **Bimolecular fluorescence complementation assay in leaf epidermal cells of *N. benthamiana***. Leaves were cotransfected with Agrobacterium carrying constructs for expression of full-length NbToc34 and either NbToc34, NbToc159A, NbToc159B, NbToc120 or NbToc90 tagged with Nt[GFP] or Ct[GFP] as indicated in the top of each panel. Only combinations that resulted in fluorescence visualization (positive interaction) by

LSCM are displayed. Images of NbToc34 homodimerization **(A-D)**, as well as its interaction with NbToc159A **(E-I)**, NbToc159B **(J-M)**, NbToc120 **(N-O)** and NbToc90 **(P)**, are shown. All images correspond to Z-stack projections taken two days after infiltration. Chlorophyll fluorescence is shown in magenta. N indicates the position of the nucleus. Scale bars correspond to 20 µm.

Next, we performed additional Y2H experiments to corroborate the above NbToc34 interactions. As negative controls, we used pGBDKT7 empty vector and pGBD-p53, a well-known tumor suppressor. The interactions were screened on the highly stringent SD-Ade-His-Leu-Trp+X-α-Gal (Figure 8, right) and replicates were made on nonselective SD-Leu-Trp plates to assess the growth of double-plasmid transformants (Figure 8, left). Growth was evident for NbToc34, NbToc159A, NbToc159B and NbToc120 baits, while no growth was observed among negative controls and NbToc90. Nevertheless, NbToc34 may interact more efficiently with NbToc34, NbToc159A and NbToc159B than NbToc120 as suggested by the comparatively faster growth, higher yield of cell mass and more intense blue staining (Figure 8). These results align with those obtained above in BiFC assays with NbToc159A and NbToc159B showing the highest number of positive combinations, and overall, indicating that NbToc34 could have an affinity higher for NbToc159A and NbToc159B than for NbToc120. Our findings also point to a lack of interaction between NbToc34 and NbToc90. Thus, differences in NbToc34 affinity could provide Toc complexes with a fine-tuning mechanism of preprotein recognition, which could depend on the availability and relative abundance of the Toc159 receptors.

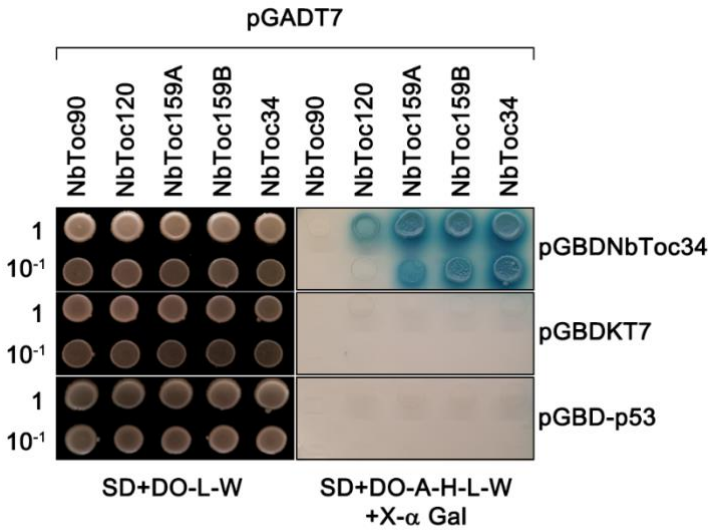

Figure 8. Yeast two-hybrid assay showing homodimerization of NbToc34 and its interaction with NbToc159A, NbToc159B and NbToc120. The cDNA of NbToc34 was fused to the GAL4 Binding Domain in pGADT to be used as bait. Besides, the cDNAs of NbToc34, NbToc159A, NbToc159B, NbToc120 and NbToc90 were fused to the GAL4 Activation Domain in pGBKT7 to be used as prey. The empty vector pGBKT7 and pGB-p53 holding a tumor suppressor were used as negative controls. Constructs were transformed into the yeast strain AH109 and double-plasmid transformants were selected by growing them in SD+DO-L-W medium. Double-plasmid

transformants were then spot-plated in ten-fold serial dilutions in selective SD+DO-A-H-L-W+X-α Gal medium to detect the activation of HIS3, ADE2, and MEL1 reporter genes (right). A replicate was done in SD+DO-L-W medium (left) to assess equal plating of double-plasmid transformants yeast cells.

DISCUSSION

Five million years ago, an ancient hybridization event occurred between members of sections *Noctiflorae* and *Sylvestres*, giving rise to the paleo-allotetraploid species *N. benthamiana*. Over the diploidization process, *N. benthamiana* has undergone extensive rearrangements between both subgenomes that only remain 19 chromosomes instead of 24, which is the sum of the parental chromosomes. Subgenome identification based on a phylogenomic approach revealed that genome downsizing mostly affected the paternally derived subgenome (50.3% of genes in NibSet-1 had a maternal origin, but only 34.4% had a paternal origin) (Schiavinato *et al.,* 2020; Schiavinato, 2021). In this way, we found duplicated orthologs in *N. benthamiana* genome v1.0.1 predicted proteins and both NibSet-1 and NbDE protein datasets for many of the *A. thaliana* Toc and Tom core components. They were tentatively designed as NbToc34, NbToc90, NbToc120, NbToc159A, NbToc159B, NbTic22-III, NbTic22-IV, NbToc75-III, NbTom20-1, NbTom20-2, NbOm64, NbToc64 and NbTom40. We have assigned a maternal origin to each pair of *N. benthamiana* orthologs identified in this work, except for NbTic-III and NbTic-IV, which had a paternal origin. These findings, together with the gene structural resemblance observed between the duplicated genes, the fact that some of them exhibit different transcriptional orientations and DNA sequence identities were close to 100% indicates that duplicated locus comes from recent segmental duplications rather than be homeologs arising from ancient whole genome duplications.

Among the databases used, the NbDE dataset gave the most accurate functional annotation. However, some relevant information about the presence/absence of isoforms was still lacking. At least two Toc34 isoforms have been found in *A. thaliana*, maize, spinach and the moss *Physcomitrella patens* (Schwenkert *et al.,* 2018). AtToc33 is the most abundant isoform that seems to be mostly in photosynthetic tissues, while AtToc34 is prominent in non-green tissues such as roots. Although AtToc34 and AtToc33 have different preferred precursor proteins, both paralogues show some functional redundancy. AtToc34 can complement AtToc33 knockout; only the double mutant is embryo-lethal (Constan *et al.,* 2004; Hust and Gutensohn,

2006). However, the presence of multiple Toc34 isoforms showing different substrate specificity is not a general feature of plants. As occurs in pea and tomato, we only found one of them in *N. benthamiana*. The absence of redundant isoforms was also suggested by the strong albino phenotype observed for NbToc34-silenced plants and its homogeneous relative expression in roots, stems and leaves. In addition, our database and literature searches from other species in genera *Nicotiana* and *Solanum*, where genomic data are available, also identified a unique Toc34 homolog for each one, suggesting that this situation could be a common feature in the family *Solanaceae*.

The Toc159 family in *A. thaliana* is composed of four members, AtToc90/120/132/159. They differ in the length of their A domains, which may contribute to the transit peptide selectivity and, thus, to the functional specialization of the Toc159 receptors (Kubis et *al.,* 2004). AtToc159 is highly expressed in young leaves and photosynthetic tissues and interacts preferentially with AtToc33. Together with AtToc75, they are assembled in Toc complexes that are important for photosynthetic preprotein import into leaf chloroplasts. AtToc159 knockout (*ppi2*) shows a severe albino phenotype that cannot grow beyond the cotyledon stage. AtToc90 is the less abundant receptor, but it also interacts with AtToc33 and partially restores *ppi2* mutant (Infanger *et al.,* 2011). AtToc132 and AtToc120, which show a high degree of aa sequence identity (89.74% in G/M domains) and especially associate with AtToc34, are more abundant than AtToc159 in roots and may be more relevant for preprotein import into root leucoplasts (Ivanova *et al.,* 2004). Single *toc132* and *toc120* mutants showed no visible phenotype, but *toc132/toc120* double homozygote resulted in a *toc159*-like bleached phenotype indicating a highly redundant functionality between them. Nevertheless, no functional overlap exists between AtToc120/132 and AtToc90/159 (Kubis *et al.,* 2004). In this work, we also found four Toc159-related receptors in *N. benthamiana* but some differences with those of *A. thaliana* were evident. As in *A. thaliana*, NbToc90 lacked the A domain and was phylogenetically related to AtToc90 and other Toc90-annotated sequences from *Nicotiana* and *Solanum sp*. AtToc120/132 counterpart in *N. benthamiana* was a unique NbToc120 protein, while that of AtToc159A was phylogenetically defined by two orthologs, NbToc159A and NbToc159B. In contrast to *A. thaliana*, all three have a molecular weight of about 150 kDa and an A domain similar in length. This situation agrees with tomato, where up

to four potential orthologs of AtToc159 (slToc159-1/4) were previously identified. Three of them (slToc159-1/2/4) were also around 150 kDa in size (Yan et al., 2014). slToc159-1 and slToc159-2 fell in the same clades that NbToc159B and NbToc159A, respectively, while slToc159-4 did in that of NbToc120. Our phylogenetic analysis suggested that this situation could be extended to other species belonging to the genera *Nicotiana* and *Solanum,* as we have stated above for NbToc34. The findings reported here also indicate that the degree of functional overlapping among Toc159-like receptors in *N. benthamiana* is higher than in *A. thaliana.* No recognizable phenotypes were observed for NbToc159-like receptor silenced plants, except for the pale one of *NbTOC159B*- and *NbTOC159A/B*-silenced plants, but albino leaf areas were observed after *NbTOC120/159A/159B* silencing. Finally, no differences in gene expression profiles between green and non-green tissues were detected for any NbToc159 receptor.

It has been reported that the specificity and fidelity of the nuclear-encoded plastid preprotein import are conferred by the initial and maybe simultaneous recognition of the transit peptides by both Toc159 and Toc34 families of receptors. Besides, AtToc34-GDP forms homodimers through interactions between the G domains in the absence of client proteins, but transit peptide binding promotes their dissociation, the GDP-GTP exchange and GTP hydrolysis (Paila *et al.,* 2015; Schnell, 2019). We have shown that NbToc34 also interacts with itself and the three receptors with an acidic domain, NbToc159A, NbToc159B and NbToc120, indicating that NbToc34 and NbToc159 receptors may also combine to form different Toc complexes. However, more detailed biochemical and genetic studies are needed to determine whether these *N. benthamiana* Toc complexes have specific functional roles. In any case, *A. thaliana* Toc complexes, which either assemble Toc33/Toc159/90 or Toc34/Toc120/132, could be more efficient in recognizing a different subset of client preproteins than those of *N. benthamiana* because they are forced to share a single form of Toc34.

Tic22 is a hydrophilic protein located in the chloroplast intermembrane space and is the first component of Tic to interact with the transit peptide. Therefore, we also address its proper annotation and functional characterization in *N. benthamiana*. *A. thaliana* has two isoforms of Tic22, AtTic22-III and atTic22-IV, that define conserved clades in land plants (Kasmati *et al.,* 2013). However, orthologs of AtTic22-III and IV in genera *Solanum* and *Nicotiana* found in NCBI

search showed no differentiation between both isoforms and presented functional annotations such as Tic22-like, Tic22 and hypothetical proteins. Nevertheless, these sequences were equally distributed into two phylogenetical groups, each including either AtTicIII or AtTicIV, perhaps indicating that both isoforms are also present in the family *Solanaceae*. Silencing of NbTic22-III did not result in a visible phenotype either indicating functional redundancy or a regulatory rather than central role in Toc-Tic communication. In this way, neither the individual disruption of AtTic22-III and AtTic22-IV nor double-mutant affected *A. thaliana* development. The double mutant phenotype, consisting of reduced growth and photosynthetic performance, was visible only under high light conditions when high import rates of proteins were needed (Rudolf *et al.,* 2013). A model was recently proposed in which Tic22 assists Toc75 POTRA domains in preprotein binding and chaperoning functions (O'Neil *et al.,* 2017).

As happened in tomato (Paul *et al.,* 2013), we could identify two AtTom20 orthologs in *N. benthamiana*, NbTom20-1 and NbTom20-2, but only one of AtOm64, which phylogenetically differed from AtToc64. Only NbDE dataset gives an annotation discerning between chloroplast and mitochondrial variants of the outer membrane protein 64. Regarding Tom20 receptors in *Nicotiana sp*., our phylogenetical analysis also revealed that most fell into two subgroups, each containing a tomato ortholog. These findings suggested that the number of Toc receptors and Tom receptors could be conserved among the species belonging to the genera *Nicotiana*. AtTom20-1 has not been identified as part of Tom complexes and its mRNA was rarely detected. Although some precursor recognition specificity has been assigned to the three remaining paralogues, only the quadruple mutant, disrupting AtTom20-2, AtTom20-3, AtTom20-4 and AtOm64 protein expression, causes embryo lethality (Lister *et al.,* 2007; Duncan et *al.,* 2013). This high functional redundancy was also supported by similar expression profiles of the four genes during development, except for a slight tendency of AtTom20-3 messenger to accumulate higher in roots than cotyledons and roots at 10 days post germination that was inverted in AtTom20-4. We observed a similar trend in the relative expression of *NbTOM20*-2 and *NbTOM20-1*/*NbOM64*, respectively. In addition, neither NbTom20-1, NbTom20-2 nor NbOm64-individually protein expression silenced plants displayed visible phenotypic abnormalities suggesting that Tom20 family members and Om64

in *N. benthamiana* as in *A. thaliana* are functionally redundant proteins. By contrast, silencing of either NbTom40 or NbToc75-III protein expression resulted in severe phenotypes indicating the absence of redundancy and their central role in protein translocation to mitochondria or chloroplast, respectively. Similarly, the corresponding null insertion mutants in *A. thaliana* showed an early embryo-lethal phenotype (Hust and Gutensohn, 2006; Hu *et al.,* 2019).

Knowledge of the specific cell compartment where a protein localizes is a major determinant in genome annotation since it determines the range of functions that the protein may perform and could help to identify the potential interacting partners. Our results showed that the subcellular localization of *A. thaliana* and *N. benthamiana* orthologs produced identical fluorescent patterns. Toc receptors and Tic22-III were dually localized in the cytoplasm and chloroplast envelope, while Toc75-III was predominantly localized in the chloroplast surface. Due to the stability of the β-barrel scaffold, GFP from recombinant proteins can partially withstand proteasomal degradation leading to cytoplasmic fluorescence. Alternatively, cytoplasm localization is consistent with previous subcellular localization studies in *A. thaliana*, pea, and *Bienertia sinuspersici* by chloroplast fractionation, immunogold, immunofluorescence, and CLSM with GFP-tagged proteins; for example, 40% of the BsToc159 and BsToc132 receptors were found in the cytoplasm (Hiltbrunner *et al.,* 2001; Lung and Chuong, 2012). At least for AtToc159, it was shown that the soluble form is active for interaction with AtToc33 lacking the membrane anchoring domain (Hiltbrunner *et al.,* 2001) and exhibits specific transit peptide binding (Smith *et al.,* 2004). Although the functional relevance of this soluble pool has been questioned (Becker *et al.,* 2004), it was also proposed that Toc complex assembly is a dynamic process in which the soluble fraction of the receptors may help preproteins to reach the translocon (Bauer *et al.,* 2002; Smith *et al.,* 2002).

Although Tom40, Om64 and Tom20 are mitochondrial outer membrane proteins, they showed different fluorescent patterns, which most likely reflect the ways each associate with the outer membrane of the mitochondria or the pathways by which they reach the mitochondrial surface. Tom40 is a β-barrel protein that requires the Tom complex and the sorting and assembly machinery (SAM) for its insertion, while Om64 and Tom20 receptors are single-spanning proteins. Om64 is a signal-anchored protein with an N-terminal transmembrane domain. Although little information about the process is available, Om64

must be inserted into the outer membrane through the mitochondrial import machinery (MIM) with Hsp70 chaperones and their co-chaperones, the J-proteins, playing an essential role in the process (Wiedemann and Pfanner, 2017; Gupta and Becker, 2021). In our study, Om64 overexpression may disrupt mitochondrial membrane permeability causing morphological alterations that result in swollen mitochondria. Finally, Tom20 receptors are tail-anchored (TA) proteins that associate with the membrane through its C-terminally located transmembrane domain. Because of their topology, they require a posttranslational pathway to be inserted into the membrane, most likely involving Guided Entry of Tail-anchored (GET) proteins such as Get3 in yeast (Farkas *et al.,* 2019). Get3 is a targeting factor that efficiently guides TA proteins to the ER but also interacts with some mitochondrial precursors. Moreover, when mitochondrial precursor accumulates in the cytoplasm, the GET pathway can direct them onto the ER surface from where they finally reach the mitochondria (Koch *et al.,* 2021). Chloroplasts and mitochondria also contain proteins that are closely related to Get3. Three GET3 paralogs of *A. thaliana* were localized to the cytosol (AtGET3a), chloroplast (AtGET3b), and mitochondria (AtGET3c) (Xing *et al.,* 2017; Mehlhorn *et al.,* 2021). GET3b has already been involved in targeting TA proteins to the thylakoids (Anderson *et al.,* 2021). Therefore, triple localization of NbTom20 and AtTom20 in the ER and mitochondrion and chloroplast envelope could be due to the oversaturation of the Get pathways.

To date, protein import systems in plants have been predominantly studied in *A. thaliana*, and a general picture of the molecular and regulation mechanisms will require studies in other species. Collectively, the findings presented are consistent with the notion that all proteins identified here are functional components of the chloroplast and mitochondrion protein import system in *N. benthamiana* and could likely be extended to other species in the genera *Nicotiana* and *Solanum*. Moreover, mitochondria and chloroplast are prime targets for viruses; in fact, many viral proteins involved in replication, movement, or plant defense overcoming are sent to these organelles. Knowing how these pathogen proteins hijack the plant import mechanisms to endosymbiotic organelles and identifying the specific host factors they use for that end will help to fight against them. Hence, we hope our results will be helpful for the further development of *N. benthamiana* as a research tool and will contribute not only

to a better knowledge of organelle protein import mechanisms but also plant-pathogen relationships.

EXPERIMENTAL PROCEDURES

Identification and gene amplification of the core components of the mitochondrion and chloroplast outer membrane translocases.

The Arabidopsis protein and DNA sequences from the Arabidopsis Information Resource (TAIR) were used as query sequences to search for the putative core components of the mitochondrion and chloroplast outer membrane translocases using the genomes and predicted proteomes of *Nicotiana benthamiana* at the Sol Genomics Network (v1.0.1) (https://solgenomics.net) and *Nicotiana benthamiana* Genome and Transcriptome Sequencing Consortium (https://benthgenome.qut.edu.au). Functional domains were determined using BLASTp available through the National Center of Biotechnology Information, NCBI (https://www.ncbi.nlm.nih.gov). TPRs and transmembrane domains were predicted using TPRpred (https://toolkit.tuebingen.mpg.de/tools/tprpred) and the Dense Alignment Surface method (https://tmdas.bioinfo.se/), respectively. Molecular weights were estimated using Compute pI/Mw (https://web.expasy.org/compute_pi) (Karpenahalli *et al.,* 2007). The coding region of NbToc90, NbToc120, NbToc159A, NbToc159B, NbToc34, NbTic22-III, NbToc75-III, NbTom20-1/-2, NbOm64 and NbTom40 were amplified by RT-PCR using SuperScript™ III One-Step RT-PCR Platinum™ Taq HiFi (Thermo Fisher Scientific, Carlsbad, CA, USA) and primers designed based on the ends of the gene sequences identified above (Supplementary Table S1). Total RNAs of *N. benthamiana*, isolated using EXTRAzol reagent following the producer's protocol (BLIRT S.A., Gdańsk, Poland), were used as RT-PCR templates. The amplified fragments were cloned into appropriate vectors (see more detailed information about them and their usage in this section) and automatically sequenced at the IBMCP DNA Sequencing Service to assess matching with database entries. Pairwise amino acid identity comparison was made using SIAS (Sequence Identity And Similarity) (http://imed.med.ucm.es/Tools/sias.html).

Phylogenetic analysis.

The Toc and Tom receptor protein sequences from some *Nicotiana sp*. and *Solanum sp*. (family *Solanaceae*), *Arabidopsis thaliana/lyrata* (family *Brassicaceae*) and *Cucumis sativus* (family *Cucurbitaceae*) were retrieved from NCBI database (Supplementary Table S2). Amino acid sequences of *N. noctiflora* proteins were obtained from the *N. tabacum* phylome (entry 251, PhylomeDB database, http://phylomedb.org/). The coat protein of the melon necrotic spot virus (GenBank: DQ339157.1) was used as an outgroup. The multiple sequence alignment was performed in MEGA XI using ClustalW with default settings (Tamura et al., 2021). Evolutionary analysis was also conducted in MEGA XI by reconstructing the bootstrap consensus tree of sequences employing the minimum evolution method with 10000 bootstrap replicates. All branches corresponding to partitions reproduced in less than 40% of bootstrap replicates were collapsed.

Molecular cloning.

For subcellular localization studies, the coding regions of NbToc90/120/159A/159B, NbToc34, NbTic22-III, NbToc75-III, NbTom20-1/-2, NbOm64 and NbTom40, obtained as indicated above, were digested with the restriction enzymes shown in the supplementary Table S1 and fused in-frame to the 5' or 3' ends of the enhanced green fluorescent protein (GFP) by cloning them into a modified pBluescriptIIKS+ already harboring a duplicated cauliflower mosaic virus (CaMV) 35S promoter and the terminator of the potato protease inhibitor II (PoPit), pKS35S-PP. Depending on the presence of internal restriction sites, the expression cassettes were liberated by digestion either with SacI, HindIII, BsaI, or BsmbI and cloned into pMOG800 (Knoester et al., 1998). We used both bimolecular fluorescence complementation (BiFC) in plants and yeast two-hybrid (Y2H) assays for interaction studies. For BiFC, we proceed similarly to before. Either an amino-terminal fragment of the green fluorescent protein (GFP) (positions 1-155, Nt-[GFP]) or a carboxyl-terminal GFP fragment (positions 156-238, Ct-[GFP]) was either fused to the amino or carboxyl terminus of NbToc90/120/159A/159B and NbToc34 coding regions. Next, recombinant cDNAs were inserted into pKS35S-PP and further, the expression cassettes were transferred to pMOG800. For Y2H, NbToc90/120/159A/159B and NbToc34 coding regions were cloned into pGBKT7 (binding domain). The coding region of NbToc34 was also cloned in pGADT7 (activation domain) (Takara Bio USA, Inc., Mountain View, CA, USA). Oligonucleotides and restriction enzymes are listed in Supplementary Table S1.

Agrobacterium tumefaciens-mediated transient expression and bimolecular fluorescence complementation (BiFC) assays.

For transient expression assays in *N. benthamiana*, binary vectors obtained before were introduced into *Agrobacterium tumefaciens* strain C58C1 by electroporation. Transformed bacteria were grown overnight in liquid Luria-Bertani (LB) medium supplemented with kanamycin and rifampicin antibiotics. Cultures were pelleted and resuspended up to the required final OD600 value (0.2) with 10 mM $MgCl_2$, 10 mM MES pH 5.6 and 150 µM acetosyringone. These suspensions were introduced in two-week-old leaves of *N. benthamiana* by gentle pressure infiltration into the abaxial side. For colocalization and BiFC experiments, which need the simultaneous expression of two different proteins, cultures were adjusted to an OD600 value of 0.5 and mixed in equal proportions before infiltration. Plants were grown under long-day photoperiods (16 h light at 25 ºC and 8 h dark at 22 ºC).

Laser scanning confocal microscopy, subcellular fluorescent markers and image analysis.

The fluorescent-tagged protein subcellular localization and BiFC were visualized with an inverted Zeiss LSM 780 laser scanning confocal microscope (Carl Zeiss, Oberkochen, Germany) two days after the agroinfiltration. eGFP and cherry fluorescent protein (ChFP) excitation were done using 488 and 561 nm wavelength lasers, respectively. The windows for emission detection were set between 492–532 nm for GFP and 590–630 nm for ChFP. The chlorophyll excitation wavelength was 488 nm, and emission was collected above 700 nm. Transit peptide of yeast cytochrome oxidase subunit IV (coxP, matrix) fused to a cherry fluorescent protein (ChFP) N-terminus (coxP-ChFP) was used as a mitochondrial matrix marker. In addition, glyrsP-ChFP consisting of the transit peptide of the *A. thaliana* glycyl-tRNA synthetase fused to the ChFP was used as a chloroplast and mitochondrion dual marker (Navarro *et al.,* 2021). Image processing and analysis, including overlays and Z-stack projections, were performed using FIJI software (Schindelin *et al.,* 2012).

Yeast two-hybrid (Y2H) assay.

Y2H assays were performed using the GAL4-based MATCHMAKER Two-Hybrid System following the manufacturer's protocol (Fields and Song, 1989) (Takara Bio USA, Inc., Mountain View, CA, USA). Full-length ORFs of NbToc90, NbToc120, NbToc159A and NbToc159B and NbToc34 were used as prey and cloned into pGADT7 (pGADNbToc90, pGADNb120,

pGADNb159A, pGADNb159B and pGADNbToc34). NbToc34 ORF was also cloned into pGBDKT7 to be used as a bait vector (pGBNbToc34) and transformed into AH109 yeast cells. Next, all pGAD constructs were transformed into AH109 cells already containing pGBNbToc34. Putative interactions were analyzed by culturing co-transformants on SD+DO-A-H-L-W+X-α Gal. To confirm the specificity of the interactions, all pGAD constructs were also transformed in yeast cells harboring pGBKT7 or pBD-p53 (tumor protein p53).

Viral-induced gene silencing in *A. thaliana.*

For VIGS, pTRV1 and pTRV2 Gateway vectors were used (Liu *et al.,* 2002). A target region of about 300 bp from NbToc90/120/159A/159B, NbToc34, NbTic22-III, NbToc75-III, NbTom20-1/-2, NbOm64 and NbTom40 genes was selected using SGN VIGS Tool (Fernandez-Pozo et al., 2015). Fragments were PCR amplified with gene-specific oligonucleotides (Supplementary Table S1) and then recombined with pDONR207. The resultant pENTRY vectors were recombined with pTRV2 according to the manufacturer's instructions (Invitrogen Life Tech, Carsland, CA, USA). A pTRV2 carrying the complete mGFP5 gene, pTRV2[GFP] (Navarro et al., 2020), was used as control. pTRV1 and all pTRV2 derivates were introduced into *A. tumefaciens* by electroporation. Agroinfiltrations for VIGS were done using the leaf infiltration method in *N. benthamiana* as described above, but, on this occasion, bacterial cultures were resuspended to a final OD600 of 1. Two-week-old *N. benthamiana* seedlings were infiltrated with bacterial cultures carrying pTRV1 and each pTRV2 derivated mixed in a 1:1 volume ratio. Gene silencing was monitored using real-time quantitative reverse transcription PCR over ten days after infiltration. Plants were grown under long-day photoperiods (16 h light at 25 ºC and 8 h dark at 22 ºC).

Real-time quantitative reverse transcription PCR.

Total RNA from at least three silenced plants of each gene was obtained by extraction with RIBOzol Reagent. Remnant genomic DNA was removed by DNase I treatment. First-strand cDNA was synthesized from 0.5 µg of total RNA using RevertAid H Minus Reverse Transcriptase and oligo(dT) (Thermo Fisher Scientific, Carlsbad, CA, USA). Real-time qPCR was carried out using QuantStudio 3 Real-Time PCR machine (Applied Biosystems, Waltham, MA, USA) and PyroTaq EvaGreen qPCR Supermix (Solis BioDyne, Tartu, Estonia), specific oligonucleotides, and recommended qPCR cycles as follows: initial denaturation for 12 min at 95 °C, followed

by 50 cycles of 15 s at 95 °C and 60 s at 60 °C. Specific oligonucleotides were designed using Primer3web version 4.1.0 (https://bioinfo.ut.ee/primer3). Oligonucleotide efficiencies were tested by qRT-PCR using tenfold serial dilutions of the corresponding cDNA. Each biological replicate was run in triplicate. Elongation factor 1-α (EF1α, TC19582), F-BOX family protein (F-BOX, Niben.v0.3.Ctg24993647) and protein phosphatase 2A (PP2A, TC21939) genes were used as endogenous controls (Liu *et al.,* 2012).

SUPPLEMENTARY MATERIAL

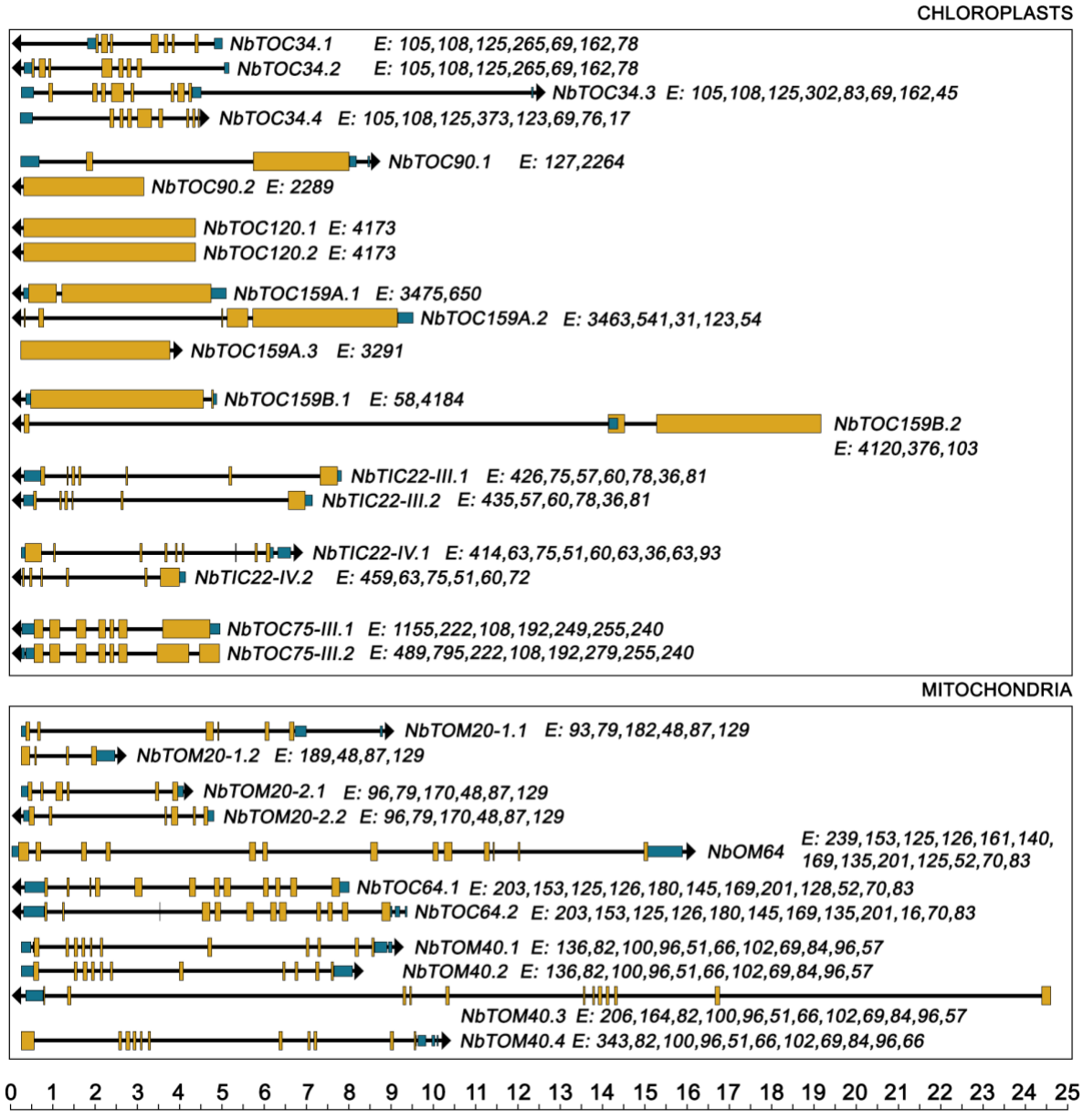

Figure S1. Gene structure of the *N. benthamiana* core components of Toc and Tom complexes, including *NbTIC22-III* and *NbTIC22-IV*. Filled orange and dark cyan boxes represent exons and UTR, respectively, and thin

lines represent introns. The size of exons (E) is indicated in the direction from the 5' to 3' end of the gene. The scale line at the bottom indicates DNA length in kb pairs.

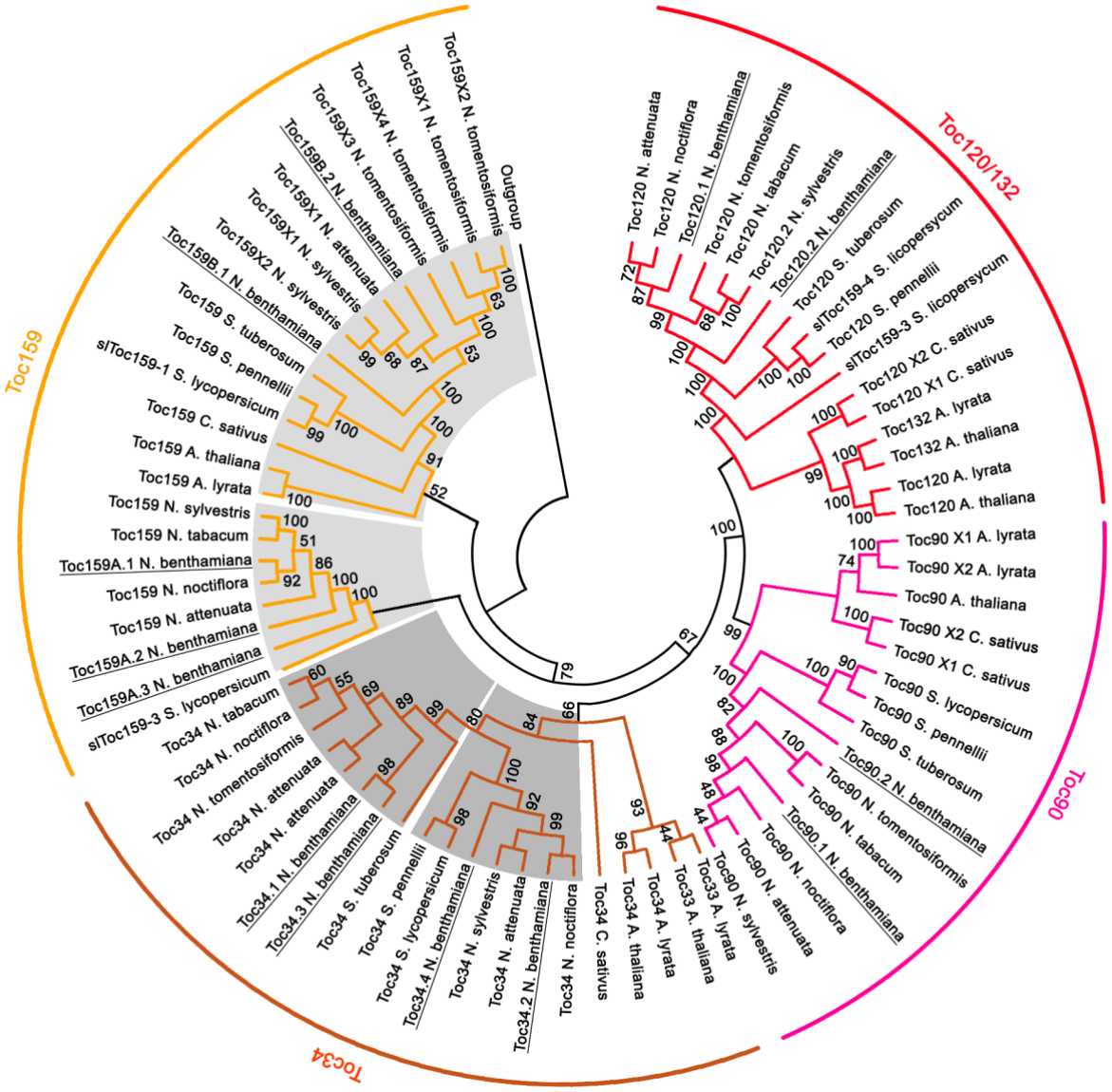

Figure S2. Phylogenetic analysis of Toc receptors Toc34, Toc90, Toc120, Toc132 and Toc159 from *Arabidopsis thaliana/lyrata* (family *Brassicaceae*), *Cucumis sativus* (family *Cucurbitaceae*) and other species from *Nicotiana sp.* and *Solanum sp.* (family *Solanaceae*) were retrieved from NCBI and PhylomeDB databases (see accession numbers in Supplementary Table S2). The coat protein of the melon necrotic spot virus (GenBank: DQ339157.1) was used as an outgroup. The multiple sequence alignment was performed in MEGA XI using ClustalW. Evolutionary analysis was also conducted in MEGA XI by reconstructing the bootstrap consensus tree of sequences employing the Minimum Evolution method with 10000 bootstrap replicates. The bootstrap values with 10000 repetitions (%) are given at the respective nodes. All branches corresponding to partitions reproduced in less than 40% of bootstrap replicates were collapsed.

Figure S3. Phylogenetic analysis of Tic receptors Tic22-III and Tic22IV from *Arabidopsis thaliana/lyrata* (family *Brassicaceae*) and other species from *Nicotiana sp*. and *Solanum sp*. (family *Solanaceae*). Sequences were retrieved from NCBI and PhylomeDB databases (see accession numbers in Figure and Supplementary Table S2). The coat protein of the melon necrotic spot virus (GenBank: DQ339157.1) was used as an outgroup. The multiple sequence alignment was performed in MEGA XI using ClustalW. Evolutionary analysis was also conducted in MEGA XI by reconstructing the bootstrap consensus tree of sequences employing the Minimum Evolution method with 10000 bootstrap replicates. The bootstrap values with 10000 repetitions (%) are given at the respective nodes. All branches corresponding to partitions reproduced in less than 40% of bootstrap replicates were collapsed.

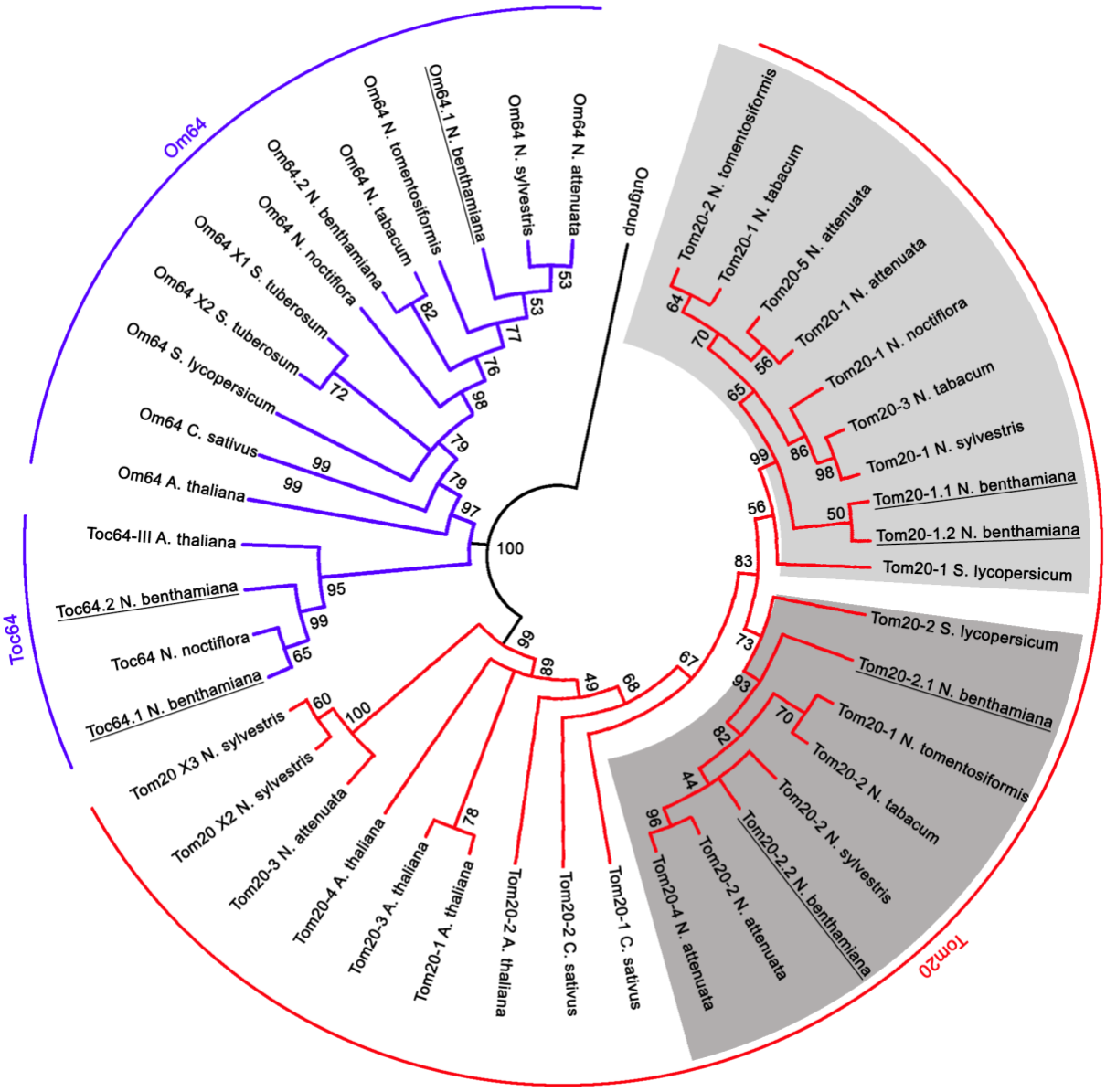

Figure S4. Phylogenetic analysis of Tom receptors Tom20 and Om64 from *Arabidopsis thaliana/lyrata* (family *Brassicaceae*), *Cucumis sativus* (family *Cucurbitaceae*) and other species from *Nicotiana sp.* and *Solanum sp.* (family *Solanaceae*) were retrieved from NCBI and PhylomeDB databases (see accession numbers in Supplementary Table S2). The coat protein of the melon necrotic spot virus (GenBank: DQ339157.1) was used as an outgroup. The multiple sequence alignment was performed in MEGA XI using ClustalW. Evolutionary analysis was also conducted in MEGA XI by reconstructing the bootstrap consensus tree of sequences employing the Minimum Evolution method with 10000 bootstrap replicates. The bootstrap values with 10000 repetitions (%) are given at the respective nodes. All branches corresponding to partitions reproduced in less than 40% of bootstrap replicates were collapsed.

Figure S5. Phylogenetic analysis of Toc75-III and Tom40 from *Arabidopsis thaliana/lyrata* (family *Brassicaceae*) and other species from *Nicotiana sp.* and *Solanum sp.* (family *Solanaceae*) were retrieved from NCBI and PhylomeDB databases (see accession numbers in Figure and Supplementary Table S2). The coat protein of the melon necrotic spot virus (GenBank: DQ339157.1) was used as an outgroup. The multiple sequence alignment was performed in MEGA XI using ClustalW. Evolutionary analysis was also conducted in MEGA XI by reconstructing the bootstrap consensus tree of sequences employing the Minimum Evolution method with 10000 bootstrap replicates. The bootstrap values with 10000 repetitions (%) are given at the respective nodes. All branches corresponding to partitions reproduced in less than 40% of bootstrap replicates were collapsed.

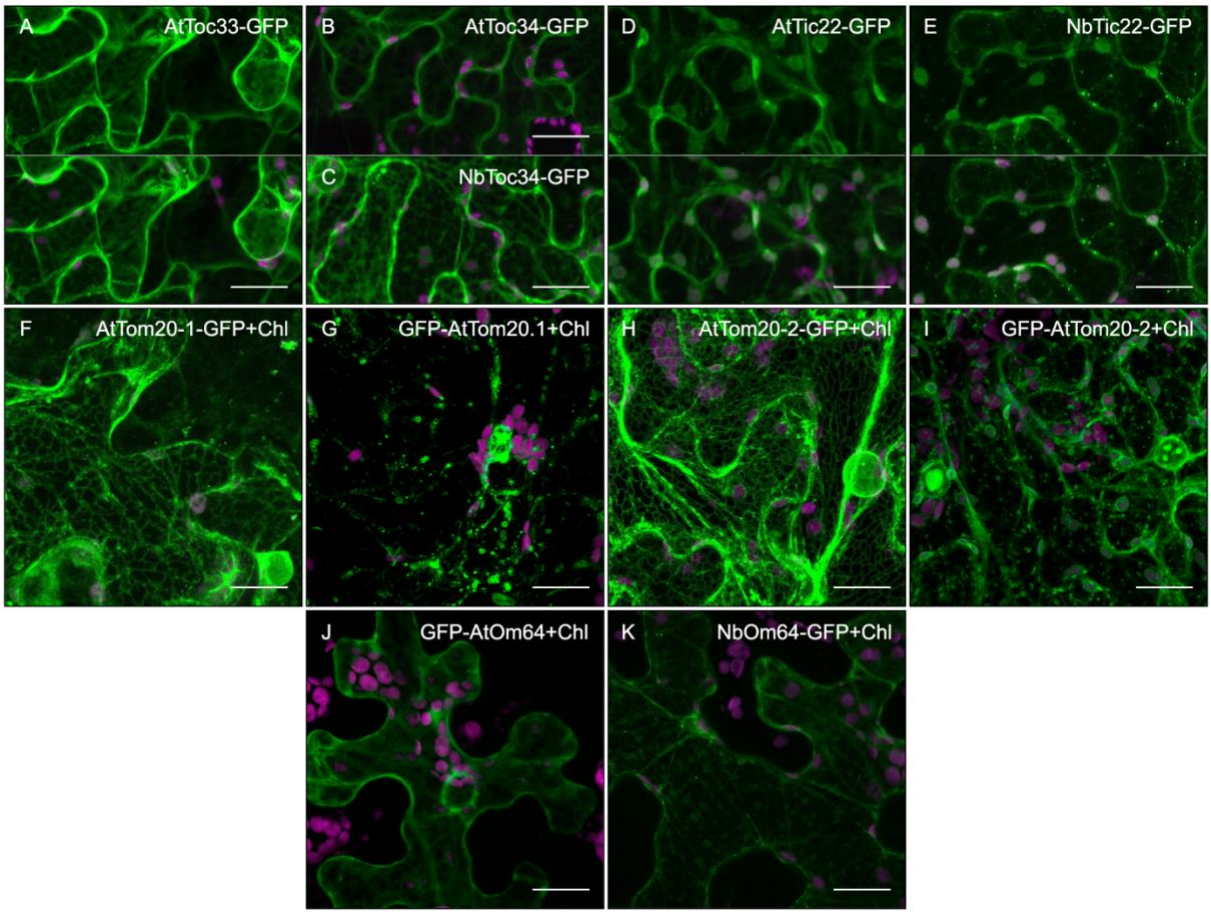

Figure S6. Subcellular localization of AtToc33-GFP **(A)**, AtToc34-GFP **(B)**, NbToc34-GFP **(C)**, AtTic22-III-GFP **(D)**, NbTic22-III-GFP **(E)**, AtTom20-1-GFP **(F)**, GFP-AtTom20-1 **(G)**, AtTom20-2-GFP **(H)**, GFP-AtTom20-1 **(I)**, GFP-AtOm64 **(J)** and GFP-NbOm64 **(K)**. GFP fusion proteins (green channel), indicated in the upper part of each panel, were expressed in epidermal cells of *N. benthamiana* by transient expression mediated by Agrobacterium. All LSCM images correspond to Z-stack projections taken two days after infiltration. Chlorophyll fluorescence is indicated (Chl) and shown in magenta. Scale bars correspond to 20 µm.

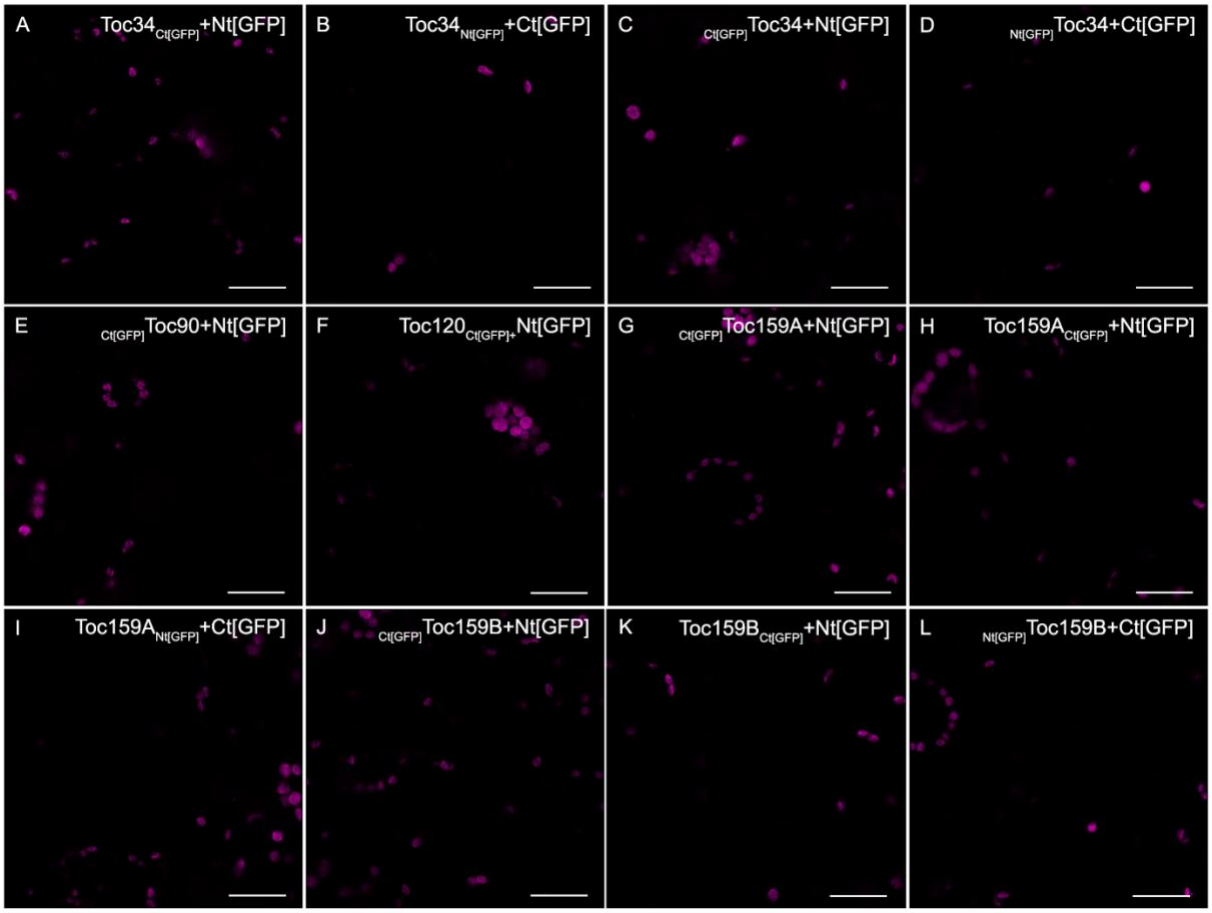

Figure S7. Negative controls of constructs involved in positive combinations from the bimolecular fluorescence complementation assay showed in Figure 6. Leaves of *N. benthamina* were cotransfected with Agrobacterium carrying the constructs for expression of either NbToc34, NbToc159A, NbToc159B, NbToc120 or NbToc90 tagged with Nt[GFP] or Ct[GFP] combined with free Nt[GFP] or Ct[GFP] as indicated in the top of each panel. All LSCM images correspond to Z-stack projections taken two days after infiltration. Chlorophyll fluorescence is shown in magenta. Scale bars correspond to 20 µm.

Supplementary Table S1. List of oligonucleotides used in this study.

Subcellular localization and BiFC studies

Plasmid	Gene	Forward primer	Reverse primer
pMOG800	AtToc75-III	ACGTGGTCTCCCATGGCCGCCTTCT CCGTCAAC BsaI[1]	ACGTGGTCTCGCTAGC**TTA**ATACCTCTC TCCAAATCGGAAG BsaI ACGTGGTCTCGCTAGCATACCTCTCTCC AAATCGGAAG BsaI
	AtToc33	ACGTCCATGGGGTCTCTCGTTCGTG A NcoI	ACGTGCTAGC**CTA**AAGTGGCTTTCCAC TTG NheI ACGTGCTAGCAAGTGGCTTTCCACTTG NheI
	AtToc34	GCATCCATGGCAGCTTTGCAAACG CTT NcoI	ACGTGCTAGC**TCA**AGACCTTCGACTTG CTA

		GCATGCTAGCAGACCTTCGACTTGCTA A NheI
AtToc90	GCATTCATGAAAGGCTTCAAAGA PagI	GCATACTAGT**TTA**GGAAACGAGAAAA SpeI GCATACTAGTGGAAACGAGAAAA SpeI
AtToc120	AGCTCGTCTCTCATGGGAGATGGG GCTGAGATTG BsmBI	AGTCCGTCTCTCTAGGTGTCCATATTGC ATTTG BsmBI AGTCCGTCTCTCTAG**TCA**GTGTCCATAT TGCATTTG BsmBI
AtToc132	AGCTCGTCTCTCATGGGAGATGGG ACTGAGTTTG BsmBI	AGCTCGTCTCTCTAGTTGTCCATATTGC GTTTG BsmBI AGCTCGTCTCTCTAG**TCA**TTGTCCATAT TGCGTTTG BsmBI
AtToc159	ACGTGGTCTCGCATGGACTCAAAG TCGGTTAC BsaI	CATGGGTCTCGCTAGCGTACATGCTGT ACTTGT BsaI CATGGGTCTCGCTAG**TCA**CGTACATGC TGTACTTGT BsaI
AtTic22-III	ATGCGGTCTCTCATGAATTCAAACA TTTTCCCACC BsaI	ATGCGGTCTCGCTAGCCTCCTGTGTTT GCTCAGTTG BsaI ATGCGGTCTCGCTAG**TTA**CCTCCTGTG TTTGCTCAGTTG BsaI
AtTom40	ACGTGGTCTCCCATGGCGGATCTTT TACCACCTC BsaI	ACGTGGTCTCGCTAGCACCAACTGTTA ATCCGAAACC BsaI ACGTGGTCTCGCTAGC**TTA**ACCAACTG TTAATCCGAAACC BsaI
AtTom20-1	GCATCCATGGATAAGCTGAATTT NcoI	GCATTCTAGACCTTAGCTTTCGA XbaI GCATTCTAGA**TCA**CCTTAGCTTTCGA XbaI
AtTom20-2	ACGTCCATGGAGTTCTCTACCGCCG NcoI	ACGTGCTAGCTCTGGCAGGAGGTGGA GGG NheI ACGTGCTAGC**TCA**TCTGGCAGGAGGT GGAGGG NheI
AtTom20-3	ACGTCCATGGATACGGAAACTGAG TTC NcoI	ACGTGCTAGCACGAGGAGGAGAGAC AGGC NheI ACGTGCTAGC**CTA**ACGAGGAGGAGAG ACAGGC NheI
AtTom20-4	ACGTCCATGGATATGCAGAATGAAA ACG NcoI	ACGTACTAGTCTGCCTTGACACCGGCG TC SpeI ACGTACTAGT**TTA**CTGCCTTGACACCG GCGTC SpeI

AtOm64	GCATCCATGGCCTCGAATACGCTTT CTTTG NcoI	ACGTGCTAGCTATGTGTTTTCGGAGTC TCTTC NheI ACGTGCTAGC**TCA**TATGTGTTTTCGGA GTCTC NheI
NbToc75-III	ACGTCGTCTCCCATGGCGTCCATCG CCGCTCC BsmBI	ACGTCGTCTCGCTAGCGAATCTCTCTCC AAAACGG BsmBI ACGTCGTCTCGCTAGC**CTA**GAATCTCTC TCCAAAACGG BsmBI
NbToc34	AGTCCCATGGCATCTCAACTAATTA GAGA NcoI	AGTCGCTAGCTGCCCATGAAGGGCTG CTCT NheI AGTCGCTAGC**TCA**TGCCCATGAAGGG CTGCTCT NheI
NbToc90	AGCTCGTCTCTCATGATGAGTTTGA AGGATTGGG BsmBI	AGTCCGTCTCTCTAGCTCCCGCTTCCA GGGA BsmBI AGTCCGTCTCTCTAGC**CTA**TCCCGCTTC CAGGGA BsmBI
NbToc120	AGCTCGTCTCTCATGGAAAATGGG GAGGAAGTATT BsmBI	AGTCCGTCTCTCTAGAAATTGCACTGG TTGAGAGAAG AGTCCGTCTCTCTAGA**TCA**AATTGCAC TGGTTGAGAGAAG
NbToc159A	AGCTCGTCTCTCATGAATTCAAAGA TTTATGGTGTTCCAC BsmBI	AGTCCGTCTCTCTAGCTATTAAGTTCTT TTCACTTGTTTGCG AGTCCGTCTCTCTAGC**CTA**TATTAAGTT CTTTTCACTTGTTTGCG
NbToc159B	AGCTCGTCTCTCATGCTGAAGTCAG TGAAGC BsmBI	AGCTCGTCTCTCTAGCGTAGATCGAGT ACTTCTCGC BsmBI AGCTCGTCTCTCTAGC**TCA**GTAGATCG AGTACTTCTCGC BsmBI
NbTic22-III	ATGCGGTCTCTCATGAATATCTTCAA ACCTAAACAGTC BsaI	AGTCGGTCTCGCTAGCCTTCTGGGAGT GATCTGTTGAA BsaI AGTCGGTCTCGCTAGC**TCA**CTTCTGGG AGTGATCTGTTGAA BsaI
NbTom40	ACGTCGTCTCCCATGGCCACTCTCA TTCCTCC BsmBI	ACGTCGTCTCGCTAGCCTCTCCCACTG TAAGCCC BsmBI ACGTCGTCTCGCTAGC**CTA**CTCTCCCAC TGTAAGCCC BsmBI
NbTom20-1	AGTCCCATGGAGCAAAACGATTTC GA NcoI	ATGCGCTAGCTCTTGGAGGAGGAGGA GGAGGCA NheI ATGCGCTAGC**TTA**TCTTGGAGGAGGA GGAGGAGGCA NheI
NbTom20-2	ACGTCCATGGATATGCAAAGCGAG NcoI	ACGTGCTAGCTTGGGTAGGAGGAGGG GGT NheI

			ACGTGCTAGC**TTA**TTGGGTAGGAGGA GGGGGT NheI
	NbOm64	AGCTGGTCTCCCATGACAAAATTAT CGAAGCTAAATG BsaI	ACGTGGTCTCGCTAGCACTAATTAGCT TTCTGAGTC BsaI ACGTGGTCTCGCTAGC**TCA**ACTAATTA GCTTTCTGAGTC BsaI
Viral induced gene silencing (VIGS)			
Plasmid	Gene	Forward primer	Reverse primer
pDONR207 **pTRV2**	GFP	*GGGGACAAGTTTGTACAAAAAAGC AGGCTTC*AGTAAAGGAGAAGAACT TTTC attB1[2]	**CCTTGAAGAAGATGGTCCTCTC**[3]
	NbToc75-III	*GGGGACAAGTTTGTACAAAAAAGC AGGC*ACAATTGTTGGTGAGAGGAA TG attB1	*GGGGACCACTTTGTACAAGAAAGCTG GGT*GCATCTCAGCAGCCAGCTCCAG attB2
	NbToc34	**GAGAGGACCATCTTCTTCAAGG**GT CCCGAAGATCAGAGG	*GGGGACCACTTTGTACAAGAAAGCTG GGTG*TGGAATGCTAATATAAAAGGAAT TA attB2
	NbToc90	**GAGAGGACCATCTTCTTCAAGG**TG ATGAGTTTGAAGG	*GGGGACCACTTTGTACAAGAAAGCTG GGTG*AGCTTCAATCTTTACCACTG attB2
	NbToc120	**GAGAGGACCATCTTCTTCAAGG**CA CAGAGGACTTGAGA	*GGGGACCACTTTGTACAAGAAAGCTG GGTG*TACCGGCTGGCACTTATTG attB2
	NbToc159A	**GAGAGGACCATCTTCTTCAAGG**CT TTGAATACTCTAA	*GGGGACCACTTTGTACAAGAAAGCTG GGTG*AGTCCCTCAATGGTATCTGC attB2
	NbToc159B	**GAGAGGACCATCTTCTTCAAGG**AC GACCAAGGCCAACA	*GGGGACCACTTTGTACAAGAAAGCTG GGTG*ATCAACAAGCAGAAAAATGTTT CTGT attB2
	NbTic22-III	**GAGAGGACCATCTTCTTCAAGG**AA GGAAAGGGAAAGGA	*GGGGACCACTTTGTACAAGAAAGCTG GGTG*ATCTGTTGAAACATCGAAAC attB2
	NbTom40	*GGGGACAAGTTTGTACAAAAAAGC AGGC*AGAACTTTTTGAAGGATTGC GC attB1	*GGGGACCACTTTGTACAAGAAAGCTG GGTA*CCATGCCATGCGACATGTGTG attB2
	NbTom20-1	**GAGAGGACCATCTTCTTCAAGG**TT TACTTTGACAAATCAGCT	*GGGGACCACTTTGTACAAGAAAGCTG GGT*GGGAGGAGGAGGAGGCACATTA GATT attB2
	NbTom20-2	**GAGAGGACCATCTTCTTCAAGG**AT TGGAATTATCACAGTTCC	*GGGGACCACTTTGTACAAGAAAGCTG GGT*GTTGTGGATTTCCAAGTGCAACTC TG attB2

	NbOm64	**GAGAGGACCATCTTCTTCAAGG**GG AAATGCTGCATATAAGG	*GGGGACCACTTTGTACAAGAAAGCTG GGT*GAGCCAAACTGGCAACCTTATT attB2
Yeast2hybrid (Y2H) studies			
Plasmid	Gene	Forward primer	Reverse primer
pGBKT7/ pGADT7	NbToc34	ACGTGGTCTCGAATTCATGGCATCT CAACTAATTAGAGA BsaI	ACGTGGTCTCGGATCCCTATGCCCATG AAGGGCTGCTCT BsaI
	NbToc90	ACGTCGTCTCGAATTCATGATGAGT TTGAAGGATTGGG BsmBI	ACGTCGTCTCGGATCCTCATCCCGCTTC CAGGGA BsmBI
	NbToc120	ACGTCGTCTCGAATTCATGCTGAAG TCAGTGAAGC BsmBI	ACGTCGTCTCGGATCCTTAGTAGATCG AGTACTTCTCGC BsmBI
	NbToc159A	ACGTCGTCTCGAATTCATGGAAAAT GGGGAGGAAGTATT BsmBI	ACGTCGTCTCGGATCCTCAAAATTGCA CTGGTTGAGAGAAG BsmBI
	NbToc159B	ACGTCGTCTCGAATTCATGAATTCA AAGATTTATGGTGTTCC BsmBI	ACGTCGTCTCGGATCCCTATATTAAGTT CTTTTCACTTGTTTGCG BsmBI
Real Time RT-qPCR			
Gene	Access	Forward primer	Reverse primer
NbToc75-III	Niben101Scf01482g01002.1 Nbv5.1tr6393264	CGCTCCTGGTATCGCACTTT	GATGAGGGTTTGGGGTTTTG
NbToc34	Niben101Scf04926g06003.1 Nbv6.1trP36581	CACCGAGGAATTGTGGTTCT	AATTGCAGCAGCCTGAATCT
NbToc90	Niben101Scf09929g01001.1 Nbv6.1trP76192	CTGGTTTATTGCCTCCCTCA	GCTTCAACAAGGGGAAATCA
NbToc120	Niben101Scf04223g01022.1 Nbv6.1trP64107	TGAGGACATGGTGGAACAAA	CTTTTCAAAGGCTGGAGTGC
NbToc159A	Niben101Scf06776g00001.1 Nbv6.1trP55981	GATGGGGACAATCAGGCTTA	AGGAAACTGACCTGCAATGG
NbToc159B	Niben101Scf07086g00019.1 Nbv6.1trA113891	CCATGGCTGGCTTTGATATT	CTTTAAGCCCGGTAACCACA
NbTic22-III	Niben101Scf28230g00015.1 Nbv6.1trP63905	CACTTTTCCGCAACTCAACA	TGCATAAACAGGCACTCCAG
NbTom40	Niben101Scf01291g00001.1 Nbv6.1trA47115	AACTTGCCTTGCCCTATTCC	TGTGGGGCCCATAAGTACAC
NbTom20-1	Niben101Scf00109g10030.1 Nbv6.1trA114286	CAGGACCTTCGACATCAACA	ATCTTGGAGGAGGAGGAGGA
NbTom20-2	Niben101Scf03766g01008.1 Nbv6.1trA6574	TGCACTTGGAAATCCACAAA	CACCCATGCAACAATACCAA
NbOm64	Niben101Scf02133g01001.1 Nbv6.1trP34412	GCATCAAACGTACCCAGCTT	GTTTCACCGCTTTCATCCAT

Supplementary Table S2. Accession numbers of Tom and Toc receptors of different plant species used in phylogenetic analysis.

Species	Protein	Accession number	Species	Protein	Accession number
A. lyrata	Toc33	XP_002892097.1			
	Toc34	XP_020876012.1			
	Toc90 X1	XP_020879152.1			
	Toc90 X2	XP_002873990.1			
	Toc120	XP_020889089.1			
	Toc132	XP_020887996.1			
	Toc159	XP_002874910.1			
A. thaliana	Toc33	AT1G02280.1	*A. thaliana*	Tom20-1	AT3G27070.1
	Toc34	AT5G05000.1		Tom20-2	AT1G27390.1
	Toc90	AT5G20300.1		Tom20-3	AT3G27080.1
	Toc120	AT3G16620.1		Tom20-4	AT5G40930.1
	Toc132	AT2G16640.1		Om64	AT5G09420.1
	Toc159	AT4G02510.1			
N. tomentosiformis	Toc34	XP_009599441.1	*N. tomentosiformis*	Tom20-1	XP_009601172.1
	Toc90	XP_009608571.1		Tom20-2	XP_009620342.1
	Toc120	XP_009610657.1		Om64	XP_009624799.1
	Toc159 X1	XP_009602186.1			
	Toc159 X2	XP_018626732.1			
	Toc159 X3	XP_018626733.1			
	Toc159 X4	XP_018626735.1			
N. attenuata	Toc34.1	XP_019231210.1	*N. attenuata*	Tom20-1	XP_019226716.1
	Toc34.2	XP_019245357.1			
	Toc90	XP_019255958.1		Tom20-2	XP_019239067.1
	Toc120.1	XP_019253520.1		Tom20-3	OIT29074.1
	Toc120.2	XP_019255958.1		Tom20-4	XP_019239067.1
	Toc159	XP_019241310.1		Tom20-5	XP_019226716.1
	Toc159	XP_019232171.1		Om64	XP_019249941.1
N. tabacum	Toc34	XP_016457516.1	*N. tabacum*	Tom20-1	XP_016457148.1
	Toc90	XP_016508006.1		Tom20-2	XP_016438094.1
	Toc120	XP_016485376.1		Tom20-3	XP_016487017.1
	Toc159	XP_009769991.1		Om64	XP_016456544.1
N. sylvestris	Toc34	XP_009779337.1	*N. sylvestris*	Tom20-1	XP_009790058.1
	Toc90	XP_009791876.1		Tom20-2	XP_009783275.1
	Toc120	XP_009768002.1		Tom20 X2	XP_009785207.1
	Toc159	XP_009769991.1		Tom20 X3	XP_009785208.1
	Toc159 X1	XP_009781898.1		Om64	XP_009776046.1

	Toc159 X2	XP_009781899.1			
N. noctiflora	Toc 34	Phy00D7QQR_118707	*N. noctiflora*	Tom20.1	Phy00D8263_118707
	Toc 90	Phy00D7QME_118707			
	Toc 120	Phy00D7YSH_118707			
	Toc 159	Phy00D830G_118707		Om64	Phy00D80ZF_118707
S. lycopersicum	Toc34	XP_004239977.2			
	Toc90	XP_004242739.1	*S. lycopersicum*	Tom20-1	XP_004231778.1
	Toc120	XP_004231012.1		Tom20-2	XP_004233293.1
	Toc159	XP_010326580.1		Om64	XP_004248799.1
S. tuberosum	Toc 34	XP_006358174.1	*S. tuberosum*	Om64 X1	XP_006341842.1
	Toc 90	XP_006359492.1			
	Toc 120	XP_006359664.1		Om64 X2	XP_015161806.1
	Toc 159	XP_015169888.1			
S. pennellii	Toc 34	XP_015074809.1			
	Toc 90	XP_015087308.1			
	Toc 120	XP_015089777.1			
	Toc 159	XP_015082300.1			
C. sativus	Toc 34	XP_004146141.1	*C. sativus*	Tom20-1	XP_004142933.1
	Toc 90 X1	XP_011648710.2		Tom20-2	XP_004145663.1
	Toc 90 X2	XP_011648711.1			
	Toc 120 X1	XP_004144917.2		Om64	XP_004136877.1
	Toc 120 X2	XP_031745274.1			
	Toc 159	XP_004152365.2			

Supplementary Table S3. List of *Nicotiana benthamiana* accession numbers of putative Tom and Toc receptors, main pores and Tic22, assignment to the parental ancestor and amino acid sequence identity

Protein	Accession number: Sol Genomics Network NibSet1-1 NbDE*	Scaffold	Parental origin	Chromosome (NbLab330 database)	Amino acid identity
NbToc75-III.1	Niben101Scf01482g01002.1 g13969.t1 (100%) NbD011778.1 (100%)	Paternal	Maternal	18	Niben101Scf01482g01002.1 vs Niben101Scf08757g00006.1 = 92.2%
NbToc75-III.2	Niben101Scf08757g00006.1 g35129.t1 (94.3%) NbD043052.1 (99.63%)	Maternal	Maternal	09	
NbToc34.1	Niben101Scf04926g06003.1 g17921.t1 (98.01) NbD001798.1 (99.66%)	Maternal	Maternal	16	Niben101Scf04926g06003.1 vs Niben101Scf00454g05025.1 = 85.4%
NbToc34.2	Niben101Scf00454g05025.1 g24833.t1 (98.33%)	Maternal	Maternal	10	

	NbD004316.1 (100%)				
NbToc34.3	Niben101Scf00163g07005.1 g39689.t1 (100%)	Maternal	Maternal	06	Niben101Scf04926g06003.1 vs Niben101Scf00163g07005.1 = 94.44%
NbToc34.4	Niben101Scf08179g01017.1 g5776.t1 (99.02%)	Paternal	orphan	15	Niben101Scf08179g01017.1 vs Niben101Scf00454g05025.1 = 96.08%
NbToc90.1	Niben101Scf09929g01001.1 g54947.t1 (100%) NbD045210.1 (100%)	Maternal	Maternal	16	Niben101Scf09929g01001.1 vs Niben101Scf04918g02009.1 = 92.51%
NbToc90.2	Niben101Scf04918g02009.1 g91899.t1 (97.9%) NbD031159.1 (99.08%)	Maternal	Maternal	07	
NbToc120.1	Niben101Scf04223g01022.1 g65878.t1 (100%) NbD028297.1 (100%)	Orphan	Maternal	08	Niben101Scf04223g01022.1 vs Niben101Scf01847g07003.1 = 93.52%
NbToc120.2	Niben101Scf01847g07003.1 g36650.t1 (100%) NbD014331.1 (100%)	Ø	Maternal	18	
NbToc159A.1	Niben101Scf06776g00001.1 g62550.t1 (100%) NbD037689.1(100%)	Maternal	Maternal	09	Niben101Scf06776g00001.1 vs Niben101Scf03857g01008.1 = 90.32%
NbToc159A.2	Niben101Scf03857g01008.1 g23395.t1 (98.01%) NbD026259.1(98.01%)	Maternal	Maternal	04	Niben101Scf06776g00001.1 vs Niben101Scf05044g00002.1= 92.81%% Niben101Scf03857g01008.1 vs Niben101Scf05044g00002.1= 95.08%%
NbToc159A.3	Niben101Scf05044g00002.1 g13934.t1 NbD031696.1	Maternal	Maternal	06	
NbToc159B.1	Niben101Scf07086g00019.1 g92014.t1 (100%) NbD038692.1 (100%)	Ø	Maternal	18	Niben101Scf07086g00019.1 vs Niben101Scf03648g02002.1 = 95.33%
NbToc159B.2	Niben101Scf03648g02002.1 g71266.t1 (99.86%) NbD025242.1(99.79%)	Maternal	Maternal	08	
NbTic22-III.1	Niben101Scf28230g00015.1 g42700.t1 (100%) NbD052702.1 (100%) NbD021651.1 (96.49%)	Paternal	Paternal	18	Niben101Scf28230g00015.1 vs Niben101Scf02964g00008.1 = 95.16%
NbTic22-III.2	Niben101Scf02964g00008.1 g16180.t1 (100%) NbE05066886.1 (95.96%)	Orphan	Orphan	08	
NbTic22-IV.1	Niben101Scf13041g02009.1 g23894.t1 (100%) NbD048958.1(99.64%) NbD001113.1 (94.14%)	Paternal	Paternal	03	Niben101Scf00090g13017.1 vs Niben101Scf13041g02009.1 = 93.00%
NbTic22-IV.2	Niben101Scf00090g13017.1 g20888.t1 (99.6%)	Orphan	Paternal	15	
NbTom40.1	Niben101Scf01291g00001.1	Maternal	Maternal	19	

	g85929.t1 (100%) NbD010422.1 (100%)				Niben101Scf01291g00001.1 vs Niben101Scf01451g05003.1 = 97.76%
NbTom40.2	Niben101Scf01451g05003.1 g78581.t1 (100%) NbD011590.1 (100%)	Maternal	Maternal	05	
NbTom40.3	Niben101Scf05971g00007.1 g18096.t1 (100%) NbD035191.1 (100%)	Maternal	Maternal	02	Niben101Scf01291g00001.1 vs Niben101Scf05971g00007.1 =92.33%
NbTom40.4	Niben101Scf04436g15042.1 g29593.t1 (100%) NbD029233.1 (100%)	Maternal	Maternal	12	Niben101Scf05971g00007.1 vs Niben101Scf04436g15042.1 = 98.17% Niben101Scf05971g00007.1 vs Niben101Scf01451g05003.1 = 92.33% Niben101Scf01291g00001.1 vs Niben101Scf04436g15042.1 = 92.33%
NbTom20-1.1	Niben101Scf00109g10030.1 g1115.t1 (100%) NbD001253.1 (100%)	Ø	Maternal	19	Niben101Scf14939g01027.1vs Niben101Scf00109g10030.1 = 95.61%
NbTom20-1.2	Niben101Scf14939g01027.1 g1115.t1 (100%) NbD001253.1 (100%)	Parental	Maternal	02	
NbTom20-2.1	Niben101Scf03766g01008.1 g8578.t1 (100%) NbD025768.1 (100%) NbD031933.1 (95.04%)	Maternal	Maternal	02	Niben101Scf03766g01008.1 vs Niben101Scf05095g01004.1 = 94.36%
NbTom20-2.2	Niben101Scf05095g01004.1 g56513.t1 (100%) NbD050116 (100%)	Orphan	Maternal	15	
NbOm64.1	Niben101Scf02133g01001.1 g93882.t1 (99.83%) NbD016248.1 (99.83%)	Paternal	Maternal	15	Niben101Scf02133g01001.1 vs NbD010896.1 = 97.64% in shared region
NbOm64.2	NbD010896.1			16	Niben101Scf02133g01001.1 vs Niben101Scf08675g00023.1 = 49.82% Niben101Scf02133g01001.1 vs Niben101Scf08653g07031.1 = 50.53 % Niben101Scf08675g00023.1 vs Niben101Scf08653g07031.1 = 95.87%
NbToc64-III.1	Niben101Scf08675g00023.1 g49103.t1 (100%) NbD042788.1 (99.63%)	Maternal	Maternal	16	
NbToc64-III.2	Niben101Scf08653g07031.1 g26195.t1 (98.96%) NbD042739.1 (98.96%)	Maternal	Orphan	6	

** percentage of identity between the aa sequences retrieved from Sol Genomics Network and NibSet1-1/NbDE datasets*

Supplementary Table S4. Results of Bimolecular fluorescence complementation assays

	NbToc34							
	$_{Nt[GFP]}$NbToc34	**+/-**	**NbToc34$_{Nt[GFP]}$**	**+/-**	**$_{Ct[GFP]}$NbToc34**	**+/-**	**NbToc34$_{Ct[GFP]}$**	**+/-**
Toc34	$_{Ct[GFP]}$NbToc34	+	$_{Ct[GFP]}$NbToc34	+				

	NbToc34 $_{Ct[GFP]}$	+	NbToc34 $_{Ct[GFP]}$	+				
TOC159 family	$_{Ct[GFP]}$NbToc90	-	$_{Ct[GFP]}$NbToc90	+	$_{Nt[GFP]}$NbToc90	-	$_{Nt[GFP]}$NbToc90	-
	NbToc90$_{Ct[GFP]}$	-	NbToc90$_{Ct[GFP]}$	-	NbToc90$_{Nt[GFP]}$	-	NbToc90$_{Nt[GFP]}$	-
	$_{Ct[GFP]}$NbToc120	-	$_{Ct[GFP]}$NbToc120	-	$_{Nt[GFP]}$NbToc120	-	$_{Nt[GFP]}$NbToc120	+
	NbToc120$_{Ct[GFP]}$	-	NbToc120$_{Ct[GFP]}$	+	NbToc120$_{Nt[GFP]}$	-	NbToc120$_{Nt[GFP]}$	-
	NbToc159A$_{Ct[GFP]}$	+	NbToc159A$_{Ct[GFP]}$	+	NbToc159A$_{Nt[GFP]}$	-	NbToc159A$_{Nt[GFP]}$	+
	$_{Ct[GFP]}$NbToc159A	+	$_{Ct[GFP]}$NbToc159A	+	$_{Nt[GFP]}$NbToc159A	-	$_{Nt[GFP]}$NbToc159A	-
	NbToc159B$_{Ct[GFP]}$	-	NbToc159B$_{Ct[GFP]}$	+	NbToc159B$_{Nt[GFP]}$	-	NbToc159B$_{Nt[GFP]}$	+
	$_{Ct[GFP]}$NbToc159B	+	$_{Ct[GFP]}$NbToc159B	+	$_{Nt[GFP]}$NbToc159B	-	$_{Nt[GFP]}$NbToc159B	-

NEGATIVE CONTROLS

	Nt[GFP]	**+/-**	**Ct[GFP]**	**+/-**
Toc34	$_{Ct[GFP]}$NbToc34	-	$_{Nt[GFP]}$NbToc34	-
TOC159 family	$_{Ct[GFP]}$NbToc90	-	$_{Nt[GFP]}$NbToc90	-
	NbToc90$_{Ct[GFP]}$	-	NbToc90$_{Nt[GFP]}$	-
	$_{Ct[GFP]}$NbToc120	-	$_{Nt[GFP]}$NbToc120	-
	NbToc120$_{Ct[GFP]}$	-	NbToc120$_{Nt[GFP]}$	-
	NbToc159A$_{Ct[GFP]}$	-	NbToc159A$_{Nt[GFP]}$	-
	$_{Ct[GFP]}$NbToc159A	-	$_{Nt[GFP]}$NbToc159A	-
	NbToc159B$_{Ct[GFP]}$	-	NbToc159B$_{Nt[GFP]}$	-
	$_{Ct[GFP]}$NbToc159B	-	$_{Nt[GFP]}$NbToc159B	-

Chapter III

A viral protein targets mitochondria and chloroplasts by hijacking general import pathways and specific receptors.

María Sáiz-Bonilla[1], Andrea Martín-Merchán[2], Vicente Pallás[1]*, Jose A. Navarro[1]*

[1]Laboratory of Plant Molecular Virology, Institute for Plant Molecular and Cell Biology, Department of Molecular and Evolutionary Plant Virology, Consejo Superior de Investigaciones Científicas-Universitat Politècnica de València, Valencia, Spain.

[2] Current address: Centre for Research in Agricultural Genomics (CRAG), CSIC-IRTA-UAB-UB, Bellaterra, Barcelona, Spain

*Corresponding authors: Vicente Pallas (vpallas@ibmcp.upv.es) and Jose Antonio Navarro (janavarr@ibmcp.upv.es)

Manuscript submitted to Journal of Virology.

Personal contribution. M.S-B and A.M-M performed molecular cloning. BiFC, Y2H, VIGS assays, qRT-PCR and analysis of the results were carried out by J.A.N. and M.S-B. All authors discussed the results.

ABSTRACT

Dual targeting is a relatively few-explored phenomenon by which some proteins are transported to two different subcellular compartments, such as chloroplasts and mitochondria. We previously showed that the R domain and the arm region of the melon necrotic spot virus coat protein could act as a dual-targeting peptide, which shares many relevant features in structure, amino acid composition, and functionality with that of the Thr-tRNA synthetases, the best-studied dual-targeted proteins by far. Here, we show that a viral coat protein hijacks the general pathways for organellar protein import and identify the coat protein-interacting organellar translocon receptors. Our findings demonstrate for the first time that an exogenous dual-targeted protein uses the general Toc and Tom import systems to reach mitochondria and chloroplasts because it depends on NbToc75 and NbTom40 availability. Interaction studies and viral infection assays in silenced plants revealed the significance of plant receptors, such as the mitochondrion NbOm64 and chloroplast NbToc159A, in this transport. We also show that chloroplast protein translocation impairment could be interlinked with retrograde communication triggering a JA-based response that incidentally promotes viral resistance. Future research may profit from our results to better comprehend cellular communication, protein import mechanisms, how preproteins interact with their receptors, and how plant pathogens manipulate host machinery to their ends.

KEY WORDS

Dual targeting, mitochondria, chloroplasts, translocon, receptor, melon necrotic spot virus, coat protein, jasmonic acid, *Nicotiana benthamiana*.

INTRODUCTION

Mitochondria and chloroplasts are bioenergetic organelles essential for plant cell function, which share a similar but sequential endosymbiotic origin (Martin *et al.*, 2015). Through the so-called retrograde signaling, they are also sensors and efficient communicators of environmental conditions to the nucleus, capable of changing the gene expression to adapt plant growth, development, and defense responses to the new situation (Mielecki *et al.*, 2020). Throughout their establishment as organelles, a large percentage of the prokaryotic ancestor genetic material was lost and transferred to the nucleus, probably to bring them under cell control. Currently, most mitochondrion and chloroplast proteins are encoded in the nucleus, synthesized in the cytoplasm as precursor polypeptides or preproteins, and, next, imported into these organelles. Due to this circumstance, two highly specialized and organelle-distinctive import types of machinery with surface receptors, proteinaceous channels, and a target signaling system have emerged (Ghifari *et al.*, 2018; Rochaix, 2022).

Mitochondrion and chloroplast import systems consist of two connected multiprotein complexes or translocons associated with their corresponding outer (Toc/Tom) and inner envelope membranes (Tic/Tim). Initially, preproteins are directed towards Toc/Tom via a guidance complex formed by cytosolic chaperones (Hsp70, Hsp90, or 14-3-3) (Lee *et al.*, 2013; Bykov *et al.*, 2020). This first sorting event is mediated by the early identification of some targeting sequences, often found at the N-terminal end of proteins intended for the chloroplast stroma and the mitochondrion matrix. Chloroplast and mitochondrion targeting sequences (cTP and mTP) share a similar amino acid (aa) composition, mainly including hydrophobic, hydroxylated, and positively but not negatively charged residues. However, they differ in length, secondary structure, and composition of the 16 N-terminal aa. The mTP, or presequence, is 42-50 aa in length. Its N-terminal region has a net positive charge and is mainly folded into amphipathic alpha-helices. The cTP is longer than mTP (approximately 58 aa long), with a serine and proline-rich N-terminal region. Moreover, cTP is generally unstructured in aqueous solutions, which improves its interaction with cytosolic chaperones and receptors, enhancing its import through the Toc complex (Shi and Theg, 2013; Murcha *et al.*, 2014).

The translocon central core is always composed of a proteinaceous channel and some surface receptors. The receptors of the Tom20 family, which has four members in Arabidopsis but

only two in *Nicotiana benthamiana*, are responsible for recognizing plant mTP (Murcha *et al.*, 2014; Bausewein *et al.*, 2020; Sáiz-Bonilla *et al.*, 2022). Besides, the plant-specific receptor outer membrane 64 (Om64) may function similarly to yeast Tom71 and mammal Tom70. Om64 may assist the sorting and assembly machinery during the insertion of hydrophobic and multispanning α-helical proteins into the outer membrane by cytosolic chaperone binding (Lister *et al.*, 2007). Instead, matrix proteins pass through Tom40, a β-barrel protein that forms a transmembrane channel connecting the cytoplasm with the mitochondrial intermembrane space (Rapaport and Neupert, 1999). Finally, mature proteins reach the matrix, where they are subjected to mTP cleavage by the mitochondrial processing peptidase, passing across the inner membranes through a specific Tim complex known as Tim17:23 (Teixeira and Glaser, 2013).

The cTP recognition is mediated by two families of receptors, Toc34 and Toc159. In Arabidopsis, the Toc34 family has two members, AtToc33 and AtToc34, whereas the Toc159 family consists of four receptors (AtToc90, AtToc120, AtToc132, and AtToc159) (Gutensohn *et al.*, 2000; Kubis *et al.*, 2004; Ivanova *et al.*, 2004). Recently, we have shown that the *N. benthamiana* genome only contains an AtToc34 orthologue (NbToc34). Although the *N. benthamiana* Toc159 family has four members, they are somewhat different from Arabidopsis (NbToc90, NbToc120, NbToc159A, and NbToc159B) (Sáiz-Bonilla *et al.*, 2022). Then, preproteins reach the chloroplast intermembrane space through the Toc75 channel (Hinnah *et al.*, 2002). There, Tic22 and the Toc75 soluble N-terminal polypeptide transport-associated domain are proposed to work as chaperones promoting the preprotein transfer to the Tic20 channel. Finally, the stromal processing peptidase complex cleaves off the cTP giving rise to the mature stromal protein (Gross et al., 2020).

Mitochondrion and chloroplast translocons operate similarly, but they have independently derived. Thus, preprotein import should be monospecific, meaning that a particular precursor is exclusively targeted into either mitochondria or chloroplasts. Although this situation occurs in most instances, certain proteins can be efficiently imported into both organelles. The concept of dual targeting was born more than two decades ago when Huang et al. identified a yeast mitochondrial leader peptide able to translocate a reporter protein into mitochondria and chloroplasts (Huang *et al.*, 1990). Five years later, Creissen et al. reported the first example

of a dual targeting protein, the *Pisum sativum* glutathione reductase (Creissen *et al.*, 1995). Since then, articles referring to dual-targeted proteins have gradually increased.

Recent research shows that dual-targeted proteins enter mitochondria and chloroplasts via regular import pathways rather than unique transport routes (Langner et al., 2014). Twin mTP and cTP may be localized in tandem at the preprotein N-terminal extreme, giving two translation products, each one holding either cTP or mTP by alternative exon splicing, alternative transcription, or translation start (Carrie *et al.*, 2009). Additionally, protein folding may control cTP or mTP accessibility to receptors (Kalderon and Pines, 2014). Nevertheless, most dual-targeted proteins involve a unique precursor with an ambiguous dual targeting peptide (dTP), which shows mTP/cTP intermediate features and is supposed to be recognized by Toc/Tom receptors (Mitschke *et al.*, 2009). There is, however, little experimental evidence to prove this last assumption. Still, the mechanism by which two different types of receptors recognize the same preprotein is unknown.

The reasons why some proteins are dual-targeted can be multiple, but it appears much more widespread than expected. In plants, approximately 5% of mitochondrion and chloroplast proteins are dual-targeted. Among them, there is a strong bias toward soluble proteins involved in basic but essential processes required in genome-containing organelles. They include tRNA biogenesis, protein synthesis, cell cycle, DNA synthesis and maintenance, proteolysis, antioxidant defense, and metabolism, which are pathways known to activate retrograde signaling. Therefore, dual targeting appears to represent a way to simultaneously coordinate the replication and/or expression of both organelle genomes, integrate the communication among chloroplasts, mitochondria, and nucleus, and regulate plant immune responses (Carrie *et al.*, 2009; Sharma *et al.*, 2018).

Since chloroplasts and mitochondria play an essential role in plant immunity, different microbial pathogens have been shown to target their effectors to one or both organelles, suppressing plant defense and promoting plant colonization. To date, such pathogens included fungi (*Melampsora larici-populina* and *Rhizoctonia solani*), bacteria (*Pseudomonas syringae*), and nematodes (*Meloidogyne javanica*), with only two fungus effectors being dual-targeted (Tzelepis *et al.*, 2021; Petre *et al.*, 2015; Stojilković *et al.*, 2022). Very recently, we

and others have shown that the coat protein (CP) of melon necrotic spot virus (MNSV) and cucumber necrosis virus (CNV), respectively, are also dual targeted to mitochondria and chloroplasts to attenuate host defense response (Alam *et al.*, 2021; Navarro *et al.*, 2021). Dual targeting of CNV CP involves a twin presequence mechanism, whereas MNSV CP holds an ambiguous dTP with combined mTP and cTP features.

Regardless of whether dual-targeted proteins are from a plant or pathogen, knowledge about their interaction with Toc/Tom receptors at a molecular level is still very limited. Here, we have used MNSV CP as a working tool to study the molecular mechanism involved in the recognition and dual transport of proteins to mitochondria and chloroplast. Our studies revealed for the first time that an exogenous protein uses the general Toc/Tom import systems to reach both mitochondria and chloroplasts but interacting with specific Toc/Tom receptors. Receptor silencing decreased infection of MNSV but not other viruses with nucleo-cytoplasmic CP localization. Remarkably, we also showed that chloroplast protein translocation disruption might prime a jasmonic acid (JA)-based defense response. Our findings may aid future studies in better understanding cellular import processes and how preprotein-receptor interaction occurs, as well as learning how plant pathogens hijack host machinery for their own benefit.

RESULTS

The MNSV CP uses the general pathways of protein transport to be imported into chloroplasts and mitochondria.

To better understand the molecular mechanisms involved in MNSV CP organellar targeting, we first investigated the NbTom40 and NbToc75-III channel contribution, both playing a predominant role in Tom and Toc complexes, respectively. For this purpose, subcellular localization of CP-GFP, a CP tagged with the green fluorescent protein, either in *NbTOM40* or *NbTOC75-III*-silenced *N. benthamiana,* was investigated. Three plants were agroinfiltrated with pTRV1 and either pTRV2[Ø], which was used as control, pTRV2[NbTom40] or pTRV2[NbToc75-III]. Ten days later, CP-GFP was transiently expressed in upper leaves. At 48 h post-infiltration, CP-GFP fluorescence was visualized under confocal laser-scanning microscopy (CLSM). We observed the CP-GFP fluorescent signal overlapping chlorophyll and

coxP-ChFP mitochondrial matrix marker fluorescence in control plants. In contrast, CP-GFP only colocalizes with chloroplast stroma or mitochondrial matrix in *NbTOM40*- or *NbTOC75-III*-silenced plants, respectively (Figure 1A), indicating that MNSV CP organellar import is dependent on the Toc and Tom complexes.

Previously, we showed that disruption of MNSV CP mitochondrion and chloroplast targeting through the deletion of its first 30 aa decreased MNSV accumulation and inhibited systemic infection (Navarro et al., 2021). Due to the CP dTP ambiguous trait, the contribution of each organelle to this effect could not be discriminated. Here, we wanted to know whether each organelle CP targeting has a specific role in MNSV infection by silencing either *NbTOM40* or *NbTOC75-III*. Ten days after the agroinfiltration of the GFP-TRV constructs in *N. benthamiana* GFP16c plants, *NbTOM40* or *NbTOC75*-III-silenced plant phenotypes were as previously described (Sáiz-Bonilla *et al.*, 2022). Then, MNSV was inoculated, and ten days later, total RNA was extracted from the upper non-inoculated leaves (henceforth systemic leaves). MNSV accumulation was analyzed by northern blot and real-time RT-qPCR. When *NbTOM40* was silenced, we found a significant decrease in the MNSV hybridization signal intensities and titer in all three replicates that were proportional to the gene silencing level (Figure 1B). Similar results were obtained with MNSV titer in *NbTOC75-III*-silenced plants, but a more consistent and robust silencing was achieved this time. On average, a half decrease in NbTom40 mRNA abundance led to more than twice the reduction of infection; meanwhile, a six-fold decrease in NbToc75-III mRNA levels resulted in a nine-fold reduction in viral accumulation (Figure 1C). Therefore, an increase in MNSV resistance was the general rule regardless of which organelle targeting was prevented.

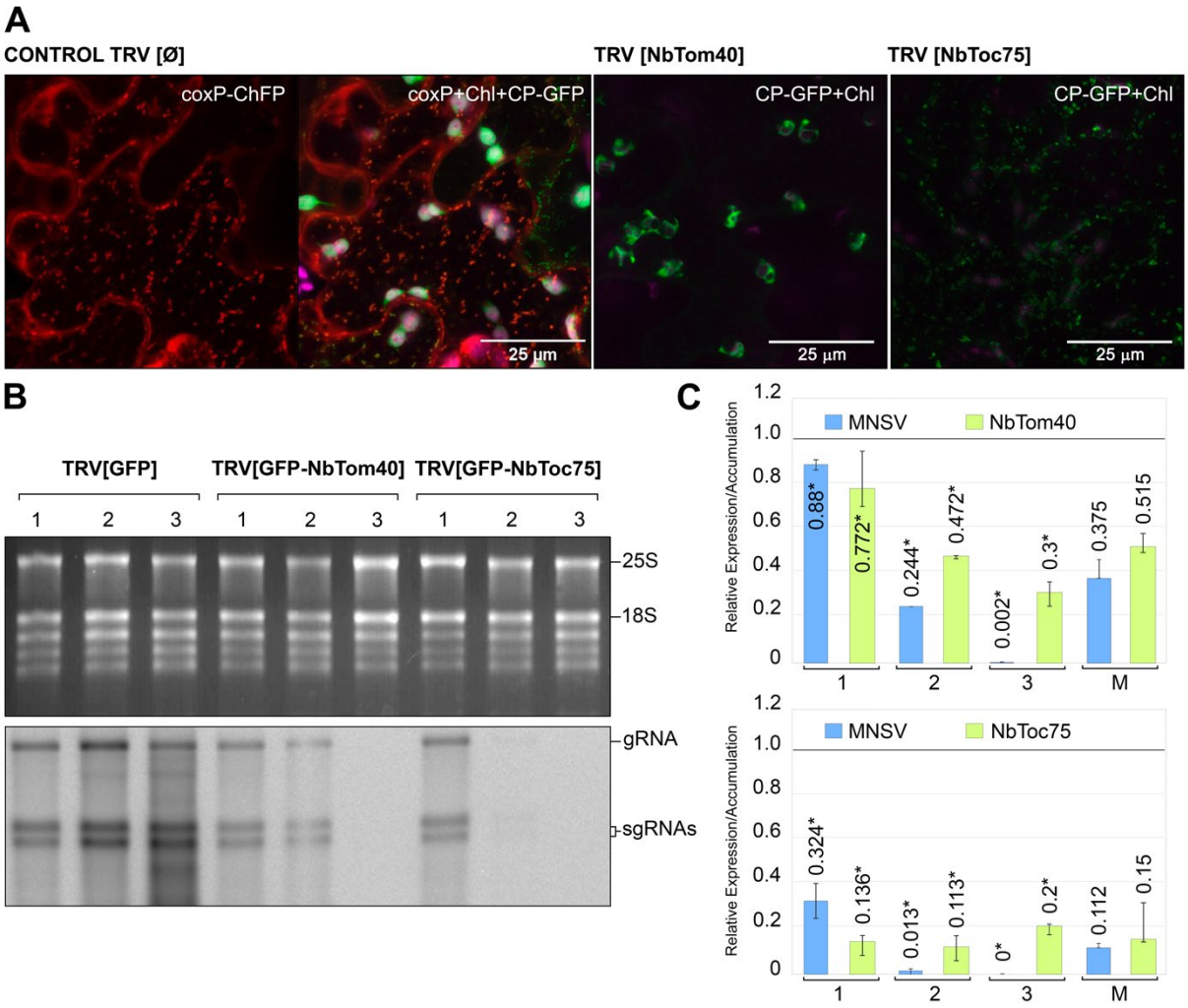

Figure 1. Effect of *NbTOM40* or *NbTOC75* silencing on subcellular localization of the MNSV CP and viral infection. **(A)** Subcellular localization of MNSV CP-GFP in control, *NbTOC75*- and *NbTOM40*-silenced *N. benthamiana* plants using VIGS mediated by tobacco rattle virus (TRV). The panel on the left shows the subcellular localization of the CP-GFP in chloroplasts and mitochondria in control TRV2[Ø] plants. The panels on the middle and right show the subcellular localization of the CP-GFP in chloroplast or mitochondria in *NbTOC40*- or *NbTOM75*-silenced plants, respectively. Chlorophyll fluorescence (Chl, magenta channel) or a mitochondrial matrix marker (coxP-ChFP, red channel) were used to visualize chloroplasts or mitochondria. **(B)** Analysis of the MNSV accumulation in non-inoculated systemic leaves of control, *NbTOM40*- and *NbTOC75*-silenced *N. benthamiana* plants at 10 dpi. The presence of MNSV genomic (gRNA) and both subgenomic RNAs (sgRNAs) was analyzed by northern blot. Three different assays are shown (1 to 3), and each lane corresponds to a mix of total RNAs from three plants. Ethidium bromide-stained agarose gel, which serves as the loading control, is shown on the top of the northern blot. The position of rRNAs 25S and 18S is indicated. **(C)** Accumulation of MNSV gRNA (blue bars) and relative expression of *NbTOM40* and *NbTOC75* (yellow-green bars) analyzed by RT-qPCR using viral p28 and gene-specific primers, respectively. The relative expression of the target gene or MNSV accumulation in control TRV2[GFP] plants was used as reference. The asterisk indicates statistically significant differences ($p<0.05$). M represents the average of the three bioassays.

By acting as sensing organelles, dysfunctional mitochondria and chloroplasts have been recently linked to innate immune responses, such as antiviral signaling and antibacterial immunity. As silencing of Toc and Tom channels could affect not only CP but also general

protein import to these organelles, we wondered if this resistance to infection was a specific effect on MNSV CP targeting or the result of a general priming effect. For that reason and considering that the coat proteins of other members of the MNSV-related genera *Alphacarmovirus* and *Betacarmovirus* as carnation mottle virus (CarMV) and turnip crinkle virus (TCV), respectively, do not have an organellar but nucleus and cytoplasm localization, infection assays of both viruses in *NbTOM40*- and *NbTOC75-III*-silenced plants were performed. Experiments were addressed as before, but viral accumulation was analyzed by quantification of the northern blot hybridization signals for genomic and subgenomic RNAs (Figure S1). As observed above, CarMV and TCV infection decreased in *NbTOM40*- and *NbTOC75-III*-silenced plants, pointing to a relevant contribution of organelle transport inhibition in providing some resistance against subsequent infections, regardless of the CP subcellular localization.

The MNSV CP interacts with specific receptors of Toc and Tom complexes.

Our knowledge of the host factors allowing proteins to target chloroplasts and mitochondria simultaneously is still very limited. To explore it, we analyzed the interaction between the MNSV CP and *N. benthamiana* Tom/Toc receptors using bimolecular fluorescence complementation (BiFC) and yeast two-hybrid (Y2H) assays. Specifically, we first searched for CP interaction with Toc receptors NbToc34, NbToc90, NbToc120, NbToc159A, and NbToc159B, and next for Tom receptors, Tom20.1, Tom20.2, and NbOm64. Because of the stromal localization of the CP, its interaction with the intermembrane space receptor/chaperone NbTic22-III was also studied By inserting the GFP between the arm region and the S domain (R/arm-GFP-SP) we previously showed that MNSV CP could be internally tagged without interfering with organellar targeting. Therefore, MNSV CP BiFC constructs were similarly obtained by inserting the C- or N-terminal GFP fragment into the same position, leading to $C_{CtGFP]}P$ and $C_{NtGFP]}P$, respectively, so that both CP ends are free to interact. However, no precise information about the position of the targeting signals used by the *N. benthamiana* translocon receptors of chloroplasts and mitochondria is available. Therefore, defining where an internal tag could be located is challenging. Instead, we fused each GFP fragment to both N-terminal or C-terminal ends of each translocon receptor, and next, they were co-expressed with $C_{CtGFP]}P$ or $C_{NtGFP]}P$ in *N. benthamiana* leaves. Two days after

agroinfiltration, we screened all four combinations for fluorescence complementation by CLSM (Table S1).

It is assumed that MNSV CP may self-interact through the shell domain to form virions. However, this ability has not been evaluated yet, so $C_{NtGFP]}P+C_{CtGFP]}P$ combination was also examined. As expected, the fluorescent signal was observed overlapping chlorophyll fluorescence (chloroplasts) and forming abundant and small spots in the cytoplasm (mitochondria) (Figure 2A). Only Toc receptors, NbToc159A and NbToc159B, were CP interaction partners in two out of four combinations (Figure 2B-E). The fluorescent signal was mainly found in the cytoplasm but occasionally observed in chloroplasts, as in NbToc159B (Figure 2E). Still being a matter of debate, Toc159 family receptors might potentially function as soluble cycling receptors that direct preproteins from the cytoplasm to the Toc translocon (Lung and Chuong, 2012; Hiltbrunner *et al.*, 2001). Then, our results also suggest that a cytoplasmic interaction between NbToc159A/B receptors and MNSV CP can happen. In a previous work, we showed that GFP-tagged NbTic22-III was located in the cytoplasm and chloroplasts regardless of the labeled protein end. Here, the interaction between CP and NbTic22-III was observed in combinations involving N-terminal tagged-NbTic22-III variants. However, the fluorescence was only detected in the cytoplasm and small cytoplasmic dots but not in chloroplasts (Figure 2F-G). A possible explanation is that proteolytic processing of the NbTic22-III N-terminal end in the intermembrane space avoids the visualization of interaction there. Neither positive interactors nor CP showed fluorescence complementation with the corresponding untagged GFP N-terminal or C-terminal fragments (Figure S2A-H).

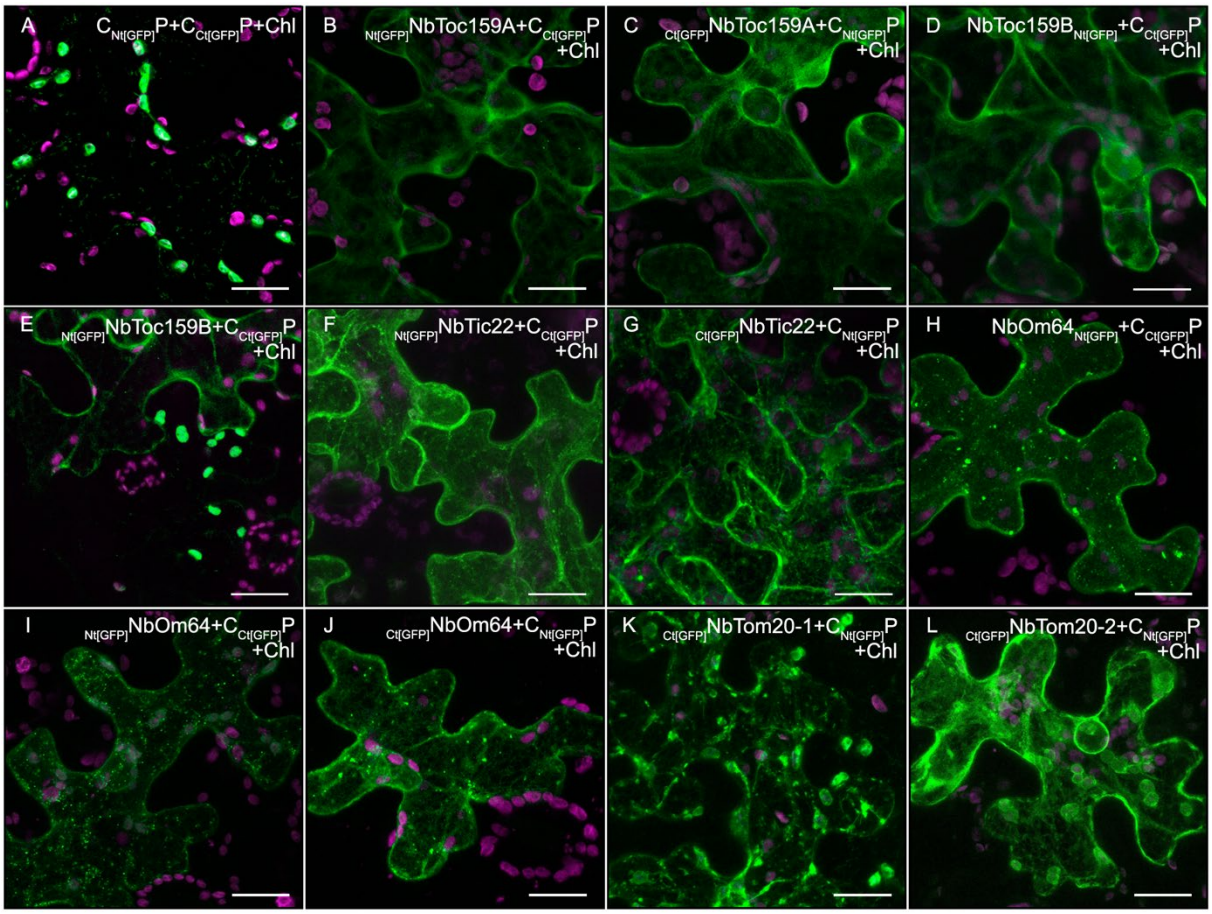

Figure 2. Bimolecular fluorescence complementation assay (BiFC) in epidermal cells of *N. benthamina* using MNSV CP and chloroplast/mitochondrion translocon receptors. Leaves were cotransfected with Agrobacterium carrying constructs for expression of full-length MNSV CP with internal Ct[GFP] or Nt[GFP]P tags ($C_{Ct[GFP]}P$ and $C_{Nt[GFP]}P$, respectively) and NbToc34, NbToc90, NbToc120, NbToc159A, NbToc159B, NbOm64, NbTom20-1 or NbTom20-2 tagged either with Nt[GFP] or Ct[GFP] in their amino or carboxyl end. $C_{Nt[GFP]}P+C_{Ct[GFP]}P$ combination was also examined. Only combinations that resulted in fluorescence visualization by microscopy are displayed. They included CP-CP self-interaction (A and B) and CP interaction with NbToc159A (C and D), NbToc159B (E and F), or NbTic22-III (G and H), NbOm64 (A-C), NbTom20-1 (D), or NbTom20-2 (E), as indicated at the top of each panel.

The CP interaction with *N. benthamiana* Tom receptors was also tested. Three out of four combinations of CP with NbOm64 (Figure 2H-J) but only one with NbTom20-1 (Figure 2K) or NbTom20-2 (Figure 2L) showed fluorescence complementation. Fluorescent signals resulting from CP-NbOm64 combinations were detected in the cytoplasm, and small cytoplasmic spots resembling mitochondria. In the case of NbTom20-1/2, the fluorescence was associated with the endoplasmic reticulum, chloroplast, and mitochondrion membranes. This localization was like that observed previously for GFP-tagged NbTom20-1/2, resulting from their overaccumulation in the cytoplasm and/or their specific posttranslational targeting mechanism involving the Guided Entry of Tail-anchored (GET) proteins (Sáiz-Bonilla *et al.*,

2022). As occurred above, none of the positive interactors showed fluorescence complementation with the corresponding untagged GFP N-terminal or C-terminal fragments (Figure S2I-M).

For Y2H assays, MNSV CP and receptors were cloned into pGBDKT7 and pGADT7. The human tumor p53 (pBD-53), the transcription factor IAA-LEUCINE RESISTANT3 (At5g54680; pAD-ILR3) (Aparicio and Pallás, 2017), and the empty vectors were used as negative controls. The interactions were screened on SD-Ade-His-Leu-Trp+X-α-Gal medium (Figure 3, right), and replicates were made on SD-Leu-Trp medium to assess double-plasmid transformant growth (Figure 3, left). In addition to pGAD-CP and pGBD-CP double transformants, yeast growth was evident for those combinations, including pGBD-NbToc159A, pGAD-NbTic22, pGBD-NbTic22, pGAD-NbOm64, pGBD-NbOm64, and pGBD-NbTom20-2 baits, while no growth was observed among negative controls. NbToc159B and NbTom20-1 also failed to interact with the MNSV CP by Y2H, supporting the involvement of NbToc159A and NbTic22-III in MNSV CP targeting to chloroplast stroma and most probably NbOm64 in its mitochondrial matrix import.

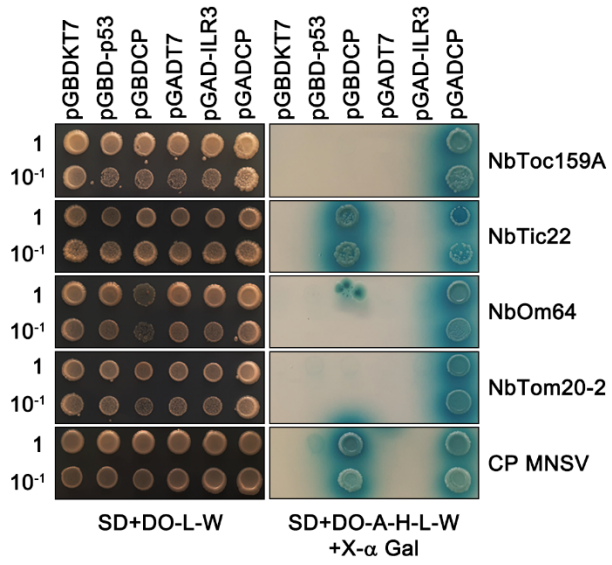

Figure 3. Yeast two-hybrid (Y2H) assay corroborating MNSV CP homodimerization and its interaction with chloroplast translocon receptors NbToc159A and NbTic22-III, and mitochondrion translocon receptors NbOm64 and NbTom20-2. AH109 yeast strain carrying plasmids expressing MNSV CP fused to the GAL4 Activation Domain in pGBKT7 (pGBDCP) or the GAL4 Binding Domain in pGADT7 (pGADCP) were co-transformed with equivalent but corresponding plasmids expressing each mitochondrion or chloroplast translocon receptor used in this work. The empty vectors, pGBKT7 or pGADT7, as well as pGB-p53 and pGAD-IL3 holding a human tumor suppressor and the transcription factor IAA-LEUCINE RESISTANT3, respectively, were used as negative controls. Double-plasmid transformants were selected by growing them in SD+DO-L-W medium and then spot-plated in ten-fold serial dilutions in selective SD+DO-A-H-L-W+X-α Gal medium to detect the activation of HIS3,

ADE2, and MEL1 reporter genes (panels on the right). A replicate was done in SD+DO-L-W medium (panels on the left) to assess equal plating of double-plasmid transformants yeast cells.

Silencing of *NbTOC34* in *N. benthamiana* might prime a jasmonic acid-based resistance against viruses.

To gain further insights into the role that Toc and Tom receptors play in MNSV infection, silenced *N. benthamiana* plants were generated by following the VIGS strategy mentioned above. *NbTOC34* disruption (4-7-fold reduction of mRNA levels) had a highly detrimental effect on the visible phenotype, resulting in dwarf and albino plants, as previously described (Sáiz-Bonilla *et al.*, 2022), and in viral accumulation at the systemic level. Although no NbToc34-CP interaction was detected, MNSV genomic and subgenomic RNAs were practically undetectable by northern blot analysis and RT-qPCR in all *NbTOC34*-silenced plants (Figure 4A and B, respectively). Considering that this plant phenotype was similar to that observed in *NbTOC75*-silenced plants (Sáiz-Bonilla *et al.*, 2022), and both Toc components have no redundant isoforms, we believed that silencing of either of two genes could result in a general disruption of protein import. Therefore, we examined again whether viral resistance was a specific effect on MNSV CP targeting or the result of a more general effect. To do this, we performed three CarMV and TCV infection assays. Similarly to MNSV, northern blot analysis revealed that no or slight hybridization signals of CarMV or TCV were detected in non-inoculated *NbTOC34*-silenced leaves (Figure 4C and 4D, respectively). These results reinforced our notion that organelle transport disruption provided remarkable resistance against viral infections.

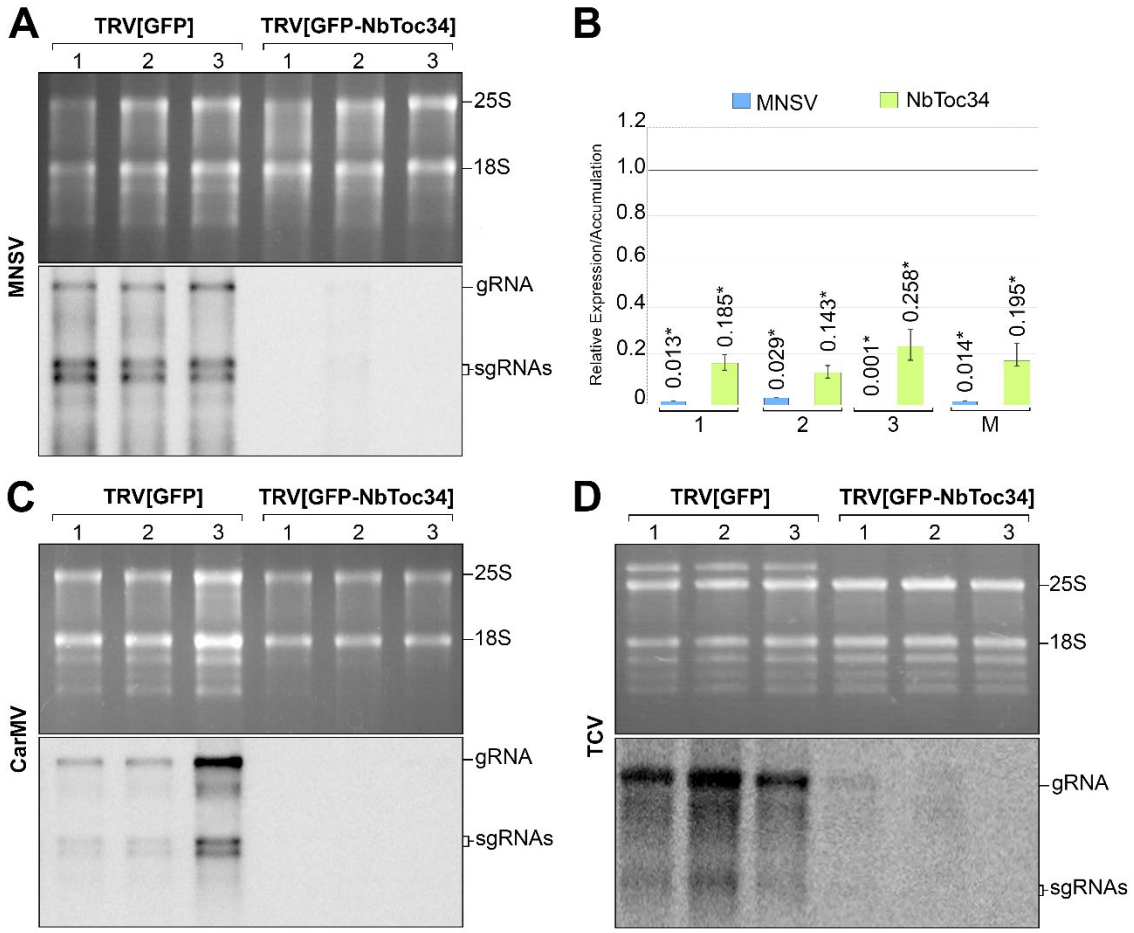

Figure 4. **Effect of *NbTOC34* silencing on MNSV, CarMV and TCV infection**. **(A)** Analysis of the MNSV accumulation in non-inoculated systemic leaves of control and *NbTOC34*-silenced *N. benthamiana* plants at 10 dpi. The presence of MNSV genomic (gRNA) and both subgenomic RNAs (sgRNAs) was analyzed by northern blot. Three different assays are shown (1 to 3), and each lane corresponds to a mix of total RNAs from three plants. Ethidium bromide-stained agarose gel, which serves as the loading control, is shown on the top of the northern blot. The position of rRNAs 25S and 18S is indicated. **(B)** Accumulation of MNSV gRNA (blue bars) and relative expression of *NbTOC34* (yellow-green bars) analyzed by RT-qPCR using viral p28 and gene-specific primers, respectively. The relative expression of the target gene or MNSV accumulation in control TRV2[GFP] plants was used as reference. The asterisk indicates statistically significant differences ($p<0.05$). M represents the average of the three bioassays. **(C-D)** Analysis of the CarMV (C) or TCV (D) accumulation in non-inoculated systemic leaves of *NbTOC34*-silenced *N. benthamiana* plants. Other indications are as in (A).

Chloroplasts play crucial roles in plant physiology as bioenergetic organelles. Nevertheless, they are also the factory for producing amino acids, fatty acids, secondary metabolites, and classical defense hormones against plant viruses, such as salicylic acid (SA) and 12-oxophytodienoic acid, the JA precursor. In addition, several studies have linked abscisic acid (ABA) to different viral resistance mechanisms (Forcat *et al.*, 2008). Therefore, we examined the SA, JA, and ABA endogenous levels in response to MNSV infection to understand better the phenomenon triggering viral resistance upon disruption of chloroplast protein import.

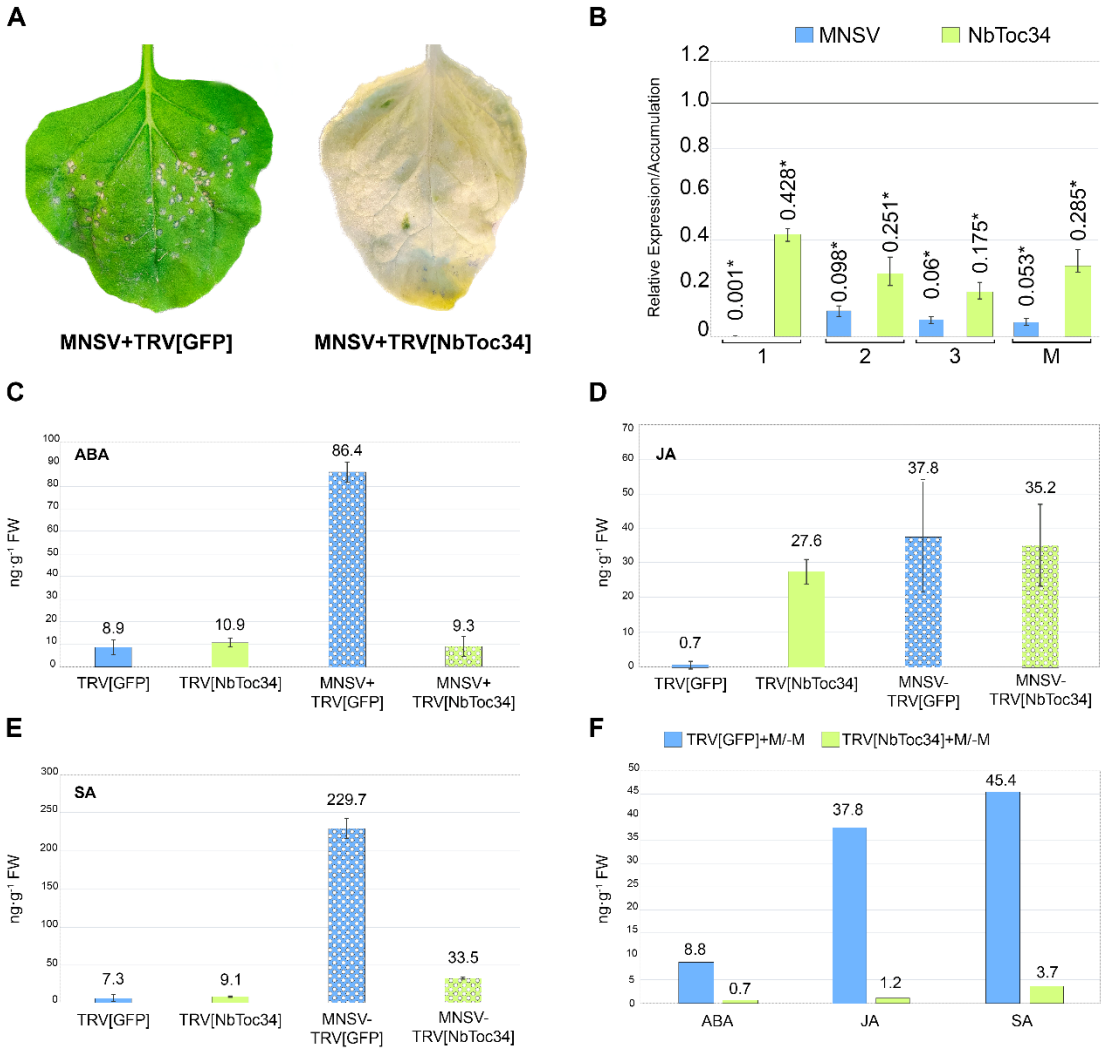

Figure 5. Analysis of the three acid hormones that primarily regulate the plant defense against viruses in plants. (A) Images of either an MNSV-inoculated control (TRV[GFP], on the right) or *NbTOC34*-silenced (TRV[NbToc34], on the right) leaf of *N. benthamiana* at 5 dpi. **(B)** RT-qPCR analysis of the MNSV gRNA (blue bars) and NbToc34 mRNA (yellow-green bars) accumulation in MNSV-inoculated leaves of *NbTOC34*-silenced *N. benthamiana* plants at 5 dpi. Three different assays are shown (1 to 3), and each lane corresponds to a mix of total RNAs from three leaves of different plants. The relative expression of the target gene or MNSV accumulation in control TRV2[GFP] plants was used as reference. The asterisk indicates statistically significant differences ($p<0.05$). **(C-E)** Bar diagrams representing the concentrations ($ng \cdot g^{-1}$ fresh weight, FW) of abscisic acid (ABA) (C), jasmonic acid (JA) (D), and salicylic acid (SA) (E) in control (TRV[GFP], blue bars), and *NbTOC34*-silenced (TRV[NbToc34], yellow-green bars) plants, before (filled bars) and 5 dpi after (polka-dotted filled bars) MNSV inoculation. **(F)** ABA, JA, and SA accumulation ratios between MNSV-inoculated (+M) and non-inoculated (-M) in control (TRV[GFP], blue bars) and *NbTOC34*-silenced *N. benthamiana* leaves.

Hormones were measured in mock and MNSV-inoculated leaves of control and *NbTOC34*-silenced plants at 5 dpi when necrotic lesions were evident in control plants (Figure 5A). Viral titer and the *NbTOC34* silencing degree were estimated by RT-qPCR (Figure 5B). As expected, MNSV infection induced the synthesis of SA, JA, and ABA in control plants, whose levels increased in inoculated leaves about 45-, 40-, and 9-fold, respectively (Figure 5C-F). Although

SA and ABA basal levels were similar in *NbTOC34*-silenced and control leaves (Figure 5C and E, respectively), those of JA in the formers were nearly 40-fold higher than in control, a value similar to the JA levels reached after infection in control plants (Figure 5D). In contrast, no significant differences were found, except for a nearly 4-fold increase in SA, after MNSV infection of *NbTOC34*-silenced leaves (Figure 5F). Therefore, the initial amplitude of JA signaling might largely influence the outcome.

Silencing of Toc receptor genes and *NbTIC22-III* supports NbToc159A as the main factor responsible for MNSV CP import to chloroplasts.

In previous work, we showed that silencing of *NbTOC90*, *NbTOC120*, *NbTOC159A*, *NbTOC159B,* or *NbTIC22* genes either resulted in none or a considerably lesser effect on the visible phenotype than *NbTOC75* or *NbTOC34* (Sáiz-Bonilla *et al.*, 2022). Then, we would like to determine the role that NbToc159 family receptors and NbTic22-III could play in MNSV infection. Gene silencing and MNSV infection assays were done using the above conditions. On the one hand, northern blot hybridization and RT-qPCR analysis revealed that disruption of *NbTOC90* expression did not affect MNSV systemic infection, resulting in higher titers than in control plants in two of three bioassays. Even though *NbTOC90* expression was not greatly altered in the third one, no systemic infection was seen, showing that viral resistance was likely caused by factors other than *NbTOC90* silencing (Figure S3).

On the other hand, a detrimental effect was observed on MNSV but not TCV and CarMV infection when the expression of any other Toc159 family component was lowered (Figure 6 and Figure S4, respectively). Nevertheless, some differences between them were appreciated. Although a direct NbToc120-CP interaction was not confirmed, MNSV accumulation was reduced by half, as shown in northern blot hybridization signals and RT-qPCR data (Figure 6A). A higher diminution of viral titer was observed when *NbTOC159A* or *NbTOC159B* was silenced (Figure 6B and C, respectively). *NbTOC159A* expression was reduced nearly seven-fold on average, leading to a ten-fold decrease in viral titer. That was the most severe reduction of MNSV accumulation detected after silencing a CP interactor, highlighting the NbToc159A pivotal role in chloroplast import of exogenous proteins. MNSV infection of *NbTOC159B*-silenced plants did not display such a drastic effect as in *NbTOC159A*-silenced plants. Compared to the control plants, a two-fold decrease in *NbTOC159B* expression resulted in a

fall in MNSV titer of about five-fold on average, even when the interaction of NbToc159B with CP could not be corroborated by Y2H (Figure 6C). It must be noted that silencing of *NbTOC159B* led to pale green plants. The possibility that this phenotype could be linked to the activation of a general defense mechanism, as happened upon silencing *NbTOC34*, was dismissed since no TCV and CarMV resistance was observed (Figure S4). CarMV and TCV CP are nucleocytoplasmic proteins lacking a dTP, then our results point to a specific effect of *NbTOC159A/B* silencing on MNSV CP targeting and hence on infection rates.

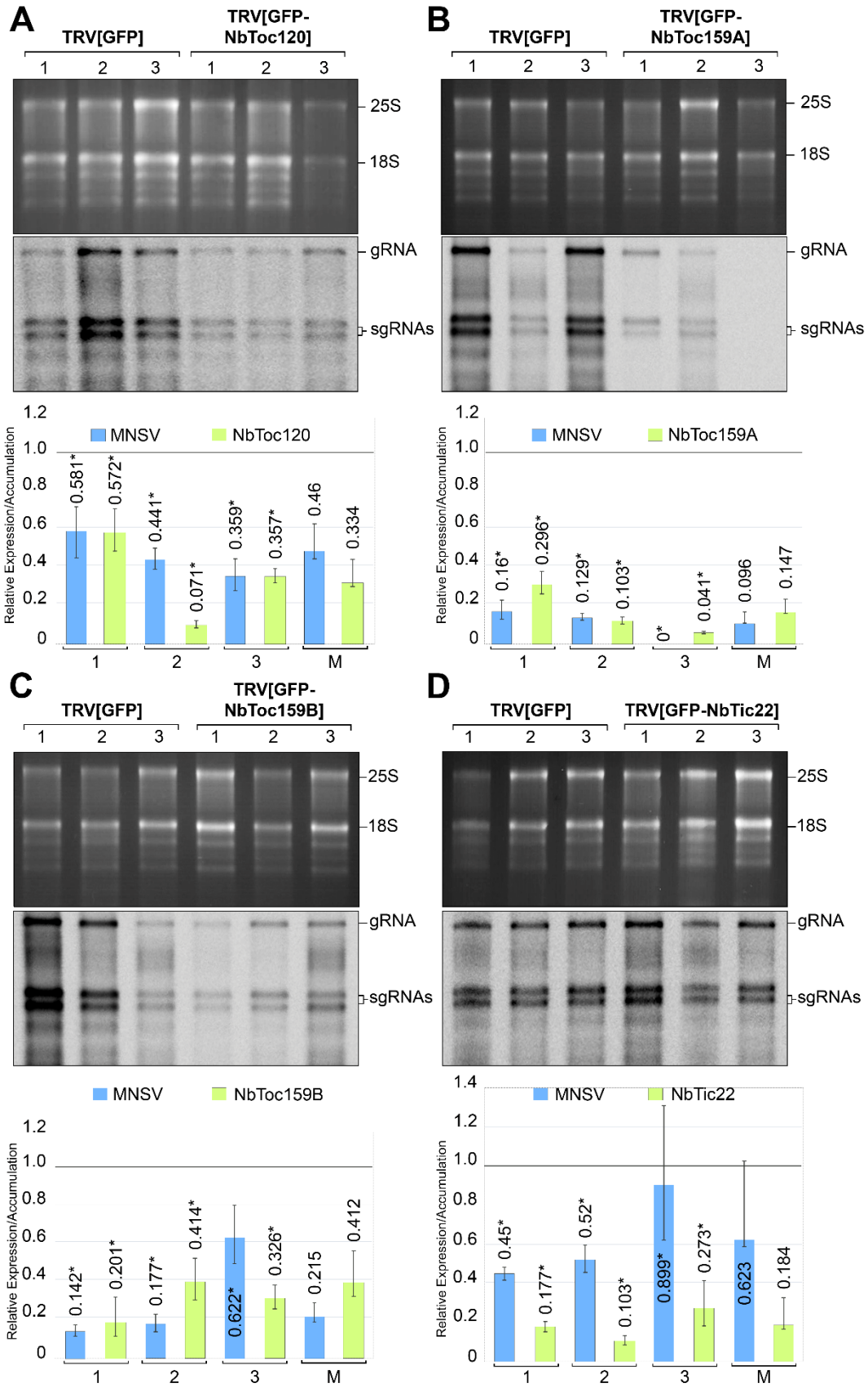

Figure 6. Effect of *NbTOC120*, *NbTOC159A*, *NbTOC159B*, or *NbTIC22-III* silencing on MNSV infection. (A) Analysis of the MNSV accumulation in non-inoculated systemic leaves of control and *NbTOC120*-silenced *N.*

benthamiana plants at 10 dpi. The presence of MNSV genomic (gRNA) and both subgenomic RNAs (sgRNAs) was analyzed by northern blot. Three different assays are shown (1 to 3), and each lane corresponds to a mix of total RNAs from three plants. Ethidium bromide-stained agarose gel, which serves as the loading control, is shown on the top of the northern blot. The position of rRNAs 25S and 18S is indicated. The bar diagram on the bottom shows the accumulation of the MNSV gRNA (blue bars) and the relative expression of *NbTOC120* (yellow-green bars) analyzed by RT-qPCR using viral p28 and gene-specific primers, respectively. The relative expression of the target gene or MNSV accumulation in control TRV2[GFP] plants was used as reference. The asterisk indicates statistically significant differences ($p<0.05$). M represents the average of the three bioassays. **(B)** Analysis of the MNSV accumulation in non-inoculated systemic leaves of control and *NbTOC159A*-silenced *N. benthamiana* plants at 10 dpi. Other indications are as in (A). **(C)** Analysis of the MNSV accumulation in non-inoculated systemic leaves of control and *NbTOC159B*-silenced *N. benthamiana* plants at 10 dpi. Other indications are as in (A). D, Analysis of the MNSV accumulation in non-inoculated systemic leaves of *NbTIC22-III*-silenced *N. benthamiana* plants at 10 dpi. Other indications are as in (A).

We finally studied the effect on MNSV infection of silencing *NbTIC22-III*, which acts in the intermembrane space as a chaperone. The northern blot and RT-qPCR analysis showed that even while NbTic22-III was a potent CP interactor, genomic and subgenomic MNSV RNA accumulation was not largely reduced after silencing (about 37 %) (Figure 6C).

The plant-specific Tom receptor Om64 plays a major role in CP import to mitochondria despite the redundancy among Tom receptors.

Next, we sought to establish whether Tom receptor silencing, including NbOm64, NbTom20-1, and NbTom20-2, affected MNSV infection. In the case of NbTom20-1 and NbTom-20.2, BiFC assays indicated an interaction with MNSV CP, which was corroborated by Y2H analysis only for NbTom20-2. However, the effect of silencing *NbTOM20-1* or *NbTOM20-2* on infection was the opposite of silencing Toc receptors. northern blot and RT-qPCR analysis showed that a five-fold or about a seven-fold decrease in *NbTOM20-1* or *NbTOM20-2* expression led to an MNSV accumulation two-fold or 1.5-fold higher than in control plants, respectively (Figure 7A and 7B). A similar increase in viral accumulation was observed in TCV but not in CarMV infections (Figure S5), which could indicate a general rather than specific effect. Although we used several *NbOM64* regions in distinct TRV2 constructs, the silencing levels were not as high as all the above genes. However, a direct relationship was observed: the greater the reduction in *NbOM64* expression, the greater the negative effect on MNSV accumulation (Figure 7C). The infection resistance of *NbOM64*-silenced plants was only observed for MNSV, while CarMV- or TCV-infected *NbOM64*-silenced plants showed higher viral RNA levels than control plants (about 1.4-fold) (Figure S5). Despite the phenomenon of functional redundancy described for mitochondrial receptors, our findings highlight the importance of NbOm64 in CP interaction and developing an efficient MNSV infection.

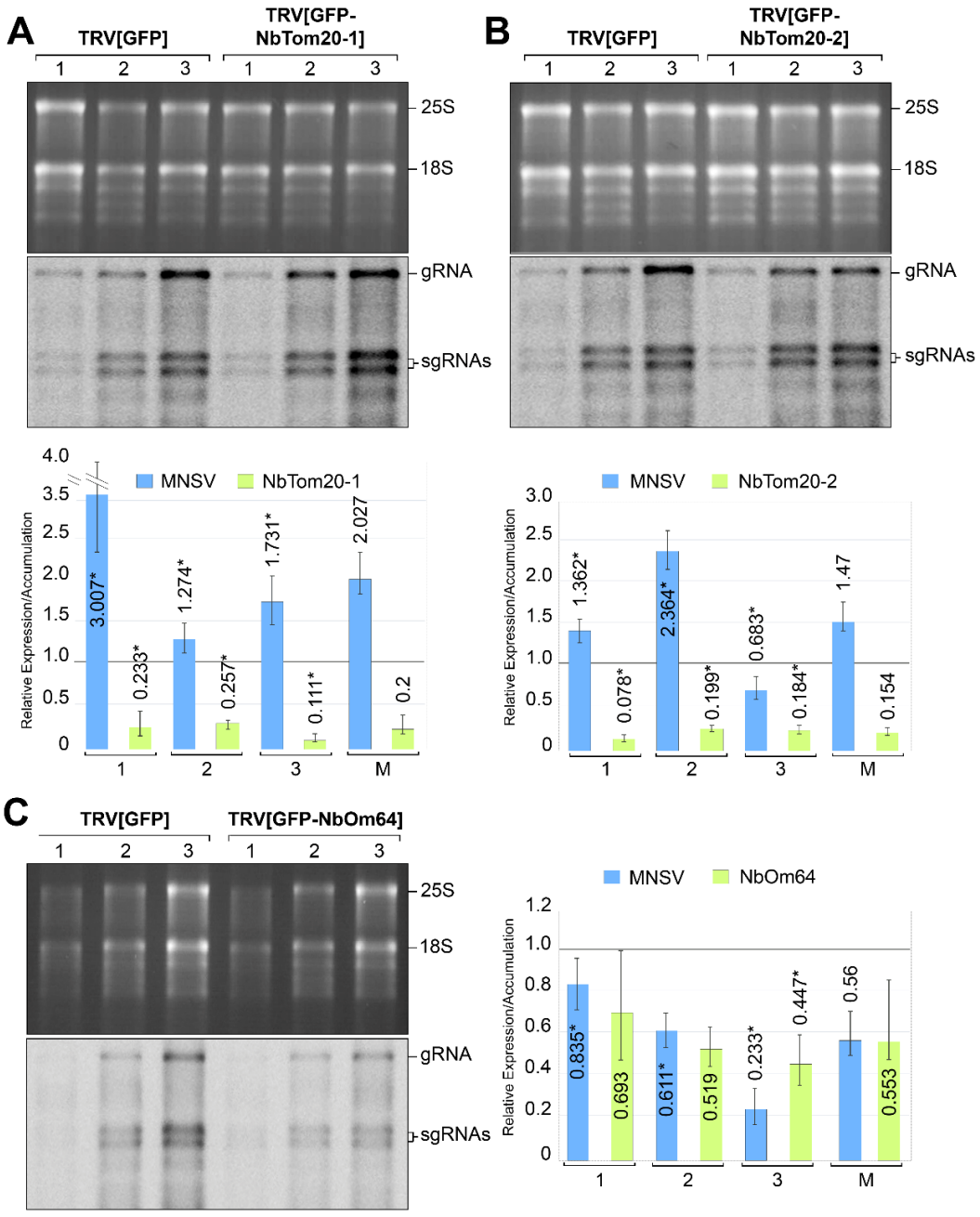

Figure 7. **Effect of NbTOM20-1, NbTOM20-2, or NbOM64 silencing on MNSV infection**. **(A)** Analysis of the MNSV accumulation in non-inoculated systemic leaves of control and NbTOM20-1-silenced *N. benthamiana* plants at 10 dpi. The presence of MNSV genomic (gRNA) and both subgenomic RNAs (sgRNAs) was analyzed by northern blot. Three different assays are shown (1 to 3), and each lane corresponds to a mix of total RNAs from three plants. Ethidium bromide-stained agarose gel, which serves as the loading control, is shown on the top of the northern blot. The position of rRNAs 25S and 18S is indicated. The bar diagram on the bottom shows the accumulation of the MNSV gRNA (blue bars) and the relative expression of NbTOM20-1 (yellow-green bars) analyzed by RT-qPCR using viral p28 and gene-specific primers, respectively. The relative expression of the target gene or MNSV accumulation in control TRV2[GFP] plants was used as reference. The asterisk indicates statistically significant differences ($p<0.05$). M represents the average of the three bioassays. **(B)** Analysis of the MNSV accumulation in non-inoculated systemic leaves of control and NbTOM20-2-silenced *N. benthamiana* plants at

10 dpi. Other indications are as in (A). **(C)** Analysis of the MNSV accumulation in non-inoculated systemic leaves of *NbOM64*-silenced *N. benthamiana* plants at 10 dpi. Other indications are as in (A).

DISCUSSION

Reports concerning the dual targeting of nuclear-encoded protein into two distinct plant cell organelles have progressively increased over the past few years. Many of them refer to the import of soluble proteins to mitochondria and chloroplasts (Sharma *et al.*, 2018). However, much of the current knowledge has been focused on identifying these cargo proteins, the structural dissection of their targeting signals, developing in silico targeting prediction tools, and implementing them. Dual-targeted proteins are supposed to be transported along the general rather than specific pathways for organellar protein import. However, little attention has been paid to how these proteins are recognized on a molecular level by the components of Toc and Tom complexes and what those components are. This inattentiveness is mainly reflected by the low number of studies published on this topic (Rödiger *et al.*, 2011; Ye *et al.*, 2012; Ye *et al.*, 2015; Woo *et al.*, 2022). In this work, we have provided experimental evidence supporting the contribution of the general pathways for organellar protein import in MNSV CP subcellular localization and identifying the specific Tom/Toc import receptors interacting with this exogenous protein.

Most mitochondrion and chloroplast dual-targeted proteins, such as Thr-tRNA synthetases (ThrRS), consist of a single precursor protein holding an ambiguous dTP rather than tandemly arrayed signals resulting from an alternative exon splicing or transcription/translation start. Likewise, the R/arm region of the MNSV CP (MNSV CP-dTP) could act as an ambiguous dTP, which would drive CP import to mitochondria and chloroplasts (Navarro *et al.*, 2021). When ThrRS-dTP and MNSV CP-dTP are compared, many relevant shared features in structure, aa composition, and functionality can be found. The most N-terminal ends of ThrRS-dTP (23 aa) and MNSV CP-dTP (30 aa) were necessary but insufficient for the organellar import. In both instances, the shortest peptide that could provide dual targeting was 60 aa long. Both dTP seem to be unstructured, albeit they had the propensity to form an amphiphilic helix in their most N terminal part. Moreover, they are overall enriched in basic, leucine, serine, and proline residues, but acidic residues are mainly found in the C terminal region. Finally, after targeting the correct organelle, both dTP undergo proteolytic processing at different positions within

the precursor protein (Navarro *et al.*, 2021; Berglund *et al.*, 2009). Then, MNSV CP can be adopted as a suitable system for studying the protein transport to organelles in plant cells.

Nuclear-encoded mitochondrial or chloroplast proteins depend on their import on the Tom/Toc complexes (Ghifari *et al.*, 2018; Rochaix, 2022). Rödiger et al. provided early evidence that dual-targeted proteins also used these pathways. They showed that mitochondrion, and chloroplast targeting of cytochrome C1 is inhibited by the ionophore valinomycin, which dissipates the electrochemical gradient, and the protonophor nigericin, which impairs thylakoidal ATP synthesis, respectively. Cytochrome C1 targeting to chloroplasts was also affected by competition with a typical chloroplast precursor protein. However, cytochrome C1 chloroplast transport was considered as a tolerated mistargeting as it does not have in chloroplasts any function equivalent to what it does in mitochondria (Rödiger et al., 2011). Although the exact MNSV CP function in organelles is still unknown, we showed that its targeting to chloroplast and mitochondria modulates chloroplast-to-nucleus communication, RNA silencing suppressor activity, encapsidation, pathogenesis and tissue tropism (Navarro *et al.*, 2021). Here we demonstrate that MNSV CP transport into both organelles proceeds along the protein general transport pathways because it depended on the availability of essential components such as NbTom40 and NbToc75-III. These findings strongly suggest that MNSV CP-dTP constitutes an evolutive hallmark selected during MNSV adaptation to its host, which in some way was shaped by endogenous plant factors.

Multiple *N. benthamiana* mitochondrial and chloroplast protein import receptors have been identified, and some functional and structural characterization has been done (Sáiz-Bonilla *et al.*, 2022). They included the Toc receptor NbToc34, and the four members of the Toc159 family (NbToc90, NbToc120, NbToc159A, and NbToc159B), the Tic receptor NbTic22-III, the Tom receptors NbTom20-1, and NbTom20-2, and the mitochondrial plant-specific receptor NbOm64. In this study, two different approaches were used to identify which receptors interact with the MNSV CP. The most confident interaction partners, verified by BiFC and Y2H, were NbToc159A, NbTic22-III, NbOm64, and NbTom20-2. Due to the *N. benthamiana* knockout unavailability, VIGS was used to unveil the role of each receptor in MNSV infection. In agreement with the interaction studies, *NbTOC159A* silencing had the highest detrimental effect on viral accumulation. However, we also observed a negative impact on MNSV infection

after *NbTOC159B* silencing, which interaction with MNSV CP was also identified by BiFC. Therefore, the involvement of NbToc159B in MNSV CP chloroplast import cannot be ruled out. Unexpectedly, the silencing of *NbTIC22-III*, which confidently interacts with MNSV CP, did not affect MNSV accumulation. We have previously shown that AtTic22-IV, the AtTic22-III redundant isoform, also exists in *N. benthamiana* (Sáiz-Bonilla *et al.*, 2022). Then, NbTic22-IV could complement the function of NbTic22-III, but it is also possible that Tic22 is not an essential element in stromal protein targeting. In this sense, the corresponding Arabidopsis double knockout was viable in normal and low-light conditions. Still, it showed a reduced import rate and photosynthetic activity when grown under high-light conditions. Therefore, it was concluded that Tic22-III and Tic22-IV mainly act when high import rates are needed (Rudolf et al., 2013).

Lister et al. classified AtOm64, together with three AtTom20 isoforms and metaxin, as Arabidopsis Tom receptors acting in the early stages of precursor recognition and import. The ability of each receptor to compensate for the loss of the other ones led them to propose very overlapping roles for these proteins. For example, Arabidopsis knockouts lacking two Tom20 isoforms showed a two-fold increase in the remaining Tom20 protein (Lister et al., 2007). Indications of such functional redundancy in *N. benthamiana* have been suggested (Sáiz-Bonilla *et al.*, 2022). In this sense, although *NbOM64* silencing had the highest detrimental effect on MNSV accumulation, the impact on viral titer reduction was not as higher as that of silencing *NbTOC159A*. These findings most likely point to a functional compensation among Tom receptors also in *N. benthamiana*. Interestingly, *NbTOM20-2*- but especially *NbTOM20-1*-silenced plants were more susceptible to viral infection. This effect was higher in MNSV than TCV but not observed in CarMV infections. Lister et al. showed that, except for *tom20-2*, the amount of Om64 protein increased in Arabidopsis *tom20* plants (Lister *et al.*, 2007). Such compensation for losing Tom20 receptors may also occur in *N. benthamiana.* Then, raising the Om64-facilitated MNSV CP transport to mitochondria could indirectly benefit viral infection.

In Arabidopsis, an NMR analysis showed how AtToc34 and AtTom20 recognize the ThrRS-dTP on the molecular level, suggesting different modes of action with the two receptors (Ye *et al.*, 2015; Ye *et al.*, 2012). More recently, Woo et al. proposed that several motifs in the signal sequence of the dual targeting protein AtSufE1 sequentially interact with metaxin and

AtTom20 for mitochondrial targeting (Woo *et al.*, 2022). However, our findings strongly indicate that MNSV CP hijacks the general import pathways for organellar protein transport for dual targeting to mitochondria and chloroplasts interacting with NbOm64 and NbToc159A specific receptors, respectively. The discrepancy observed between our results in *N. benthamiana* and those published in Arabidopsis, where AtToc34 and AtTom20 seem to play major roles in dual targeting, may arise from several factors. According to previous studies in Arabidopsis, the initial and simultaneous identification of the transit peptides by the Toc159 and Toc34 families of receptors and the functional similarity of Toc33 and Toc34 suggests that different Toc complexes are present in chloroplasts. In this sense, AtToc33/AtToc159 was involved preferentially in the import of photosynthetic proteins while, AtToc34/AtToc120/132 was associated with non-photosynthetic proteins. NbToc34 and NbToc159 receptors can also combine to form different Toc complexes, but they are forced to share a single form of Toc34. Therefore, they could be less efficient in recognizing a subset of client preproteins than the Toc complexes of *A. thaliana*. Moreover, when each Toc159-related receptor of *N. benthamiana* was silenced, the resulting phenotypes showed substantial differences from those of the corresponding Arabidopsis knockouts, including also a higher degree of functional redundancy (Constan et al., 2004; Kubis et al., 2004; Sáiz-Bonilla et al., 2022). All these observations largely reflect a functional specialization of each receptor in *N. benthamiana* distinct from Arabidopsis, which could result in different mechanisms for cargo sorting.

Another possibility is that preprotein recognition may not always happen similarly. There are two distinct models explaining how Toc receptors work. On the one hand, the "targeting model", which could be adopted by MNSV CP (Figure 8A), proposes that a cytosolic Toc159 recognizes the preprotein transit peptide through the G/A domains, forming a complex that tethers to the outer envelope membrane by a homotypic interaction with the Toc34 G domain. Finally, the preprotein is transferred to Toc75. On the other hand, in the "motor model", the membrane-associated Toc34 constitutes the initial point of contact for transit peptides. Next, preproteins are transferred to Toc159, which also remains stably associated with the outer membrane and acts as a GTP-driven motor pushing preproteins through Toc75 (Jarvis, 2008). Therefore, Toc159 may sometimes operate as the primary receptor, while Toc34 may play this role on other occasions or with alternative preproteins. Despite the

redundancy and overlapping functions of Om64 and Tom20 receptors, our results suggest that Om64 would recognize MNSV CP dual transit peptide through its interaction with Hsp70 and Hsp90 (Nickel *et al.*, 2019). Afterward, MNSV CP is transferred to the Tom complex reaching the mitochondrion intermembrane space through Tom40 (Figure 8B).

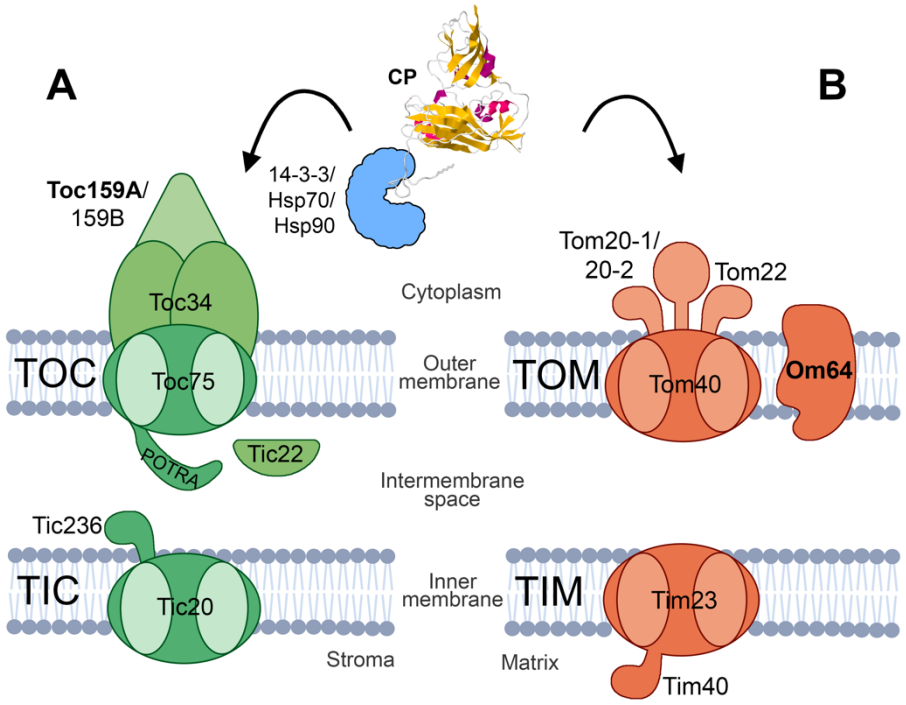

Figure 8. Graphic model of the interaction between MNSV CP and translocon receptors of chloroplast and mitochondria. The CP is targeted to the envelope of both organelles through the interaction of its R domain, which then acts as a dual transit peptide, with 14-3-3, Hsp70 and Hdp90 proteins. **(A)** In chloroplasts, MNSV CP dual transit peptide could be mainly recognized by Toc159A, and translocated through the translocon of the outer membrane of the chloroplast (Toc) by the Toc75 channel. Once into the intermembrane space, the CP could interact with Tic22-III to facilitate its transport to the stroma. **(B)** In mitochondria, MNSV CP dual transit peptide could be recognized mainly by Om64 but not excluding the possibility of interaction with other Tom receptors. Once there, it could be translocated through the translocon of the outer membrane of mitochondria (Tom) by the Tom40 channel to the intermembrane space. Finally, the CP could reach the mitochondrial matrix through the translocon of the inner membrane of mitochondria (Tim) by interacting with unknown factors.

Our studies incidentally provide solid evidence regarding the relevance of the mitochondrion and chloroplast physiological state in the defensive response since the downregulation of *NbTOM40*, *NbTOC75-III,* or *NbTOC34* led to the induction of general resistance against MNSV, CarMV, and TCV. Considering that these viruses replicate in mitochondria, which is morphologically altered after the membrane insertion of the virus-encoded auxiliary replicase, the *NbTOM40* silencing could directly impact viral infection (Blake *et al.*, 2007; Gomez-Aix *et al.*, 2015). Neither TCV, CarMV nor MNSV proteins, instead of MNSV CP, have been found in

chloroplasts; however, *NbTOC75-III-* and *NbTOC34*-silenced plants displayed the same resistance to infection. Here we showed that *NbTOC34*-silenced plants accumulated higher levels of JA than control plants, which is critical for antiviral defense (Wu and Ye, 2020). The mechanism by which disruption of organellar protein import and JA synthesis are linked is unknown. Nevertheless, mitochondria and chloroplasts have been postulated to function also as a source of signaling molecules, including RNA, reactive oxygen species (ROS), proteins, and other metabolites, in retrograde communication with the nucleus (Mielecki *et al.*, 2020), which is of essential relevance, especially during plastid formation and under stressful circumstances. Some reports have recently emphasized the significance of the organelle protein import status and protein homeostasis in retrograde communication. Alteration of chloroplast protein import capacity by GENOMES UNCOUPLED1 (GUN1) depletion, when high import rates are necessary, results in folding stress due to the cytosolic overaccumulation of unimported preproteins. This situation induces the HSP90 upregulation that mediates retrograde communication by either repressing/activating negative/positive transcription regulators and, in turn, maintaining the photosynthesis-associated nuclear gene expression (Wu et al., 2019). Furthermore, *AtTIC100* disruption, a component of the Tic translocon, impaired protein transport and initiated antero-retrograde signaling, maintaining plastids in an immature state and postponing their transition to chloroplasts (Loudya *et al.*, 2022). Therefore, chloroplast protein import disruption by *NbTOC34*, and probably *NbTOC75* silencing, could activate some signaling pathways triggering JA synthesis. For example, OXIDATIVE SIGNAL INDUCIBLE 1, in response to chloroplast ROS, induced JA biosynthesis and programmed cell death (Mielecki *et al.*, 2020).

Our research demonstrated for the first time that an exogenous dual-targeted protein exploits the common Toc and Tom import systems to enter both mitochondria and chloroplasts while interacting with specific Toc/Tom receptors. We have also revealed that significant impairment of the chloroplast protein translocation could be interlinked with retrograde communication triggering a JA-based response that incidentally promotes viral resistance. Future research may profit from our results to better comprehend cellular communication, protein import mechanisms, how preproteins interact with their receptors, and how plant pathogens manipulate host machinery to their ends.

EXPERIMENTAL PROCEDURES

Molecular cloning.

Tom receptor constructions for BiFC were made as previously described for Toc receptors (Sáiz-Bonilla *et al.*, 2022). Additionally, MNSV CP R/arm and S/P domain were PCR-amplificated from an MNSV clone. Next, the GFP amino-terminal (positions 1-155, Nt-[GFP]) or carboxyl-terminal (positions 156-238, Ct-[GFP]) fragments was fused *in frame* between the R/arm and S/P domains and cloned into a modified pSKII+ containing a 35Sx2 promoter and potato protease inhibitor II terminator. Finally, the expression cassettes were transferred to pMOG800 by endonuclease restriction methods as previously described (Sáiz-Bonilla *et al.*, 2022). For Y2H, MNSV CP cDNA was PCR-amplificated and cloned into pGBKT7 and pGADT7 (Takara Bio USA, Inc., Mountain View, CA, USA), resulting in pBDCP and pGADCP, respectively.

The pTRV1 and pTRV2 gateway vectors were used for VIGS (Liu *et al.*, 2002). The 300 nt-length target region selected to silence Tom/Toc receptors, and channels was determined by SGN VIGS tool. The corresponding cDNAs were RT-PCR amplified using SuperScript™ III One-Step RT-PCR Platinum™ Taq HiFi following the supplier protocol (Thermo Fisher Scientific, Carlsbad, CA, USA), and *N. benthamiana* RNAs. Through overlap extension PCR, each fragment was assembled *in tandem* with a 300 nt-length GFP fragment. The resulting cDNA was cloned into the pDONR207, and next, the resultant pENTRY vector was recombined with pTRV2 according to the manufacturer's instructions (Invitrogen Life Tech, Carsland, CA, USA). pTRV2[GFP], a pTRV2 containing the whole mGFP5 gene, was used as a control. Table S2 provides a list of the oligonucleotides and restriction enzymes utilized.

Yeast two-hybrid assays.

Y2H assays were carried out using the GAL4-based MATCHMAKER Two-Hybrid System, following the manufacturer's instructions (Takara Bio USA, Inc., Mountain View, CA, USA). Yeast strain AH109 was transformed using TRAFO protocol (Gietz and Woods, 2002) with pGADCP and pBDCP constructions. Transformant cells were selected by culturing on SD+DO-L for pGADCP and SD+DO-W for pBDCP. Next, all pGAD or pGB receptor constructs were transformed into AH109 containing pGBCP or pGADCP, respectively. Putative interactions were analyzed by culturing yeast co-transformants on SD+DO-A-H-L-W+X-α Gal. As negative

controls, all pGAD and pGBD constructs were also transformed in AH109 harboring pGBKT7 or pBD-p53 and pGADT7 or pGAD-ILR3, respectively.

Agrobacterium tumefaciens-mediated protein transient expression.

For protein transient expression assays in *N. benthamiana*, binary constructs were introduced into *Agrobacterium tumefaciens* C58C1 by electroporation. Transformed bacteria were grown at 28 °C. Cultures were resuspended in 10 mM $MgCl_2$, 10 mM MES pH 5.6, and 150 μM acetosyringone (OD600, 0.2) and infiltrated into the abaxial side of *N. benthamiana* two-week-old leaves. For BiFC, cultures containing the corresponding vectors were mixed before infiltration. Four-week-old plants were kept in growth chambers under long-day photoperiods (16 h light at 25 °C and 8 h dark at 22 °C).

Confocal laser scanning microscopy and fluorescent markers.

An inverted Zeiss LSM 780 confocal microscope (Zeiss, Jena, Germany) was used. Chlorophyll and GFP were excited with the 488 nm line of an argon-ion laser. GFP emission was collected between 492-532 nm, and chlorophyll autofluorescence above 700 nm. For imaging of cherry fluorescent protein (ChFP) fluorescence, excitation at 561 nm was used, and emission was observed at 590–630 nm. The mitochondrial matrix marker coxP-ChFP consisted of the yeast cytochrome oxidase subunit IV transit peptide fused to the ChFP (Navarro *et al.*, 2021). Image processing and analysis were performed using FIJI software.

Viral infection studies in virus-induced gene-silenced plants for Tom and Toc receptors and channels.

Two-week-old *N. benthamiana* plants constitutively expressing GFP (line GFP16c) were used for viral infection studies. Two leaves per plant were infiltrated with bacteria harboring pTRV1 or each pTRV2 construct (1:1 ratio, OD600 = 1). Ten days after TRV agroinoculation, when GFP was silenced in the whole plant as visualized using a UV lamp, plants were mechanically inoculated either with carnation mottle virus (CarMV-Dixie), turnip crinkle virus (TCV-M) or melon necrotic spot virus (MNSV(Al/264)) virions. Three plants per target were inoculated in two non-agroinfiltrated upper leaves. Next, virion-inoculated (local) and upper virion-non-inoculated (systemic) leaves were collected five and ten days post-inoculation, respectively. Virions were purified from *N. benthamiana* as previously described (Díez *et al.*, 1998).

Total RNA extraction and northern blot analysis.

Total RNA from *N. benthamiana* local and systemic leaves were obtained using RiboZol™ RNA Extraction Reagent (VWR Life Science, Matsonford Radnor, PA, USA). 0.5 µg per sample were analyzed on a denaturing gel (3-(N-morpholino) propane sulfonic acid, 5% formaldehyde, 1.3% agarose) and capillary-transferred to nylon membranes in 10X SSC (1.5 M NaCl, 0.15 M sodium citrate). For northern blot hybridization, a digoxigenin-labeled riboprobe for MNSV, CarMV, or TCV CP and CSPD chemiluminescent substrate was used as previously described (Pallás *et al.*, 1998). For detecting viral RNAs, we used a Fujifilm LAS-3000 Imager *(Fuji* Photo Film, Tokyo, Japan).

Real-time quantitative reverse transcription PCR.

RNA samples were treated with DNase I following supplier instructions (Thermo Fisher Scientific, Carlsbad, CA, USA). The first-strand cDNA was obtained using RevertAid H Minus Reverse Transcriptase and random hexamers (Thermo Fisher Scientific, Carlsbad, CA, USA). RT-qPCR was done with a QuantStudio 3 Real-Time PCR machine (Applied Biosystems, Waltham, MA, USA) and PyroTaq EvaGreen qPCR Supermix (Solis BioDyne, Tartu, Estonia), specific oligonucleotides (Table Ssupplementañ2), and recommended qPCR cycles. For designing specific oligonucleotides, Primer3Web 4.1.0 was used (https://bioinfo.ut.ee/primer3). Three systemic leaves from MNSV-inoculated plants for each construct, control, and assay were grouped, generating three biological replicates. The protein phosphatase 2A (PP2A, TC21930) was used to normalize the expression levels using specific oligonucleotides (Liu *et al.*, 2012). Statistical significances at the 95% confidence level (α = 0.05) were determined using Graphpad Prism ($p < 0.05$) through unpaired parametric t-test with Welch's correction as well as one-way ANOVA and Tukey's post-hoc test for multiple comparisons.

Free acid hormone analysis and quantification.

Two-week-old GFP16c *N. benthamiana* plants were agroinfiltrated with pTRV2-GFP, and pTRV2-NbToc34. Ten days after agroinoculation, plants were infected with MNSV virions. At five dpi, 100-200 mg of nitrogen-ground tissue from three biological replicates were sent to the IBMCP plant hormone quantification facility (UPV-CSIC). Free hormones, jasmonic acid,

salicylic acid, and abscisic acid, were analyzed and quantified using a Q Exactive Orbitrap Mass Spectrometer (Thermo Fisher Scientific, Carlsbad, CA, USA).

SUPPLEMENTARY MATERIAL

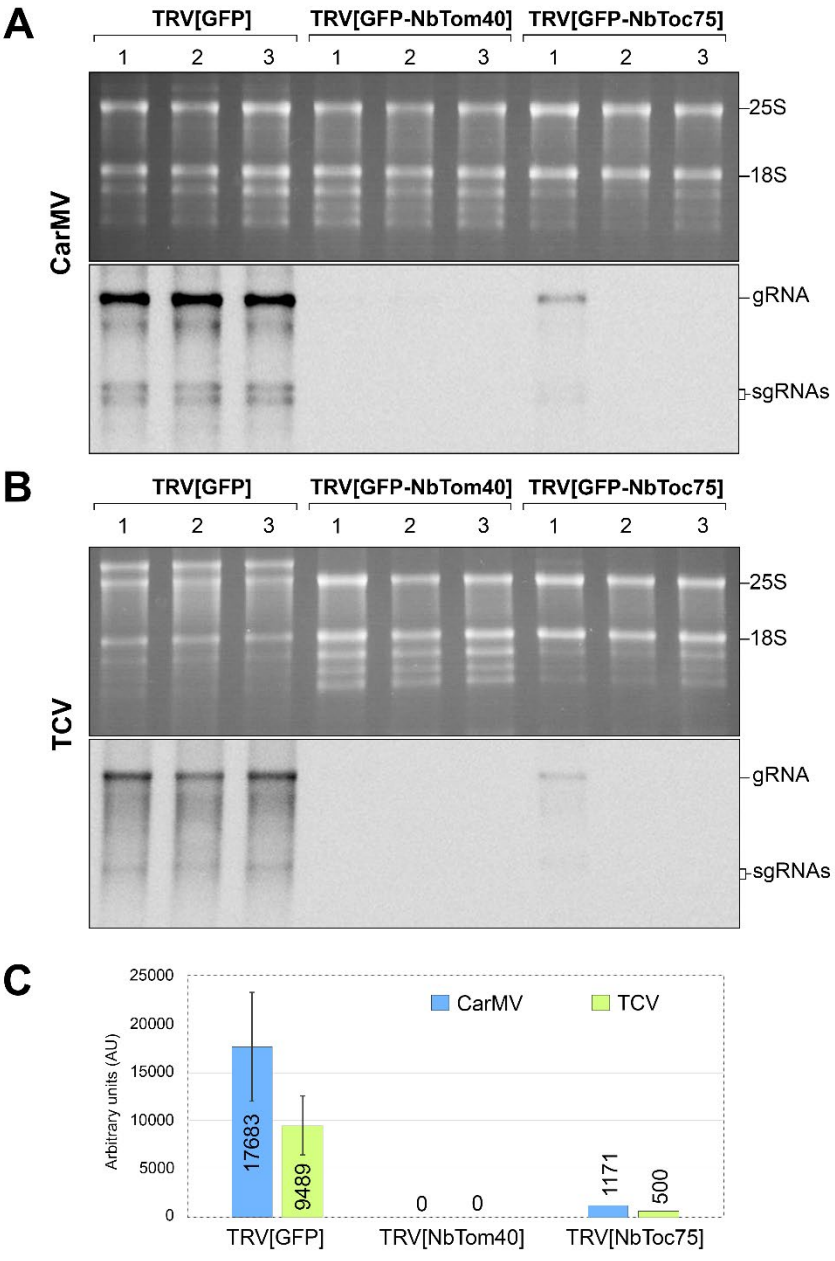

Figure S1. Effect of *NbTOM40* or *NbTOC75* silencing on CarMV and TCV infection.

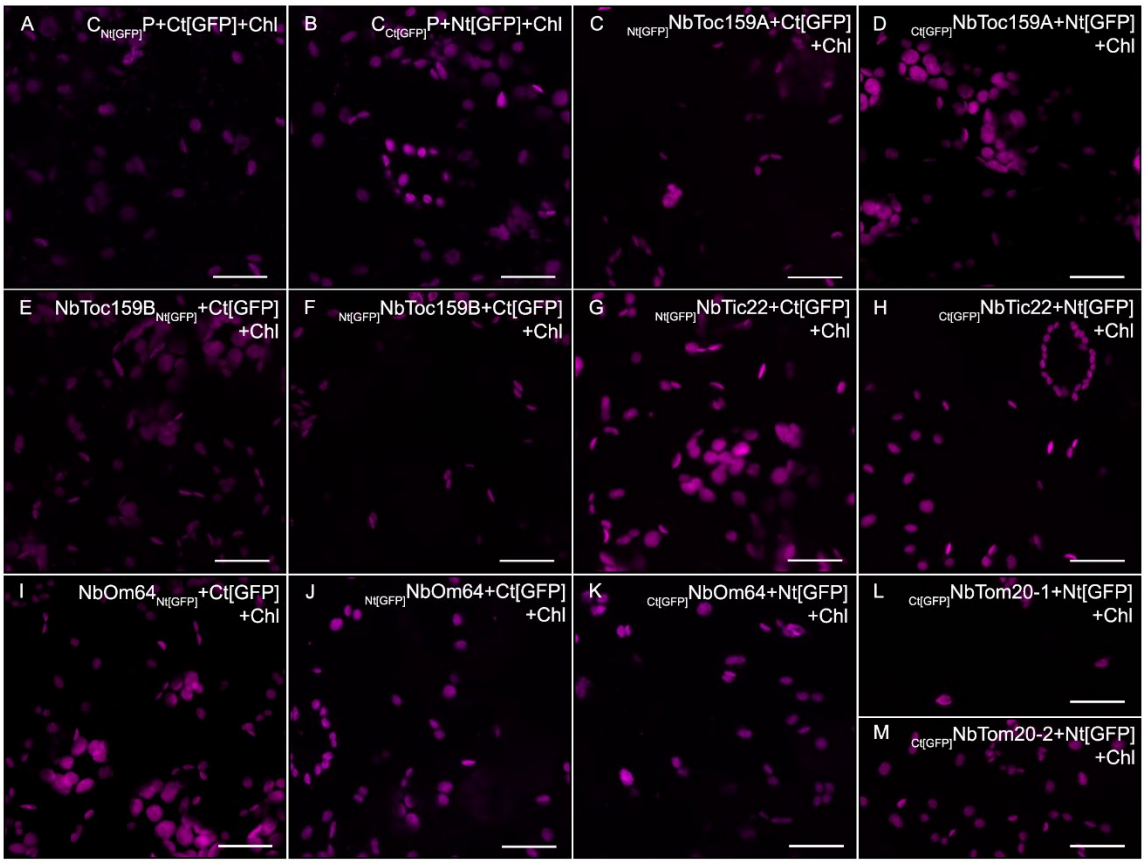

Figure S2. Negative controls of the bimolecular fluorescence complementation assay.

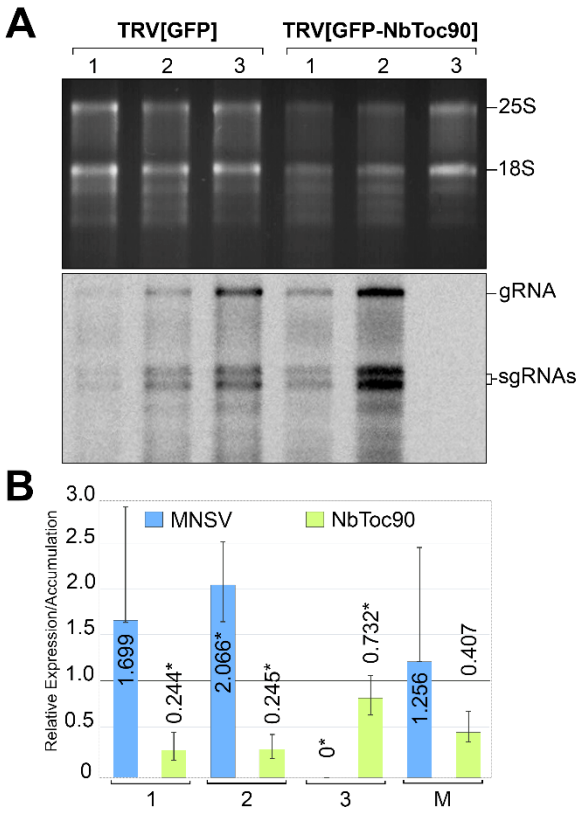

Figure S3. Effect of *NbTOC90* silencing on MNSV infection.

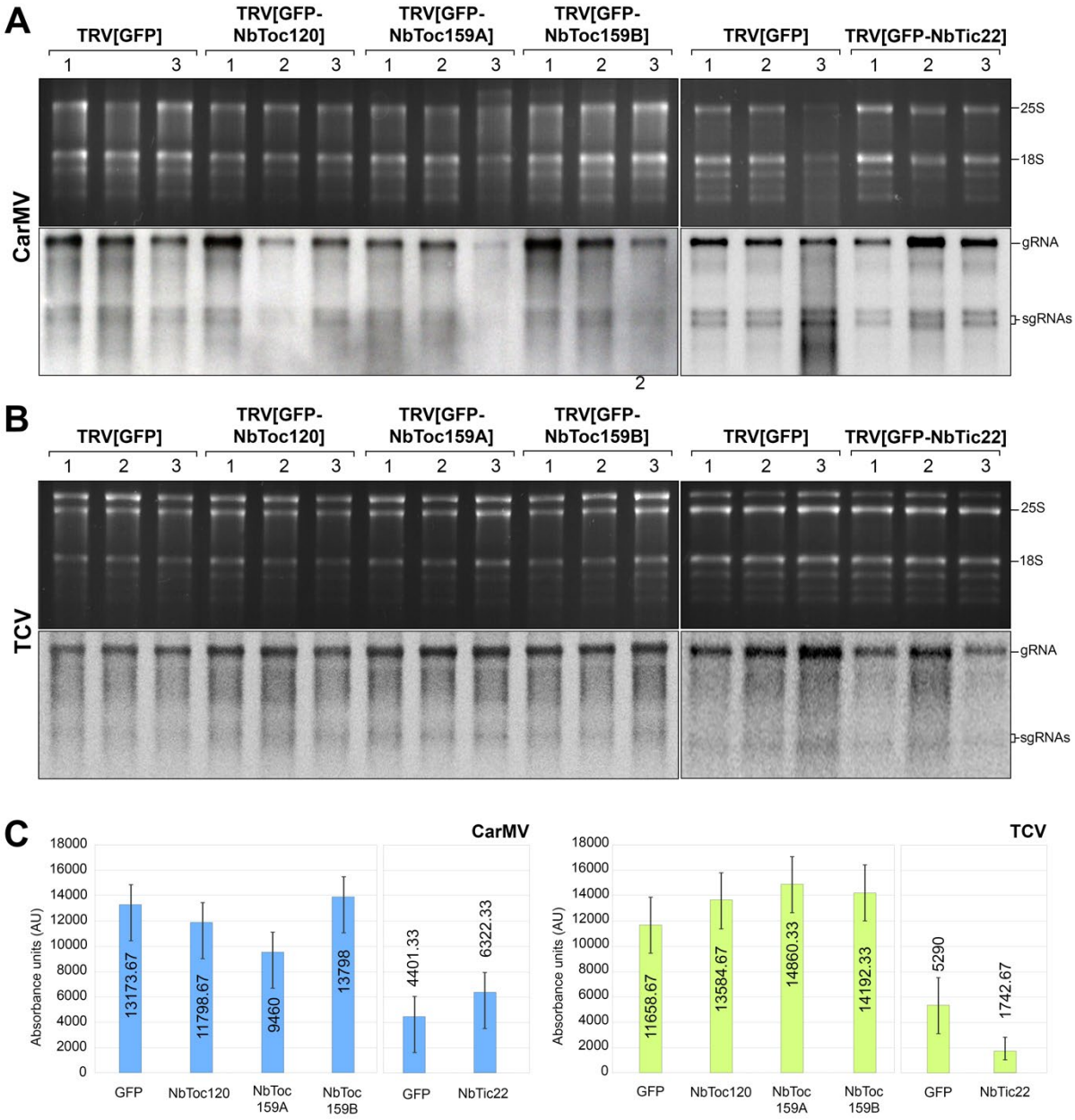

Figure S4. Effect of *NbTOC120, NbTOC159A, NbTOC159B* or *NbTIC22-III* silencing on CarMV and TCV infection.

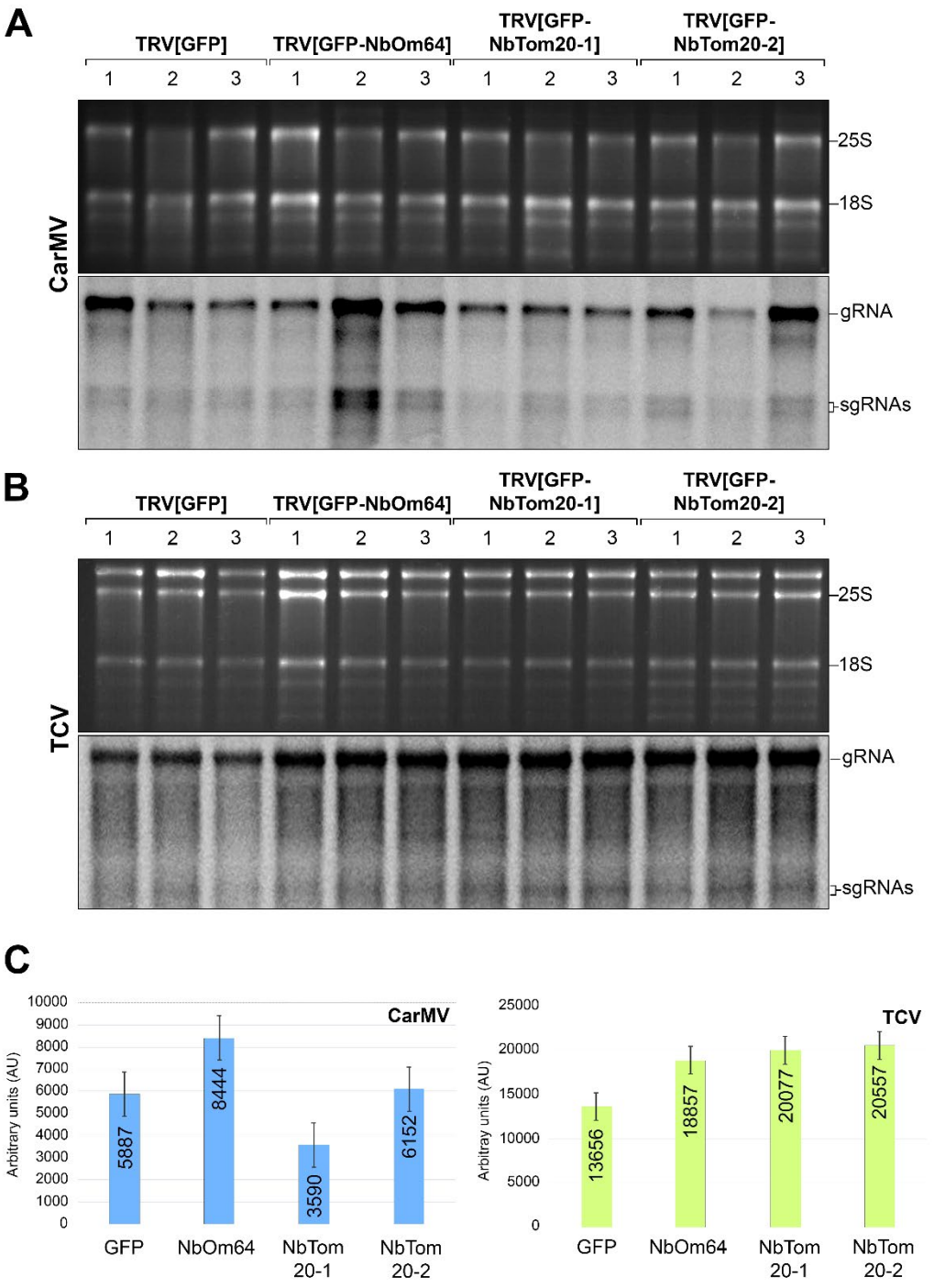

Figure S5. Effect of *NbTOM20-1, NbTOM20-2, or NbOM64* silencing on CarMV and TCV infection.

Supplementary Table S1. Bimolecular fluorescence complementation assays

	MNSV CP				NEGATIVE CONTROLS			
CP	$C_{Nt[GFP]}P+C_{Ct[GFP]}P$	+			$C_{Nt[GFP]}P$+Ct[GFP]	-	$C_{Ct[GFP]}P$+Nt[GFP]	-
TOC	NbToc90$_{Nt[GFP]}$+$C_{Ct[GFP]}P$	-	$_{Nt[GFP]}$NbToc90+$C_{Ct[GFP]}P$	-	NbToc90$_{Nt[GFP]}$+Ct[GFP]	-	$_{Nt[GFP]}$NbToc90+Ct[GFP]	-
	NbToc90$_{Ct[GFP]}$+$C_{Nt[GFP]}P$	-	$_{Ct[GFP]}$NbToc90+$C_{Nt[GFP]}P$	-	NbToc90$_{Ct[GFP]}$+Nt[GFP]	-	$_{Ct[GFP]}$NbToc90+Nt[GFP]	-
	NbToc120$_{Nt[GFP]}$+$C_{Ct[GFP]}P$	-	$_{Nt[GFP]}$NbToc120+$C_{Ct[GFP]}P$	-	NbToc120$_{Nt[GFP]}$+Ct[GFP]	-	$_{Nt[GFP]}$NbToc120+Ct[GFP]	-
	NbToc120$_{Ct[GFP]}$+$C_{Nt[GFP]}P$	-	$_{Ct[GFP]}$NbToc120+$C_{Nt[GFP]}P$	-	NbToc120$_{Ct[GFP]}$+Nt[GFP]	-	$_{Ct[GFP]}$NbToc120+Nt[GFP]	-
	NbToc159A$_{Nt[GFP]}$+$C_{Ct[GFP]}P$	-	$_{Nt[GFP]}$NbToc159A+$C_{Ct[GFP]}P$	+	NbToc159A$_{Nt[GFP]}$+Ct[GFP]	-	$_{Nt[GFP]}$NbToc159A+Ct[GFP]	-
	NbToc159A$_{Ct[GFP]}$+$C_{Nt[GFP]}P$	-	$_{Ct[GFP]}$NbToc159A+$C_{Nt[GFP]}P$	+	NbToc159A$_{Ct[GFP]}$+Nt[GFP]	-	$_{Ct[GFP]}$NbToc159A+Nt[GFP]	-
	NbToc159B$_{Nt[GFP]}$+$C_{Ct[GFP]}P$	+	$_{Nt[GFP]}$NbToc159B+$C_{Ct[GFP]}P$	+	NbToc159B$_{Nt[GFP]}$+Ct[GFP]	-	$_{Nt[GFP]}$NbToc159B+Ct[GFP]	-
	NbToc159B$_{Ct[GFP]}$+$C_{Nt[GFP]}P$	-	$_{Ct[GFP]}$NbToc159B+$C_{Nt[GFP]}P$	-	NbToc159B$_{Ct[GFP]}$+Nt[GFP]	-	$_{Ct[GFP]}$NbToc159B+Nt[GFP]	-
TIC	NbTic22$_{Nt[GFP]}$+$C_{Ct[GFP]}P$	-	$_{Nt[GFP]}$NbTic22+$C_{Ct[GFP]}P$	+	NbTic22$_{Nt[GFP]}$+Ct[GFP]	-	$_{Nt[GFP]}$NbTic22+Ct[GFP]	-
	NbTic22$_{Ct[GFP]}$+$C_{Nt[GFP]}P$	-	$_{Ct[GFP]}$NbTic22+$C_{Nt[GFP]}P$	+	NbTic22$_{Ct[GFP]}$+Nt[GFP]	-	$_{Ct[GFP]}$NbTic22+Nt[GFP]	-
TOM	NbOm64$_{Nt[GFP]}$+$C_{Ct[GFP]}P$	+	$_{Nt[GFP]}$NbOm64+$C_{Ct[GFP]}P$	+	NbOm64$_{Nt[GFP]}$+Ct[GFP]	-	$_{Nt[GFP]}$NbOm64+Ct[GFP]	-
	NbOm64$_{Ct[GFP]}$+$C_{Nt[GFP]}P$	-	$_{Ct[GFP]}$NbOm64+$C_{Nt[GFP]}P$	-	NbOm64$_{Ct[GFP]}$+Nt[GFP]	-	$_{Ct[GFP]}$NbOm64+Nt[GFP]	-
	NbTom20-1$_{Nt[GFP]}$+$C_{Ct[GFP]}P$	-	$_{Nt[GFP]}$NbTom20.1+$C_{Ct[GFP]}P$	-	NbTom20-1$_{Nt[GFP]}$+Ct[GFP]	-	$_{Nt[GFP]}$NbTom20.1+Ct[GFP]	-
	NbTom20-1$_{Ct[GFP]}$+$C_{Nt[GFP]}P$	-	$_{Ct[GFP]}$NbTom20.1+$C_{Nt[GFP]}P$	+	NbTom20-1$_{Ct[GFP]}$+Nt[GFP]	-	$_{Ct[GFP]}$NbTom20.1+Nt[GFP]	-
	NbTom20-2$_{Nt[GFP]}$+$C_{Ct[GFP]}P$	-	$_{Nt[GFP]}$NbTom20.2+$C_{Ct[GFP]}P$	-	NbTom20-2$_{Nt[GFP]}$+Ct[GFP]	-	$_{Nt[GFP]}$NbTom20.2+Ct[GFP]	-
	NbTom20-2$_{Ct[GFP]}$+$C_{Nt[GFP]}P$	-	$_{Ct[GFP]}$NbTom20.2+$C_{Nt[GFP]}P$	+	NbTom20-2$_{Ct[GFP]}$+Nt[GFP]	-	$_{Ct[GFP]}$NbTom20.2+Nt[GFP]	-

Supplemental Table S2. List of oligonucleotides used

Oligonucleotides used for quantitative RT-PCR

Name	**sense**	**sequence**
qPCR-MNSV	Forward	ggtgcgtttgatcgcttaac
qPCR-MNSV	Reverse	taacccctccaacgatttca

Oligonucleotides used for generating $C_{Ct[GFP]}P$ and $C_{Nt[GFP]}P$ BiFC clones by GB

Name	**sense**	**sequence**
GB-CPMNSV-S BsmBI	Forward	gcgccgtctcgctcgtaccatggcgatggttagacgcat
NtCP-BsmBI	Reverse	acgtcgtctcctcgaacaaacctaggcttcatac
Linker-BsmBI	Forward	acgtcgtctcttcgagctagcgccggtgcaggagc
CtYFP-BsmBI	Reverse	acgtcgtctctccgagaccttgtacagctcgtcc
NtYFP-BsmBI	Reverse	acgtcgtctctccgaggccatgatatagacgttgtggctg
CtCP-BsmBI	Forward	acgtcgtctcctcggaaggatctgtgaagatagttc
GB-CPMNSV	Reverse	gcgccgtctcgctcacgctggcgaggtaggctgtttctg
CP-PagI	Forward	acgttcatgacgatggttagacgc
CP-Stop-XbaI	Reverse	acgttctagactaggcgaggtaggctgtttc
CP-MNSV(BsaI-EcoRI)	Forward	acgtggtctcgaattcatggcgatggttagacgc
CP-MNSV(BsaI-BamHI)	Reverse	acgtggtctcggatccctaggcgaggtaggctgtttc

Y2H Cloning of translocon receptors		
Name	**Sense**	**sequence**
NbOm64(BsaI-EcoRI)S	Forward	acgtggtctcgaattcatgacaaaattatcgaagctaaatg
NbOm64(BsaI-BamHI)A	Reverse	acgtggtctcggatcctcaactaattagctttctgag
NbTom20.1(BsaI-EcoRI)S	Forward	acgtggtctcgaattcatggagcaaaacgatttcga
NbTom20.1(BsaI-BamHI)A	Reverse	acgtggtctcggatccttatcttggaggaggaggaggaggca
NbTom20.2(BsaI-EcoRI)S	Forward	acgtggtctcgaattcatggatatgcaaagcgag
NbTom20.2(BsaI-BamHI)A	Reverse	acgtggtctcggatccctattgggtaggaggaggggt
NbTic22-III(BsaI-EcoRI)S	Forward	acgtggtctcgaattcatgaatatcttcaaacctaaacagtc
NbTic22-III(BsaI-BamHI)A	Reverse	acgtggtctcggatccctacttctgggagtgatctgttgaa

Chapter IV

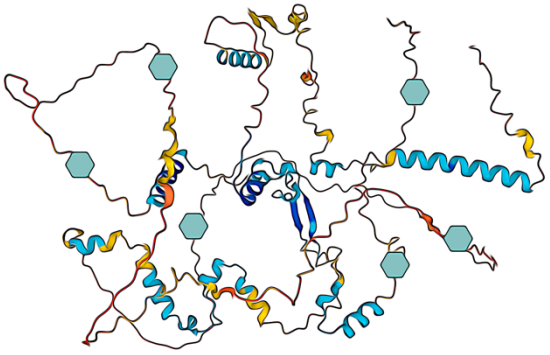

The interactome of a plant viral protein revealed by proximity labeling shows MAPK cascade and splicing components as proviral factors.

María Sáiz-Bonilla[1], Yuanyuan Li[2], Justin W. Walley[3], Savithramma P. Dinesh-Kumar[2], Vicente Pallás[1] & Jose A. Navarro[1]

[1]Laboratory of Plant Molecular Virology, Institute for Plant Molecular and Cell Biology, Department of Molecular and Evolutionary Plant Virology, Consejo Superior de Investigaciones Científicas-Universitat Politècnica de València, Valencia, Spain

[2]Department of Plant Biology and The Genome Center, College of Biological Sciences, University of California, Davis, Davis, CA, 95616, USA.

[3]Department of Plant Pathology and Microbiology, Iowa State University, Ames, IA, 50011, USA.

Part of the work included in this chapter was performed in Dinesh-Kumar laboratory (University of Davis, California).

Manuscript in preparation.

Personal contribution. M.S-B performed all experiments except the LC-MS/MS analysis which was carried out by J.W.W. M.S-B, J.A.N and V.P. analyzed the results and discuss them.

ABSTRACT

The coat protein (CP) of melon necrotic spot virus (MNSV) is dually targeted to chloroplast and mitochondria, and this import is required for viral infection. The search for CP interactors is interesting not only for understanding how plant viruses co-opt or subvert basic cell biological processes but also for indetifying potential antiviral targets. Using TurboID-based proximity labeling, a novel and powerful tool for detecting protein-protein interactors, we identified a large list of host proteins interacting with the CP of MNSV and its cytoplasmic mutant lacking the dual transit peptide. From eight proteins initially selected, the most detrimental effect on viral accumulation was observed after the silencing of *NbSIK1*, *NbSMU2,* and *NbMAP3K*, which encode a MAP4 Kinase, a splicing factor, and a MAP3 Kinase, respectively. However, only the interaction of the CP with NbSMU2 and NbMAP3K was verified by bimolecular fluorescence complementation. NbMAP3K-NbSIK1 interaction was also evidenced, suggesting an indirect interaction between the MNSV CP and NbSIK1 that NbMAP3K could facilitate. Due to protein functionality and interaction localization, two main hypotheses were raised. On the one hand, NbSMU2 hijacking by CP MNSV would result in mRNA splicing changes in favor of MNSV infection. On the other hand, it has been reported that *NbSIK1*-silenced plants accumulate high levels of salicylic acid that could restrict viral infection. This protein is also considered a positive regulator of PAMP-triggered immunity (PTI). The silencing of *NbMAP3K*, a negative regulator of PTI, also limits MNSV infection. Consequently, our findings support the participation of a mitogen-activated protein kinase cascade during MNSV infection, modulated by positive and negative PTI regulators.

KEY WORDS

TurboID, proximity labeling, coat protein, protein-protein interaction, melon necrotic spot virus, mRNA splicing, MAPK cascade, *Nicotiana benthamiana*.

INTRODUCTION

Due to their structural role in cellular membranes, proteins are the most abundant component in the cells of any living organism. Plant proteins also play enzymatic and functional roles in pivotal processes such as photosynthesis, biosynthesis, transport, or immunity (Rasheed *et al.*, 2020). In this line, protein-protein interactions (PPI) are crucial for coordinating developmental and physiological cellular pathways (Zhang *et al.*, 2010). Indeed, the study of the plant interactome is necessary to expand our knowledge about the adaptation processes that take place inside the cell in response to biotic and abiotic stresses (Fukao, 2012).

PPIs could be assorted as permanent or transient according to their stability or lifetime. The first ones involve the formation of long-life stable complexes, while the second ones include short-lived interactions. Frequently, they can also be described as specific, direct, or indirect physical associations. If the molecular surfaces of two proteins come into contact, the interaction is referred to as *direct*; otherwise, it is referred to as *indirect* if the two proteins are physically apart but interact through other intermediaries to form a complex (Peng *et al.*, 2017). PPI detection methods are classified as: (i) *in vivo*, when the method takes place inside a living organism, like in the yeast two-hybrid (Y2H) approach; (ii) *in vitro*, when the technique is performed in a regulated environment but outside of a living organism, such as in the affinity complex purification (AP) and (iii) *in silico*, when the interaction is predicted by computational analysis, like in the ortholog-based sequence approach (Rao *et al.*, 2014). Y2H and AP have been widely used in the last few years. However, the use and the results obtained with these conventional techniques are restricted to *in vitro* or non-physiological conditions, which implies the recognition of only highly stable PPIs. Indeed, proteome mapping of organelles and their minor components is pivotal for determining the protein interactome (Kim and Roux, 2016).

The Proximity Labeling (PL) methodology was developed to resolve some issues presented by the traditional methods for PPI detection. In PL, a genetically encoded biotin ligase is fused to a protein of interest, previously tagged with a conventional epitope to assure its expression, or a localization signal peptide to target it to a particular organelle. This synthetic and promiscuous biotin ligase transforms the infiltrated biotin into transient, diffuse, and activated biotin adenylate intermediates that react with surface lysine residues of nearby

proteins in a radius of 10 nm, leaving labeling even short-lived protein complexes (Kim *et al.*, 2014; Samavarchi-Tehrani *et al.*, 2020). Then, the modified proteins can be isolated from total extracts by standard pulldown methods. Streptavidin beads are specifically used to enrich the biotinylated proteins, which will be later identified by mass spectrometry (MS) (Xu *et al.*, 2023; Qin *et al.*, 2021).

The first biotin ligases used for PL, such as BioID or BioID2, had incubation times of around 18-24 hours and an incubation temperature of 37 °C, making them unsuitable for plants. So, TurboID and miniTurboID versions were introduced to have a biotin ligase that works optimally in all organisms. With sizes of 35 and 28 kDa for TuboID and miniTurboID, respectively, both enzymes present a temperature of incubation of 25 °C and labeling times of around 10 minutes, which is enough to capture short and transient PPIs (Branon *et al.*, 2018; Yang *et al.*, 2021). PL provides many noteworthy benefits that make it a modern and competitive technique. First, PL enables the tagging of proteins in a physiological environment because the engineered enzyme is genetically encoded and produced *in vivo* joined to the protein of interest. Secondly, due to biotin tagging and capture by streptavidin beads, PPIs remain intact during lysis and protein purification. Consequently, PL is not only used to study PPIs but also for subcellular proteomes, cell type-specific proteomes, protein-nucleotide interactions, and interactome of a meiotic protein. Even PL could be coupled with clustered regularly interspaced short palindromic repeats (CRISPR) (Feng *et al.*, 2023; Dionne and Gingras, 2022; Myers *et al.*, 2018; Rees *et al.*, 2015; Trinkle-Mulcahy, 2019; Yi *et al.*, 2020).

The coat proteins (CP) of numerous plant RNA viruses have been characterized as multifunctional proteins assisting in the infectious cycle development (Callaway *et al.*, 2001; Weber and Bujarski, 2015). Melon necrotic spot virus (MNSV) is a positive and polycistronic RNA virus that, according to the phylogenetic analysis of its RNA-dependent RNA polymerase (RdRP), belongs to the genus *Gammacarmovirus* (Adams *et al.*, 2016). MNSV genome codes for five different proteins that fulfill functions such as replication, movement, and encapsidation (Genovés *et al.*, 2006; Navarro and Pallás, 2017). Among them, the CP is a multifunctional protein, which acts like a moonlighting protein because it performs different functions in different steps of the viral cycle. Indeed, the MNSV CP can be localized in chloroplasts and mitochondria due to the presence of a dual transit peptide (dTP) in its first

90-95 amino acids. It can also be located in the cell cytoplasm to a lesser extent. Thus, the MNSV CP may fulfill different functions depending on its subcellular localization. Cytoplasmic CP could act in mitochondrial viral replication complexes (VRC) formation, virion assembly, vector transmission, and RNA-silencing suppression. Meanwhile, chloroplast and mitochondrion-targeted CP could serve as an effector interfering with plant defense signaling or as a mechanism to modulate the levels of cytoplasmic CP and thus the intensity of the RNA silencing suppression (Navarro *et al.*, 2021).

Due to the parasitic nature of viruses, these pathogens must not only overcome the defensive barriers of the plant but also hijack host factors in order to perpetuate themselves. Host factors could either facilitate the establishment of virus infection (Hyodo and Okuno, 2020) or by the contrary, act as antiviral factors limiting the infection progress by activation of resitance mechanims such as autophagy, ubiquitination, mRNA decay and gene silencing, that target viral components (Garcia-Ruiz, 2019). Therefore, the identification of host factors subverted or co-opted by viruses will further our understanding of the viral life cycle and the knowledge of novel resistance targets (García and Pallás, 2015; Hsu and Spindler, 2012; Wang, 2015).

Pathogen effector proteins are mainly responsible for host factors hijacking, and their interaction partners could be mainly detected by appropriate PPIs methods. In this study, we use a TurboID proximity labeling approach (Zhang *et al.*, 2019) to identify the host factors associated with the MNSV CP. This viral protein and its dTP deletion mutant were cloned, fused *in frame* to the TurboID-engineered catalytic enzyme, and expressed in *N. benthamiana* leaves. Next, many host factors were identified by mass spectrometry analysis (MS), and some of them were selected for further analysis. Under virus-induced gene silencing (VIGS) of *NbSMU2*, *NbSIK1*, or *NbMAP3K*, the viral RNA levels showed a significant reduction. The splicing factor NbSMU2 has been previously described to interact with the nematode protein effector 30D08 (Verma *et al.*, 2018), suggesting that mRNA splicing changes could accelerate MNSV infection. Furthermore, NbSIK1 is a MAP4 kinase protein that takes part in antibacterial plant immunity (Zhang *et al.*, 2018), whereas NbMAP3K is a MAP3 Kinase that acts as a negative regulator affecting the PAMP-triggered immunity (PTI) immunity pathway of *A. thaliana* (Mithoe *et al.*, 2016), which supports the initiation of a mitogen-activated protein kinase (MAPK) cascade after MNSV infection. However, only the interaction of the CP with

NbSMU2 and NbMAP3K was verified by BiFC. Nevertheless, NbMAP3K-NbSIK1 interaction was also evidenced, suggesting an indirect interaction between the MNSV CP and NbSIK1 that NbMAP3K could facilitate.

RESULTS

Refining the setting parameters for optimal expression of TurboID-fused proteins and MNSV CP TurboID Proximity Labelling assays.

To determine as many interactors of the MNSV CP as possible, including transient/indirect, and stable/direct interactions, a proximity labeling technique was developed. From previous chapters, it is clear that after transient expression, the MNSV CP is fast-targeted to chloroplasts and mitochondria. Therefore, to identify the putative cytoplasmic CP interactors, a deletion mutant (ΔNtCP) lacking the dual targeting peptide, which corresponds to the first amino-terminal 95 amino acids, was also used. Both were cloned into the p35S::gN-TurboID plasmid resulting in CP-TurboID-3xHA and ΔNtCP-TurboID-3xHA. As control for CP-TurboID-3xHA, the dual targeting peptide of the glycyl-tRNA synthetase (GlyRS) was also fused to the TurboID-3xHA, resulting in the GlyRS-TurboID-3xHA, which is also targeted to mitochondria and chloroplasts. The TurboID-3xHA expressed from the "empty vector p35S::gN-TurboID" was used as the control for ΔNtCP-TurboID-3xHA (Duchêne *et al.*, 2001). Each TurboID-fused construction was then transformed into *Agrobacterium tumefaciens* GV3101, and their expression in *N. benthamiana* leaves were tested at 24-, 36-, 48-, and 72-hours post-infiltration (hpi). Protein extraction and immunoblotting with anti-HA antibody proved 48 hours post-infiltration as the optimal time (data not shown). Then, the accumulation of biotinylated proteins after incubation with exogen biotin was analyzed at different time points. For that, a 200 µM biotin solution was infiltrated in *N. benthamiana* leaves previously agroinfiltrated with each Turbo-ID fusion construct and incubated at room temperature (RT). Infiltrated leaves were collected at 1, 3, and 6 hpi, followed by protein extraction. Immunoblot with Streptavidin-HRT antibody shows that the longer the incubation time, the higher the increase in biotinylated proteins (Figure 1, upper panel). Moreover, the expression of the TuboID fusion proteins was also confirmed with an anti-HA antibody (Figure 1, bottom panel). From these results, 48 hours after infiltration for protein expression and 6 hours for biotin incubation were established as optimal time points for TurboID Proximity Labeling assays.

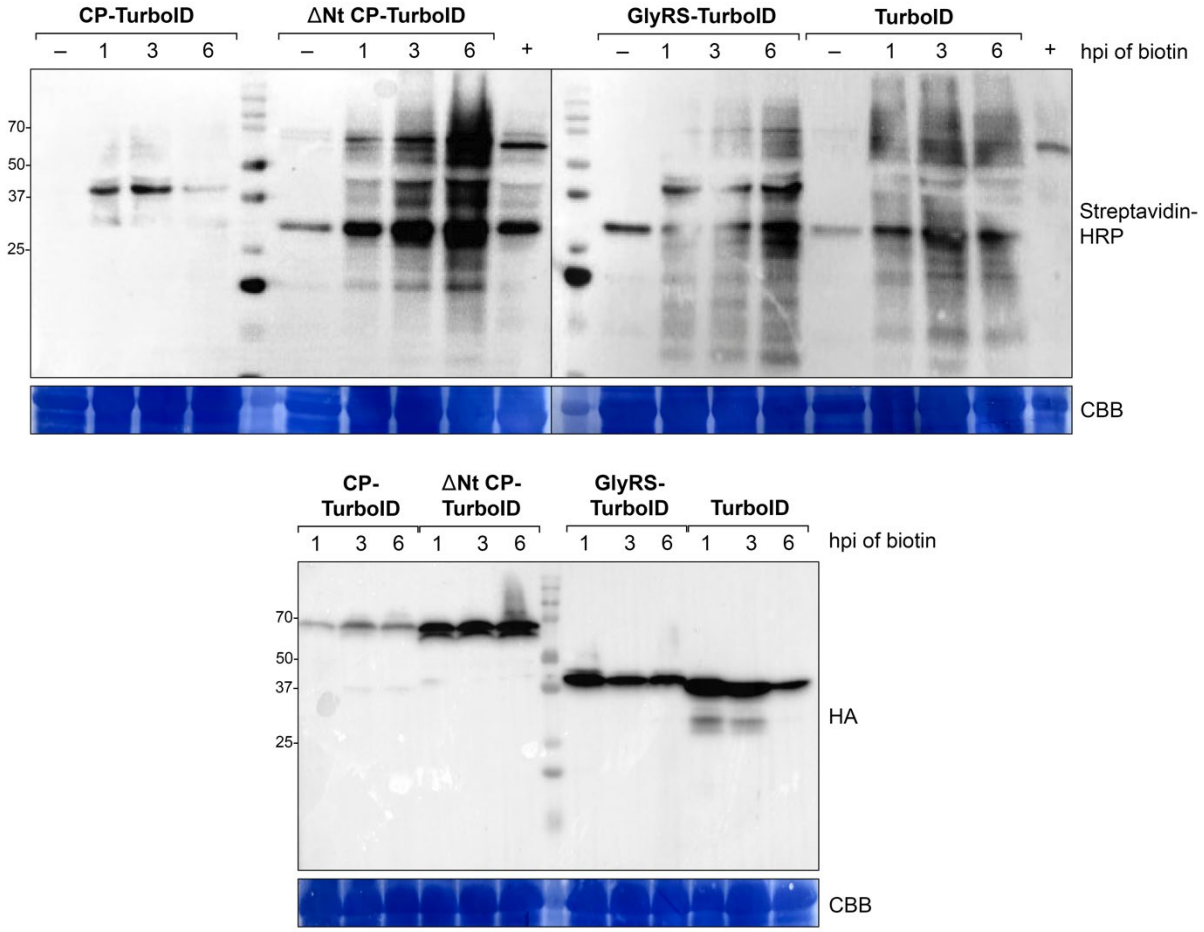

Figure 1. Refining the setting parameters for optimal expression of TurboID-fused proteins and MNSV-CP TurboID Proximity Labelling assays. *Nicotiana benthamiana* plants were agroinfiltrated with CP-TurboID, ΔNtCP-TurboID, and their corresponding controls GlyRS-TurboID and TurboID, respectively. 48 hours post-agroinfiltation (hpi) of constructions, leaves were infiltrated with either 200 µM biotin (+) or medium containing the buffer (-) and incubated at RT. Leaves were collected at various time intervals as shown in the panels (1, 3, and 6 hours) (upper panels). Streptavidin-HRP and anti-HA antibodies were used to detect the biotinylated proteins and the TurboID-fused constructions, respectively (upper and lower panels). As loading and transfer control, membranes were stained with Coomassie Brilliant Blue (CBB). Each panel has a molecular weight size indicator in kDa on the left.

TurboID proximity labeling technique identifies a large variety of potential MNSV CP interactors.

After determining the optimal experimental setting for protein expression and exogen biotin incubation, we continued this study following the TurboID Proximity Labeling procedure previously described (Zhang *et al.*, 2019). The basic steps of the method are shown in Figure 2.

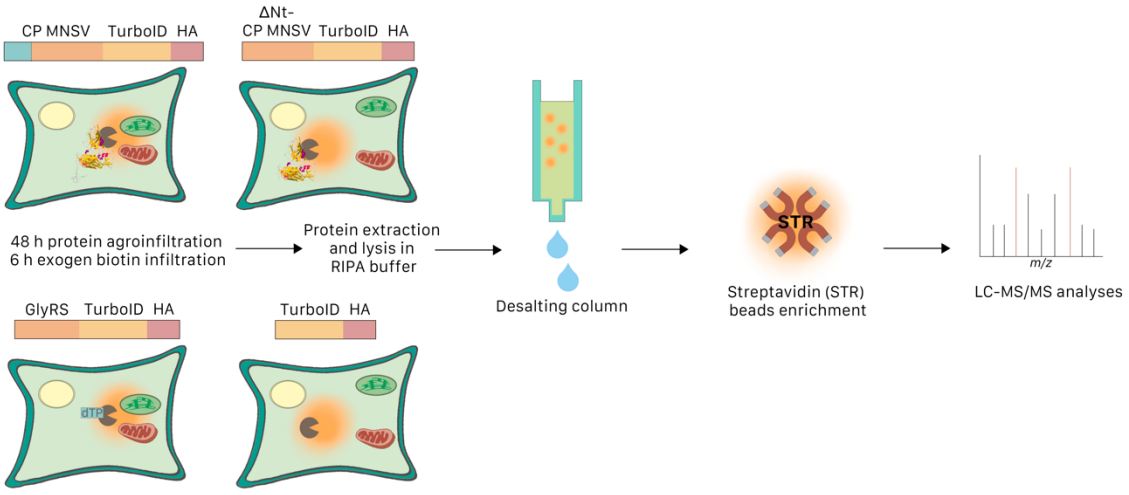

Figure 2. Workflow carried out for the characterization of protein-protein interactions of the CP of MNSV and the ΔNtCP deletion mutant without the dual transit peptide by proximity labeling. First, CP and ΔNtCP were cloned and fused to the TurboID enzyme, the same as the GlyRS dual targeting sequence, which was used as control for the CP-TurboID fusion. The free TurboID was used as control for ΔNtCP. Biotin-labeled proteins were isolated using streptavidin (STR) beads and analyzed by liquid chromatography-mass spectrometry (LC-MS/MS). The Nt region of the MNSV CP harboring the dual transit peptide is represented in blue color.

A. tumefaciens cultures carrying the CP-TurboID-3xHA, GlyRS-TurboID-3xHA, ΔNtCP-TurboID-3xHA, and TurboID-3xHA constructions were infiltrated into two week-*N. benthamiana* plants. Biotin labeling was performed following the conditions optimized above. Afterward, infiltrated leaves were collected and ground with liquid nitrogen, and proteins were extracted with RIPA lysis buffer. Then, a desalting method was carried out to remove the remaining soluble biotin that could still be present in protein extracts. Indeed, the desalting step is crucial because, in contrast to desalted samples, immunoblot examination of the affinity-purified proteins found fewer biotinylated proteins in non-desalted than in desalted samples. Next, a fraction of the protein samples for each construction and replicate were taken out at three points along the TurboID PL protocol and analyzed by Western blot to ensure the proper development of the technique. First, a portion of the input proteins was saved after extraction with RIPA buffer; a second fraction was taken out to show proteins after the desalting column step. Finally, the third fraction corresponded to the streptavidin pull-down enriched proteins before LC-MS/MS analysis. The immunoblot at these three points with anti-HA and Streptavidin-HRT antibodies ensured the proper expression of the TurboID-fused proteins and the accurate capture of biotinylated proteins, respectively. The membrane staining of the PVDF membranes with Coomassie brilliant blue (CBB) revealed that the total protein quantity

decreases drastically from the initial input to the final enriched biotinylated-protein samples (Figure 3).

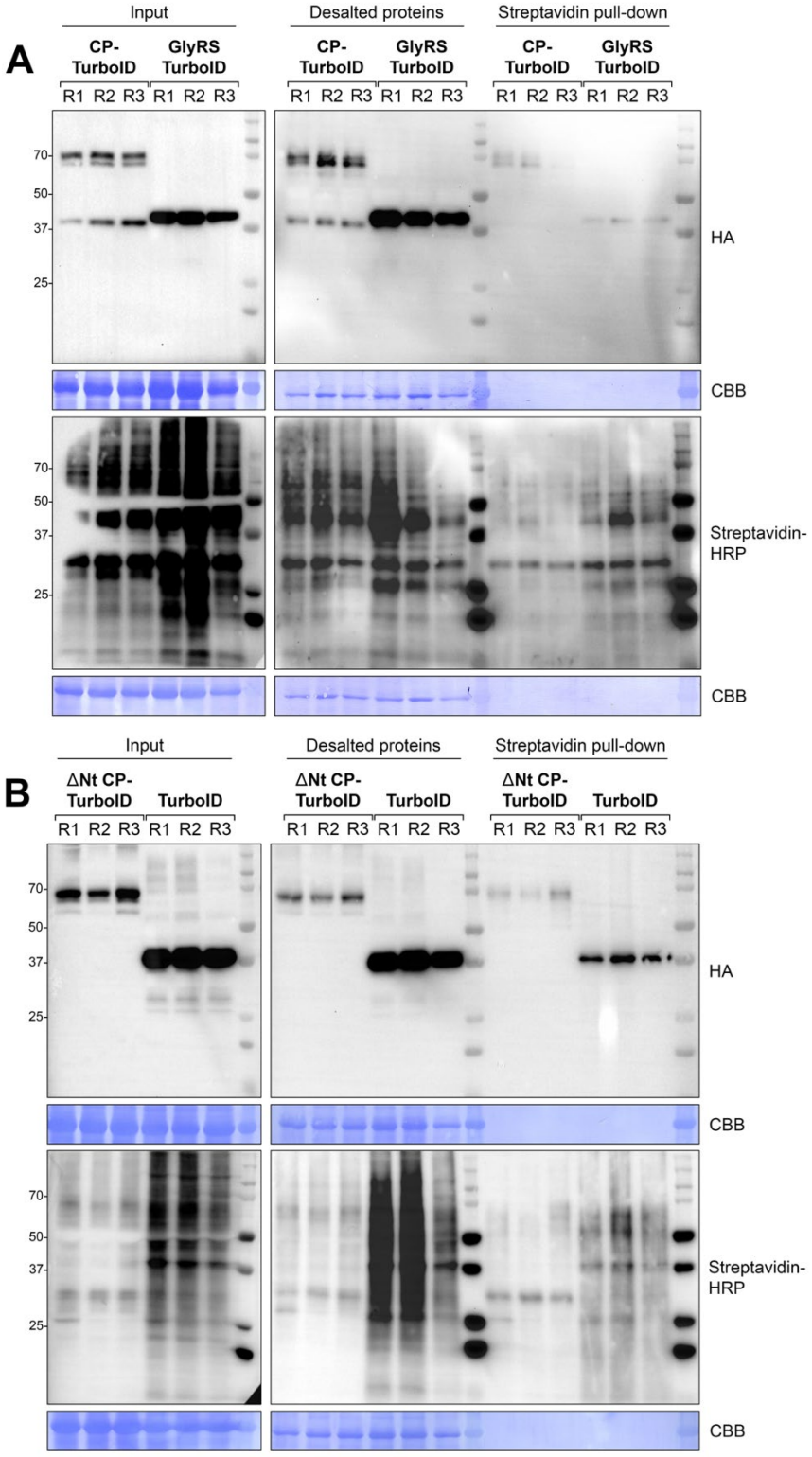

Figure 3. Assessment of the correct development of the TurboID PL assay for CP-TurboID-3xHA (A) and ΔNtCP-TurboID-3xHA (B) by Western blot analysis at different steps. Three replicates for each target and its control were agroinfiltrated with the indicated constructions. A 200 µM biotin solution was infiltrated at 48 hpi,

and plants were further incubated at RT for 6 hours. After that, leaves were collected, and proteins were extracted by RIPA buffer (input). Total protein extracts were passed through a desalting column to remove the remaining free biotin (desalted proteins). About 6 mg of each desalted protein extract were prepared for affinity purification by streptavidin magnetic beads (streptavidin pull-down). Western blots confirmed the biotinylated protein enrichment in the samples before their analysis by LC-MS/MS. Anti-HA and Streptavidin-HRP antibodies were used to identify TurboID-fused proteins and biotinylated proteins, respectively (upper and lower panels, respectively). As loading control, the PVDF membranes were stained with Coomassie Brilliant Blue (CBB) after Western blot. Each panel has a molecular weight size marker indicated in kDa on the left.

Before LC-MS/MS analysis, on-bead digestion was used to separate the enriched proteins from the streptavidin beads, and the resultant peptides were then chemically labeled with isotopically different tandem mass tag (TMT) labels (McAlister *et al.*, 2012; Thompson *et al.*, 2003). TMT labeled samples were combined, and 15 g were subjected to a 2-Dimensional (2D) LC-MS/MS analysis. Peptides were delivered to a Q Exactive Plus mass spectrometer utilizing 2D-LC-MS/MS, which uses low pH reverse-phase as the second dimension and online strong cation exchange (SCX) as the first dimension (Song *et al.*, 2018; Walley *et al.*, 2018). Finally, we quantified the relative amounts of each affinity-purified protein in CP-TurboID-3xHA vs. GlyRS-TurboID-3xHA and ΔNtCP-TurboID-3xHA vs. TurboID-3xHA and identified peptides using MaxQuant33. Using the Perseus34 software, we computed two-sample t-tests and carried out permutation-based false discovery rate (FDR) correction (q-value) to identify enriched interactors. Comparing two datasets obtained from Sol Genomics Network (solgenomics) and the National Center for Biotechnology Information (NCBI), we found 161 and 151 protein candidates, respectively, that had log2 fold change (FC) values higher than zero for CP-TurboID-HA vs. GlyRS-TurboID-HA. For ΔNtCP-TurboID-HA vs. TurboID-HA, we obtained 729 and 779 candidate proteins, respectively (Supplementary Table 2). Additionally, to reduce the list of candidates, we considered putative interactors of the CP if they showed an FC higher than 1.5 and had a p-value lesser than 0.05. After applying these restrictions and combining both datasets, a total of 30 potential interactors for CP-TurboID-3xHA vs. GlyRS-TurboID-3xHA and 156 for ΔNtCP-TurboID-3xHA vs. TurboID-3xHA were identified (Figure 4 and Supplementary Table 3). A large difference in the number of proteins detected from both assays was notable, and it was also found that they did not share any protein. This result is most likely due to the different subcellular localization of each pair of TurboID-fused proteins. CP-TurboID-3xHA and GlyRS-TurboID-HA are mainly located in chloroplast and mitochondria whereas ΔNtCP-TurboID-3xHA and TurboID-HA stay in the cytoplasm.

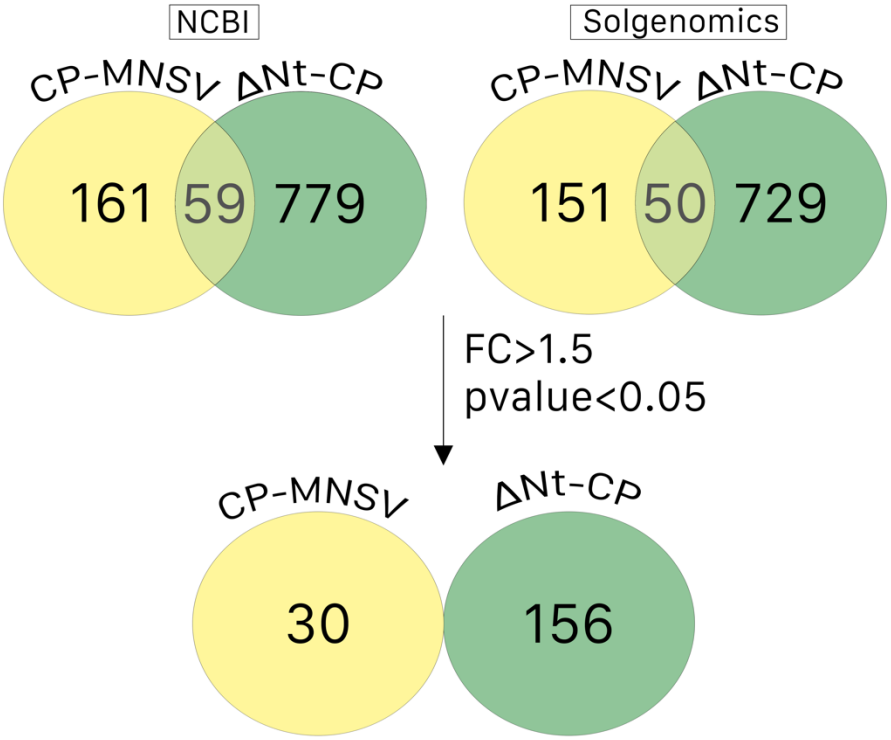

Figure 4. Vent diagram showing the total number of proteins obtained from LC-MS/MS analysis for both targets: MNSV CP and ΔNtCP. Two data sets, from the National Center for Biotechnology Information (NCBI) and Sol Genomics Network (solgenomics), with positive Log2 fold change (FC), were used. Both databases were combined, and proteins with FC > 1.5 and p-value < 0.05 were selected for further analysis.

Selection of CP-interacting candidate proteins for reverse genetics studies.

From all potential candidates above pre-selected with FC higher than 1.5 and a p-value lesser than 0.05, we chosed 18 proteins at the top of the solgenomics and NCBI database lists for further bibliographic research. Next, the most interesting in terms of defense and pathogenesis were selected for functional analysis. On the one hand, three serine threonine-protein kinases, NbSIK1 (Niben101Scf02043g06009.1) and two isoforms of NbEDR1 (Niben101Scf01068g01003.1, Niben101Scf16132g00002.1), a spliceosomal protein, NbSMU2 (Niben101Scf37685g00004.1), and a kinesin-related protein, NbKIN7 (Niben101Scf05711g04009.1) were chosen for CP-TurboID-3xHA/GlyRS-TurboID-3xHA. On the other hand, an E3 ubiquitin-protein ligase NbUPL4 (Niben101Scf05710g03032.1), a protein having a domain of unknown function NbDUF724 (Niben101Scf02831g07010.1), a NAD(P)H-ubiquinone oxidoreductase NbNDC1 (Niben101Scf02280g04013.1) and a protein kinase NbMAP3K (Niben101Scf01587g02009.1) were selected for ΔNtCP-TurboID-

3xHA/TurboID-3xHA (Table 1). The functional relevance of these selected proteins in viral infection was analyzed by reverse genetics using viral gene-induced silencing (VIGS).

Table 1. Candidate proteins detected and selected from CP-TurboID-3xHA/GlyRS-TurboID-3xHA and ΔNtCP-TurboID-3xHA/TurboID-3xHA for VIGS analysis.

Input	Protein	Log2FC	p-value	Peptides	Sequence coverage
CP-TurboID-HA vs. GlyRS-TurboID-HA	NbSIK1	2.67	0.00	1	5
	NbEDR1	2.63	0.00	1	1, 2
	NbSMU2	2.19	0.00	4	7, 9
	NbKIN7	1.96	0.00	1	1, 2
	NbEDR1-X1	1.65	0.00	2	3, 1
ΔNtCP-TurboID-HA vs. TurboID-HA	NbUPL4	3.89	0.00	1	11, 3
	NbDUF724	3.68	0.00	1	11, 3
	NbNDC1	3.53	0.00	1	1, 8
	NbMAP3K	3,39	0.00	3	2, 3

VIGS assays for studying the functional implication of the putative MNSV CP interactors in viral infection.

For determining the effect of gene silencing on MNSV CP functionality and infection, a tobacco rattle virus (TRV) virus-induced gene silencing (VIGS) strategy was developed for each candidate. In this way, pTRV2 constructs were generated for each putative interactor generating pTRV2[NbSIK1], pTRV2[NbEDR1-X1], pTRV2[NbSMU2], pTRV2[NbKIN7], pTRV2[NbUPL4], pTRV2[NbDUF724], pTRV2[NbNDC1] and pTRV2[NbMAP3K] that together with pTRV1 were agroinfiltrated in leaves of transgenic *N. benthamiana* (GFP16c line, Ruiz et

al., 1998). pTRV2[GFP] was used as control. Ten days after the agroinfiltration, when the GFP transgene was nearly silenced (plants were visualized under UV light), MNSV virion was inoculated in upper non-agroinfiltrated leaves. At this point, a visible phenotype was only observed in *NbSMU2*- and *NbMAP3K*-silenced plants; meanwhile, the rest showed phenotypes highly similar to the *GFP*-silenced control (Figure 5 shows the visible phenotype of NbSMU2-, NbMAP3K-, and GFP-silenced healthy plants three weeks after TRV construct agroinfiltration). The upper non-inoculated leaves (systemic leaves) were collected seven days later, and the total RNA was extracted.

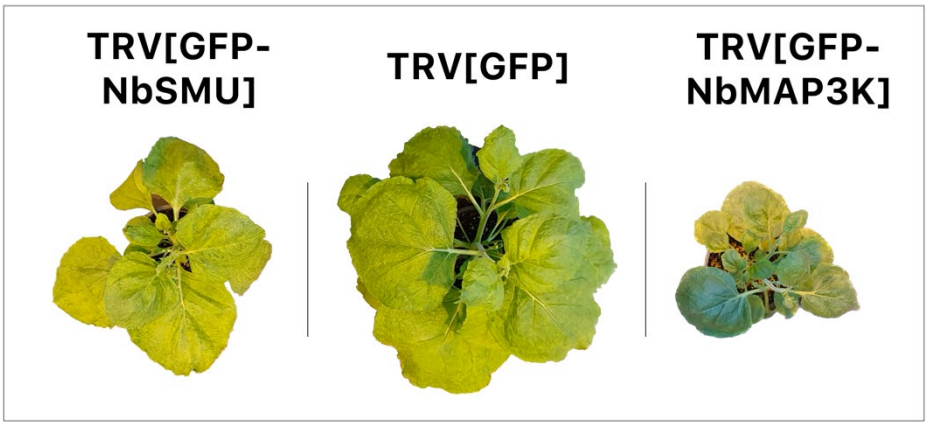

Figure 5. Visible phenotypes of the *N. benthamiana* plants silenced for *NbSMU2*, GFP (control), and *NbMAP3K* by tobacco rattle virus (TRV)-induced gene silencing (VIGS). Images were taken three weeks after pTRV1, and each indicated pTRV2 variant agroinfiltration.

The MNSV RNA accumulation was analyzed by Northern blot in three different assays consisting of three plants per silenced target. From all the examined candidates, silencing of *NbSIK1*, *NbSMU2*, and *NbMAP3K* negatively affected MNSV accumulation on a consistent basis (Figure 6A). Specifically, this effect was more notable in *NbSMU2*- and *NbMAP3K-silenced plants*, which could be related to their visible phenotype (Figure 5). MNSV accumulation was also affected in *NbEDR1-X1-*, *NbKIN7-,* and *NbNDC1*-silenced plants but more slightly. Meanwhile, the silencing of *NbUPL4* or *NbDUF724* intensifies viral accumulation compared with control plants (Figure 7). The RT-qPCR results showed a direct relationship between the degree of gene silencing and viral accumulation. On average, half silencing of *NbSIK1* expression leads to a half decrease in MNSV accumulation. A six-fold decline in viral titer was caused by a more than eight-fold reduction in *NbSMU2* expression. Meanwhile, the MNSV accumulation dropped by roughly eight times compared to the control plants due to a nearly nine-fold reduction in *NbMAP3K* expression (Figure 6B).

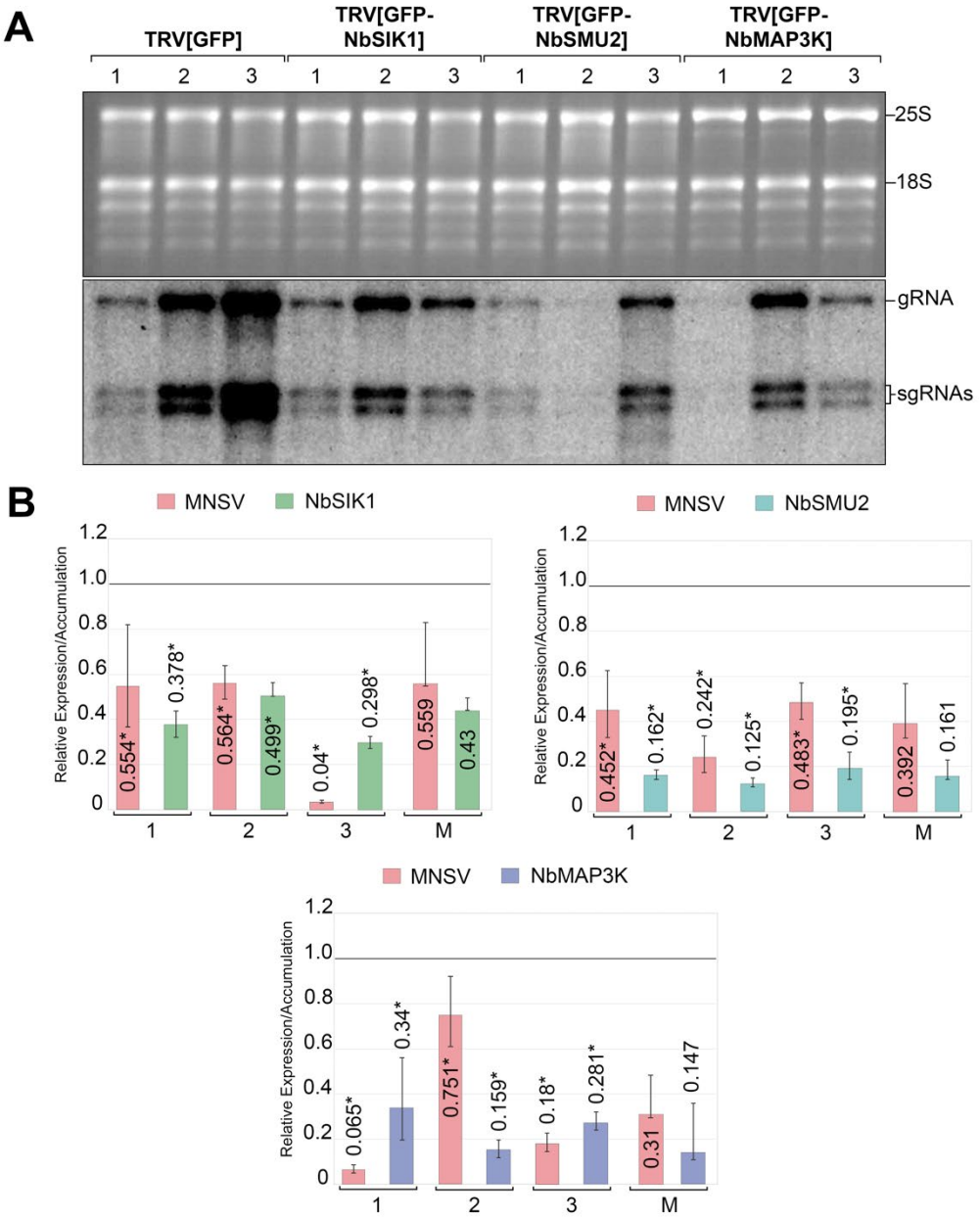

Figure 6. Effect of *NbSIK1*, *NbSMU2,* or *NbMAP3K* silencing on MNSV infection. **(A)** Northern blot analysis was used to determine the accumulation of the genomic and subgenomic RNAs (gRNA and sgRNAs) of MNSV at 7 days post-inoculation. Three different assays are shown (1 to 3), and each lane corresponds to a mix of total RNAs from three plants. As loading control, the ethidium bromide staining of the gel before the membrane transfer is displayed. The positions of the 25S and 18S rRNAs are shown (upper panel). **(B)** Bar diagrams obtained from RT-qPCR analysis showing the MNSV relative accumulation (pink bars) and the relative expression of *NbSIK* (green bars), *NbSMU2* (blue bars) and *NbMAP3K* (purple bars). Three different assays are shown (1 to 3), and M represents the average of the three bioassays. The relative expression of the target gene or MNSV accumulation in control *GFP*-plants was used as reference. The asterisk indicates statistically significant differences ($p<0.05$).

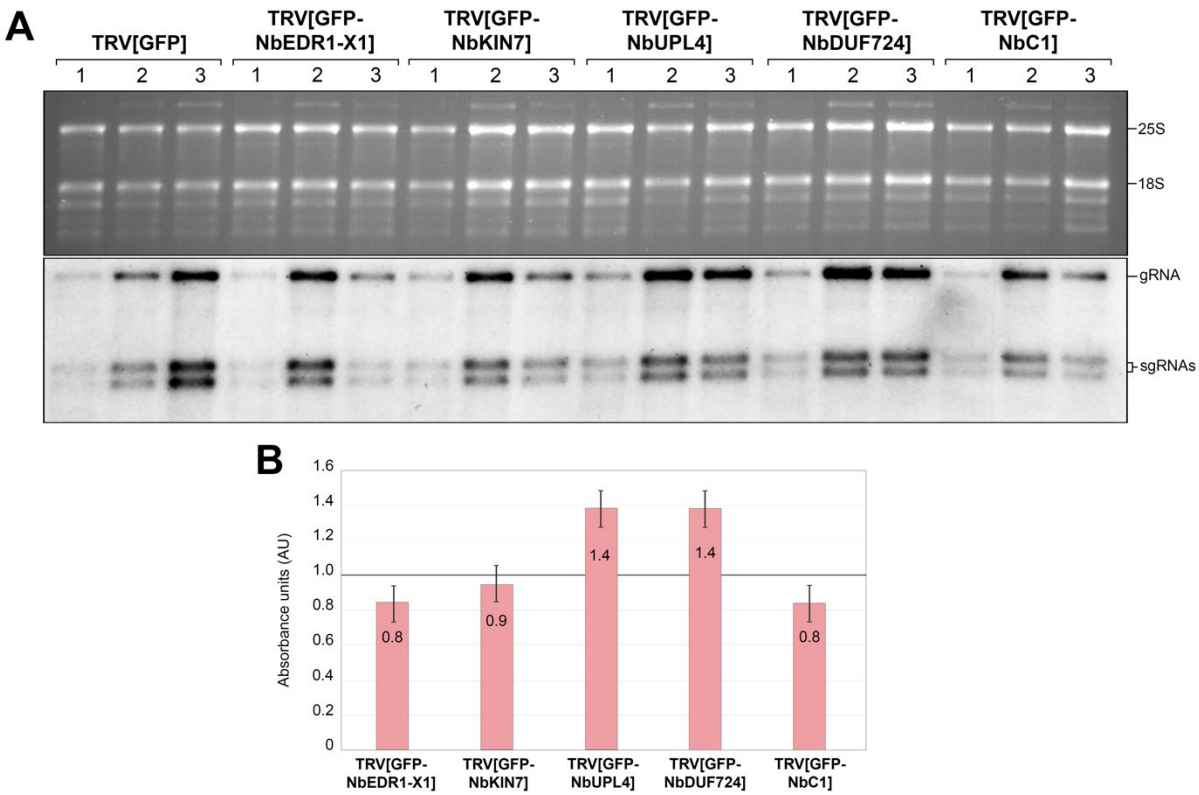

Figure 7. Effect of NbEDR1-X1, NbKIN7, NbUPL3, NbDUF724 and NbC1 silencing on MNSV infection. **(A)** Northern blot analysis was used to determine genomic and subgenomic RNAs (gRNA and sgRNAs) of MNSV at 7 days post inoculation. Three different assays are shown (1 to 3) and each lane corresponds to a mix of total RNAs from three plants. As loading control, ethidium bromide staining with 25S and 18S rRNAs are shown (upper panel). **(B)** Bar diagrams obtained from MNSV gRNAs accumulation measurement by intensity of hybridization for *NbEDR1-X1, NbKIN7, NbUPL3, NbDUF724 and NbC1-silenced N. benthamiana* plants at 10 dpi. The relative hybridation signal in of the gRNAs MNSV accumulation in control *GFP*-plants was used as reference.

NbSMU2, and NbMAP3K are positive interactors of the MNSV CP.

Proteins whose gene silencing had the greatest negative effect on viral infection, NbSIK1, NbSMU and NbMAP3K, were selected to verify their interaction with MNSV CP and ΔNtCP by bimolecular fluorescence complementation (BiFC) assays. The amino-terminal (positions 1-155, Nt[GFP]) or carboxyl-terminal (positions 156-238, Ct[GFP]) GFP fragments were fused to the C- and N-terminal end of the ΔNtCP or each interactor generating, NbSIK1-, SMU2-, MAP3K-, or ΔNtCP-Nt[GFP], NbSIK1-, SMU2-, MAP3K-, or ΔNtCP-Ct[GFP], Nt[GFP]-NbSIK1, -SMU2, -MAP3K, or -ΔNtCP and Ct[GFP]-NbSIK1, -SMU2, -MAP3K, or -ΔNtCP constructions.

Before analyzing the interactions, it is pivotal to evaluate the subcellular localization of the candidates in *N. benthamiana*. Therefore, NbSIK1-GFP, SMU2-GFP, and MAP3K-GFP fusions were also made for subcellular studies. On the one hand, SIK1 from *Arabidopsis thaliana* has been previously reported to be localized in the plasma membrane, trans-Golgi network, and

early endosomes (Xiong *et al.*, 2016). NbSIK1-GFP was mainly distributed in the plasma membrane and small bodies following the cytoplasmic streaming. Albeit, it also seems to be in the nucleus of the cell, although this signal might be originated by passive macromolecular diffusion through nuclear pore complexes (Figure 8A and B). On the other side, AtSMU2-GFP was reported to localize in the nucleus of root cells (Chung *et al.*, 2009), as we observed with NbSMU2-GFP in epidermal cells. However, fluorescence was also detected in cytoplasm structures that might correspond to mitochondria due to their morphology and quantity (Figure 8C and D). Finally, AtMAP3K was identified by an flg22 treatment to be a phosphoprotein associated to the plasma membrane (Benschop *et al.*, 2007). In contrast, NbMAP3K-GFP was mainly localized in the cytoplasm and small granules along the cytoplasm streaming (Figure 8E and F).

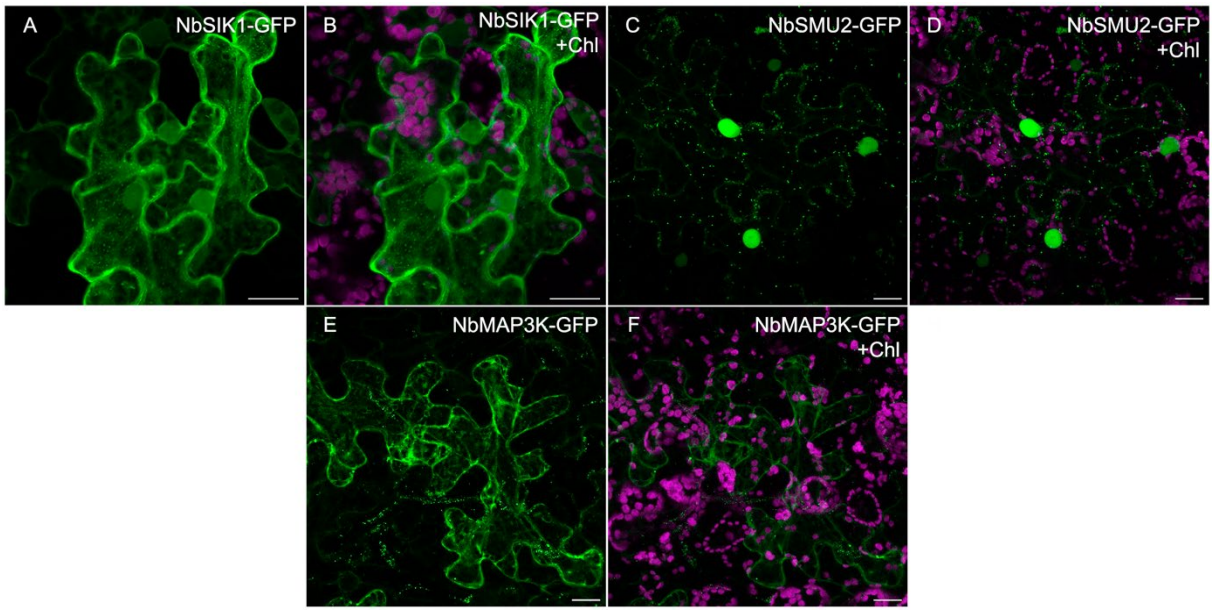

Figure 8. Subcellular localization of NbSIK1-GFP, NbSMU2-GFP, and NbMAP3K-GFP. GFP fusion proteins were expressed in *Nicotiana benthamiana* epidermal cells, Z-stack projections were acquired two days after infiltration. Magenta represents the fluorescence of chlorophyll. Scale bars represent 20 micrometers.

Next, the interaction of the candidates with the MNSV CP and ΔNtCP were re-evaluated by BiFC. With this purpose, the constructions of each interactor with the corresponding GFP fragments were co-expressed in *N. benthamiana* leaves with $C_{Ct[GFP]}$P or $C_{Nt[GFP]}$P (Navarro et al., 2021) and Ct[GFP]-ΔNtCP, Nt[GFP]-ΔNtCP, ΔNtCP-Ct[GFP] or ΔNtCP-Nt[GFP] and Ct[GFP]-ΔNtCP, Nt[GFP]-ΔNtCP, ΔNtCP-Ct[GFP] or ΔNtCP-Nt[GFP] (see combinations in Supplementary Table 4). First, the ΔNtCP-ΔNtCP interaction was demonstrated in four combinations tested (Figure 9A-B and Supplementary Table 4). The fluorescence was observed in the nucleo-

cytoplasm according to that previously shown for ΔNtCP-GFP (Navarro et *al.*, 2021). This result proved that the R domain or arm region does not participate in CP-CP selfinteraction. NbSMU2 and NbMAP3K but not NbSIK1 were positive interactors of ΔNtCP at least in one combination (Figure 9C-F and Supplementary Table 4). On the one hand, NbSMU2 exhibits positive interaction in the cell nucleus with ΔNtCP in two of the four combinations tested (Figure 9C-D and Supplementary Table 4). On the other side, the interaction of NbMAP3K with ΔNtCP was proven only in one combination in cytoplasmic granules (Figure 9E-F and Supplementary Table 4). Due to their functional role in mitogen-activated protein kinase cascades in plants, NbSIK1 and NbMAP3K interaction was also evaluated, resulting in a positive association of both kinases that localized similarly to that observed in NbMAP3K-ΔNtCP interaction (Figure 9G-H). Thus, our BiFC results indicate an indirect interaction between NbSIK1 and MNSV CP that the putative formation of a complex between NbSIK1 and NbMAP3K could explain. Unfortunately, the interaction of the complete CP was not observed neither with NbSIK1, NbSMU2, nor NbMAP3K, even though NbSIK1 and NbSMU2 were identified as interactors of the CP-TurboID-3xHA (Figure 9J-L and Supplementary Table 4). Since the targeting of the MNSV CP to chloroplasts and mitochondria is a fast process, its transit through the cytoplasm may be very short. Moreover, one BiFC limitation is that the visibility of transient interactions in cells is disrupted by the sluggish maturation process of fluorophores (Kerppola, 2008). Therefore, BiFC assays could not be sensitive enough to detect a transient interaction of the CP with NbSMU2 or NbMAP3K.

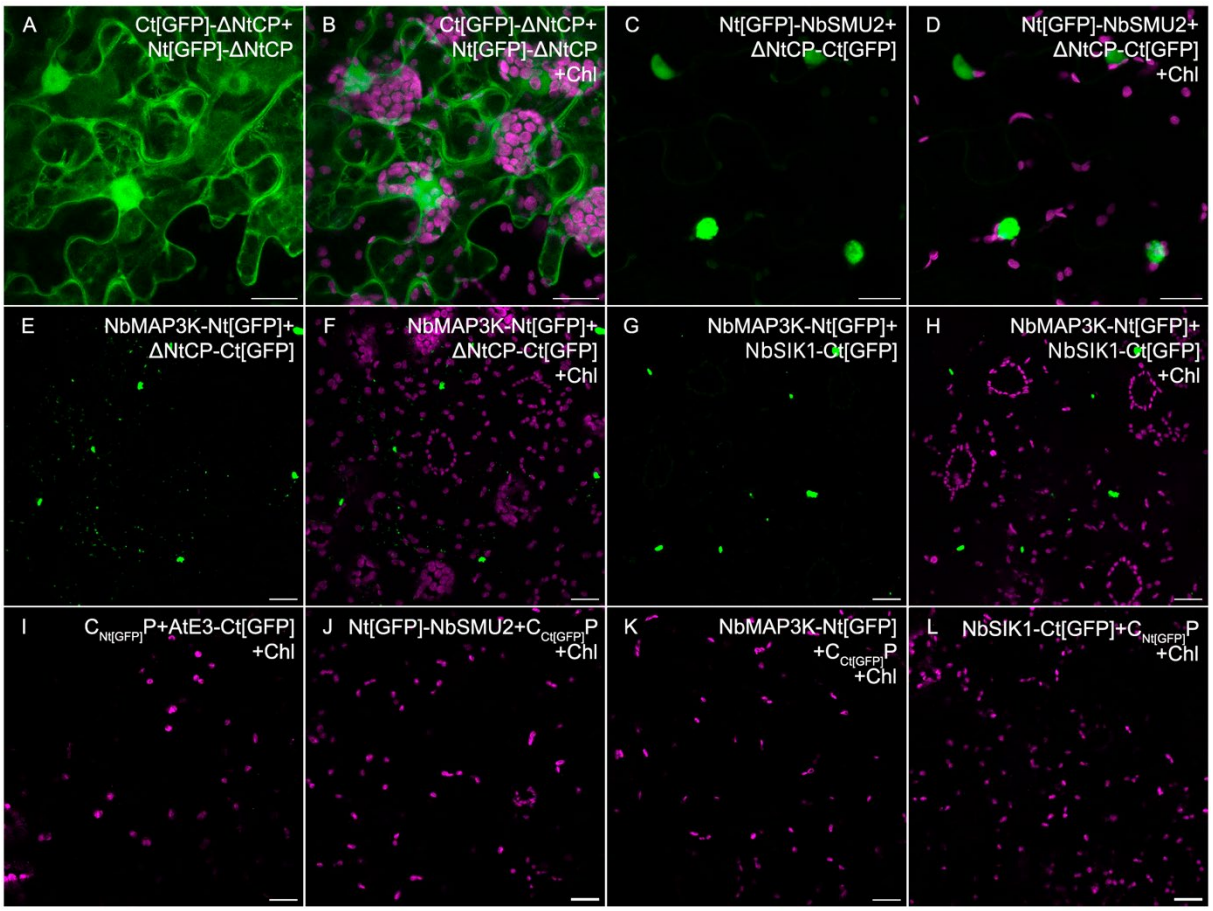

Figure 9. Bimolecular fluorescence complementation assay (BiFC) in epidermal cells of *N. benthamina* using ΔNtCP, NbSIK1, NbSMU2, and NbMAP3K. Leaves were co-infiltrated with agrobacterium carrying the constructs for expression of Ct[GFP]-ΔNtCP, Nt[GFP]-ΔNtCP, ΔNtCP-Ct[GFP], and ΔNtCP-Nt[GFP] and NbSIK1, NbSMU2 NbMAP3K tagged either with Nt[GFP] or Ct[GFP] in their amino or carboxyl end. A representative combination of ΔNtCP interacting with ΔNtCP (A-B), NbSMU2 (C-D), and NbMAP3K (E-F) is shown. Panels G-H show the NbMAP3K-NbSIK1 interaction. A representative negative control with an Arabidopsis E3 ligase (At3G48070) is shown (I). No interaction was observed between the complete CP and NbSMU2 (J), NbMAP3K (K), and NbSIK (L). The scale bars correspond to 20 µm.

To examine if the silencing of the above genes affected the organellar targeting of the MNSV CP, its subcellular localization was tested in *NbSIK1*-, *NbSMU2*- and *NbMAP3K*-silenced *N. benthamiana* plants. First, wild-type *N. benthamiana* plants were silenced as previously described for VIGS but using the empty vector pTRV2[Ø] as control. The previously obtained $C_{[GFP]}P$ fusion, which contains the GFP between the R/arm domain and the S/P domains (Navarro *et al.*, 2021), was agroinfiltrated in upper leaves ten days following the TRV agroinfiltration. Next, the fluorescence was viewed using confocal laser-scanning microscopy (CLSM) 48 hours post-agroinfiltration. As previously reported (Navarro *et al.*, 2021), the dual subcellular localization of the MNSV CP inside the chloroplasts and mitochondria was observed in control plants (Figure 10A-B). This pattern was similar under *NbSIK1* (Figure 10C-D) and *NbSMU2* (Figure 10E-F) silencing; however, chloroplast morphology and the initiation

of chloroplast stromule formation in *NbSMU2*-silenced plants highlighted an intensification of the stress response. In contrast, under *NbMAP3K* silencing, CP localization in chloroplast stroma was disrupted; instead, it was mainly anchored to the chloroplast membrane. A drastic reduction of the mitochondrion-located CP was also noticed, while fluorescence mainly seemed to be in the cell cytoplasm (Figure 10G-H).

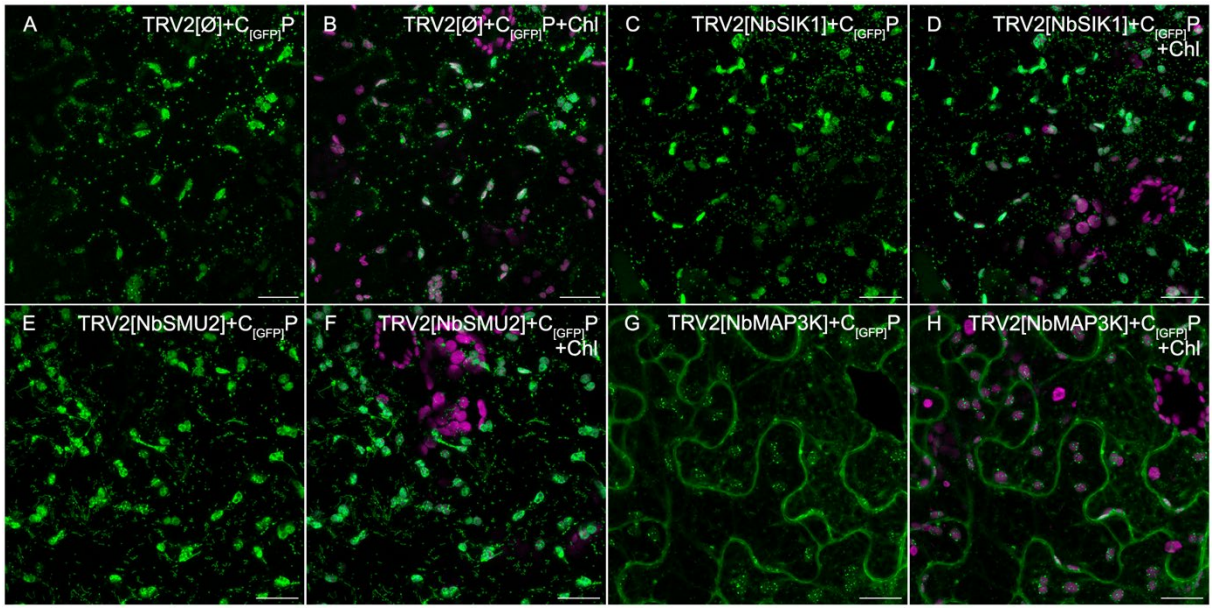

Figure 10. Subcellular localization of MNSV $C_{[GFP]}P$ in control (A-B), *NbSIK1*- (C-D), *NbSMU2*- (E-F) and *NbMAP3K*- (G-H) silenced *N. benthamiana* plants using VIGS mediated by tobacco rattle virus (TRV). Chlorophyll fluorescence (Chl, magenta channel) was used to visualize chloroplasts. The scale bars correspond to 20 µm.

DISCUSSION

Proximity labeling technology using modified biotin ligase enzymes has become an effective method for protein-protein interaction identification and analysis of cellular protein networks. Specifically, TurboID enables highly effective labeling in a short interval of time (as fast as 10 minutes) and a wide range of operating temperatures for different organisms (Xu *et al.*, 2023). In brief, TurboID PL might be considered a new tool for the reliable identification of transient and stable interactors of a protein of interest, complementing the conventional approaches for identifying protein-protein interactions such as yeast two-hybrid (Y2H) or affinity complex purification (AP).

However, there are some points to consider when choosing suitable controls for TurboID PL. They must be located in the same subcellular localization of the protein of interest to eliminate false positives (Zhang *et al.*, 2019). In this sense, we used GlyRS-TurboID-3xHA, which has the dTP of the Arabidopsis glycyl-tRNA synthetase with mitochondrial and chloroplastic localization, to discriminate false positive interactors obtained with CP-TurboID-3xHA (Duchêne *et al.*, 2001). Otherwise, TurboID-3xHA, which remains in the cell cytoplasm, was used as control of the ΔNtCP-TurboID-3xHA, the mutated MNSV ΔNtCP, which without its dual transit peptide has a nucleo-cytoplasm localization.

We identified 30 proteins for CP-TurboID-3xHA/GlyRS-TurboID-3xHA and 156 for ΔNtCP-TurboID-3xHA/TurboID-3xHA. This list of potential interactors also provides an interactive map of direct and indirect interactions as a function of protein localization (Zhang *et al.*, 2019). We selected eight of them, mainly for their higher Log2foldchange and functionality concerning plant pathogenesis and immunity. From those proteins interacting with the MNSV, the main role of SIK1 in Arabidopsis has been related to cell proliferation and expansion. Nevertheless, this protein also acts as a positive regulator of PTI response (Zhang *et al.*, 2018; Duhart and Raftery, 2020). The two isoforms of NbEDR1 selected, NbEDR1 and NbEDR1-X1, are homologous to the MAP3K family, acting as negative regulators of plant defense (Neubauer *et al.*, 2020; Zhao *et al.*, 2014). NbSMU2 is an auxiliary spliceosomal protein recently identified to interact with the nematode effector 30D08 in the nucleus. This interaction alters the pre-mRNA splicing and nuclear gene expression at the feeding site, increasing the susceptibility to parasite infection (Verma *et al.*, 2018). Finally, NbKIN7.3, known as Kin7/separase complex (KISC) in *A. thaliana*, where its main function is related to microtubule regulation (Moschou *et al.*, 2016). Other four proteins were selected from the list of ΔNtCP interactors. They included NbUPL4, which encodes a ubiquitin-protein ligase containing a Homologous to the E6-AP Carboxyl Terminus (HECT) domain, and NbDUF724, a protein of unknown function. Also, NbNDC1, a NAD(P)H dehydrogenase localized in the chloroplast thylakoid and mitochondrial membrane in *A. thaliana*, catalyzes an important reaction for vitamin K1 production (Fatihi *et al.*, 2015). Finally, NbMAP3K, whose principal role is related to pollen development, has also been described as a negative regulator of Flagellin-sensing 2-mediated signaling (Chaiwongsar *et al.*, 2012; Mithoe *et al.*, 2016). Further functional analysis by reverse genetics of selected genes was required; however, *N.*

benthamiana currently has few genetic resources. Therefore, VIGS was used to elucidate whether or not each of these proteins has a role in MNSV infection. Our finding indicated that positive, negative, and non-significant effects in viral infection were noticed depending on the silenced gene. However, the most confident and repetitive result was always the antiviral effect observed in *NbSIK1*, *NbSMU2,* or *NbMAP3K*-silenced plants that showed, in all bioassays performed, a reduction of the MNSV titer directly related to the mRNA levels of the silenced gene.

In our experimental conditions, only VIGS silencing of *NbSMU2* and *NbMAP3K* resulted in a visible phenotype. Similar developmental abnormalities have been reported in the *smu2* mutant of *A. thaliana*, which shows altered splicing of a common set of pre-mRNAs (Chung *et al.*, 2009). Instead, due to Arabidopsis redundancy, the single *map3k* mutant does not show any visible phenotype; meanwhile, *map3kε1;map3kε2* double-mutant combination causes pollen lethality, abnormal callose accumulation, and increasing level of jasmonic acid (JA) (Chaiwongsar *et al.*, 2012). Finally, *NbSIK1*-silenced plants were phenotypically similar to the control, albeit, *AtSIK1* mutant has a dwarf phenotype, and it is compromised in PTI response (Zhang *et al.*, 2018). The effect on PTI response might be related to the decrease in MNSV accumulation in *NbSIK1*-silenced plants; meanwhile, the developmental function of AtSIK1 in the *N. benthamiana* orthologous would be replaced.

SMU2 has been described as a suppressor of mec-8 and unc52 factors for humans and *A. thaliana*. It is a RED family protein member because of its two RED domains (arginine (R)/glutamic acid (E) or arginine/aspartic acid (D) region) at its N- and C-terminal parts. Regarding its molecular function, SMU2 acts as a secondary protein in the spliceosome of *Caenorhabditis elegans* and *A. thaliana*. Therefore, SMU2 might control the splicing of particular pre-mRNAs (Spartz *et al.*, 2004; Ulrich *et al.*, 2016; Chung *et al.*, 2009). Protein-protein interaction studies determined that SMU2 binds to SMU1, forming a complex that takes part in mRNA splicing and phosphatase regulation (Lee *et al.*, 2014). Moreover, the SMU1-SMU2 complex has been previously shown to interact with the viral replicase of the influenza A virus, promoting its replication by controlling viral RNA splicing and protein production. Previous reports also highlight the association of this complex with a human immunodeficiency virus protein (Jäger *et al.*, 2011). In this line, SMU1-SMU2 might be

targeted by a large number of viruses because both have some motifs that promote the assembly of multi-protein complexes: coiled-coil motifs in the RED N terminal domain, two nuclear receptor binding motifs, and WD-40 repeats in N and C terminal domains of SMU1 (Fournier *et al.*, 2014).

As mentioned above, SMU2 is also targeted by the effector protein 30D08 of the soybean cyst nematode, *Heterodera glycines*. The SMU2-30D08A nuclear interaction alters the pre-mRNA splicing and expression of a subset of genes crucial for developing feeding sites. Consequently, the *smu2* mutant was less susceptible to nematode infection (Verma *et al.*, 2018), similar to what happens with the MNSV infection in *NbSMU2*-silenced plants. mRNA splicing acts as a pivotal gene regulation process in eukaryotes, which is not widely studied under virus-plant interactions, nor when a pathogen causes splicing alterations (Boudreault *et al.*, 2019; Syed *et al.*, 2012; Reddy *et al.*, 2013). Nevertheless, alterations in alternative splicing of host transcripts have been observed in plants infected by bacteria, fungi, oomycetes, viruses, and viroids (Dinesh-Kumar and Baker, 2000; Nellist *et al.*, 2014; Mandadi and Scholthof, 2015; Liu *et al.*, 2016; Huang *et al.*, 2017; Jiang *et al.*, 2018). This finding suggests that altering splicing activity represents a significant front in the conflict between pathogens and their hosts. Indeed, Du et al., 2020 have discovered how mRNA splicing changes under a viral infection promote the synthesis of proviral factors, which preferentially accumulate supporting viral infection. In this line, CP could hijack NbSMU2 function on mRNA splicing with the same purpose, causing alternative splicing of host genes and gene expression changes to assist MNSV infection. How NbSMU2-CP nuclear interaction could happen is represented on the bottom of Figure 11.

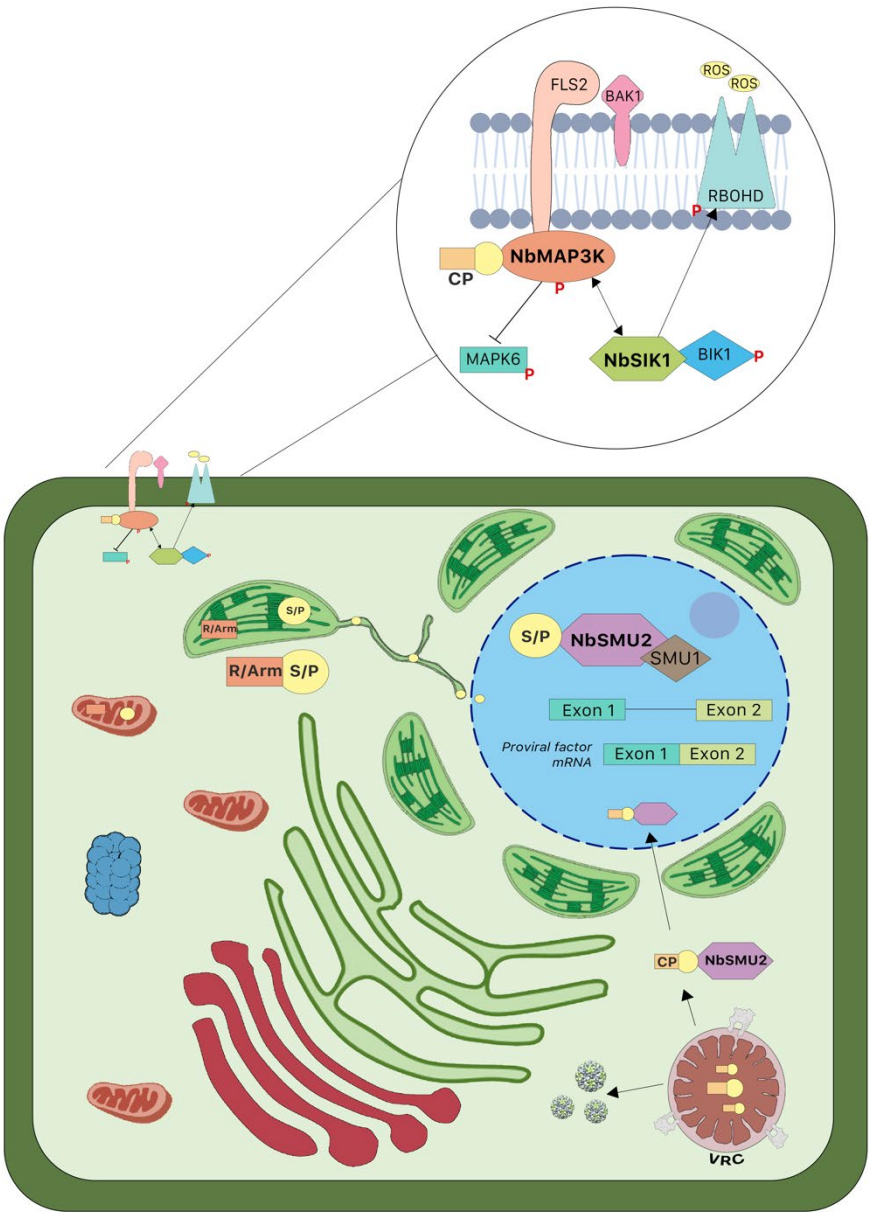

Figure 11. **Model for a role of NbSMU2, NbSIK1 and NbMAP3K during MNSV infection.** To induce alternative splicing of proviral factor mRNAs, NbSMU2-CP interaction would occurs in two different ways. First, the S/P domains of MNSV CP could reach the nucleus through stromules after CP processing in chloroplast stroma. Second, in late infection, non-processed CP produced inside viral replication complexes (VRC) in cytoplasm, would interact with NbSMU2. Next, transport to the nucleus would be driven by NbSMU2. On the other side, it has been described that NbMAP3K interacts with the flagellin receptor FLAGELLIN-SENSITIVE 2 (FLS2) and its co-receptor BRASSINOSTEROID INSENSITIVE 1-ASSOCIATED KINASE 1 (BAK1) inhibitin the MAPK cascade (MAPK6). On the other side, NbSIK1 directly phosphorylates RBOHD and interact with BIK1. In this line, our results show that NbMAP3K and NbSIK1 have antagonistic functions as negative and positive regulators of PTI, respectively. Both proteins interact between them and with the MNSV CP, which might limit PTI development to facilitate MNSV infection.

In Arabidopsis, 20 genes encode MAP kinases (MAPKs), 10 genes encode MAP kinase kinases (MAP2Ks), 80 genes encode MAP kinase kinase kinases (MAP3Ks), and 10 genes encode MAP kinase kinase kinase kinases (MAP4Ks). Consequently, the more genes encoded, the more

redundancy among these families (Su and Krysan, 2016). Pathogen-associated molecular pattern (PAMP) of *Pseudomonas syringae* sensing results in both early reactions, such as the generation of reactive oxygen species (ROS), ion fluxes across the plasma membrane, and activation of MAPK cascades, as well as delayed reactions, such as the activation of genes related to defense. The result of these immune responses boosts a first line of defense known as PAMP-triggered immunity (PTI), similar to virus infection. Pathogens could evade PTI responses and interfere with plant defense by injecting or secreting a group of effectors into the host. For instance, Bacterial flagellin 2 (flg22) is recognized by its main receptor FLAGELLIN-SENSITIVE 2 (FLS2), a leucine-rich repeat (LRR) receptor kinase, and a co-receptor BRASSINOSTEROID INSENSITIVE 1-ASSOCIATED KINASE 1 (BAK1) (Mithoe et al., 2016). SIK1 from *A. thaliana* is a MAP4K involved in cell expansion and proliferation. Still, it is crucial to plant immune responses because it positively controls extracellular ROS and boosts PTI against bacterial pathogens. To strengthen the ROS burst, SIK1 directly phosphorylates RBOHD and forms an association with and stabilizes BIK1, the major immunological regulator (Zhang *et al.*, 2018). The *sik1* mutant of *A. thaliana* has been described to have exacerbated levels of salicylic acid (SA), which in *NbSIK1*-silenced plants might be causing hormonal priming enabling viral infection (Zhang *et al.*, 2018).

The *A. thaliana* MAP3K acts as a negative regulator of FLS2 signaling, attenuating plant defense responses, and immunity. Principally, MAP3K interacts with FLS2 attenuating the MAPK cascade and PTI (Mithoe *et al.*, 2016). In this line, the absence of MAP3K negative regulator in *NbMAP3K*-silenced plants would entail PTI response development, ROS production, and MAPK cascade signaling, leading to a restriction on MNSV infection development. In addition, MAP4K can phosphorylate MAP3K and is a hotspot and hub in MAPK and other signaling pathways due to their various subcellular locations (Mu *et al.*, 2022). AtSIK1 and AtMAP3K have been described as antagonistic for plant immunity. They act as a positive and negative regulator of PTI, respectively. Moreover, Mithoe et al., 2016 suggest that MAP3K could compete with a positive regulator for FLS2 interaction. Thus, given the NbSIK1-NbMAP3K positive interaction by BiFC and their immunity roles, both proteins could compete for FLS2, resulting in a balance between positive or negative regulation of PTI (Figure 11, top).

Our results confirm TurboID PL as a potential tool for detecting transient/stable and direct/indirect protein-protein interactions. Our findings also provide indirect clues supporting the participation of a mitogen-activated protein kinase cascade during MNSV infection, modulated by positive and negative PTI regulators. They also indicated that RNA splicing changes could happen under MNSV infection, requiring further study.

EXPERIMENTAL PROCEDURES

Plant growth conditions.

Nicotiana benthamiana plants were grown at controlled conditions: 16 h light and 8 h photoperiod at 22 °C.

Molecular cloning for TurboID PL, BiFC, and VIGS.

For TurboID Proximity Labelling (PL) fusion clones, CP, ΔNtCP deletion mutant lacking the most amino-terminal 90 amino acids, and the dual targeting peptide of an Arabidopsis glycyl-tRNA synthetase (GlyRS), which was used as control for the CP clone, were amplified by PCR, digested with *MluI/XmaI* and ligated into *MluI/XmaI* p35S::gN-TurboID resulting in p35S::CP-TurboID, p35S::ΔNtCP -TurboID, and p35S::GlyRS-TurboID. p35S::TurboID was used as control for p35S::ΔNtCP-TurboID. Three influenza hemagglutinin (3xHA) epitopes at the TurboID C terminus were also included to facilitate the detection. Primers used for plasmid construction are described in Supplementary Table 1.

To generate the clones for Bimolecular Fluorescence Complementation (BiFC) assays, CP and ΔNtCP were cloned as previously described (Navarro *et al.*, 2021). Meanwhile, the coding regions of NbSIK1, NbSMU2, and NbMAP3K were amplified through RT-PCR and SuperScript™ III One-Step RT-PCR Platinum™ Taq HiFi (Thermo Fisher Scientific, Carlsbad, CA, USA) with the primers described in Supplementary Table 1. The amplified fragments were digested with *NcoI/NheI* for NbSIK1 or *BsaI* for NbSMU2 and NbMAP3K and ligated into a pBluescript II SK(+) that contains a CamV 35Sx2 promoter and the potato protease inhibitor II terminator (Popit) with the amino-terminal (positions 1-155, Nt-[GFP]) or carboxyl-terminal (positions 156-238, Ct-[GFP]) GFP fragments. Finally, the expression cassette was liberated with *BsaI* digestion with *HindIII*-compatible ends and introduced into pMOG800, previously digested with *HindIII*.

To perform the virus-induce gene silencing (VIGS) constructs, we used pTRV1 and pTRV2 gateway vectors (Liu *et al.*, 2002). A region of 300 nt-length from each protein was selected by SGN VIGS Tool from the Sol Genomics network (https://vigs.solgenomics.net/). Fragments were amplified by RT-PCR as previously described and assembled *in tandem* with a 300 nt-length GFP region. The resulting cDNA was then cloned into pDONR207, and then, in accordance with the manufacturer instructions, the resulting pENTRY vector was recombined with pTRV2 (Invitrogen Life Tech, Carsland, CA, USA). The control was pTRV2[GFP], a pTRV2 containing the whole mGFP5 gene.

Agroinfiltration.

Agrobacterium tumefaciens strain GV3101, with the TurboID-fused expression constructs previously generated, was infiltrated into *N. benthamiana* leaves. The OD600 values of the Agrobacterium cultures carrying p35S::CP-TurboID and p35S::GlyRS-TurboID were set to 1.0, while the OD600 for p35S::ANtCP-TurboID and p35S::TurboID was 0.8. The same leaf sections were infiltrated with 200 µM of biotin and 10 mM $MgCl_2$, 48 hours after the agroinfiltration of the constructs and 6 hours before sample collection.

For assays of protein transient expression, pMOG800 constructions were transformed by electroporation in *A. tumefaciens* C58C1. Then, bacterial cultures were grown at 28 °C overnight in Luria-Bertani medium with the proper antibiotic. Cultures were adapted to an OD600 of 0.2 with 10 mM $MgCl_2$, 10 mM MES pH 5.6, and 150 µM acetosyringone and infiltrated into the abaxial side of two-week-old *N. benthamiana* leaves.

For BiFC analysis, bacterial cultures of each vector carrying the corresponding Nt[GFP] or Ct[GFP]-fused protein were mixed and infiltrated in the leaves of four weeks-old *N. benthamiana* plants.

Protein extraction for Mass Spectrometry (MS) analysis.

Three biological replicates were evaluated by MS for each TurboID-fused construct (CP-TurboID-3xHA, GlyRS-TurboID-3xHA, ΔNtCP-TurboID-3xHA, and TurboID-3xHA). Four infiltrated leaves from each plant were collected 6 hours after biotin infiltration and immediately frozen in liquid nitrogen. To extract the proteins, 1 ml of RIPA lysis buffer [50 mM Tris-HCl (pH 7.5), 1 mM EDTA, 500 mM NaCl, 1% NP40 (v/v), 0.1% SDS (w/v), 0.5% sodium

deoxycholate (w/v), 1 mM DTT, and 1 tablet of cOmplete™ Protease Inhibitor Cocktail (Roche, Catalog number 11697498001)] were added to 700 mg of leaf tissue previously powdered. The tubes were immediately centrifuged at 16.500xg for 10 minutes after vortex mixing to eliminate the biotin excess in the lysates. The top soluble fraction was next passed through the Zeba™ Spin Desalting Column (Thermo Fisher Scientific, Catalog number 89893). Then, 100 µl of the desalted extract lysate was reserved and utilized to calculate the protein content using the Pierce™ BCA Protein Assay Kit (Thermo Fisher Scientific, Catalog number 23225).

To enrich biotinylated proteins from the protein extracts, 200 µl of streptavidin-coated magnetic beads (Dynabeads™ MyOne™ Streptavidin C1, Invitrogen, Catalog number 65001) were washed twice with RIPA lysis buffer. The desalted lysates containing ~ 6 mg of total protein were incubated overnight at 4 °C with the equilibrated beads on a rotator. Next, the beads were washed with 1 ml of buffer I (2% SDS in water), 1 ml of buffer II (50 mM HEPES, pH 7.5, 500 mM NaCl, 1 mM EDTA, 0.1% deoxycholic acid (w/v), and 1% Triton X-100), and 1 ml of buffer III (250 mM LiCl, 1 mM EDTA, 0.1% deoxycholic acid (w/v), 1% NP40 (v/v)). The beads were washed twice in 50 mM Tris-HCl, pH 7.5, then six times in 50 mM ammonium bicarbonate, pH 8.0, to remove the residual detergent thoroughly. Finally, 1 ml of 50 mM ammonium bicarbonate was used to resuspend the beads. 100 µl of the suspension was used for Western blot analysis in order to verify that the biotinylated proteins were successfully enriched, and the remaining beads were either flash-frozen in liquid nitrogen and kept at -80 °C or shipped right away on dry ice for liquid chromatography-mass spectrometry (LC-MS/MS) analysis. On-bead trypsin digestion of biotinylated proteins, TMT labeling, liquid chromatography, and mass spectrometry were performed as previously described (Zhang et al., 2019).

MS data analysis.

In order to analyze the raw data, MaxQuant version 1.6.1.033 was used. Spectra were searched against either the *Nicotiana benthamiana* data set of NCBI or the *Nicotiana benthamiana* (N. benthamiana sequence v1.0.1 proteome file entitled "Niben101 annotation.proteins.wdesc.fasta") downloaded from SOL Genomics (ftp:/ftp. solgenomics.net/genomes/Nicotiana benthamiana). MaxQuant added reverse decoy sequences and typical contaminants to the proteome data. Methionine oxidation and protein

N-terminal acetylation were specified as variable modifications, whereas carbamidomethyl cysteine was set as a fixed modification. "Reporter Ion MS2" was chosen as the sample type, and "TMT10plex" was chosen for the lysine and N-termini. The MaxQuant adjustments tab was used to configure TMT batch-specific correction parameters (TMT Lot No. TB260979). “Specific” and “Trypsin/P;LysC” were chosen as the digestion parameters. Missed cleavages were permitted up to two times. It was necessary to have a false discovery rate of less than 0.01 at both the protein identification level and the peptide spectral match level, as determined by MaxQuant employing a target-decoy strategy70. The MaxQuant functionality that compares runs was not used.

TMT intensity measurements were median-centered to equalize the total TMT intensity across all samples in order to normalize the data. Perseus34 was used to perform statistical analyses and hierarchical clustering on the proteomics data. There was no imputation for missing values. Two-sample t-tests combined with permutation-based false discovery rate (FDR) correction were used in statistical analysis to find enriched interacting proteins. If a protein has a q-value of less than 0.05 and a fold enrichment of greater than 1.5, it was referred to as a strongly enriched interactor.

Western blot analysis.

The plant tissue that expressed the desired protein or proteins was ground using liquid nitrogen. Total protein extracts were analyzed by SDS-PAGE, and then transferred to Immobilon-P PVDF membrane using the Trans-Blot Turbo Transfer System (Millipore, Catalog number IPVH00010) (Bio-Rad). Membranes were incubated with the appropriate primary antibodies or streptavidin-HRP, followed by incubation with the corresponding secondary antibodies. Membranes were blocked for 1.5 h in 5% fat-free milk in phosphate-buffered saline with 0.1% Tween20 (PBST) (for immunoblot HA detection) or 2.5% BSA in PBST (for streptavidin-HRP detection). Western blotting antibodies used were the rat anti-HA (Roche, Catalog number 11867423001; 1:5000 dilution), Streptavidin-HRP (Abcam, Catalog number ab7403; 1:10000 dilution); anti-HA-HRP (Roche, Catalog number 12013819001; 1:5000 dilution). According to the manufacturer instructions, chemiluminiscent signals were seen using either the Bio-Rad Clarity™ Western ECL Substrate (Catalog number 1705060 from Bio-Rad) or the ThermoFisher SuperSignal™ West Pico PLUS Chemiluminescent Substrate

(ThermoFisher, Catalog number 34577). A ChemiDoc™ Touch Imaging System was used to collect chemiluminescent signals (Bio-Rad).

Confocal laser scanning microscopy.

We employed an inverted Zeiss LSM 780 confocal microscope (Zeiss, Jena, Germany) to examine the subcellular localization of proteins and BiFC interactions in N. benthamiana leaf dishes. An objective plan-apochromat 40x/1.4 Oil DIC M27 with a diameter of 0.5 cm was used to capture the images. The chlorophyll autofluorescence and the green fluorescent protein (GFP) were excited using a 488 nm line argon-ion laser. Chlorophyll and GFP fluorescence emitted above 700 nm, and in the 480-520 nm range, respectively, were measured. FIJI software was used for image processing and analysis, including overlays and Z-stack projections.

MNSV infection assays in virus-induced gene-silenced plants for host factors.

Two-week-old *N. benthamiana* plants constitutively expressing GFP (line GFP16c) were employed for viral infection research. Bacterial cultures carrying either pTRV1 or each pTRV2 construct (1:1 ratio, OD600 = 1) were infiltrated into two leaves per plant, and plants were mechanically inoculated ten days after TRV agroinoculation with melon necrotic spot virus (MNSV(Al/264)) virions. Previously to MNSV infection, GFP silencing in the plants was evaluated with a UV lamp. Then, seven days after viral inoculation, systemic (virion-non-inoculated) leaves were collected.

Total RNA extraction and Northern blot analysis.

Total RNA from systemic leaves, previously recollected, was obtained by RiboZol™ RNA Extraction Reagent (VWR Life Science, Matsonford Radnor, PA, USA). A denaturing gel (3-(N-morpholino) propane sulfonic acid, 5% formaldehyde, 1.3% agarose) was used to analyze around 0.5 g of RNA from each sample, which was then capillary-transferred to nylon membranes in 10X SSC (1.5 M NaCl, 0.15 M sodium citrate). A digoxigenin-labeled riboprobe against the MNSV CP gene and the CSPD chemiluminescent substrate was employed for Northern blot hybridization as previously described (Pallás *et al.*, 1998). We utilized a Fujifilm LAS-3000 Imager to visualize the chemiluminescent hybridization signals from the viral RNAs (Fuji Photo Film, Tokyo, Japan).

Quantitative reverse transcription PCR in real time (RT-qPCR).

Following the supplier recommendations, the genomic DNA was removed from the RNA samples using DNase I. (Thermo Fisher Scientific, Carlsbad, CA, USA). The first-strand cDNA was then amplified from 0.5 g of total RNA using RevertAid H Minus Reverse Transcriptase and random hexamers (Thermo Fisher Scientific, Carlsbad, CA, USA). The QuantStudio 3 Real-Time PCR system (Applied Biosystems, Waltham, MA, USA), PyroTaq EvaGreen qPCR Supermix (Solis BioDyne, Tartu, Estonia), specific oligonucleotides (Supplementary Table 2), and the manufacturer suggested qPCR cycles were used to perform the RT-qPCR. Primer3Web 4.1.0 was employed to design the oligonucleotides for each gene (https://bioinfo.ut.ee/primer3). For each target, control, and assay, three systemic leaves from MNSV-inoculated plants were pooled, creating three biological replicates. Together with the previously mentioned oligonucleotides, the protein phosphatase 2A (PP2A, TC21930) was employed as an endogenous control to normalize the expression levels (Liu *et al.*, 2012). GraphPad Prism was used to calculate the statistical significance at the 95% confidence level ($\alpha = 0.05$; $p < 0.05$) using the unpaired parametric t-test with Welch's correction. One-way ANOVA and Tukey's post-hoc test for multiple comparisons were also used.

SUPPLEMENTARY MATERIAL

Supplementary Table S1. List of oligonucleotides used

Oligonucleotides used for TurboID		
Name	**sense**	**sequence**
MNSV-CP-D/Mlu-Xma	Forward	aatctgagtttttctgattaacagatggcgatggttagacgcattaat
MNSV-CP-R/Mlu-Xma	Reverse	gaggcacagtattgtctttcccgggggcgaggtaggctgtttctggagag
ΔNt-CP-D/Mlu-Xma	Forward	aatctgagtttttctgattaacagatggtgaagatagttcatagggagttta
GlyRS-D/Mlu-Xma	Forward	aatctgagtttttctgattaacagatggccatcctccatttctctcttc
GlyRS-R/Mlu-Xma	Reverse	gaggcacagtattgtctttcccgggctggaggcgttgaatcgcttgttg
Oligonucleotides used for BiFC		
Name	**sense**	**sequence**
NbSIK-D(Nco)	Forward	gcatccatggaatttcgtccctcgtc
NbSIK-R(Nhe)-STOP	Reverse	gcatgctagcctaatgaaatttatttacct
NbSIK-R(Nhe)-NO-STOP	Reverse	gcatgctagcatgaaatttatttacctttt
NbSMU-D(Bsa+Nco)	Forward	acgtggtctcgcatgtcttcctccaaacggaa
NbSMU-R(Bsa+Nhe)-STOP	Reverse	catgggtctcgctagcttatacacgcagcttctttc
NbSMU-R(Bsa+Nhe)-NO-STOP	Reverse	catgggtctcgctagctacacgcagcttctttcc
NbMAP3K-D(Bsa+Nco)	Forward	acgtggtctcgcatgtctaggcaaatggcaaa
NbMAP3K-R(Bsa+Nhe)-STOP	Reverse	catgggtctcgctagttacaaaactgtgtttatat
NbMAP3K-R(Bsa+Nhe)-NO-STOP	Reverse	catgggtctcgctagccaaaactgtgtttatatg
Host proteins silencing by VIGS		

Name	sense	sequence
attB1-NbSIK1	Forward	ggggacaagtttgtacaaaaaagcaggcttcggaagatccttcaactaagt
attB2-NbSIK1	Reverse	ggggaccactttgtacaagaaagctgggtggcttcatctgtgacattcat
attB1-NbSMU2	Forward	ggggacaagtttgtacaaaaaagcaggcttcaatggatatgatgctatgca
attB2-NbSMU2	Reverse	ggggaccactttgtacaagaaagctgggtgaccaggatagcactcagaat
attB1-NbMAP3K	Forward	ggggacaagtttgtacaaaaaagcaggcttcgaatttgaaccacaaaaaca
attB2-NbMAP3K	Reverse	ggggaccactttgtacaagaaagctgggtggcctctgtcaactttgttgc
attB1-NbEDR1	Forward	ggggacaagtttgtacaaaaaagcaggcttctactccagaaattggtgatg
NbEDR1-X1-R	Reverse	tagcacccataaaacacctgccccttctt
NbEDR1-X1-D	Forward	aagaaggggcaggtgttttatgggtgcta
attB2-NbEDR1	Reverse	ggggaccactttgtacaagaaagctgggtgctgtcgatttggatgacaaa
attB1-NbKIN7	Forward	ggggacaagtttgtacaaaaaagcaggcttcaacgcagacacttctgatga
attB2-NbKIN7	Reverse	ggggaccactttgtacaagaaagctgggtgagtctcctggtccaaaaggt
attB1-NbUPL4	Forward	ggggacaagtttgtacaaaaaagcaggcttctggaaactcggagccggaag
attB2-NbUPL4	Reverse	ggggaccactttgtacaagaaagctgggtgattattatctttatcggaac
attB1-NbDUF724	Forward	ggggacaagtttgtacaaaaaagcaggcttcgaacggatttgatgttattc
attB2-NbDUF724	Reverse	ggggaccactttgtacaagaaagctgggtgcgaattttgccacatatggc
attB1-NbC1	Forward	ggggacaagtttgtacaaaaaagcaggcttctgatgctccacgtcttaatt
attB2-NbC1	Reverse	ggggaccactttgtacaagaaagctgggtgcatggatataggcattttac
Oligonucleotides used for RT-qPCR		
Name	**sense**	**sequence**
NbSIK1-qPCR-D	Forward	agttaaaagtgaaggcgtggg
NbSIK1-qPCR-R	Reverse	ccctgtggcctcaatgtagt
NbSMU2-qPCR-D	Forward	agaaactgtgcctcaatctgc
NbSMU2-qPCR-R	Reverse	tgacccatatctccagcagg
NbMAP3K-qPCR-D	Forward	tccctcttctgcatgcatct
NbMAP3K-qPCR-R	Reverse	caactttcttggtggcagct

Access to Supplementary Table 2:

https://docs.google.com/spreadsheets/d/1BDSRM7visjRRpG7ZSPWsBJF06cHn6gm2/edit?usp=sharing&ouid=117083687904204348341&rtpof=true&sd=true

Acces to Supplementary Table 3:

https://docs.google.com/spreadsheets/d/1EEewKHWYHeakPUWDcwPnR4UF_dhwdwz9/edit?usp=sharing&ouid=117083687904204348341&rtpof=true&sd=true

Supplementary Table 4. Results of Bimolecular fluorescence complementation assays

	NbSMU2 – /+		
Nt-NtSMU2	Ct-NbSMU2	NbSMU2-Nt	NbSMU2-Ct

– $C_{Ct[GFP]}P$	– $C_{Nt[GFP]}P$	– $C_{Ct[GFP]}P$	– $C_{Nt[GFP]}P$
+ ΔNtCP-Ct[GFP]	+ ΔNtCP-Nt[GFP]	– ΔNtCP-Ct[GFP]	– ΔNtCP-Nt[GFP]
+ Ct[GFP]-ΔNtCP	– Nt[GFP]-ΔNtCP	– Ct[GFP]-ΔNtCP	– Nt[GFP]-ΔNtCP
– AtE3-Ct[GFP]	– AtE3-Nt[GFP]	– AtE3-Ct[GFP]	– AtE3-Nt[GFP]
NbSIK1 – /+			
Nt-NtSIK1	Ct-NbSIK1	NbSIK1-Nt	NbSIK1-Ct
– $C_{Ct[GFP]}P$	– $C_{Nt[GFP]}P$	– $C_{Ct[GFP]}P$	– $C_{Nt[GFP]}P$
– ΔNtCP-Ct[GFP]	– ΔNtCP-Nt[GFP]	– ΔNtCP-Ct[GFP]	– ΔNtCP-Nt[GFP]
– Ct[GFP]-ΔNtCP	– Nt[GFP]-ΔNtCP	– Ct[GFP]-ΔNtCP	– Nt[GFP]-ΔNtCP
– AtE3-Ct[GFP]	– AtE3-Nt[GFP]	– AtE3-Ct[GFP]	– AtE3-Nt[GFP]
NbMAP3K – /+			
	Ct-NbMAP3K	NbMAP3K-Nt	NbMAP3K-Ct
	– $C_{Nt[GFP]}P$	– $C_{Ct[GFP]}P$	– $C_{Nt[GFP]}P$
	– ΔNtCP-Nt[GFP]	+ ΔNtCP-Ct[GFP]	– ΔNtCP-Nt[GFP]
	– Nt[GFP]-ΔNtCP	– Ct[GFP]-ΔNtCP	– Nt[GFP]-ΔNtCP
	– AtE3-Nt[GFP]	– AtE3-Ct[GFP]	– AtE3-Nt[GFP]

General discussion

GENERAL DISCUSSION

In a general way, all results presented in this thesis could be divided into two main parts, the description of the mechanisms that govern the dual targeting of the coat protein (CP) of melon necrotic spot virus (MNSV), and a study of the functional relevance of the CP transport and the final destination.

The description of the mechanisms that govern the CP dual targeting starts in *chapter I,* where its N-terminal end, formed by the R domain and the arm region, was showed to act as a dual transit peptide (dTP). The vast majority of the proteins dually targeted to mitochondrion matrix and chloroplast stroma have a single precursor with an ambiguous dual-targeting peptide (dTP) that exhibits intermediate characteristics from mitochondrial presequences (mTP) and chloroplasts targeting sequence (cTP) (Mitschke *et al.*, 2009). For instance, Thr-tRNA synthetases (ThrRS) proteins, which also are dually transported, have an ambiguous dTP, similar to the R domain and the arm regions of the MNSV CP. As stated in the introduction section, the R domain is enriched in arginines, lysines, prolines, and glutamines and can be split into two subdomains, R_1 and R_2. Deletion assays showed that the R_1 subdomain is an essential component, and the structure of the R_2 subdomain and the arm region is also required for mitochondrial and chloroplast dual transport but just acts as a spacer.

It is important to emphasize that the CP of MNSV has been previously reported to be more similar to that of tombusviruses than the gammacarmoviruses because of its primary sequence, the length of R and P domains, and its three-dimensional structure (Riviere *et al.*, 1989; Wada *et al.*, 2008). According to our studies with other tombusvirus CPs, together with that of CNV (Alam *et al.*, 2021), chloroplast and/or mitochondrial targeting could be a general rule among the CP of the tombusviruses. The organelle translocons involved in protein import are not homologous, but they operate mechanistically in a similar way (Peeters and Small, 2001). The first sorting event in this process is mediated by the early identification of the N-terminal targeting sequences by some families of receptors of the outer translocons, which are located on the outer membranes facing the cytoplasm. Due to its genome annotation availability and resources, functional and mechanistic studies of translocon receptors from both organelles have been mainly done for the model plant *Arabidopsis thaliana.* MNSV and

tombusviruses cannot infect Arabidopsis, making it extremely difficult to experimentally study the relationship between the CP organelle import and the viral infection. Nevertheless, *Nicotiana benthamiana* has emerged as an interesting tool for studying innate immunity and defensive signaling during host-microbe interactions because of its extreme vulnerability to numerous pathogens, including bacteria, fungi, and viruses such as MNSV. Therefore, taking advantage of the recent availability of the *N. benthamiana* genome and proteome, our first step was to characterize the essential elements of the mitochondrial and chloroplasts outer membrane translocases that we initially designed as, NbToc75-III, NbToc34, NbToc90, NbToc120, NbToc159A, NbToc159B, NbTic22-III for chloroplasts (Figure 1, top) and NbTom40, NbTom20-1, NbTom20-2, NbOm64 for mitochondria (Figure 1, bottom).

Chloroplast receptors of the outer membrane translocon (Toc) have been divided into two families, Toc34 family and Toc159 (Jarvis, 2008). In *A. thaliana*, both families present different isoforms (AtToc33/34 and AtToc90/120/132/159), resulting in at least some redundancy. Consequently, a severe phenotype was not visible in most of the corresponding single-knockout mutants, except for the strong albino plants of the *toc159* mutant. Nevertheless, this appears not to be an extensive feature for other plants. In *chapter II*, NbToc34 was characterized as the unique member of the Toc34 family, whose silencing caused a strong albino phenotype. For the Toc159 family, NbToc90, like AtToc90, lacks the A domain; meanwhile, AtToc120 and AtToc132 were represented in a unique protein NbToc120, which was more similar in size to AtToc159. Finally, two orthologs, NbToc159A, and NbToc159B, were found to define Toc159 phylogenetically. In Arabidopsis, double knockout mutant *toc120/132* showed an albino phenotype similar to *toc159*. However, the silencing of NbToc159A had no visible effect, while the silencing of NbToc159B only produced a pale phenotype. We had to silence NbToc120/159A/159B to obtain a variegated phenotype with green and albino areas. Therefore, the members of the *N. benthamiana* Toc159 family are functionally more redundant than those of Arabidopsis.

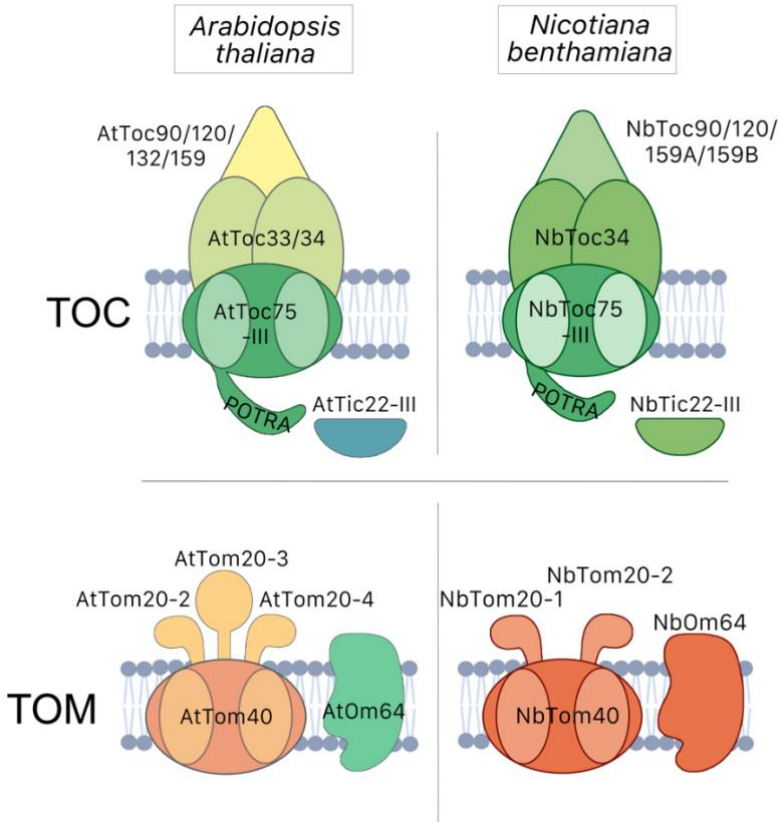

Figure 1. Schematic comparison of the core components of the Toc and Tom complexes in *A. thaliana* (left) and *N. benthamiana* (right). See text for details.

The first component of the chloroplast inner membrane translocon complex (Tic) to interact with the Toc-emerging transit peptide is the hydrophilic protein Tic22, which is found in the chloroplast intermembrane space (Kasmati *et al.*, 2013). Two isoforms were characterized for *A. thaliana,* AtTic22-III, and AtTic22-IV, similar to *N. benthamiana*. Nevertheless, NbTic22-III-silenced plants did not show any visual phenotype after silencing, which suggests a functional redundancy or a regulatory chaperone function rather than a pivotal role in Toc-Tic communication.

Regarding the receptors of the mitochondrial outer membrane translocon complex (Tom), two orthologs of the four-member AtTom20 family were found, NbTom20-1 and NbTom20-2 but only one for AtOm64, which was also phylogenetically distinct from AtToc64, NbOm64. Redundancy was also reported for Arabidopsis Tom complex receptors because embryo lethality was only caused by the quadruple mutant *attom20-2/-3/-4/atom64* (Lister *et al.*, 2007; Duncan *et al.*, 2013). In this sense, the four Tom20 genes in *A. thaliana* had similar expression patterns during development, with a minimal variation in the accumulation of

AtTom20-3 mRNA in roots and cotyledons. Our results also found that the NbTom20-2 and NbTom20-1/NbOm64 corresponding genes in *N. benthamiana* had a similar expression trend. However, individual silencing of these genes did not result in visible abnormalities, suggesting that the members of the Tom20 family and Om64 in both plant species are functionally redundant proteins.

In addition to the translocon receptor complex of both organelles, preproteins are mainly translocated through a pore, being Tom40 for mitochondria and Toc75 for chloroplasts. The null mutants of the pores in *A. thaliana* are embryo-lethal (Hust and Gutensohn, 2006; Hu *et al.*, 2019). Similarly, severe abnormalities were developed in *N. benthamiana* plants after silencing NbTom40 and NbToc75-III, showing no redundancy, the absence of other functional isoforms, and the crucial role of these pores for protein translocation.

Our findings also demonstrated that orthologs from *A. thaliana* and *N. benthamiana* presented identical fluorescence patterns when GFP fusions were localized within cells. Toc receptors and Tic22-III had dual localization in the cytoplasm and chloroplast envelope, while Toc75-III was mainly found on the chloroplast surface. Even though Tom40, Om64, and Tom20 are mitochondrial outer membrane proteins, they displayed a different fluorescence pattern, which is most likely a result of how each of them is associated with the outer membrane or how they reach the mitochondrial surface. These results are consistent with the notion that all proteins identified were functional components of the chloroplast and mitochondrion protein import system in *N. benthamiana*.

After performing the complete characterization of the core components of the mitochondria and chloroplast translocon complexes, we presented experimental evidence about the contribution of the general organellar protein import pathways to the subcellular localization of the MNSV CP. We identified the specific Tom/Toc import receptors interacting with this viral protein. NbToc159A, NbTic22-III, NbOm64, and NbTom20-2 were determined as interaction partners of the MNSV CP by BiFC and Y2H. Because *N. benthamiana* knockouts were unavailable, VIGS tool was employed to examine each receptor function in MNSV infection. For instance, NbToc159A silencing showed the most significant negative impact on viral accumulation, consistent with the interaction results. The NbToc159B and MNSV CP

interaction was detected only by BiFC, but we also noticed a detrimental effect on MNSV infection because of the NbToc159B silencing. Therefore, the NbToc159B involvement in the chloroplast import of the MNSV CP cannot be avoided. Unexpectedly, MNSV accumulation was unaffected by NbTic22-III silencing. However, we have previously demonstrated that AtTic22-IV, the redundant isoform of AtTic22-III, also exists in *N. benthamiana*. NbTic22-IV might supplement the role of NbTic22-III, while it is also plausible that Tic22 is not a necessary component for stromal protein targeting. In this sense, the double knockout from *A. thaliana* was functional but displayed a decreased import protein rate and photosynthetic activity. So, Tic22-III and Tic22-IV only could be necessary when high import rates are required (Rudolf *et al.*, 2013).

AtOm64 and AtTom20 isoforms were determined as Tom receptors in preprotein recognition. Moreover, significantly overlapping roles have been proposed for these proteins since one receptor can compensate for the loss of the other (Lister *et al.*, 2007). In *chapter III*, the functional redundancy for the *N. benthamiana* orthologues was also proposed. Although silencing of NbOm64 had the most significant negative influence on MNSV accumulation, the effect on viral titer reduction was not as larger as that of silencing NbToc159A. These results presumably indicate that functional compensation also occurs among Tom receptors in *N. benthamiana*. Nevertheless, silenced plants for NbTom20-1 and NbTom20-2 were also vulnerable to viral infection. Albeit, it has been demonstrated that Arabidopsis *tom20* mutant plants produced more Om64 protein (Lister *et al.*, 2007). Compensation for Tom20 receptors loss could also happen in *N. benthamiana,* where an Om64 level increase would facilitate MNSV CP transport to mitochondria.

Previous studies have determined AtToc34 and AtTom20 as central translocon receptors for *A. thaliana* (Ye *et al.*, 2012; Ye *et al.*, 2015; Woo *et al.*, 2022). Nevertheless, our results strongly suggest that MNSV CP hijacks the general import pathways for organellar protein transport for dual targeting to mitochondria and chloroplasts because of its interaction with NbOm64 and NbToc159A receptors. The differences between our findings in *N. benthamiana* and those reported in Arabidopsis, where AtToc34 and AtTom20 appear to play significant roles in dual targeting, could result from several variables. Previous research in Arabidopsis indicates that various Toc complexes are present in chloroplasts based on the innitial and simultaneous

identification of the transit peptides by the Toc159 and Toc34 families of receptors and the functional similarities of Toc33 and Toc34. In this regard, AtToc33/AtToc159 played a preferential role in the import of proteins involved in photosynthesis, whereas AtToc34/AtToc120/132 were linked to non-photosynthetic proteins. Although the NbToc34 and NbToc159 receptors can interact to generate other Toc complexes, they have to share the same Toc34 variant. In comparison to *A. thaliana* Toc complexes, they might be less effective at recognizing a particular subset of client preproteins. Additionally, after silencing each Toc159-related receptor in *N. benthamiana*, the phenotypes were significantly different from those of the corresponding Arabidopsis knockouts, including a higher level of functional redundancy. Each receptor in *N. benthamiana* differs from Arabidopsis regarding functional specialization, which may lead to various cargo sorting systems.

Preprotein recognition might not always occur similarly since two different models describe Toc receptor function. On the one hand, the *targeting model*, which MNSV CP may adopt, postulates that cytosolic Toc159 identifies the preprotein transit peptide through the G/A domains, generating a complex that associates with the outer envelope membrane by contact with the Toc34 G domain. Next, Toc75 receives the preprotein. On the other hand, the Toc34 membrane-associated protein serves as the transit peptide first point of contact in the *motor model*. Preproteins are then transported to Toc159, which stays permanently attached to the outer membrane and functions as a GTP-driven motor pushing preproteins through Toc75 (Jarvis, 2008). Therefore, Toc159 may occasionally act as the major receptor, whereas Toc34 may do so occasionally or in the presence of different preproteins. Our findings also imply that Om64 would recognize MNSV CP dual transit peptide through its interaction with Hsp70 and Hsp90 despite the redundant and overlapping functions of Om64 and Tom20 receptors (Nickel *et al.*, 2019). Then, the MNSV CP is passed to the Tom complex, which uses Tom40 pore to access the mitochondrion intermembrane space.

One proposed role for mitochondria and chloroplasts is to act as a source of signaling molecules, such as reactive oxygen species (ROS), proteins, RNA, and other metabolites, in retrograde communication with the nucleus triggering plant responses to environmental changes and adaptation. This signaling pathway is activated by the physiological and developmental states of these organelles and could be initiated by a pathogen infection

generating changes in nuclear expression and cell death (Reape *et al.*, 2015; Li *et al.*, 2016; Zhao *et al.*, 2016; Wang *et al.*, 2020). For this reason, both organelles have been reported to be targets for pathogenic effectors of fungi, bacteria, nematodes, and viruses, such as the CP of MNSV to control plant defense responses and retrograde signaling effectively (Petre *et al.*, 2015; Liu *et al.*, 2018). Knowing how these pathogen proteins hijack the plant import mechanisms to endosymbiotic organelles and identifying the specific host factors they use for that end will help to fight against them.

As shown in *chapter III*, silencing of NbToc40, NbToc75-III, or NbToc34 resulted in a general resistance against MNSV, CarMV, and TCV. Thus, our studies provide strong evidence for the significance of the mitochondrion and chloroplast physiological state in the defensive response. NbTom40 silencing could directly impact viral infection because these viruses replicate in mitochondria, which is morphologically changed after the membrane insertion of the virus-encoded auxiliary replicase (Blake *et al.*, 2007; Gómez-Aix *et al.*, 2015). Besides MNSV CP, no other viral protein of CarMV or TCV has been identified in chloroplasts, yet, both *NbToc75-III*- and *NbToc34*-silenced plants exhibited the same level of viral infection resistance. We have also demonstrated that NbToc34 silencing leads to a high increase in jasmonic acid (JA), an essential component of antiviral defense (Wu and Ye, 2020). Although other viral coat proteins have been shown to induce the accumulation of JA (Han *et al.*, 2020), the mechanism that relates JA production and organellar protein import disruption is unknown.

On the other side, different hypotheses for the functional relevance of the CP transport were raised in *chapter I*. The early proposed roles for the MNSV CP included RNA silencing suppression through siRNA sequestration, viral genome binding/encapsidation, and attachment to the transmission vector (Serra-Soriano *et al.*, 2017). Here, we also suggest that MNSV CP has a further role related with its organelle targeting in controlling the equilibrium between plant defense and virus counter-defense responses, which results in a compatible interaction (see significant statement in *chapter I*).

To avoid an excessive viral replication that could result in a very early plant defense response, some plant viruses suppress their genome translation, posttranslational modifications, and

degradation through host pathways to prevent the accumulation and/or function of essential viral effectors and persist in the host (Paudel and Sanfaçon, 2018). The MNSV CP was demonstrated to act as an RNA silencing suppressor (RSS) by siRNA sequestration through the R_2/arm region and inhibiting the spread of systemic silencing. Our results suggested that CP organelle targeting and processing will dismiss viral counter-defense. In this sense, we have demonstrated that p29 dose-dependent necrosis induction might directly correlate with high infection levels via antiviral RNA silencing suppression. Thus, with high amounts of CP in the cytoplasm, viral RSS activity is probably enhanced, promoting early p29 overaccumulation. Instead of increasing MNSV replication, this situation could amplify mitochondrial modification, accelerating and strengthening antiviral defense activation. Thus, CP targeting and processing could alleviate excessive RSS activity in green areas, and uncoated replicating genomes can be spread inside motile VRCs. Once viral replication reaches a certain threshold, organellar targeting of CP may be prevented. For instance, masking dTP through interactions with other CP molecules or various viral and host proteins leads to the accumulation of a subpopulation of unprocessed cytoplasmic CP suitable for RNA silencing suppression and genome encapsidation. Moreover, this strategy may facilitate horizontal transmission by interacting the vector fungus zoospores with the virions accumulated in roots. Indeed, it has been previously reported that RNA silencing occurs in melon roots which are vastly more infected than cotyledons or leaves (Gosalvez *et al.*, 2003; Herranz *et al.*, 2015).

Alternatively, the proteolytic processing of the MNSV CP after targeting mitochondria and chloroplasts could result in two CP-derived peptides, both unsuitable for RNA silencing suppression and genome encapsidation. The overaccumulation of the split R/arm region could be perceived as a signal molecule for danger, acting then as an elicitor. In contrast, the rest of the CP (S/P domains) could be considered an effector interfering with plant defense signaling starting in these organelles.

Whether MNSV CP organelle targeting function is beyond a self-attenuation mechanism not prematurely harming plant host or has a more direct implication interfering with the antiviral plant signaling initiated in mitochondria and chloroplasts needs further investigation. Therefore, a search for potential host factors that interact with the MNSV CP and its cytoplasmic mutant ΔNtCP was performed by biotin proximity labeling with TurboID ligase.

This methodology enables highly effective labeling in minutes and a higher range of operating temperatures (Xu *et al.*, 2023). In our initial hypothesis, we expected that a significant part of selected proteins was from mitochondria and chloroplast because of the early and fast targeting of the CP. However, the candidates obtained were mainly localized in the cytoplasm. The functional relevance of eight selected host factors under MNSV infection was determined by VIGS. NbSMU2, NbMAP3K, and NbSIK1 showed the most confident and repetitive detrimental effect on viral RNA accumulation. SMU2 is a RED domain protein that localizes in the nucleus and has been described to control the splicing of a particular set of pre-mRNAs in *C. elegans* and *A. thaliana* by forming a complex with SMU1 (Spartz *et al.*, 2004; Chung *et al.*, 2009; Ulrich *et al.*, 2016). NbSMU2 interaction with the CP was also studied by BiFC and localized inside the nucleus where the mRNA splicing regulation takes place. Besides, mRNA splicing acts as a pivotal gene regulation process in eukaryotes which is not widely studied under virus-plant interactions, nor when a pathogen causes splicing alterations (Boudreault *et al.*, 2019; Syed *et al.*, 2012; Reddy *et al.*, 2013). Nevertheless, alterations in alternative splicing of host transcripts have been observed in plants infected by bacteria, fungi, oomycetes, viruses, and viroids (Dinesh-Kumar and Baker, 2000; Nellist *et al.*, 2014; Mandadi and Scholthof, 2015; Liu *et al.*, 2016; Huang *et al.*, 2017; Jiang *et al.*, 2018). This finding suggests that altering splicing activity could represent a significant front in the conflict between pathogens and their hosts. Indeed, Du et al., 2020 discovered how mRNA splicing changes under a viral infection promote the synthesis of proviral factors, which preferentially accumulate supporting viral infection. In this line, CP might hijack NbSMU2 function on mRNA splicing with the same purpose, causing alternative splicing of host genes that could assist MNSV infection.

Pathogen-associated molecular pattern (PAMP) of *Pseudomonas syringae* sensing results in both early reactions, such as the generation of reactive oxygen species (ROS), ion fluxes across the plasma membrane, and activation of mitogen-activated protein kinase (MAPK) cascade, as well as delayed reactions, such the activation of genes related to defense. These immune responses boost a first line of defense known as PAMP-triggered immunity (PTI). There has been some recent indirect evidence for PTI-like responses against viral infection (Macho and Lozano-Duran, 2019; Teixeira *et al.,* 2019) Pathogens could evade PTI responses and interfere with plant defense by injecting or secreting a group of effectors into the host. For instance,

Bacterial flagellin 2 (flg22) is recognized by its main receptor FLAGELLIN-SENSITIVE 2 (FLS2), a leucine-rich repeat (LRR) receptor kinase, and a co-receptor BRASSINOSTEROID INSENSITIVE 1-ASSOCIATED KINASE 1 (BAK1) (Mithoe et al., 2016). SIK1 from *A. thaliana* has been characterized as a MAP4K involved in cell expansion and proliferation. It is also a crucial element of plant immune responses because it positively controls extracellular ROS and boosts PTI against bacterial pathogens. To strengthen the ROS burst, SIK1 directly phosphorylates RBOHD and associates with and stabilizes the major immunological regulator BIK1 (Zhang *et al.*, 2018). Moreover, the *sik1* mutant of *A. thaliana* has been described to have exacerbated levels of salicylic acid (SA). Therefore, a comparable SA priming might be happening in *NbSIK1*-silenced *N. benthamiana* plants enabling MNSV infection, as it has been similarly described in *chapter III* with *NbToc34*-silenced plants and jasmonic acid (JA) levels. NbSIK1 was not an ΔNtCP or CP positive BIFC interactor, but it might be considered an indirect interactor because of its interaction with NbMAP3K and its detection by TurboID PL.

Finally, *A. thaliana* MAP3K acts as negative regulator of FLS2 signaling, attenuating plant defense responses and immunity. MAP3K interacts with FLS2 attenuating MAPK cascade and PTI (Mithoe *et al.*, 2016). In this line, the absence of MAP3K negative regulator in *NbMAP3K*-silenced plants would entail PTI response development, ROS production, and MAPK cascade signaling, restricting MNSV infection development. In addition, MAP4K can phosphorylate MAP3K and is a hotspot and hub in MAPK and other signaling pathways due to their various subcellular locations (Mu *et al.*, 2022). AtSIK1 and AtMAP3K have been described as antagonistic for plant immunity; both act as positive and negative regulators of PTI, respectively. Moreover, Mithoe et al. suggested that MAP3K could compete with a positive regulator for FLS2 interaction. Thus, given the NbSIK1-NbMAP3K positive interaction by BiFC and their immunity roles, both proteins could compete for FLS2 interaction, resulting in positive or negative regulation of PTI.

In summary, the results obtained in this Thesis shed light on how a plant viral coat protein is dually targeted to two essential cell organelles, chloroplasts and mitochondria, and which could be the potential benefits from the pathogen side of this unusual scenario in the plant virus world. It is expected that in the future these results can facilitate the design of strategies that allow mitigating the harmful effects of viral infections in plants.

Conclusions

CONCLUSIONS

1. The MNSV CP is dually transported to chloroplast stroma and mitochondrial matrix due to the presence of a dual transit peptide in its N-terminal extreme, which embraces the R/arm domain and is cleaved after the import. The organelle localization should impact the viral cycle since the proteolytic cleavage could be considered, *a priori*, unhelpful for viral infection, as both genome binding during encapsidation and RNA silencing suppression (RSS) activity, which are dependent on the R/arm domain, are compromised.
2. An elevated RSS activity of the CP could result in enhanced viral replication, p29 overaccumulation, and increased VRC biogenesis that finally cause extensive alterations in mitochondria. This situation could enhance the initial plant defense response resulting in early necrosis development and viral systemic spreading inhibition. Thus, MNSV could moderate its replication and p29 accumulation by regulating CP RSS activity through organelle targeting and eluding early-triggered antiviral response.
3. A direct effect of the subcellular localization of the S/P domain in mitochondria and chloroplasts on plant defense response attenuation cannot be ruled out since its deletion resulted in a precarious balance between defense and counter-defense responses, generating either p29-cytopathic alteration and MNSV cell-to-cell movement restriction.
4. The receptors of the chloroplast outer membrane translocon in *Nicotiana benthamiana* were functionally classified into two families, NbToc34, with a single member, and NbToc159, with four members (NbToc90/120/159A/159B). Regarding the receptors of the mitochondrion outer membrane translocon in *N. benthamiana*, two NbTom20 isoforms (NbTom20-1 and NbTom20-2) and NbOm64 were characterized. Silencing phenotypes and relative expression analysis in different tissues revealed that, except for the Toc and Tom channel forming components (NbToc75 and NbTom40) and NbToc34, functional redundancy could be a rule either among the members of the Toc159 family or all mitochondrial receptors. Finally, heterodimer formation between NbToc34 and the NbToc159 family receptors was confirmed by two alternative techniques indicating that different Toc34/159 complexes could be assembled.

5. The MNSV CP subverts the general Toc and Tom protein import systems to reach mitochondria and chloroplasts. Interaction studies and viral infection assays in silenced plants revealed the significance of the mitochondrion NbOm64 and chloroplast NbToc159A plant receptors in the CP organelle transport.
6. Chloroplast protein translocation impairment in *NbToc34*-silenced plants could be interlinked with retrograde communication triggering a JA-based response that incidentally promotes viral resistance.
7. Using TurboID proximity labeling methodology, NbSIK1, NbSMU2, and NbMAP3K, among other host factors, were found to associate with the MNSV CP. All of them played a proviral role since their silencing had a detrimental effect on MNSV accumulation. On the one hand, the CP might hijack NbSMU2, an mRNA regulation protein, to cause alternative splicing of host genes to assist MNSV infection development. Remarkably, our findings support the participation of a mitogen-activated protein kinase cascade, modulated by positive and negative PTI regulators such as NbSIK1 and NbMAP3K, respectively, during MNSV infection.

References

REFERENCES

AbuQamar, S., Chen, X., Dhawan, R., Bluhm, B., Salmeron, J., Lam, S., Dietrich, R.A. and Mengiste, T. (2006) Expression profiling and mutant analysis reveals complex regulatory networks involved in Arabidopsis response to Botrytis infection. *Plant J.*, **48**, 28–44.

Adams, M.J., Lefkowitz, E.J., King, A.M.Q., et al. (2016) Ratification vote on taxonomic proposals to the International Committee on Taxonomy of Viruses. *Arch Virol*, **161**, 2921–2949.

Aken, O. van, Zhang, B., Law, S., Narsai, R. and Whelan, J. (2013) AtWRKY40 and AtWRKY63 modulate the expression of stress-responsive nuclear genes encoding mitochondrial and chloroplast proteins. *Plant Physiol*, **162**, 254–271.

Alam, S. B., Reade, R., Maghodia, A. B., Ghoshal, B., Theilmann, J., and Rochon, D.A. (2021) Targeting of cucumber necrosis virus coat protein to the chloroplast stroma attenuates host defense response. *Virology*, **554**, 106–119.

Alazem, M. and Lin, N.S. (2015) Roles of plant hormones in the regulation of host-virus interactions. *Mol Plant Pathol*, **16**, 529–540.

Alvarado-Marchena, L., Marquez-Molins, J., Martinez-Perez, M., Aparicio, F. and Pallás, V. (2021) Mapping of Functional Subdomains in the atALKBH9B m6A-Demethylase Required for Its Binding to the Viral RNA and to the Coat Protein of Alfalfa Mosaic Virus. *Front Plant Sci*, **12**, 1346.

Anderson, S.A., Satyanarayan, M.B., Wessendorf, R.L., Lu, Y., and Fernandez, D.E. (2021) A homolog of guided entry of tail-anchored proteins 3 functions in membrane-specific protein targeting in chloroplasts of Arabidopsis. *Plant Cell,* **33**, 2812–2833.

Andrès, C., Agne, B. and Kessler, F. (2010) The TOC complex: Preprotein gateway to the chloroplast. *Biochimica et Biophysica Acta (BBA) - Molecular Cell Research*, **1803**, 715–723.

Aparicio, F. and Pallás, V. (2017) The coat protein of Alfalfa mosaic virus interacts and interferes with the transcriptional activity of the bHLH transcription factor ILR3 promoting salicylic acid-dependent defence signalling response. *Mol Plant Pathol*, **18**, 173–186.

Aparicio, F., Vilar, M., Perez-Payá, E. and Pallás, V. (2003) The coat protein of prunus necrotic ringspot virus specifically binds to and regulates the conformation of its genomic RNA. *Virology*, **313**, 213–223.

Ascencio-Ibáñez, J.T., Sozzani, R., Lee, T.J., Chu, T.M., Wolfinger, R.D., Cella, R. and Hanley-Bowdoin, L. (2008) Global analysis of Arabidopsis gene expression uncovers a complex array of changes impacting pathogen response and cell cycle during geminivirus infection. *Plant Physiol*, **148**, 436–454.

Atkinson, N.J. and Urwin, P.E. (2012) The interaction of plant biotic and abiotic stresses: from genes to the field. *J Exp Bot*, **63**, 3523–3544.

Ayllón, M.A., Cambra, M., Llave, C. and Moriones, E. (2016) *Enfermedades de plantas causadas por virus y viroides*, Bubok Editorial.

Baebler, Š., Witek, K., Petek, M., et al. (2014) Salicylic acid is an indispensable component of the Ny-1 resistance-gene-mediated response against Potato virus Y infection in potato. *J Exp Bot*, **65**.

Baldwin, A., Wardle, A., Patel, R., Dudley, P., Park, S. K., Twell, D., et al. (2005) A molecular-genetic study of the Arabidopsis Toc75 gene family. *Plant Physiol.,* **138**, 715–733.

Balint-Kurti, P. (2019) The plant hypersensitive response: concepts, control and consequences. *Mol. Plant Pathol.*, **20**, 1163–1178.

Bally, J., Jung, H., Mortimer, C., Naim, F., Philips, J. G., Hellens, R., et al. (2018) The rise and rise of *Nicotiana benthamiana*: A plant for all reasons. *Annu. Rev. Phytopathol.,* **56**, 405–426.

Baquero-Perez, B., Geers, D. and Díez, J. (2021) From A to m6A: The emerging viral epitranscriptome. *Viruses*, **13**, 1049.

Bauer, J., Hiltbrunner, A., Weibel, P., Vidi, P.A., Alvarez-Huerta, M., Smith, M.D., et al. (2002) Essential role of the G-domain in targeting of the protein import receptor atToc159 to the chloroplast outer membrane. *J. Cell Biol.,* **159**, 845-854.

Bauer, M.F., Hofmann, S., Neupert, W. and Brunner, M. (2000) Protein translocation into mitochondria: the role of TIM complexes. *Trends Cell Biol*, **10**, 25–31.

Bausewein, T., Naveed, H., Liang, J. and Nussberger, S. (2020) The structure of the TOM core complex in the mitochondrial outer membrane. *Biol. Chem.*, **401**, 687–697.

Becker, T., Jelic, M., Vojta, A., Radunz, A., Soll, J., and Schleiff, E. (2004) Preprotein recognition by the Toc complex. *EMBO J.,* **23**, 520–530.

Benschop, J.J., Mohammed, S., O'Flaherty, M., Heck, A.J.R., Slijper, M. and Menke, F.L.H. (2007) Quantitative Phosphoproteomics of Early Elicitor Signaling in Arabidopsis. *Molecular & Cellular Proteomics*, **6**, 1198–1214.

Berardini, T.Z., Reiser, L., Li, D., Mezheritsky, Y., Muller, R., Strait, E., et al. (2015) The arabidopsis information resource: Making and mining the "gold standard" annotated reference plant genome. *Genesis,* **53**, 474–485.

Berglund, A.K., Pujol, C., Duchene, A.M. and Glaser, E. (2009) Defining the determinants for dual targeting of amino acyl-tRNA synthetases to mitochondria and chloroplasts. *J Mol Biol*, **393**, 803–814.

Berglund, A.K., Spånning, E., Biverståhl, H., Maddalo, G., Tellgren-Roth, C., Mäler, L. and Glaser, E. (2009) Dual targeting to mitochondria and chloroplasts: Characterization of Thr-tRNA synthetase targeting peptide. *Mol Plant*, **2**, 1298–1309.

Blake, J.A., Lee, K.W., Morris, T.J. and Elthon, T.E. (2007) Effects of turnip crinkle virus infection on the structure and function of mitochondria and expression of stress proteins in turnips. *Physiol Plant*, **129**, 698–706.

Blanco-Pérez, M., Pérez-Cañamás, M., Ruiz, L. and Hernández, C. (2016) Efficient Translation of Pelargonium line pattern virus RNAs Relies on a TED-Like 3´-Translational Enhancer that Communicates with the Corresponding 5´-Region through a Long-Distance RNA-RNA Interaction. *PLoS One*, **11**, e0152593.

Böhm, H., Albert, I., Fan, L., Reinhard, A. and Nürnberger, T. (2014) Immune receptor complexes at the plant cell surface. *Curr Opin Plant Biol*, **20**, 47–54.

Bol, J.F. (1999) Alfalfa mosaic virus and ilarviruses: Involvement of coat protein in multiple steps of the replication cycle. *Journal of General Virology*, **80**, 1089–1102.

Bol, J.F. (2008) Role of capsid proteins. *Methods in Molecular Biology*, **451**, 21–31.

Bouché, N., and Bouchez, D. (2001) Arabidopsis gene knockout: Phenotypes wanted. *Curr. Opin. Plant Biol.,* **4**, 111–117.

Boudreault, S., Roy, P., Lemay, G. and Bisaillon, M. (2019) Viral modulation of cellular RNA alternative splicing: A new key player in virus–host interactions? *Wiley Interdiscip Rev RNA*, **10**.

Boulila, M. (2011) Positive selection, molecular recombination structure and phylogenetic reconstruction of members of the family Tombusviridae: implication in virus taxonomy. *Genet Mol Biol*, **34**, 647–660.

Branon, T.C., Bosch, J.A., Sanchez, A.D., Udeshi, N.D., Svinkina, T., Carr, S.A., Feldman, J.L., Perrimon, N. and Ting, A.Y. (2018) Efficient proximity labeling in living cells and organisms with TurboID. *Nat Biotechnol*, **36**, 880–898.

Briesemeister, S., Rahnenführer, J. and Kohlbacher, O. (2010) YLoc—an interpretable web server for predicting subcellular localization. *Nucleic Acids Res.*, **38**, 497–502.

Brizard, J.P., Carapito, C., Delalande, F., Dorsselaer, A. Van and Brugidou, C. (2006) Proteome analysis of plant-virus interactome: comprehensive data for virus multiplication inside their hosts. *Mol Cell Proteomics*, **5**, 2279–2297.

Burgyán, J., Hornyik, C., Szittya, G., Silhavy, D. and Bisztray, G. (2000) The ORF1 products of tombusviruses play a crucial role in lethal necrosis of virus-infected plants. *J. Virol.*, **74**, 73–81.

Bykov, Y.S., Rapaport, D., Herrmann, J.M., and Schuldiner, M. (2020) Cytosolic events in the biogenesis of mitochondrial proteins. *Trends Biochem. Sci.,* **45**, 650–667.

Calil, I.P. and Fontes, E.P.B. (2017) Plant immunity against viruses: Antiviral immune receptors in focus. *Ann Bot*, **119**, 711–723.

Callaway, A., Giesman-Cookmeyer, D., Gillock, E.T., Sit, T.L. and Lommel, S.A. (2001) The multifunctional capsid proteins of plant RNA viruses. *Annu Rev Phytopathol*, **39**, 419–460.

Campbell, J.H., Hoang, T., Jelokhani-Niaraki, M. and Smith, M.D. (2014) Folding and self-association of atTic20 in lipid membranes: implications for understanding protein transport across the inner envelope membrane of chloroplasts. *BMC Biochem*, **15**, 1–13.

Canto, T., Uhrig, J.F., Swanson, M., Wright, K.M. and MacFarlane, S.A. (2006) Translocation of tomato bushy stunt virus P19 protein into the nucleus by ALY proteins compromises its silencing suppressor activity. *J. Virol.*, **80**, 9064–9072.

Caplan, J.L., Kumar, A.S., Park, E., Padmanabhan, M.S., Hoban, K., Modla, S., Czymmek, K. and Dinesh-Kumar, S.P. (2015) Chloroplast stromules function during innate immunity. *Dev. Cell*, **34**, 45–57.

Caplan, J.L., Mamillapalli, P., Burch-Smith, T.M., Czymmek, K. and Dinesh-Kumar, S.P. (2008) Chloroplastic protein NRIP1 mediates innate immune receptor recognition of a viral effector. *Cell*, **132**, 449–462.

Carli, M. Di, Villani, M.E., Bianco, L., Lombardi, R., Perrotta, G., Benvenuto, E. and Donini, M. (2010) Proteomic analysis of the plant-virus interaction in cucumber mosaic virus (CMV) resistant transgenic tomato. *J Proteome Res*, **9**, 5684–5697.

Carrie, C. and Small, I. (2013) A reevaluation of dual-targeting of proteins to mitochondria and chloroplasts. *Biochim Biophys Acta*, **1833**, 253–259.

Carrie, C., Giraud, E. and Whelan, J. (2009) Protein transport in organelles: Dual targeting of proteins to mitochondria and chloroplasts. *FEBS Journal*, **276**, 1187–1195.

Carrie, C., Murcha, M.W., and Whelan, J. (2010) An in silico analysis of the mitochondrial protein import apparatus of plants. *BMC Plant Biol.,* **10**, 1-15.

Caverzan, A., Passaia, G., Rosa, S.B., Ribeiro, C.W., Lazzarotto, F. and Margis-Pinheiro, M. (2012) Plant responses to stresses: Role of ascorbate peroxidase in the antioxidant protection. *Genet. Mol. Biol.*, **35**, 1011–1019.

Chaiwongsar, S., Strohm, A.K., Su, S.H. and Krysan, P.J. (2012) Genetic analysis of the Arabidopsis protein kinases MAP3Kε1 and MAP3Kε2 indicates roles in cell expansion and embryo development. *Front Plant Sci*, **3**, 228.

Chaudhary, A. and Yadav, R.D. (2019) A review on virus protein self-assembly. *J. Nanoparticle Res.*, **21**, 254.

Chen, Smith, Fitzpatrick and Schnell (2002) In vivo analysis of the role of atTic20 in protein import into chloroplasts. *Plant Cell*, **14**, 641–654.

Chen, Y.L., Chen, L.J., Chu, C.C., Huang, P.K., Wen, J.R. and Li, H. (2018) TIC236 links the outer and inner membrane translocons of the chloroplast. *Nature 2018 564:7734*, **564**, 125–129.

Chisholm, S.T., Parra, M.A., Anderberg, R.J. and Carrington, J.C. (2001) Arabidopsis RTM1 and RTM2 genes function in phloem to restrict long-distance movement of tobacco etch virus. *Plant Physiol*, **127**, 1667–1675.

Chiu, M.H., Chen, I.H., Baulcombe, D.C. and Tsai, C.H. (2010) The silencing suppressor P25 of Potato virus X interacts with Argonaute1 and mediates its degradation through the proteasome pathway. *Mol Plant Pathol*, **11**, 641–649.

Chung, T., Wang, D., Kim, C.S., Yadegari, R. and Larkins, B.A. (2009) Plant SMU-1 and SMU-2 Homologues Regulate Pre-mRNA Splicing and Multiple Aspects of Development. *Plant Physiol*, **151**, 1498–1512.

Constan, D., Patel, R., Keegstra, K. and Jarvis, P. (2004) An outer envelope membrane component of the plastid protein import apparatus plays an essential role in Arabidopsis. *Plant J.*, **38**, 93–106.

Cooley, M.B., Pathirana, S., Wu, H.J., Kachroo, P. and Klessig, D.F. (2000) Members of the Arabidopsis HRT/RPP8 family of resistance genes confer resistance to both viral and oomycete pathogens. *Plant Cell*, **12**, 663–676.

Creissen, G., Reynolds, H., Xue, Y. and Mullineaux, P. (1995) Simultaneous targeting of pea glutathione reductase and of a bacterial fusion protein to chloroplasts and mitochondria in transgenic tobacco. *Plant J*, **8**, 167–175.

Csorba, T., Kontra, L. and Burgyán, J. (2015) Viral silencing suppressors: Tools forged to fine-tune host-pathogen coexistence. *Virology*, **479–480**, 85–103.

Csorba, T., Pantaleo, V. and Burgyán, J. (2009) RNA silencing: an antiviral mechanism. *Adv Virus Res*, **75**, 35–71.

Dawson, W. 0. (1992) Tobamovirus-plant interactions. *Virology*, **186**, 359–367.

de Pinto, M.C., Locato, V. and Gara, L. (2012) Redox regulation in plant programmed cell death. *Plant. Cell Environ.*, **35**, 234–244.

Decroocq, V., Salvador, B., Sicard, O., Glasa, M., Cosson, P., Svanella-Dumas, L., Revers, F., Garcia, J.A. and Candresse, T. (2009) The determinant of potyvirus ability to overcome the RTM resistance of *Arabidopsis thaliana* maps to the N-terminal region of the coat protein. *Mol Plant Microbe Interact*, **22**, 1302–1311.

Dellaporta, S.L., Wood, J. and Hicks, J.B. (1983) A plant DNA minipreparation: Version II. *Plant Mol. Biol. Report.*, **1**, 19–21.

Díaz, J.A., Nieto, C., Moriones, E., Truniger, V. and Aranda, M.A. (2004) Molecular characterization of a Melon necrotic spot virus strain that overcomes the resistance in melon and nonhost plants. *Mol. Plant-Microbe Interact.*, **17**, 668–675.

Díaz, M.G., Hernández-Verdeja, T., Kremnev, D., Crawford, T., Dubreuil, C. and Strand, Å. (2018) Redox regulation of PEP activity during seedling establishment in *Arabidopsis thaliana*. *Nature Communications 2017 9:1*, **9**, 1–12.

Díez, J., Marcos, J.F. and Pallás, V. (1998) Carmovirus isolation and RNA extraction. *Methods Mol Biol*, **81**, 211–217.

Dinesh-Kumar, S.P. and Baker, B.J. (2000) Alternatively spliced N resistance gene transcripts: Their possible role in tobacco mosaic virus resistance. *Proc Natl Acad Sci U S A*, **97**, 1908–1913.

Ding, X., Jimenez-Gongora, T., Krenz, B. and Lozano-Duran, R. (2019) Chloroplast clustering around the nucleus is a general response to pathogen perception in *Nicotiana benthamiana*. *Mol Plant Pathol*, **20**, 1298–1306.

Dionne, U. and Gingras, A.C. (2022) Proximity-Dependent Biotinylation Approaches to Explore the Dynamic Compartmentalized Proteome. *Front Mol Biosci*, **9**.

Dominissini, D., Moshitch-Moshkovitz, S., Schwartz, S., et al. (2012) Topology of the human and mouse m6A RNA methylomes revealed by m6A-seq. *Nature*, **485**, 201–206.

Drozdetskiy, A., Cole, C., Procter, J. and Barton, G.J. (2015) JPred4: a protein secondary structure prediction server. *Nucleic Acids Res.*, **43**, 389–394.

Du, K., Jiang, T., Chen, H., Murphy, A.M., Carr, J.P., Du, Z., Li, X., Fan, Z. and Zhou, T. (2020) Viral Perturbation of Alternative Splicing of a Host Transcript Benefits Infection. *Plant Physiol*, **184**, 1514–1531.

Duchêne, A.M., Peeters, N., Dietrich, A., Cosset, A., Small, I.D. and Wintz, H. (2001) Overlapping destinations for two dual targeted glycyl-tRNA synthetases in *Arabidopsis thaliana* and Phaseolus vulgaris. *J. Biol. Chem.*, **276**, 15275–15283.

Duhart, J.C. and Raftery, L.A. (2020) Mob Family Proteins: Regulatory Partners in Hippo and Hippo-Like Intracellular Signaling Pathways. *Front Cell Dev Biol*, **8**, 161.

Duncan, O., Murcha, M. W., and Whelan, J. (2013) Unique components of the plant mitochondrial protein import apparatus. *Biochim. Biophys. Acta Mol. Cel. Res.,* **1833**, 304–313.

Duncan, O., Murcha, M.W. and Whelan, J. (2013) Unique components of the plant mitochondrial protein import apparatus. *Biochimica et Biophysica Acta (BBA) - Molecular Cell Research*, **1833**, 304–313.

Dutta, S., Teresinski, H.J., and Smith, M.D. (2014) A split-ubiquitin yeast two-hybrid screen to examine the substrate specificity of atToc159 and atToc132, two arabidopsis chloroplast preprotein import receptors. *PLoS ONE,* **9**, e95026.

Eckart, K., Eichacker, L., Sohrt, K., Schleiff, E., Heins, L., and Soll, J. (2002) A Toc75-like protein import channel is abundant in chloroplasts. *EMBO Rep.,* **3**, 557–562.

Elena, S.F., Fraile, A. and García-Arenal, F. (2014) Evolution and emergence of plant viruses. In *Advances in Virus Research*. Academic Press Inc., pp. 161–191.

Espinosa-Cantú, A., Cruz-Bonilla, E., Noda-Garcia, L. and DeLuna, A. (2020) Multiple Forms of Multifunctional Proteins in Health and Disease. *Front Cell Dev Biol*, **8**, 451.

Estavillo, G.M., Crisp, P.A., Pornsiriwong, W., et al. (2011) Evidence for a SAL1-PAP Chloroplast Retrograde Pathway That Functions in Drought and High Light Signaling in Arabidopsis. *Plant Cell*, **23**, 3992–4012.

Exposito-Rodriguez, M., Laissue, P.P., Yvon-Durocher, G., Smirnoff, N. and Mullineaux, P.M. (2017) Photosynthesis-dependent H2O2 transfer from chloroplasts to nuclei provides a high-light signalling mechanism. *Nature Communications 2017 8:1*, **8**, 1–11.

Farkas, Á., de Laurentiis, E. I., and Schwappach, B. (2019) The natural history of Get3-like chaperones. *Traffic,* **20**, 311–324.

Fatihi, A., Latimer, S., Schmollinger, S., Block, A., Dussault, P.H., Vermaas, W.F.J., Merchant, S.S. and Basset, G.J. (2015) A Dedicated Type II NADPH Dehydrogenase Performs the Penultimate Step in the Biosynthesis of Vitamin K1 in Synechocystis and Arabidopsis. *Plant Cell*, **27**, 1730–1741.

Feng, C., Roitinger, E., Hudecz, O., et al. (2023) TurboID-based proteomic profiling of meiotic chromosome axes in Arabidopsis thaliana. *Nat Plants*, **9**, 616-630.

Fernández-Crespo, E., Navarro, J.A., Serra-Soriano, M., Finiti, I., García-Agustín, P., Pallás, V. and González-Bosch, C. (2017) Hexanoic acid treatment prevents systemic MNSV movement in Cucumis melo plants by priming callose deposition correlating SA and OPDA accumulation. *Front. Plant Sci.*, **8**, 1793.

Fernandez-Pozo, N., Rosli, H.G., Martin, G.B., and Mueller, L.A. (2015) The SGN VIGS tool: User-Friendly software to design virus-induced gene silencing (VIGS) constructs for functional genomics. *Mol. Plant,* **8**, 486–488.

Fields, S., and Song, O. (1989) A novel genetic system to detect protein-protein interactions. *Nature,* **340**, 245–246.

Fister, A.S., Mejia, L.C., Zhang, Y., Herre, E.A., Maximova, S.N. and Guiltinan, M.J. (2016) Theobroma cacao L. pathogenesis-related gene tandem array members show diverse expression dynamics in response to pathogen colonization. *BMC Genomics*, **17**, 363.

Flores-Pérez, Ú., and Jarvis, P. (2013) Molecular chaperone involvement in chloroplast protein import. *Biochim. Biophys. Acta Mol. Cel. Res.,* **1833**, 332–340.

Forcat, S., Bennett, M.H., Mansfield, J.W. and Grant, M.R. (2008) A rapid and robust method for simultaneously measuring changes in the phytohormones ABA, JA and SA in plants following biotic and abiotic stress. *Plant Methods*, **4**, 16.

Fournier, G., Chiang, C., Munier, S., Tomoiu, A., Demeret, C., Vidalain, P.O., Jacob, Y. and Naffakh, N. (2014) Recruitment of RED-SMU1 Complex by Influenza A Virus RNA Polymerase to Control Viral mRNA Splicing. *PLoS Pathog*, **10**, e1004164.

Freed, E.O. (2004) HIV-1 and the host cell: An intimate association. *Trends Microbiol*, **12**, 170–177.

Fujita, Y., Fujita, M., Yamaguchi-Shinozaki, K. and Director, K. (2009) Transcription factors involved in the crosstalk between abiotic and biotic stress-signaling networks. In K. Yoshioka and K. Shinozaki, eds. *Signal crosstalk in plant stress responses*. Hoboken: Wiley-Blackwell, pp. 43–58.

Fukao, Y. (2012) Protein-protein interactions in plants. *Plant Cell Physiol*, **53**, 617–625.

Garcia-Ruiz, H. (2019) Host factors against plant viruses. *Mol Plant Pathol*, **20**, 1588–1601.

García, J.A. and Pallás, V. (2015) Viral factors involved in plant pathogenesis. *Curr Opin Virol*, **11**, 21–30.

Gautier, R., Douguet, D., Antonny, B. and Drin, G. (2008) HELIQUEST: a web server to screen sequences with specific alpha-helical properties. *Bioinformatics*, **24**, 2101–2102.

Ge, C., Spånning, E., Glaser, E. and Wieslander, Å. (2014) Import determinants of organelle-specific and dual targeting peptides of mitochondria and chloroplasts in arabidopsis thaliana. *Mol. Plant*, **7**, 121–136.

Genovés, A., Navarro, J.A. and Pallás, V. (2006) Functional analysis of the five Melon necrotic spot virus genome-encoded proteins. *J Gen Virol*, **87**, 2371–2380.

Genovés, A., Navarro, J.A. and Pallás, V. (2009) A self-interacting carmovirus movement protein plays a role in binding of viral RNA during the cell-to-cell movement and shows an actin cytoskeleton dependent location in cell periphery. *Virology*, **395**, 133–142.

Genovés, A., Navarro, J.A. and Pallas, V. (2010) The Intra- and Intercellular Movement of Melon necrotic spot virus (MNSV) Depends on an Active Secretory Pathway. *Mol Plant Microbe Interact*, **23**, 263–272.

Ghifari, A.S., Gill-Hille, M., and Murcha, M.W. (2018) Plant mitochondrial protein import: the ins and outs. *Biochem. J.,* **475**, 2191–2208.

Ghoshal, K., Theilmann, J., Reade, R., Maghodia, A. and Rochon, D. (2015) Encapsidation of host RNAs by cucumber necrosis virus coat protein during both agroinfiltration and infection. *J. Virol.*, **89**, 10748–10761.

Gietz, R.D. and Woods, R.A. (2002) Transformation of yeast by lithium acetate/single-stranded carrier DNA/polyethylene glycol method. *Methods Enzymol.*, **350**, 87–96.

Giraud, E., Aken, O. van, Ho, L.H.M. and Whelan, J. (2009) The transcription factor ABI4 is a regulator of mitochondrial retrograde expression of ALTERNATIVE OXIDASE1a. *Plant Physiol*, **150**, 1286–1296.

Glingston, R.S., Deb, R., Kumar, S. and Nagotu, S. (2019) Organelle dynamics and viral infections: at cross roads. *Microbes Infect*, **21**, 20–32.

Gomez-Aix, C., García-García, M., Aranda, M.A. and Sanchez-Pina, M.A. (2015) Melon necrotic spot virus replication occurs in association with altered mitochondria. *Mol Plant-Microbe Interact*, **28**, 387–397.

Gómez-Aix, C., Pascual, L., Cañizares, J., Sánchez-Pina, M.A. and Aranda, M.A. (2016) Transcriptomic profiling of Melon necrotic spot virus-infected melon plants revealed virus strain and plant cultivar-specific alterations. *BMC Genomics*, **17**, 429.

Gopalan, S., Wei, W. and He, S.Y. (1996) hrp gene-dependent induction of hin1: A plant gene activated rapidly by both harpins and the avrPto gene-mediated signal. *Plant J.*, **10**, 591–600.

Gosalvez-Bernal, B., Genoves, A., Navarro, J.A., Pallas, V. and Sanchez-Pina, M.A. (2008) Distribution and pathway for phloem-dependent movement of Melon necrotic spot virus in melon plants. *Mol. Plant Pathol.*, **9**, 447–461.

Gosalvez, B., Navarro, J.A., Lorca, A., Botella, F., Sánchez-Pina, M.A. and Pallás, V. (2003) Detection of Melon necrotic spot virus in water samples and melon plants by molecular methods. In *Journal of Virological Methods*. pp. 87–93.

Grangeon, R., Agbeci, M., Chen, J., Grondin, G., Zheng, H. and Laliberté, J.-F. (2012) Impact on the endoplasmic reticulum and Golgi apparatus of turnip mosaic virus infection. *J Virol*, **86**, 9255–9265.

Gross, L.E., Spies, N., Simm, S., and Schleiff, E. (2020) Toc75-V/OEP80 is processed during translocation into chloroplasts, and the membrane-embedded form exposes its POTRA domain to the intermembrane space. *FEBS Open Bio.,* **10**, 444–454.

Gupta, A., and Becker, T. (2021) Mechanisms and pathways of mitochondrial outer membrane protein biogenesis. *Biochim. Biophys. Acta Bioenerg.,* **1862**, 148323.

Gutensohn, M., Schulz, B., Nicolay, P. and Flügge, U.I. (2000) Functional analysis of the two Arabidopsis homologues of Toc34, a component of the chloroplast protein import apparatus. *Plant J*, **23**, 771–783.

Hafrén, A., Macia, J.L., Love, A.J., Milner, J.J., Drucker, M. and Hofius, D. (2017) Selective autophagy limits cauliflower mosaic virus infection by NBR1-mediated targeting of viral capsid protein and particles. *Proc Natl Acad Sci U S A*, **114**, E2026–E2035.

Hafrén, A., Üstün, S., Hochmuth, A., Svenning, S., Johansen, T. and Hofius, D. (2018) Turnip Mosaic Virus Counteracts Selective Autophagy of the Viral Silencing Suppressor HCpro. *Plant Physiol*, **176**, 649–662.

Han, K., Huang, H., Zheng, H., et al. (2020) Rice stripe virus coat protein induces the accumulation of jasmonic acid, activating plant defence against the virus while also attracting its vector to feed. *Mol Plant Pathol*, **21**, 1647–1653.

Hanley-Bowdoin, L., Bejarano, E.R., Robertson, D. and Mansoor, S. (2013) Geminiviruses: masters at redirecting and reprogramming plant processes. *Nat Rev Microbiol*, **11**, 777–788.

Hanson, M.R. and Hines, K.M. (2018) Stromules: Probing formation and function. *Plant Physiol.*, **176**, 128–137.

Hao, X., Lu, A., Sokal, N., et al. (2011) Cucumber necrosis virus p20 is a viral suppressor of RNA silencing. *Virus Res.*, **155**, 423–432.

He, H., Ge, L., Li, Z., Zhou, X. and Li, F. (2023) Pepino mosaic virus antagonizes plant m6A modification by promoting the autophagic degradation of the m6A writer HAKAI. *aBIOTECH 2023*, 1–14.

Heath, M.C. (2000) Hypersensitive response-related death. *Plant Mol. Biol.*, **44**, 321–334.

Heijne, G. von and Nishikawa, K. (1991) Chloroplast transit peptides. The perfect random coil? *FEBS Lett*, **278**, 1–3.

Hernández, J.A., Gullner, G., Clemente-Moreno, M.J., Künstler, A., Juhász, C., Díaz-Vivancos, P. and Király, L. (2016) Oxidative stress and antioxidative responses in plant–virus interactions. *Physiol. Mol. Plant Pathol.*, **94**, 134–148.

Herranz, M.C., Navarro, J.A., Sommen, E. and Pallas, V. (2015) Comparative analysis among the small RNA populations of source, sink and conductive tissues in two different plant-virus pathosystems. *BMC Genomics*, **16**, 117.

Hiltbrunner, A., Bauer, J., Vidi, P.A., Infanger, S., Weibel, P., Hohwy, M. and Kessler, F. (2001) Targeting of an abundant cytosolic form of the protein import receptor at Toc159 to the outer chloroplast membrane. *J Cell Biol*, **154**, 309–316.

Hinnah, S. C., Wagner, R., Sveshnikova, N., Harrer, R., and Soll, J. (2002) The chloroplast protein import channel Toc75: Pore properties and interaction with transit peptides. *Biophys. J.,* **83**, 899–911.

Hirabayashi, Y., Kikuchi, S., Oishi, M. and Nakai, M. (2011) In vivo studies on the roles of two closely related Arabidopsis Tic20 proteins, AtTic20-I and AtTic20-IV. *Plant Cell Physiol*, **52**, 469–478.

Horton, P., Park, K.-J., Obayashi, T., Fujita, N., Harada, H., Adams-Collier, C.J. and Nakai, K. (2007) WoLF PSORT: protein localization predictor. *Nucleic Acids Res.*, **35**, 585–587.

Hsu, T.H. and Spindler, K.R. (2012) Identifying host factors that regulate viral infection. *PLoS Pathog*, **8**, 3.

Hu, Ying, Zou, W., Wang, Z., Zhang, Y., Hu, Yuanyuan, Qian, J., Wu, X., Ren, Y. and Zhao, J. (2019) Translocase of the outer mitochondrial membrane 40 is required for mitochondrial biogenesis and embryo development in arabidopsis. *Front Plant Sci*, **10**, 389.

Huang, J., Gu, L., Zhang, Y., et al. (2017) An oomycete plant pathogen reprograms host pre-mRNA splicing to subvert immunity. *Nature Communications 2017 8:1*, **8**, 1–15.

Huang, J., Hack, E., Thornburg, R.W. and Myers, A.M. (1990) A yeast mitochondrial leader peptide functions in vivo as a dual targeting signal for both chloroplasts and mitochondria. *Plant Cell*, **2**, 1249–1260.

Huang, S., Aken, O. van, Schwarzländer, M., Belt, K. and Millar, A.H. (2016) The Roles of Mitochondrial Reactive Oxygen Species in Cellular Signaling and Stress Response in Plants. *Plant Physiol*, **171**, 1551–1559.

Huh, S.U., Kim, M.J. and Paek, K.H. (2013) Arabidopsis Pumilio protein APUM5 suppresses Cucumber mosaic virus infection via direct binding of viral RNAs. *Proc Natl Acad Sci U S A*, **110**, 779–784.

Huh, S.U., Kim, M.J., Ham, B.K. and Paek, K.H. (2011) A zinc finger protein Tsip1 controls Cucumber mosaic virus infection by interacting with the replication complex on vacuolar membranes of the tobacco plant. *New Phytol*, **191**, 746–762.

Hui, E., Xiang, Y. and Rochon, D. (2010) Distinct regions at the N-terminus of the cucumber necrosis virus coat protein target chloroplasts and mitochondria. *Virus Res.*, **153**, 8–19.

Hull, R. (2002) Induction of Disease 1: Virus Movement through the Plant and Effects on Plant Metabolism. In L. Academic Press, ed. *Matthew's Plant Virology*. Hull, R., pp. 373–436.

Humphries, A. D., Streimann, I. C., Stojanovski, D., Johnston, A. J., Yano, M., Hoogenraad, N. J., et al. (2005) Dissection of the mitochondrial import and assembly pathway for human Tom40. *J. Bio. Chem.,* **280**, 11535–11543.

Hust, B., and Gutensohn, M. (2006) Deletion of core components of the plastid protein import machinery causes differential arrest of embryo development in Arabidopsis thaliana. *Plant Biol.,* **8**, 18–30.

Hyodo, K. and Okuno, T. (2016) Pathogenesis mediated by proviral host factors involved in translation and replication of plant positive-strand RNA viruses. *Curr Opin Virol*, **17**, 11–18.

Hyodo, K. and Okuno, T. (2020) Hijacking of host cellular components as proviral factors by plant-infecting viruses. *Adv Virus Res*, **107**, 37–86.

Hyodo, K., Kaido, M. and Okuno, T. (2014) Traffic jam on the cellular secretory pathway generated by a replication protein from a plant RNA virus. *Plant Signal Behav*, **9**, e28644.

Hyodo, K., Taniguchi, T., Manabe, Y., Kaido, M., Mise, K., Sugawara, T., Taniguchi, H. and Okuno, T. (2015) Phosphatidic Acid Produced by Phospholipase D Promotes RNA Replication of a Plant RNA Virus. *PLoS Pathog*, **11**, 1–28.

Infanger, S., Bischof, S., Hiltbrunner, A., Agne, B., Baginsky, S. and Kessler, F. (2011) The Chloroplast Import Receptor Toc90 Partially Restores the Accumulation of Toc159 Client Proteins in the *Arabidopsis thaliana* ppi2 Mutant. *Mol Plant*, **4**, 252–263.

Ivanova, Y., Smith, M.D., Chen, K. and Schnell, D.J. (2004) Members of the Toc159 import receptor family represent distinct pathways for protein targeting to plastids. *Mol. Biol. Cell*, **15**.

Jäger, S., Cimermancic, P., Gulbahce, N., et al. (2011) Global landscape of HIV-human protein complexes. *Nature*, **481**, 365–370.

Jarvis, P. (2008) Targeting of nucleus-encoded proteins to chloroplasts in plants. *New Phytol*, **179**, 257–285.

Jarvis, P. and Soll, J. (2002) Erratum to: “Toc, Tic, and chloroplast protein import” [Biochim. Biophys. Acta 1541 (2001) 64–79]. *Biochimica et Biophysica Acta (BBA) - Molecular Cell Research*, **1590**, 177–189.

Jiang, J. and Laliberté, J.F. (2011) The genome-linked protein VPg of plant viruses-a protein with many partners. *Curr Opin Virol*, **1**, 347–354.

Jiang, J., Smith, H.N., Ren, D., Mudiyanselage, S.D.D., Dawe, A.L., Wang, L. and Wang, Y. (2018) Potato Spindle Tuber Viroid Modulates Its Replication through a Direct Interaction with a Splicing Regulator. *J Virol*, **92**, e01004-18.

Jin, X., Cao, X., Wang, X., Jiang, J., Wan, J., Laliberté, J.-F. and Zhang, Y. (2018) Three-dimensional architecture and biogenesis of membrane structures associated with plant virus replication. *Front. Plant Sci.*, **9**, 57.

Jones, J.D.G. and Dangl, J.L. (2006) The plant immune system. *Nature 2006 444:7117*, **444**, 323–329.

Ju, H.-J., Samuels, T.D., Wang, Y.-S., Blancaflor, E., Payton, M., Mitra, R., Krishnamurthy, K., Nelson, R.S. and Verchot-Lubicz, J. (2005) The potato virus X TGBp2 movement protein associates with endoplasmic reticulum-derived vesicles during virus infection. *Plant Physiol*, **138**, 1877–1895.

Kakani, K., Sgro, J.-Y. and Rochon, D. (2001) Identification of Specific Cucumber Necrosis Virus Coat Protein Amino Acids Affecting Fungus Transmission and Zoospore Attachment. *J Virol*, **75**, 5576–5583.

Kalderon, B. and Pines, O. (2014) Protein folding as a driving force for dual protein targeting in eukaryotes. *Front Mol Biosci*, **1**, 23.

Kamenski, P.A., Vinogradova, E.N., Krasheninnikov, I.A. and Tarassov, I.A. (2007) Directed import of macromolecules into mitochondria. *Mol Biol*, **41**, 187–202.

Karpenahalli, M. R., Lupas, A. N., and Söding, J. (2007) TPRpred: A tool for prediction of TPR-, PPR- and SEL1-like repeats from protein sequences. *BMC Bioinform.,* **8**, 1–8.

Kasmati, A.R., Töpel, M., Khan, N.Z., Patel, R., Ling, Q., Karim, S., Aronsson, H. and Jarvis, P. (2013) Evolutionary, molecular and genetic analyses of Tic22 homologues in *Arabidopsis thaliana* chloroplasts. *PLoS One*, **8**, e63863.

Kaul, S., Koo, H.L., Jenkins, J., et al. (2000) Analysis of the genome sequence of the flowering plant *Arabidopsis thaliana*. *Nature*, **408**, 796–815.

Kerppola, T.K. (2008) Bimolecular fluorescence complementation (BiFC) analysis as a probe of protein interactions in living cells. *Annu Rev Biophys*, **37**, 465.

Kikuchi, S., Oishi, M., Hirabayashi, Y., Lee, D.W., Hwang, I. and Nakai, M. (2009) A 1-megadalton translocation complex containing Tic20 and Tic21 mediates chloroplast protein import at the inner envelope membrane. *Plant Cell*, **21**, 1781–1797.

Kim, D.I. and Roux, K.J. (2016) Filling the Void: Proximity-Based Labeling of Proteins in Living Cells. *Trends Cell Biol*, **26**, 804–817.

Kim, D.I., Birendra, K.C., Zhu, W., Motamedchaboki, K., Doye, V. and Roux, K.J. (2014) Probing nuclear pore complex architecture with proximity-dependent biotinylation. *Proc Natl Acad Sci U S A*, **111**, E2453–E2461.

Kleine, T. and Leister, D. (2013) Retrograde signals galore. *Front Plant Sci*, **4**, 45.

Kleine, T. and Leister, D. (2016) Retrograde signaling: Organelles go networking. *Biochim Biophys Acta Bioenerg*, **1857**, 1313–1325.

Kmiec, B., Teixeira, P.F. and Glaser, E. (2014) Shredding the signal: Targeting peptide degradation in mitochondria and chloroplasts. *Trends Plant Sci.*, **19**, 771–778.

Knoester, M., va Loon, L.C., van den Heuvel, J., Hennig, J., Bol, J.F. and Linthorst, H.J.M. (1998) Ethylene-insensitive tobacco lacks nonhost resistance against soil-borne fungi. *Proc. Natl. Acad. Sci. U. S. A.*, **95**, 1933–1937.

Kobayashi, K. and Masuda, T. (2013) Spatial and temporal regulation of chloroplast development in arabidopsis root. In T. Kuang, C. Lu, and L. Zhang, eds. *Photosynthesis research for food, fuel and the future*. Berlin, Heidelberg: Springer, pp. 389–393.

Koch, C., Schuldiner, M., and Herrmann, J.M. (2021). ER-SURF: Riding the endoplasmic reticulum surface to mitochondria. *Int. J. Mol. Sci.,* **22**, 9655.

Köhler, R.H., Zipfel, W.R., Webb, W.W. and Hanson, M.R. (1997) The green fluorescent protein as a marker to visualize plant mitochondria in vivo. *Plant J.*, **11**, 613–621.

Kormelink, R.J.M. (2011) The Molecular Biology of Tospoviruses and Resistance Strategies. In A. Plyusnin and R. M. Elliot, eds. *Bunyaviridae: Molecular and Cellular Biology*. Caister Academic Press, pp. 163–191.

Kourelis, J., Kaschani, F., Grosse-Holz, F. M., Homma, F., Kaiser, M., and van der Hoorn, R.A.L. (2019) A homology-guided, genome-based proteome for improved proteomics in the alloploid *Nicotiana benthamiana*. *BMC Genom.,* **20**, 1–15.

Koussevitzky, S., Nott, A., Mockler, T.C., Hong, F., Sachetto-Martins, G., Surpin, M., Lim, J., Mittler, R. and Chory, J. (2007) Signals from Chloroplasts Converge to Regulate Nuclear Gene Expression. *Science (1979)*, **316**, 715–719.

Kovács-Bogdán, E., Benz, J.P., Soll, J. and Bölter, B. (2011) Tic20 forms a channel independent of Tic110 in chloroplasts. *BMC Plant Biol*, **11**, 1–16.

Krab, I.M., Caldwell, C., Gallie, D.R. and Bol, J.F. (2005) Coat protein enhances translational efficiency of Alfalfa mosaic virus RNAs and interacts with the eIF4G component of initiation factor eIF4F. *Journal of General Virology*, **86**, 1841–1849.

Krenz, B., Jeske, H. and Kleinow, T. (2012) The induction of stromule formation by a plant DNA-virus in epidermal leaf tissues suggests a novel intra- and intercellular macromolecular trafficking route. *Front. Plant Sci.*, **3**, 291.

Kubis, S., Patel, R., Combe, J., Bédard, J., Kovacheva, S., Lilley, K., et al. (2004) Functional specialization amongst the arabidopsis Toc159 Family of chloroplast protein import receptors. *Plant Cell,* **16**, 2059–2077.

Kunze, M., and Berger, J. (2015) The similarity between N-terminal targeting signals for protein import into different organelles and its evolutionary relevance. *Front. Physiol,* **6**, 259.

Laliberté, J.-F. and Sanfaçon, H. (2010) Cellular remodeling during plant virus infection. *Annu. Rev. Phytopathol.*, **48**, 69–91.

Laliberté, J.-F. and Zheng, H. (2014) Viral manipulation of plant host membranes. *Annu. Rev. Virol.*, **1**, 237–259.

Landeo-Ríos, Y., Navas-Castillo, J., Moriones, E. and Cañizares, M.C. (2016) The p22 RNA silencing suppressor of the crinivirus Tomato chlorosis virus preferentially binds long dsRNAs preventing them from cleavage. *Virology*, **488**, 129.

Langner, U., Baudisch, B. and Klösgen, R.B. (2014) Organelle import of proteins with dual targeting properties into mitochondria and chloroplasts takes place by the general import pathways. *Plant Signal Behav*, **9**, e29301.

Lee, D.W., Jung, C. and Hwang, I. (2013) Cytosolic events involved in chloroplast protein targeting. *Biochim Biophys Acta Mol Cell Res*, **1833**, 245–252.

Lee, S., Han, S., Jeong, A.L., Park, J.S. and Yang, Y. (2014) Depletion of IK causes mitotic arrest through aberrant regulation of mitotic kinases and phosphatases. *FEBS Lett*, **588**, 2844–2850.

Lee, S.C. and Luan, S. (2012) ABA signal transduction at the crossroad of biotic and abiotic stress responses. *Plant Cell Environ*, **35**, 53–60.

Li, H.M. and Chiu, C.C. (2010) Protein transport into chloroplasts. *Annu Rev Plant Biol*, **61**, 157–180.

Li, W., Xu, Y.P., Zhang, Z.X., Cao, W.Y., Li, F., Zhou, X., Chen, G.Y. and Cai, X.Z. (2012) Identification of genes required for nonhost resistance to Xanthomonas oryzae pv. oryzae reveals novel signaling components. *PLoS One*, **7**, e42796.

Li, Y., Cui, H., Cui, X. and Wang, A. (2016) The altered photosynthetic machinery during compatible virus infection. *Curr. Opin. Virol.*, **17**, 19–24.

Li, Z., Shi, J., Yu, L., Zhao, X., Ran, L., Hu, D. and Song, B. (2018) N 6 -methyl-adenosine level in *Nicotiana tabacum* is associated with tobacco mosaic virus. *Virol J*, **15**, 1–10

Lin, B. and Heaton, L.A. (1999) Mutational Analyses of the Putative Calcium Binding Site and Hinge of the Turnip Crinkle Virus Coat Protein. *Virology*, **259**, 34–42.

Lister, R., Carrie, C., Duncan, O., Ho, L.H.M., Howell, K.A., Murcha, M.W. and Whelan, J. (2007) Functional definition of outer membrane proteins involved in preprotein import into mitochondria. *Plant Cell*, **19**, 3739–3759.

Liu, D., Shi, L., Han, C., Yu, J., Li, D. and Zhang, Y. (2012) Validation of reference genes for gene expression studies in virus-infected *Nicotiana benthamiana* using quantitative real-time PCR. *PLoS One*, **7**, e46451.

Liu, H. and Jeffery, C.J. (2020) Moonlighting proteins in the fuzzy logic of cellular metabolism. *Molecules*, **25**, 3440.

Liu, Jiqin, Chen, X., Liang, X., Zhou, X., Yang, F., Liu, Jia, He, S.Y. and Guo, Z. (2016) Alternative Splicing of Rice WRKY62 and WRKY76 Transcription Factor Genes in Pathogen Defense. *Plant Physiol*, **171**, 1427–1442.

Liu, Jiqin, Chen, X., Liang, X., Zhou, X., Yang, F., Liu, Jia, He, S.Y. and Guo, Z. (2016) Alternative Splicing of Rice WRKY62 and WRKY76 Transcription Factor Genes in Pathogen Defense. *Plant Physiol*, **171**, 1427–1442.

Liu, Y., Lan, X., Song, S., Yin, L., Dry, I.B., Qu, J., Xiang, J. and Lu, J. (2018) In planta functional analysis and subcellular localization of the oomycete pathogen *Plasmopara viticola* candidate RXLR effector repertoire. *Front. Plant Sci.*, **9**, 286.

Liu, Y., Schiff, M. and Dinesh-Kumar, S.P. (2002) Virus-induced gene silencing in tomato. *Plant J.*, **31**, 777–786.

Liu, Y., Schiff, M., Marathe, R. and Dinesh-Kumar, S.P. (2002) Tobacco Rar1, EDS1 and NPR1/NIM1 like genes are required for N-mediated resistance to tobacco mosaic virus. *Plant J*, **30**, 415–429.

Loebenstein, G. (2009) Local Lesions and Induced Resistance. In Academic Press, pp. 73–117.

Loudya, N., Maffei, D.P.F., Bédard, J., Ali, S.M., Devlin, P.F., Jarvis, R.P. and López-Juez, E. (2022) Mutations in the chloroplast inner envelope protein TIC100 impair and repair chloroplast protein import and impact retrograde signalling. *Plant Cell*, **34**, 3028-3046.

Lough, T.J., Netzler, N.E., Emerson, S.J., Sutherland, P., Carr, F., Beck, D.L., Lucas, W.J. and Forster, R.L.S. (2007) Cell-to-Cell Movement of Potexviruses: Evidence for a Ribonucleoprotein Complex Involving the Coat Protein and First Triple Gene Block Protein. *Mol Plant Microbe Interact*, **13**, 962–974.

Lozano-Durán, R. (2016) Geminiviruses for biotechnology: the art of parasite taming. *New Phytologist*, **210**, 58–64.

Lozano-Durán, R., Rosas-Díaz, T., Gusmaroli, G., Luna, A.P., Taconnat, L., Deng, X.W. and Bejarano, E.R. (2011) Geminiviruses Subvert Ubiquitination by Altering CSN-Mediated Derubylation of SCF E3 Ligase Complexes and Inhibit Jasmonate Signaling in *Arabidopsis thaliana*. *Plant Cell*, **23**.

Lu, H., Zhou, Q., He, J., Jiang, Z., Peng, C., Tong, R. and Shi, J. (2020) Recent advances in the development of protein–protein interactions modulators: mechanisms and clinical trials. *Signal Transduct Target Ther*, **5**, 1–23.

Lung, S.C., and Chuong, S.D.X. (2012) A transit peptide-like sorting signal at the C terminus directs the bienertia sinuspersici preprotein receptor toc159 to the chloroplast outer membrane. *Plant Cell,* **24**, 1560–1578.

Luo, G.Z., Macqueen, A., Zheng, G., et al. (2014) Unique features of the m6A methylome in *Arabidopsis thaliana*. *Nat Commun*, **5**, 1–8.

Macasev, D., Newbigin, E., Whelan, J. and Lithgow, T. (2000) How Do Plant Mitochondria Avoid Importing Chloroplast Proteins? Components of the Import Apparatus Tom20 and Tom22 from Arabidopsis Differ from Their Fungal Counterparts. *Plant Physiol*, **123**, 811.

MacFarlane, S. and Popovich, A. (2000) Efficient expression of foreign proteins in roots from tobravirus vectors. *Virology*, **267**, 29–35.

Macho, A.P. and Lozano-Duran, R. (2019) Molecular dialogues between viruses and receptor-like kinases in plants. Mol. Plant Pathol. **20**, 1191–1195.

Maksymowych, R., Dollahon, N., di Cola, L.P. and Orkwiszewski, J.A.J. (1993) Chloroplasts in tissues of some herbaceous stems. *Acta Soc. Bot. Pol.*, **62**, 123–126.

Mandadi, K.K. and Scholthof, K.B.G. (2015) Genome-Wide Analysis of Alternative Splicing Landscapes Modulated during Plant-Virus Interactions in Brachypodium distachyon. *Plant Cell*, **27**, 71.

Marsh, M. and Helenius, A. (2006) Virus entry: open sesame. *Cell*, **124**, 729–740.

Martin, W.F., Garg, S. and Zimorski, V. (2015) Endosymbiotic theories for eukaryote origin. *Philosophical Transactions of the Royal Society B: Biological Sciences*, **370**, 20140330.

Martínez-Pérez, M., Aparicio, F., López-Gresa, M.P., Bellés, J.M., Sánchez-Navarro, J.A. and Pallás, V. (2017) Arabidopsis m6A demethylase activity modulates viral infection of a plant virus and the m6A abundance in its genomic RNAs. *Proc Natl Acad Sci U S A*, **114**, 10755–10760.

Martínez-Pérez, M., Gómez-Mena, C., Alvarado-Marchena, L., Nadi, R., Micol, J.L., Pallas, V. and Aparicio, F. (2021) The m6A RNA Demethylase ALKBH9B Plays a Critical Role for Vascular Movement of Alfalfa Mosaic Virus in Arabidopsis. *Front Microbiol*, **12**.

Martínez-Pérez, M., Navarro, J.A., Pallás, V. and Sánchez-Navarro, J.A. (2019) A sensitive and rapid RNA silencing suppressor activity assay based on alfalfa mosaic virus expression vector. *Virus Res.*, **272**, 197733.

Martínez-Turiño, S. and Hernández, C. (2009) Inhibition of RNA silencing by the coat protein of Pelargonium flower break virus: distinctions from closely related suppressors. *Journal of General Virology*, **90**, 519–525.

May, T., and Soll, J. (2000) 14-3-3 proteins form a guidance complex with chloroplast precursor proteins in plants. *Plant Cell,* **12**, 53–64.

McAlister, G.C., Huttlin, E.L., Haas, W., et al. (2012) Increasing the multiplexing capacity of TMTs using reporter ion isotopologues with isobaric masses. *Anal Chem*, **84**, 7469–7478.

McCartney, A.W., Greenwood, J.S., Fabian, M.R., White, K.A. and Mullen, R.T. (2005) Localization of the tomato bushy stunt virus replication protein p33 reveals a peroxisome-to-endoplasmic reticulum sorting pathway. *Plant Cell*, **17**, 3513–3531.

Medina-Puche, L. and Lozano-Duran, R. (2019) Tailoring the cell: a glimpse of how plant viruses manipulate their hosts. *Curr Opin Plant Biol*, **52**, 164–173.

Medina-Puche, L., Tan, H., Dogra, V., et al. (2020) A Defense Pathway Linking Plasma Membrane and Chloroplasts and Co-opted by Pathogens. *Cell*, **182**, 1109-1124.

Mehlhorn, D. G., Asseck, L. Y., and Grefen, C. (2021) Looking for a safe haven: tail-anchored proteins and their membrane insertion pathways. *Plant Physiol.,* **187**, 1916–1928.

Meyer, K.D., Saletore, Y., Zumbo, P., Elemento, O., Mason, C.E. and Jaffrey, S.R. (2012) Comprehensive Analysis of mRNA Methylation Reveals Enrichment in 3' UTRs and Near Stop Codons. *Cell*, **149**, 1635.

Mielecki, J., Gawroński, P. and Karpiński, S. (2020) Retrograde signaling: Understanding the communication between organelles. *Int J Mol Sci*, **21**, 1–24.

Miller, W.A. and Koev, G. (2000) Synthesis of subgenomic RNAs by positive-strand RNA viruses. *Virology*, **273**, 1–8.

Miras, M., Allen Miller, W., Truniger, V. and Aranda, M.A. (2017) Non-canonical translation in Plant RNA viruses. *Front Plant Sci*, **8**, 494.

Miras, M., Torre, C., Gómez-Aix, C., Hernando, Y. and Aranda, M.A. (2020) Development of monoclonal antibodies against melon necrotic spot virus and their use for virus detection. *J. Virol. Methods*, **278**, 113837.

Mithoe, S.C., Ludwig, C., Pel, M.J., et al. (2016) Attenuation of pattern recognition receptor signaling is mediated by a MAP kinase kinase kinase. *EMBO Rep*, **17**, 441–454.

Mitschke, J., Fuss, J., Blum, T., Höglund, A., Reski, R., Kohlbacher, O. and Rensing, S.A. (2009) Prediction of dual protein targeting to plant organelles. *New Phytol*, **183**, 224–236.

Miyazono, Y., Hirashima, S., Ishihara, N., Kusukawa, J., Nakamura, K.I. and Ohta, K. (2018) Uncoupled mitochondria quickly shorten along their long axis to form indented spheroids, instead of rings, in a fission-independent manner. *Sci. Rep.*, **8**, 1–14.

Mochizuki, T., Hirai, K., Kanda, A., Ohnishi, J., Ohki, T. and Tsuda, S. (2009) Induction of necrosis via mitochondrial targeting of Melon necrotic spot virus replication protein p29 by its second transmembrane domain. *Virology*, **390**, 239–249.

Mochizuki, T., Ohnishi, J., Ohki, T., Kanda, A. and Tsuda, S. (2008) Amino acid substitution in the coat protein of Melon necrotic spot virus causes loss of binding to the surface of *Olpidium bornocanus* zoospores. *Journal of General Plant Pathology*, **74**, 176–181.

Moffett, P. (2009) Mechanisms of Recognition in Dominant R Gene Mediated Resistance. *Adv Virus Res*, **75**, 1–229.

Moschou, P.N., Gutierrez-Beltran, E., Bozhkov, P. V. and Smertenko, A. (2016) Separase Promotes Microtubule Polymerization by Activating CENP-E-Related Kinesin Kin7. *Dev Cell*, **37**, 350–361.

Mu, J., Zhou, J., Gong, Q. and Xu, Q. (2022) An allosteric regulation mechanism of Arabidopsis Serine/Threonine kinase 1 (SIK1) through phosphorylation. *Comput Struct Biotechnol J*, **20**, 368–379.

Mur, L.A.J.J., Kenton, P., Lloyd, A.J., Ougham, H. and Prats, E. (2007) The hypersensitive response; the centenary is upon us but how much do we know? *J. Exp. Bot.*, **59**, 501–520.

Murcha, M. W., Kmiec, B., Kubiszewski-Jakubiak, S., Teixeira, P. F., Glaser, E., and Whelan, J. (2014) Protein import into plant mitochondria: signals, machinery, processing, and regulation. *J. Exp. Bot.,* **65**, 6301–6335.

Myers, S.A., Wright, J., Peckner, R., Kalish, B.T., Zhang, F. and Carr, S.A. (2018) Discovery of proteins associated with a predefined genomic locus via dCas9-APEX-mediated proximity labeling. *Nat Methods*, **15**, 437–439.

Nagy, P.D. (2016) Tombusvirus-host interactions: co-opted evolutionarily conserved host factors take center court. *Annu. Rev. Virol.*, **3**, 491–515.

Nagy, P.D. (2020) Exploitation of Host Factors and Cellular Pathways by Tombusviruses for the Biogenesis of the Viral Replication Organelles. *Proceedings*, **50**, 18.

Nakai, M. (2018) New Perspectives on Chloroplast Protein Import. *Plant Cell Physiol*, **59**, 1111–1119.

Navarro, J.A. and Pallás, V. (2017) An Update on the Intracellular and Intercellular Trafficking of Carmoviruses. *Front. Plant Sci*, **8**, 1801.

Navarro, J.A., Saiz-Bonilla, M., Sanchez-Navarro, J.A., and Pallas, V. (2021) The mitochondrial and chloroplast dual targeting of a multifunctional plant viral protein modulates chloroplast-to-nucleus communication, RNA silencing suppressor activity, encapsidation, pathogenesis and tissue tropism. *Plant J.,* **108**, 197–218.

Navarro, J.A., Sanchez-Navarro, J.A. and Pallas, V. (2019) Key checkpoints in the movement of plant viruses through the host. *Adv Virus Res*, **104**, 1–64.

Navarro, J.A., Serra-Soriano, M., Corachán-Valencia, L., and Pallás, V. (2020) A conserved motif in three viral movement proteins from different genera is required for host factor recruitment and cell-to-cell movement. *Sci. Rep.,* **10**, 1–15.

Nellist, C.F., Qian, W., Jenner, C.E., et al. (2014) Multiple copies of eukaryotic translation initiation factors in Brassica rapa facilitate redundancy, enabling diversification through variation in splicing and broad-spectrum virus resistance. *Plant J*, **77**, 261–268.

Neubauer, M., Serrano, I., Rodibaugh, N., Bhandari, D.D., Bautor, J., Parker, J.E. and Innes, R.W. (2020) Arabidopsis EDR1 Protein Kinase Regulates the Association of EDS1 and PAD4 to Inhibit Cell Death. *Mol Plant Microbe Interact*, **33**, 693.

Nickel, C., Horneff, R., Heermann, R., Neumann, B., Jung, K., Soll, J. and Schwenkert, S. (2019) Phosphorylation of the outer membrane mitochondrial protein OM64 influences protein import into mitochondria. *Mitochondrion*, **44**, 93–102.

Nott, A., Jung, H.-S., Koussevitzky, S. and Chory, J. (2006) Plastid-to-nucleus retrograde signaling. *Annu. Rev. Plant Biol.*, **57**, 739–759.

O'Neil, P.K., Richardson, L.G.L., Paila, Y.D., Piszczek, G., Chakravarthy, S., Noinaj, N., et al. (2017) The POTRA domains of Toc75 exhibit chaperone-like function to facilitate import into chloroplasts. *Proc. Natl. Acad. Sci. U. S. A.,* **114**, E4868–E4876.

Ohki, T., Akita, F., Mochizuki, T., Kanda, A., Sasaya, T. and Tsuda, S. (2010) The protuding domain of the coat protein of Melon necrotic spot virus is involved in compatibility with and transmission by the fungal vector *Olpidium bornovanus*. *Virology*, **402**, 129–134.

Ohki, T., Sako, I., Kanda, A., Mochizuki, T., Honda, Y. and Tsuda, S. (2008) A new strain of Melon necrotic spot virus that is unable to systemically infect Cucumis melo. *Phytopathology*, **98**, 1165–1170.

Oikawa, K., Yamasato, A., Kong, S.G., Kasahara, M., Nakai, M., Takahashi, F., Ogura, Y., Kagawa, T. and Wada, M. (2008) Chloroplast outer envelope protein Chup1 is essential for chloroplast anchorage to the plasma membrane and chloroplast movement. *Plant Physiol.*, **148**, 829–842.

Paila, Y.D., Richardson, L.G.L., and Schnell, D.J. (2015) New insights into the mechanism of chloroplast protein import and its integration with protein quality control, organelle biogenesis and development. *J. Mol. Biol.,* **427**, 1038–1060.

Pallás, V. (2007) *En el límite de la vida. Un siglo de Virus* La Voz de Galicia.

Pallas, V. and García, J.A. (2011) How do plant viruses induce disease? Interactions and interference with host components. *Journal of General Virology*, **92**, 2691–2705.

Pallas, V., Aparicio, F., Herranz, M.C., Sanchez-Navarro, J.A. and Scott, S.W. (2013) The Molecular Biology of Ilarviruses. *Adv Virus Res*, **87**, 139–181.

Pallás, V., Más, P. and Sánchez-Navarro, J.A. (1998) Detection of plant RNA viruses by nonisotopic dot-blot hybridization. *Methods Mol Biol*, **81**, 461–468.

Panavas, T., Hawkins, C.M., Panaviene, Z. and Nagy, P.D. (2005) The role of the p33:p33/p92 interaction domain in RNA replication and intracellular localization of p33 and p92 proteins of Cucumber necrosis tombusvirus. *Virology*, **338**, 81–95.

Panigrahi, R., Kubiszewski-Jakubiak, S., Whelan, J., and Vrielink, A. (2015). The design and structure of outer membrane receptors from peroxisomes, mitochondria, and chloroplasts. *Structure,* **23**, 1783–1800.

Paudel, D.B. and Sanfaçon, H. (2018) Exploring the diversity of mechanisms associated with plant tolerance to virus infection. *Front. Plant Sci.*, **9**, 1575.

Paul, P., Simm, S., Blaumeiser, A., Scharf, K. D., Fragkostefanakis, S., Mirus, O., et al. (2013) The protein translocation systems in plants - composition and variability on the example of *Solanum lycopersicum*. *BMC Genom.,* **14**, 189.

Peeters, N. and Small, I. (2001) Dual targeting to mitochondria and chloroplasts. *Biochimica et Biophysica Acta (BBA) - Molecular Cell Research*, **1541**, 54–63.

Peng, X., Wang, J., Peng, W., Wu, F.X. and Pan, Y. (2017) Protein-protein interactions: detection, reliability assessment and applications. *Brief Bioinform*, **18**, 798–819.

Perello, C., Llamas, E., Burlat, V., Ortiz-Alcaide, M., Phillips, M.A., Pulido, P. and Rodriguez-Concepcion, M. (2016) Differential subplastidial localization and turnover of enzymes involved in isoprenoid biosynthesis in chloroplasts. *PLoS One*, **11**, e0150539.

Petre, B., Saunders, D.G.O., Sklenar, J., Lorrain, C., Win, J., Duplessis, S. and Kamoun, S. (2015) Candidate effector proteins of the rust pathogen Melampsora larici-populina target diverse plant cell compartments. *Mol Plant-Microbe Interact*, **28**, 689–700.

Piatigorsky, J., O'Brien, W.E., Norman, B.L., Kalumuck, K., Wistow, G.J., Borras, T., Nickerson, J.M. and Wawrousek, E.F. (1988) Gene sharing by delta-crystallin and argininosuccinate lyase. *Proc Natl Acad Sci U S A*, **85**, 3479–3483.

Pogson, B.J., Woo, N.S., Förster, B. and Small, I.D. (2008) Plastid signalling to the nucleus and beyond. *Trends Plant Sci*, **13**, 602–609.

Pontier, D., Tronchet, M., Rogowsky, P., Lam, E. and Roby, D. (1998) Activation of hsr203, a plant gene expressed during incompatible plant-pathogen interactions, is correlated with programmed cell death. *Mol. Plant. Microbe. Interact.*, **11**, 544–554.

Priesnitz, C., and Becker, T. (2018) Pathways to balance mitochondrial translation and protein import. *Genes Dev.,* **32**, 1285–1296.

Pu, X.J., Li, Y.N., Wei, L.J., Xi, D.H. and Lin, H.H. (2016) Mitochondrial energy-dissipation pathway and cellular redox disruption compromises Arabidopsis resistance to turnip crinkle virus infection. *Biochem Biophys Res Commun*, **473**, 421–427.

Pujol, C., Maréchal-Drouard, L. and Duchêne, A.M. (2007) How can organellar protein N-terminal sequences be dual targeting signals? in silico analysis and mutagenesis approach. *J. Mol. Biol.*, **369**, 356–367.

Pumplin, N. and Voinnet, O. (2013) RNA silencing suppression by plant pathogens: defence, counter-defence and counter-counter-defence. *Nat Rev Microbiol*, **11**, 745–760.

Qin, W., Cho, K.F., Cavanagh, P.E. and Ting, A.Y. (2021) Deciphering molecular interactions by proximity labeling. *Nat Methods*, **18**, 133–143.

Qu, F., Ren, T. and Morris, T.J. (2003) The Coat Protein of Turnip Crinkle Virus Suppresses Posttranscriptional Gene Silencing at an Early Initiation Step. *J Virol*, **77**, 511.

Rajjou, L., Duval, M., Gallardo, K., Catusse, J., Bally, J., Job, C. and Job, D. (2012) Seed Germination and Vigor. *Annual review of plant biology*, **63**, 507–533.

Ralph, S.A., Foth, B.J., Hall, N. and McFadden, G.I. (2004) Evolutionary pressures on apicoplast transit peptides. *Mol. Biol. Evol.*, **21**, 2183–2194.

Ramundo, S., Asakura, Y., Salomé, P.A., Strenkert, D., Boone, M., Mackinder, L.C.M., et al. (2020) Coexpressed subunits of dual genetic origin define a conserved supercomplex mediating essential protein import into chloroplasts. *Proc. Natl. Acad. Sci. U.S.A.,* **117**, 32739–32749.

Rao, V.S., Srinivas, K., Sujini, G.N. and Kumar, G.N.S. (2014) Protein-Protein Interaction Detection: Methods and Analysis. *Int J Proteomics*, **2014**, 1–12.

Rapaport, D. and Neupert, W. (1999) Biogenesis of Tom40, core component of the Tom complex of mitochondria. *J. Cell Biol.*, **146**, 321–332.

Rasheed, F., Markgren, J., Hedenqvist, M. and Johansson, E. (2020) Modeling to understand plant protein structure-function relationships—implications for seed storage proteins. *Molecules*, **25**.

Reape, T.J., Brogan, N.P. and McCabe, P.F. (2015) Mitochondrion and chloroplast regulation of plant programmed cell death. In A. Gunawardena and P. McCabe, eds. *Plant programmed cell death*. Cham: Springer, pp. 33–53.

Reddy, A.S.N., Marquez, Y., Kalyna, M. and Barta, A. (2013) Complexity of the Alternative Splicing Landscape in Plants. *Plant Cell*, **25**, 3657–3683.

Rees, J.S., Li, X.W., Perrett, S., Lilley, K.S. and Jackson, A.P. (2015) Protein Neighbors and Proximity Proteomics. *Mol Cell Proteomics*, **14**, 2848–2856.

Reichert, V.L., Choi, M., Petrillo, J.E. and Gehrke, L. (2007) Alfalfa mosaic virus coat protein bridges RNA and RNA-dependent RNA polymerase in vitro. *Virology*, **364**, 214–226

Richardson, L.G.L., Paila, Y.D., Siman, S.R., Chen, Y., Smith, M.D., and Schnell, D.J. (2014) Targeting and assembly of components of the TOC protein import complex at the chloroplast outer envelope membrane. *Front. Plant Sci.,* **5**, 269.

Richardson, L.G.L., Small, E.L., Inoue, H. and Schnell, D.J. (2018) Molecular Topology of the Transit Peptide during Chloroplast Protein Import. *Plant Cell*, **30**, 1789–1806.

Riviere, C.J., Pot, J., Tremaine, J.H. and Rochon, D.M. (1989) Coat protein of melon necrotic spot carmovirus is more similar to those of tombusviruses than those of carmoviruses. *J. Gen. Virol.*, **70**, 3033–3042.

Rochaix, J.D. (2022) Chloroplast protein import machinery and quality control. *FEBS J*, **289**, 6908–6918.

Rochon, D., Singh, B., Reade, R., Theilmann, J., Ghoshal, K., Alam, S.B. and Maghodia, A. (2014) The p33 auxiliary replicase protein of Cucumber necrosis virus targets peroxisomes and infection induces de novo peroxisome formation from the endoplasmic reticulum. *Virology*, **452**–**453**, 133–142.

Rödiger, A., Baudisch, B., Langner, U. and Klösgen, R.B. (2011) Dual targeting of a mitochondrial protein: the case study of cytochrome c1. *Mol Plant*, **4**, 679–687.

Rossel, J.B., Wilson, P.B., Hussain, D., et al. (2007) Systemic and intracellular responses to photooxidative stress in Arabidopsis. *Plant Cell*, **19**, 4091–4110.

Roux, K.J., Kim, D.I., Raida, M. and Burke, B. (2012) A promiscuous biotin ligase fusion protein identifies proximal and interacting proteins in mammalian cells. *J Cell Biol*, **196**, 801.

Rudolf, M., MacHettira, A. B., Groß, L. E., Weber, K. L., Bolte, K., Bionda, T., et al. (2013) In vivo function of Tic22, a protein import component of the intermembrane space of chloroplasts. *Mol. Plant,* **6**, 817–829.

Ruiz, T.M., Voinnet, O. and Baulcombe, D.C. (1998) Initiation and maintenance of virus-induced gene silencing. *Plant Cell*, **10**, 937–946.

Russo, M., Burgyan, J. and Martelli, G.P. (1994) Molecular Biology of Tombusviridae. *Adv Virus Res*, **44**, 381–428.

Russo, M., Franco, A. di and Martelli, G.P. (1983) The fine structure of Cymbidium ringspot virus infections in host tissues. III. Role of peroxisomes in the genesis of multivesicular bodies. *J Ultrastruct Res*, **82**, 52–63.

Sáiz-Bonilla, M., Martín-Merchan, A., Pallás, V. and Navarro, J.A. (2022) Molecular characterization, targeting and expression analysis of chloroplast and mitochondrion protein import components in *Nicotiana benthamiana*. *Front Plant Sci*, **13**, 1040688.

Samavarchi-Tehrani, P., Samson, R. and Gingras, A.C. (2020) Proximity Dependent Biotinylation: Key Enzymes and Adaptation to Proteomics Approaches. *Mol Cell Proteomics*, **19**, 757–773.

Sanchez-Navarro, J., Miglino, R., Ragozzino, A. and Bol, J.F. (2001) Engineering of alfalfa mosaic virus RNA 3 into an expression vector. *Arch. Virol.*, **146**, 923–939.

Sasvari, Z., Gonzalez, P.A., Rachubinski, R.A. and Nagy, P.D. (2013) Tombusvirus replication depends on Sec39p endoplasmic reticulum-associated transport protein. *Virology*, **447**, 21–31.

Schiavinato, M. (2021) Subgenome evolution in allotetraploid plants *Nicotiana benthamiana*. *Plant J.,* **106**, 672–688.

Schiavinato, M., Marcet-Houben, M., Dohm, J.C., Gabaldón, T., and Himmelbauer, H. (2020) Parental origin of the allotetraploid tobacco *Nicotiana benthamiana*. *Plant J.,* **102**, 541–554.

Schiavinato, M., Strasser, R., Mach, L., Dohm, J.C., and Himmelbauer, H. (2019) Genome and transcriptome characterization of the glycoengineered *Nicotiana benthamiana* line ΔxT/FT. *BMC Genom.,* **20**, 1–16.

Schindelin, J., Arganda-Carreras, I., Frise, E., Kaynig, V., Longair, M., Pietzsch, T., et al. (2012) Fiji: an open-source platform for biological-image analysis. *Nat. Methods,* **9**, 676–682.

Schnell, D.J. (2019) The TOC GTPase receptors: Regulators of the fidelity, specificity and substrate profiles of the general protein import machinery of chloroplasts. *Protein J.,* **38**, 343–350.

Scholthof, H.B. (2005) Plant virus transport: Motions of functional equivalence. *Trends Plant Sci*, **10**, 376–382.

Scholthof, K.B.G. (2004) Tobacco Mosaic Virus: A model system for plant biology. *Annu Rev Phytopathol*, **42**, 13–34.

Schwenkert, S., Dittmer, S., and Soll, J. (2018). Structural components involved in plastid protein import. *Essays Biochem.,* **62**, 65–75.

Scott, I. and Logan, D.C. (2008) Mitochondrial morphology transition is an early indicator of subsequent cell death in Arabidopsis. *New Phytol.*, **177**, 90–101.

Serra-Soriano, M., Navarro, J.A. and Pallas, V. (2017) Dissecting the multifunctional role of the N-terminal domain of the Melon necrotic spot virus coat protein in RNA packaging, viral movement and interference with antiviral plant defence. *Mol. Plant Pathol.*, **18**, 837–849.

Serra-Soriano, M., Navarro, J.A., Genoves, A. and Pallás, V. (2015) Comparative proteomic analysis of melon phloem exudates in response to viral infection. *J. Proteomics*, **124**, 11–24.

Sett, S., Prasad, A. and Prasad, M. (2022) Resistance genes on the verge of plant-virus interaction. *Trends Plant Sci*, **27**, 1242–1252.

Shang, Y., Yan, L., Liu, Z.Q., et al. (2010) The Mg-chelatase H subunit of Arabidopsis antagonizes a group of WRKY transcription repressors to relieve ABA-responsive genes of inhibition. *Plant Cell*, **22**, 1909–1935.

Sharma, M., Bennewitz, B. and Klösgen, R.B. (2018) Rather rule than exception? How to evaluate the relevance of dual protein targeting to mitochondria and chloroplasts. *Photosynth Res*, **138**, 335–343.

Shen, B.R., Zhu, C.H., Yao, Z., Cui, L.L., Zhang, J.J., Yang, C.W., He, Z.H. and Peng, X.X. (2017) An optimized transit peptide for effective targeting of diverse foreign proteins into chloroplasts in rice. *Sci. Rep.*, **7**, 1–12.

Shi, L.X., and Theg, S.M. (2013) The chloroplast protein import system: From algae to trees. *Biochim. Biophys. Acta Mol. Cell Res.,* **1833**, 314–331.

Simon, A.E. (2015) 3'UTRs of carmoviruses. *Virus Res*, **206**, 27–36.

Simon, A.E. and Miller, W.A. (2013) 3' cap-independent translation enhancers of plant viruses. *Annu Rev Microbiol*, **67**, 21–42.

Smith, M.D., Hiltbrunner, A., Kessler, F., and Schnell, D.J. (2002) The targeting of the atToc159 preprotein receptor to the chloroplast outer membrane is mediated by its GTPase domain and is regulated by GTP. *J. Cell Biol.,* **159**, 833–843.

Smith, M.D., Rounds, C.M., Wang, F., Chen, K., Afitlhile, M., and Schnell, D.J. (2004) atToc159 is a selective transit peptide receptor for the import of nucleus-encoded chloroplast proteins. *J. Cell Biol.,* **165**, 323–334.

Sommer M.S., Daum B., Gross L.E., Weis, B.L., Mirus, O., Abram, L., Maier, U.G., Kühlbrandt, W., Schleiff, E. (2011) Chloroplast Omp85 proteins change orientation during evolution. *Proc Natl Acad Sci USA,* **108**, 13841–13846.

Song, G., Hsu, P.Y. and Walley, J.W. (2018) Assessment and Refinement of Sample Preparation Methods for Deep and Quantitative Plant Proteome Profiling. *Proteomics*, **18**, 1800220.

Soosaar, J.L.M., Burch-Smith, T.M. and Dinesh-Kumar, S.P. (2005) Mechanisms of plant resistance to viruses. *Nat Rev Microbiol*, **3**, 789–798.

Spartz, A.K., Herman, R.K. and Shaw, J.E. (2004) SMU-2 and SMU-1, Caenorhabditis elegans homologs of mammalian spliceosome-associated proteins RED and fSAP57, work together to affect splice site choice. *Mol Cell Biol*, **24**, 6811–6823.

Sperschneider, J., Catanzariti, A.M., Deboer, K., Petre, B., Gardiner, D.M., Singh, K.B., Dodds, P.N. and Taylor, J.M. (2017) LOCALIZER: Subcellular localization prediction of both plant and effector proteins in the plant cell. *Sci. Rep.*, **7**, 1-14.

Stojilković, B., Xiang, H., Chen, Y., Bauters, L., Put, H. Van de, Steppe, K., Liao, J., Engler, J. de A. and Gheysen, G. (2022) The nematode effector Mj-NEROSs interacts with ISP influencing plastid ROS production to suppress plant immunity. *bioRxiv*, **2022**, 10.

Su, S.H. and Krysan, P.J. (2016) A double-mutant collection targeting MAP kinase related genes in Arabidopsis for studying genetic interactions. *Plant J*, **88**, 867–878.

Su, T., Li, W., Wang, P. and Ma, C. (2019) Dynamics of peroxisome homeostasis and its role in stress response and signaling in plants. *Front. Plant Sci.*, **10**, 705.

Sugiyama, M., Sato, H., Karasawa, A., Hase, S., Takahashi, H. and Ehara, Y. (2000) Characterization of symptom determinants in two mutants of cucumber mosaic virus Y strain, causing distinct mild green mosaic symptoms in tobacco. *Physiol Mol Plant Pathol*, **56**, 85–90.

Syed, N.H., Kalyna, M., Marquez, Y., Barta, A. and Brown, J.W.S. (2012) Alternative splicing in plants--coming of age. *Trends Plant Sci*, **17**, 616–623.

Talbot, N.J. and Kershaw, M.J. (2009) The emerging role of autophagy in plant pathogen attack and host defence. *Curr Opin Plant Biol*, **12**, 444–450.

Tamura, K., Stecher, G., and Kumar, S. (2021) MEGA11: Molecular evolutionary genetics analysis version 11. *Mol. Biol. Evol.,* **38**, 3022–3027.

Tanz, S.K., Castleden, I., Small, I.D. and Harvey Millar, A. (2013) Fluorescent protein tagging as a tool to define the subcellular distribution of proteins in plants. *Front. Plant Sci.*, **4**, 214.

Teixeira, R.M., Ferreira, M.A., Raimundo, G.A.S., Loriato, V.A., Reis, P.A.B. and Fontes, E.P.B. (2019) Virus perception at the cell surface: revisiting the roles of receptor-like kinases as viral pattern recognition receptors. Mol. Plant Pathol. **20**, 1196–1202.

Teixeira, P. F., and Glaser, E. (2013) Processing peptidases in mitochondria and chloroplasts. *Biochim. Biophys. Acta Mol. Cell Res.,* **1833**, 360–370.

Thaler, J.S., Owen, B. and Higgins, V.J. (2004) The Role of the Jasmonate Response in Plant Susceptibility to Diverse Pathogens with a Range of Lifestyles. *Plant Physiol*, **135**, 530.

Thomas, C.L., Leh, V., Lederer, C. and Maule, A.J. (2003) Turnip crinkle virus coat protein mediates suppression of RNA silencing in *Nicotiana benthamiana*. *Virology*, **306**, 33–41.

Thompson, A., Schäfer, J., Kuhn, K., Kienle, S., Schwarz, J., Schmidt, G., Neumann, T. and Hamon, C. (2003) Tandem Mass Tags: A Novel Quantification Strategy for Comparative Analysis of Complex Protein Mixtures by MS/MS. *Anal Chem*, **75**, 1895–1904.

Tranel, P. J., and Keegstra, K. (1996) A novel, bipartite transit peptide targets OEP75 to the outer membrane of the chloroplastic envelope. *Plant Cell,* **8**, 2093–2104.

Trinkle-Mulcahy, L. (2019) Recent advances in proximity-based labeling methods for interactome mapping [version 1; referees: 2 approved]. *F1000Res*, **8**.

Truniger, V., Miras, M. and Aranda, M.A. (2017) Structural and functional diversity of plant virus 3'-cap-independent translation enhancers (3'-CITEs). *Front Plant Sci*, **8**, 2047.

Tzelepis, G., Dölfors, F., Holmquist, L. and Dixelius, C. (2021) Plant mitochondria and chloroplasts are targeted by the Rhizoctonia solani RsCRP1 effector. *Biochem Biophys Res Commun*, **544**, 86–90.

Ulrich, A.K.C., Schulz, J.F., Kamprad, A., Schütze, T. and Wahl, M.C. (2016) Structural Basis for the Functional Coupling of the Alternative Splicing Factors Smu1 and RED. *Structure*, **24**, 762–773.

van Aken, O. and van Breusegem, F. (2015) Licensed to kill: mitochondria, chloroplasts, and cell death. *Trends Plant Sci.*, **20**, 754–766.

van Loon, L.C. (1997) Induced resistance in plants and the role of pathogenesis-related proteins. *Eur. J. Plant Pathol.*, **103**, 753–765.

Verchot, J. (2016) How does the stressed out ER find relief during virus infection? *Curr. Opin. Virol.*, **17**, 74–79.

Verma, A., Lee, C., Morriss, S., et al. (2018) The novel cyst nematode effector protein 30D08 targets host nuclear functions to alter gene expression in feeding sites. *New Phytologist*, **219**, 697–713.

Voos, W., and Röttgers, K. (2002). Molecular chaperones as essential mediators of mitochondrial biogenesis. *Biochim. Biophys. Acta,* **1592**, 51–62.

Wada, Y., Tanaka, H., Yamashita, E., Kubo, C., Ichiki-Uehara, T., Nakazono-Nagaoka, E., Omura, T. and Tsukihara, T. (2008) The structure of melon necrotic spot virus determined at 2.8 Å resolution. *Acta Crystallogr Sect F Struct Biol Cryst Commun*, **64**, 8–13.

Waigmann, E., Ueki, S., Trutnyeva, K. and Citovsky, V. (2010) The Ins and Outs of Nondestructive Cell-to-Cell and Systemic Movement of Plant Viruses. *CRC Crit Rev Plant Sci*, **23**, 195–250.

Walley, J.W., Shen, Z., McReynolds, M.R., Schmelz, E.A. and Briggs, S.P. (2018) Fungal-induced protein hyperacetylation in maize identified by acetylome profiling. *Proc Natl Acad Sci U S A*, **115**, 210–215.

Wan, J., Cabanillas, D.G., Zheng, H. and Laliberte, J.-F. (2015) Turnip mosaic virus moves systemically through both phloem and xylem as membrane-associated complexes. *Plant Physiol.*, **167**, 1374–1388.

Wang, A. (2015) Dissecting the Molecular Network of Virus-Plant Interactions: The Complex Roles of Host Factors. *Annu Rev Phytopathol*, **53**, 45–66.

Wang, J., Xu, G., Ning, Y., Wang, X. and Wang, G.L. (2022) Mitochondrial functions in plant immunity. *Trends Plant Sci*, **27**, 1063–1076.

Wang, Y., Selinski, J., Mao, C., Zhu, Y., Berkowitz, O. and Whelan, J. (2020) Linking mitochondrial and chloroplast retrograde signalling in plants. *Philosophical Transactions of the Royal Society B: Biological Sciences*, **375**, 1–12.

Wang, Z., Tang, K., Zhang, D., Wan, Y., Wen, Y., Lu, Q. and Wang, L. (2017) High-throughput m6A-seq reveals RNA m6A methylation patterns in the chloroplast and mitochondria transcriptomes of *Arabidopsis thaliana*. *PLoS One*, **12**, e0185612.

Want, J.P.H. van der and Dijkstra, J. (2006) A history of plant virology. *Arch Virol*, **151**, 1467–1498.

Weber, P.H. and Bujarski, J.J. (2015) Multiple functions of capsid proteins in (+) stranded RNA viruses during plant-virus interactions. *Virus Res*, **196**, 140–149.

Weiss, R.A. (2002) Virulence and pathogenesis. *Trends Microbiol*, **10**, 314–317.

Whitham, S., Dinesh-Kumar, S.P., Choi, D., Hehl, R., Corr, C. and Baker, B. (1994) The product of the tobacco mosaic virus resistance gene N: similarity to toll and the interleukin-1 receptor. *Cell*, **78**, 1101–1115.

Wiedemann, N., and Pfanner, N. (2017) Mitochondrial machineries for protein import and assembly. *Annu. Rev. Biochem.,* **86**, 685–714.

Wiesemann, K., Simm, S., Mirus, O., Ladig, R. and Schleiff, E. (2019) Regulation of two GTPases Toc159 and Toc34 in the translocon of the outer envelope of chloroplasts. *Biochim Biophys Acta Proteins Proteom*, **1867**, 627–636.

Woo, S., Moon, B. and Hwang, I. (2022) Both metaxin and Tom20 together with two mitochondria-specific motifs support mitochondrial targeting of dual-targeting AtSufE1. *J Integr Plant Biol*, **64**, 1596–1613.

Woodson, J.D. and Chory, J. (2008) Coordination of gene expression between organellar and nuclear genomes. *Nature Reviews Genetics 2008 9:5*, **9**, 383–395.

Wu, G.Z., Meyer, E.H., Richter, A.S., et al. (2019) Control of retrograde signalling by protein import and cytosolic folding stress. *Nat Plants 2019 5:5*, **5**, 525–538.

Wu, X. and Ye, J. (2020) Manipulation of Jasmonate Signaling by Plant Viruses and Their Insect Vectors. *Viruses*, **12**, 148.

Xiang, Y., Kakani, K., Reade, R., Hui, E. and Rochon, D. (2006) A 38-amino-acid sequence encompassing the arm domain of the cucumber necrosis virus coat protein functions as a chloroplast transit peptide in infected plants. *J. Virol.*, **80**, 7952–7964.

Xing, S., Mehlhorn, D.G., Wallmeroth, N., Asseck, L.Y., Kar, R., Voss, A., et al. (2017) Loss of GET pathway orthologs in *Arabidopsis thaliana* causes root hair growth defects and affects SNARE abundance. *Proc. Natl. Acad. Sci. U.S.A.,* **114**, E1544–E1553.

Xiong, J., Cui, X., Yuan, X., Yu, X., Sun, J. and Gong, Q. (2016) The Hippo/STE20 homolog SIK1 interacts with MOB1 to regulate cell proliferation and cell expansion in Arabidopsis. *J Exp Bot*, **67**, 1461–1475.

Xu, S.L., Shrestha, R., Karunadasa, S.S. and Xie, P.Q. (2023) Proximity Labeling in Plants. *Annual Review of Plant Biology*, **74.**

Yan, J., Campbell, J. H., Glick, B. R., Smith, M. D., and Liang, Y. (2014) Molecular characterization and expression analysis of chloroplast protein import components in tomato (*Solanum lycopersicum*). *PLoS ONE,* **9**, e95088.

Yang, F., Xiao, K., Pan, H. and Liu, J. (2021) Chloroplast: The Emerging Battlefield in Plant–Microbe Interactions. *Front Plant Sci*, **12**, 218.

Yang, X., Zhiyan, W., Zhang, D., Li, Z., Nagalakshmi, U., Dinesh-Kumar, S.P. and Zhang, Y. (2021) Proximity labeling: an emerging tool for probing in planta molecular interactions. *Plant Commun*, **2**, 100137.

Yang, Z., Huang, Y., Yang, J., et al. (2020) Jasmonate Signaling Enhances RNA Silencing and Antiviral Defense in Rice. *Cell Host Microbe*, **28**, 89-103.

Ye, W., Spånning, E., Glaser, E. and Mäler, L. (2015) Interaction of the dual targeting peptide of Thr-tRNA synthetase with the chloroplastic receptor Toc34 in *Arabidopsis thaliana*. *FEBS Open Bio*, **5**, 405–412.

Ye, W., Spãnning, E., Unnerstãle, S., Gotthold, D., Glaser, E. and Mäler, L. (2012) NMR investigations of the dual targeting peptide of Thr-tRNA synthetase and its interaction with the mitochondrial Tom20 receptor in *Arabidopsis thaliana*. *FEBS J*, **279**, 3738–3748.

Yi, W., Li, J., Zhu, X., et al. (2020) CRISPR-assisted detection of RNA-protein interactions in living cells. *Nat Methods*, **17**, 685–688.

Yogev, O., Naamati, A. and Pines, O. (2011) Fumarase: A paradigm of dual targeting and dual localized functions. *FEBS J.*, **278**, 4230–4242.

Young, J.C., Hoogenraad, N.J. and Hartl, F.U. (2003) Molecular chaperones Hsp90 and Hsp70 deliver preproteins to the mitochondrial import receptor Tom70. *Cell*, **112**, 41–50.

Yue, J., Wei, Y. and Zhao, M. (2022) The Reversible Methylation of m6A Is Involved in Plant Virus Infection. *Biology (Basel)*, **11**, 271.

Zhang, C., Wu, Z., Li, Y. and Wu, J. (2015) Biogenesis, function, and applications of virus-derived small RNAs in plants. *Front Microbiol*, **6**, 1237.

Zhang, L., Hanada, K. and Palukaitis, P. (1994) Mapping local and systemic symptom determinants of cucumber mosaic cucumovirus in tobacco. *Journal of General Virology*, **75**, 3185–3191.

Zhang, M., Chiang, Y.H., Toruño, T.Y., et al. (2018) The MAP4 Kinase SIK1 Ensures Robust Extracellular ROS Burst and Antibacterial Immunity in Plants. *Cell Host Microbe*, **24**, 379-391.

Zhang, T.Y., Wang, Z.Q., Hu, H.C., et al. (2021) Transcriptome-Wide N6-Methyladenosine (m6A) Profiling of Susceptible and Resistant Wheat Varieties Reveals the Involvement of Variety-Specific m6A Modification Involved in Virus-Host Interaction Pathways. *Front Microbiol*, **12**.

Zhang, X.P. and Glaser, E. (2002) Interaction of plant mitochondrial and chloroplast signal peptides with the Hsp70 molecular chaperone. *Trends Plant Sci*, **7**, 14–21.

Zhang, Y., Gao, P. and Yuan, J.S. (2010) Plant Protein-Protein Interaction Network and Interactome, *Current genomics*, **11**, 40-46.

Zhang, Y., Song, G., Lal, N.K., et al. (2019) TurboID-based proximity labeling reveals that UBR7 is a regulator of N NLR immune receptor-mediated immunity. *Nat Commun*, **10**, 3252.

Zhao, C., Nie, H., Shen, Q., Zhang, S., Lukowitz, W. and Tang, D. (2014) EDR1 Physically Interacts with MKK4/MKK5 and Negatively Regulates a MAP Kinase Cascade to Modulate Plant Innate Immunity. *PLoS Genet*, **10**, e1004389.

Zhao, J., Zhang, X., Hong, Y. and Liu, Y. (2016) Chloroplast in plant-virus interaction. *Front. Microbiol.*, **7**, 1565.

Zhao, S. and Li, Y. (2021) Current understanding of the interplays between host hormones and plant viral infections. *PLoS Pathog*, **17**, e1009242.

ANNEX I.

List of parental plasmids for the development of the different constructs used in this thesis.

Plasmid	Resistance	Experimental Procedure
pBluescript-35S-Popit (pSK35S-PP)	Amp	Subcellular localization
pMOG800	Kan	
pMNSV(Al/264)	Amp	Subcellular localization under MNSV infection
pMNSV(CP-GFP)	Amp	
pMNSV(CP-HA)	Amp	
pMNSV(CPΔR_1[6-30]-GFP)	Amp	
pMNSV(CPΔR_1[6-30]-HA)	Amp	
pMNSV(CPΔR_1)	Amp	
pMNSV(R/arm-GFP)	Amp	
pTRV1	Kan	Expression
$pTRV2_{promPEBV}$[CP-HA]	Kan	
$pTRV2_{promPEBV}$[ChFP]	Kan	
pGBKT7	Kan	Yeast two-hybrid
pGADT7	Amp	
pTRV1	Kan	VIGS
pTRV2-X	Kan	
p35S::gN-TurboID-3xHA	Amp	TurboID


ibmcp
Instituto de Biología Molecular
y Celular de Plantas


CSIC
Consejo Superior de Investigaciones Científicas